国立病院機構鹿児島医療センター

研究業績集　第 25 号

令和6年4月～令和7年3月（2024年4月～2025年3月）

国立病院機構鹿児島医療センター

臨床研究部

巻頭言

鹿児島医療センター研究業績集第 25 号の発刊にあたって

国立病院機構の誇るべき特色の１つとして、それぞれの病院が独立した臨床研究部門を持ち、成果を上げていることが挙げられます。残念ながら、我が国においては独立した研究部門を維持している病院というのは民間はもちろんのこと公立系でも国立病院機構以外には多くはないと思います。これは、国立病院機構が『質の高い臨床研究を推進する』という理念を掲げており、それを実行していくという決意の表れだと理解しています。

さて、鹿児島医療センターの令和 6 年度の研究面での成果を臨床研究部でここにまとめていただきました。当センターの皆さんが、日頃、臨床の duty に追われて忙しく働き、その上に働き方改革にまで迫られる中で、このように大変立派な成果を出していただいていることに感謝致します。当センターから多くの学会発表、論文が生まれていることに誇りを感じると共に、当センターで健全に医療が行われていると実感いたします。

医は仁術であり、医療は医学に基づく社会実装された技術と言えます。したがって我々がより良い医療を提供すには、博愛の精神、奉仕の心、そして高度な技術や豊かな知識など人間的な側面と学術的な側面からの研鑽が必要なことは言うまでもありません。実際、欧米の病院では教会が運営設立しているところも少なくありませんが、そういうところでも研究部門を有し、アカデミックに医学研究を推進させています。医療を心理や人間性、そして技術や経済性の観点から見るのと同時にサイエンスとして見ることも極めて重要です。その意味で鹿児島医療センターでは、臨床研究部が当センターの医療をサイエンス面からしっかりサポートしてくれているのは心強い限りです。今回まとめていただいた業績集を当センターの提供する医療のサイエンス面からの成果だと見ていただければ、我々の提供する医療は決して偏った医療ではないことがわかっていただけると同時に、今後もますます期待していただけるものと確信します。

独立行政法人国立病院機構鹿児島医療センター
院長　西尾　善彦

目次

1. 臨床研究部の組織概要

1. 名称・所在地

独立行政法人国立病院機構鹿児島医療センター臨床研究部
鹿児島県鹿児島市城山町８－１

2. 沿革

臨床研究部は 1999 年 10 月に設置されました。当初は病態生理研究室、医用工学研究室、画像診断研究室、臨床疫学研究室、治療評価研究室の 5 室で運営されていましたが、2007 年に治療評価研究室を臨床研究推進室と名称変更を行い、さらに 2013 年からは治験管理室を加え、現在 1 部 6 室で活動しています。2006 年からは東病棟 8 階に臨床研究部・治験管理室がありましたが、2018 年 4 月の逓信病院機能移転に伴い、2017 年 11 月に臨床研究部は旧更衣棟に、治験管理室は事務棟に移転しました。

3. 組織構成

臨床研究部長の総括のもとに以下の研究室を設置しています。

1. 病態生理研究室
2. 医用工学研究室
3. 画像診断研究室
4. 臨床疫学研究室
5. 臨床研究推進室
6. 治験管理室

令和 6 年度の臨床研究部の各室の体制は以下に示す通りです。

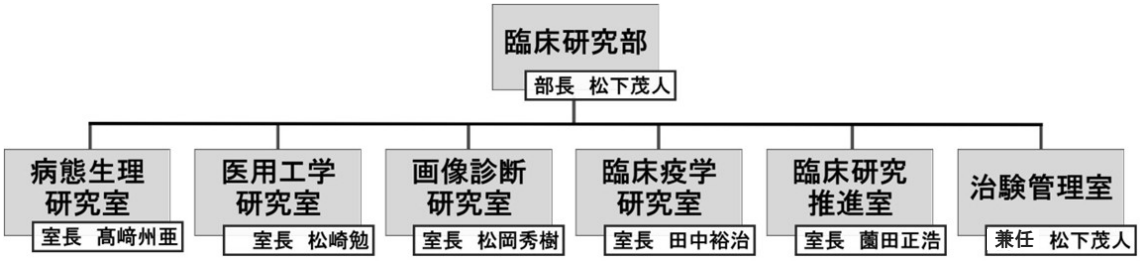

4. 鹿児島大学大学院医歯学総合研究科

当院は 2009 年より、鹿児島大学の連携大学院として教育・研究活動を行なっております。2024 年度からは、先進医療学講座（連携講座）「臨床情報医工学」を新たに開講し、臨床と基礎研究を融合した先進的な研究体制を整備いたしました。
本講座「臨床情報医工学」では、優秀で実践的な医療人材の育成を目的に、多分野の教官による指導体制を確立し、当院での高度な臨床経験と鹿児島大学大学院における基礎的研究との連携を図っています。これにより、大学院生が先進的かつ包括的な臨床研究を遂行できるよう支援しています。
2023 年 10 月からは第 2 循環器内科の伊集院駿先生が博士課程に進学し、主指導教官である東健作先生の指導のもと、臨床研究部において研究を進めております。

2. 臨床研究と治験

① 臨床研究

(ア) EBM・ネットワーク共同臨床研究

領域・課題番号	研究責任医師	研究課題名
H28－NHO(血液)－02	大塚眞紀	成人初発未治療びまん性大細胞型 B 細胞リンパ腫における R-CHOP 単独治療と放射線併用療法の治療成績、QOL、費用、費用対効果の多施設共同前向きコホート研究
H30－NHO(外科)－01	塗木健介	本邦における成人鼠経ヘルニア術後慢性疼痛の実態調査とそのリスク因子解析 -多施設共同前向きコホート研究-（HERNIA STUDY）
H31－NHO(血液)－01	大塚眞紀	未治療濾胞性リンパ腫における Obinutuzumab の治療成績、QOL、費用対効果、予後に関する多施設前向きコホート研究（PEACE-FL)
H31－NHO(多共)－02	野元三治	メトトレキサート(MTX)関連リンパ増殖性疾患の遺伝子変異プロファイルの解析
R2－NHO(心脳)－04	髙﨑州亜	がん化学療法関連心筋症の予測、早期発見、早期治療 ～心臓超音波検査 speckle tracking 法、タイチン truncating 変異の検出、尿中タイチン N フラグメント測定、血中心筋トロポニン I 高感度測定の比較検討～
R3－NHO(血液)－01	大塚眞紀	レジストリーデータを利用した AYA 世代 DLBCL の臨床的・生物学的特性を明らかにする観察研究（NHO-DLBCL-AYA 研究）
R3－NHO(他研)－01	中村康典	DOAC 服用患者における抜歯の安全性の確立に関する研究：ガイドライン確立のための多施設共同前向き研究
R4－NHO(心脳)－01	松岡秀樹	急性期 BAD 型脳梗塞に対する抗血栓療法の種類と神経学的予後に関する前向き探索研究

(イ) 競争的研究費等

I. 公費臨床試験

財源	課題名	研究者名	金額（円）
日本医療研究開発機構研究費	頭頸部基底細胞癌縮小マージン切除による新たな低侵襲標準治療の開発	分担研究者 松下茂人	1,300,000
日本医療研究開発機構研究費	爪部悪性黒色腫への指趾骨温存切除による新たな低侵襲標準治療の開発	分担研究者 松下茂人	260,000
日本医療研究開発機構研究費	ロメリジン塩酸塩による CADASIL 患者に対する脳虚血イベント再発抑制	分担研究者 松岡秀樹	650,000
文部科学省 科学研究費助成事業 基盤研究(C)	唇裂患者の顔貌評価を三次元から四次元へ進化させる分析方法の開発(22K10125)	主任研究者 大河内孝子	520,000
		分担研究者 中村康典	130,000

財源	課題名	研究者名	金額(円)
文部科学省 科学研究費助成事業　基盤研究(C)	口腔機能評価と健康指標のデータビジュアライズと口腔機能管理アウトカムの検討(23K09483)	分担研究者 中村康典	65,000
文部科学省 科学研究費助成事業　基盤研究(C)	心房細動の早期発見への道を拓く唾液内マクロRNA の探索(23K0735)	主任研究者 二宮雄一	195,000
文部科学省 科学研究費助成事業　基盤研究(C)	血管老化の早期発見を目指した　唾液診断の可能性(24K13060)	分担研究者 二宮雄一	130,000
文部科学省 科学研究費助成事業　基盤研究(C)	PACAP-PACI 受容体シグナルの乾癬の病態に与える影響と治療応用の可能性(24K11500)	主任研究者 藤井一恭	780,000
文部科学省 科学研究費助成事業　基盤研究(C)	掻痒疾患における中枢および抹消 PACAP 受容体シグナル伝達の比較解析(22K06647)	分担研究者 藤井一恭	130,000
厚生労働省 厚生労働科学研究費補助金	小児から成人期発症遺伝性 QT 延長症候群とその類縁疾患の突然死予防に関する研究(23FC1003)	分担研究者 二宮由美子	100,000

Ⅱ．民間セクターからの寄付金

課題名/依頼業者名	研究者名	金額(円)
高齢者の血管疾患に対する外科治療の研究助成	金城　玉洋	600,000
肝細胞がんに対する冠動脈塞栓療法に関する研究	櫻井　一宏	150,000
弁膜症外科治療における研究(心臓血管外科)	金城　玉洋	500,000

(ウ)臨床研究課題

	部署	研究内容・課題名
1	第 1 循環器内科	動脈硬化を基盤とした虚血性心臓病における新規血液マーカーの確立
2	第 1 循環器内科 中島　均	エベロリムス溶出性コバルトクロムステント(CoCr-EES[XIENCE])留置後の DAPT 投与期間を 1 か月に短縮することの安全性を評価する多施設前向きオープンラベル無作為化比較試験(ShorT and Optimal duration of Dual AntiPlatelet Therapy study-2(STOPDAPT-2)
3	第 1 循環器内科 中島　均	日本心血管インターベンション学会内登録データを用いた統合的解析
4	第 1 循環器内科	日本経カテーテル心臓弁治療学会(JTVT)内登録データを用いた統合的解析
5	第 1 循環器内科 片岡哲郎	鹿児島県における急性冠症候群(ACS)のレジストリー(OK－ACS　Registry)

	部署	研究内容・課題名
6	第 1 循環器内科 片岡哲郎	1・2 世代薬剤溶出性ステント留置後のステント血栓症に関するレトロスペクティブ多施設レジストリー
7	心臓血管外科 立石直毅	胸部正中切開創の表皮細菌が及ぼす影響と皮膚ドレッシング剤の効果
8	脳・血管内科 松岡秀樹	非弁膜症性心房細動とアテローム血栓症を合併する脳梗塞例の二次予防における最適な抗血栓療法に関する多施設共同ランダム化比較試験（Optimal Antithrombotic Therapy in Ischemic Stroke Patients with Non-Valvular Atrial Fibrillation and Atherothrombosis：ATIS-NVAF)
9	脳・血管内科 松岡秀樹	K-RESOLVE Network 研究
10	脳・血管内科 濵田祐樹	機械的血栓回収療法による再開通後の脳循環時間と再潅流障害との関連についての研究
11	脳・血管内科 松岡秀樹	レセプト等情報を用いた脳卒中・脳神経外科医療疫学調査（J-ASPECT study : Nationwide survey of Acute Stroke care capacity for Proper dEsignation of Comprehensive stroke CenTer in Japan）
12	脳・血管内科 濵田祐樹	血管モデルを用いた有効な血栓回収療法手技の確立に関する研究
13	脳・血管内科 松岡秀樹	ロメリジン塩酸塩による CADASIL 患者に対する脳虚血イベント再発抑制
14	脳・血管内科 松岡秀樹	急性期 BAD 型脳梗塞に対する 抗血栓療法の種類と神経学的予後に関する前向き探索研究
15	脳・血管内科 松岡秀樹	脳梗塞再発のリスク因子を有する急性期アテローム血栓性脳梗塞及びハイリスク TIA 患者を対象としたプラスグレルのクロピドグレルとの血小板凝集能の比較臨床研究 (ACUTE-PRAS)
16	脳・血管内科 松岡秀樹	第 Xa 因子阻害薬による治療下で大出血を認めた患者の特性、医療介入、健康状態の転帰を記録する、多国籍、縦断的、観察研究（REVERXaL）
17	脳・血管内科 濵田祐樹	血栓吸引カテーテルを用いた機械的血栓回収療法の効果と安全性に関する多施設共同登録研究(REACT AIS Registry)
18	脳・血管内科 濵田祐樹	最終健常確認時刻から 24-72 時間経過した前方循環主幹動脈閉塞を有する脳梗塞例に対する血管内治療の有効性検証の為の多施設共同ランダム化比較研究
19	脳・血管内科 濵田祐樹	急性期脳主幹動脈閉塞における機械的血栓回収療法例の後ろ向きコホート研究
20	脳・血管内科 松岡秀樹	抗凝固療法下に発症した心房細動関連脳梗塞の多機関共同前向きコホート研究 (AFIDA-1)
21	脳・血管内科 松岡秀樹	心原性脳塞栓撲滅のために心房細動の早期発見・適切治療を目指すシステム開発と社会実装-SEGODON Project-
22	脳・血管内科 佐藤健朗	鹿児島医療センター脳卒中データベース研究
23	小児科 二宮由美子	小児から成人期発症遺伝性 QT 延長症候群とその類縁疾患の突然死予防に関する研究
24	血液内科 大塚眞紀	レジストリ―データを利用した AYA 世代 DLBCL の臨床的・生物学的特性を明らかにする観察研究
25	血液内科 大塚眞紀	未治療 CCR4 陽性高齢者 ATL に対するモガムリズマブ併用 CHOP-14 の第II相試験
26	血液内科 大塚眞紀	骨髄増殖性腫瘍の実態と遺伝子変異検索

	部署	研究内容・課題名
27	血液内科 大塚眞紀	B細胞性急性リンパ性白血病におけるターゲットキャプチャーRNA-seq を用いたサブタイプ診断の実行可能性に関する研究
28	血液内科 大塚眞紀	成人T細胞白血病リンパ腫における CCR4 遺伝子変異と予後の検討
29	血液内科 大塚眞紀	80 歳以上未治療びまん性大細胞型 B 細胞リンパ腫に対するポラツズマブベドチン＋R-miniCHP 療法の有効性と安全性を検証する多施設共同非盲検無対照試験
30	血液内科 大塚眞紀	COVID-19 に関するレジストリ研究
31	糖尿病・内分泌内科 郡山暢之	電子カルテ情報活用型多施設症例データベースを利用した糖尿病に対する臨床情報収集に関する研究（J-DREAMS）
32	消化器内科 森内昭博	肝細胞癌に対するアテゾリズマブ＋ベバシズマブ併用療法の治療効果と安全性の検討
33	消化器内科 櫻井一宏	C型肝炎ウイルス排除治療による肝硬変患者のアウトカムに関する多施設共同観察研究
34	婦人科 神尾真樹	卵巣を摘出した有経女性の骨量についての研究
35	婦人科 神尾真樹	VAIN に対するレーザー蒸散術の治療効果
36	外科・消化器外科 塗木健介	免疫抑制患者に対する 13 価蛋白結合型肺炎球菌ワクチンと 23 価莢膜多糖体型肺炎球菌ワクチンの連続摂取と 23 価莢膜多糖体型肺炎球菌ワクチン単独摂取の有効性の比較 -二重盲検無作為化比較試験-（CPI Study）
37	外科・消化器外科 塗木健介	本邦における成人鼠経ヘルニア術後慢性疼痛の実態調査とそのリスク因子解析 -多施設共同前向きコホート研究-（HERNIASTUDY）
38	麻酔科 今林 徹	当センター集中治療におけるレミフェンタニル使用状況の調査
39	麻酔科 今林 徹	重症患者への経腸栄養チューブ挿入におけるポータブルX線撮影装置の有効性の検証
40	病理診断科 野元三治	T 細胞大顆粒リンパ球性白血病の 5 例についての研究
41	病理診断科 野元三治	メトトレキサート(MTX)関連リンパ増殖性疾患の病態解明のための多施設共同研究（H28-NHO(多共)-02）
42	病理診断科 野元三治	メトトレキサート(MTX)関連リンパ増殖性疾患の遺伝子変異プロファイルの解析（H31-NHO(多共)-02）
43	病理診断科 後藤正道	耳下腺ワルチン腫瘍の病理学的特徴と疫学に関する研究（耳下腺リンパ上皮のう胞と鰓原性のう胞に関する研究）
44	歯科口腔外科 中村康典	急性期医療におけるフレイル予防に対する口腔機能管理
45	歯科口腔外科 福永莉々亜	放射線化学療法患者における周術期口腔機能管理に対する口腔支持療法の構築
46	歯科口腔外科 中村康典	口腔機能評価と健康指標のデータビジュアライズと口腔機能管理アウトカムの検討
47	歯科口腔外科 中村康典	DOAC 服用患者における抜歯の安全性の確立に関する研究：ガイドライン確立のための多施設共同前向き研究(STEPD) 研究 R3-NHO（他研）-[01]
48	歯科口腔外科 大河内孝子	唇裂患者の顔貌評価を三次元から四次元へ進化させる分析方法の開発
49	皮膚腫瘍科 松下茂人	爪部悪性黒色腫への指趾骨温存切除による新たな低侵襲標準治療の開発

	部署	研究内容・課題名
50	皮膚腫瘍科 松下茂人	頭頸部基底細胞癌縮小マージン切除による新たな低侵襲標準治療の開発
51	皮膚腫瘍科 松下茂人	メラノサイト系の悪性腫瘍に関する角層解析の有用性
52	皮膚腫瘍科 松下茂人	皮膚腫瘍における免疫応答解析に基づくがん免疫療法予測診断法の確立
53	皮膚腫瘍科 松下茂人	JCOG1605：パクリタキセル既治療原発性皮膚血管肉腫に対するパゾパニブ療法の非ランダム化検証的試験
54	皮膚腫瘍科 松下茂人	ニボルマブ+イピリムマブで治療される悪性黒色腫患者における腸内細菌代謝産物の臨床的意義に関する前向き観察研究
55	皮膚腫瘍科 松下茂人	結合組織性皮膚疾患における病態解明
56	皮膚腫瘍科 松下茂人	皮膚疾患画像ナショナルデータベースの構築と AI 活用診療支援システムの開発
57	皮膚腫瘍科 松下茂人	BRAF 陽性悪性黒色腫に対する BRAF･MEK 阻害薬および免疫チェックポイント阻害薬の臨床効果に関する多機関共同後ろ向き観察研究
58	皮膚腫瘍科 松下茂人	悪性黒色腫のリンパ節郭清範囲に関する多施設共同観察研究
59	皮膚腫瘍科 佐々木奈津子	毛巣洞の外科的治療に関する多施設共同後ろ向き研究
60	皮膚腫瘍科 松下茂人	汗孔癌の予後および再発に関する観察研究
61	皮膚腫瘍科 後藤啓介	皮膚原発 NUT 癌の解析検討
62	皮膚腫瘍科 松下茂人	apocrine carcinoma with sebaceous differentiation の一例
63	皮膚腫瘍科 松下茂人	JCOG-バイオバンク・ジャパン連携バイオバンク
64	皮膚腫瘍科 松下茂人	掌蹠末端黒子型黒色腫の外科的深部マージンと予後に関する多機関共同後方視的観察研究 Correlation between surgical deep margin and prognosis of palm and sole acral melanoma: A multi-institutional retrospective study
65	皮膚腫瘍科 松下茂人	BRAF 陽性悪性黒色腫に対する BRAF･MEK 阻害薬 および抗 PD-1 抗体を用いた術後補助療法の臨床効果 に関する多機関共同後ろ向き観察研究
66	皮膚腫瘍科 松下茂人	皮膚悪性腫瘍(non-melanoma skin cancer)の Sentinel node 同定に関する研究
67	皮膚腫瘍科 松下茂人	皮膚リンパ腫臨床統計調査研究
68	皮膚腫瘍科 青木恵美	リンパ節転移を伴う皮膚がんに対する手術アプローチに関する観察研究
69	皮膚腫瘍科 藤井一恭	掻痒疾患における中枢および末梢 PACAP 受容体シグナル伝達の比較解析
70	皮膚腫瘍科 藤井一恭	PACAP-PAC1 受容体シグナルの乾癬の病態に与える影響と治療応用の可能性
71	皮膚腫瘍科 松下茂人	進行期 BRAF 陽性悪性黒色腫(メラノーマ)に対する免疫チェックポイント阻害薬または BRAF/MEK 阻害薬を先行する逐次療法の実臨床における薬剤選択や有用性を探索する多機関共同前向き観察研究 (B-CHECK-SW study)

	部署	研究内容・課題名
72	皮膚腫瘍科 松下茂人	皮膚がんにおける個別化医療推進を目的とした癌ゲノムパネル使用法の解析:多施設共同後ろ向き観察研究
73	皮膚腫瘍科 青木恵美	術後 stage IIB-C, III 爪部悪性黒色腫における術後補助療法および無治療経過観察の予後比較に関する多機関共同後ろ向き研究
74	皮膚腫瘍科 松下茂人	免疫チェックポイント阻害薬投与に伴う類天疱瘡の全国調査
75	皮膚腫瘍科 青木恵美	頭頸部皮膚血管肉腫に対する一次治療に関する多施設共同後ろ向き研究
76	不整脈治療科 塗木徳人	カテーテルアブレーション症例全例登録プロジェクト(J-AB レジストリ)
77	不整脈治療科 塗木徳人	リード抜去症例の実態調査(J-LEX レジストリ)
78	不整脈治療科 塗木徳人	Micra Acute Performance(MAP) AV Japan Registry
79	不整脈治療科 塗木徳人	循環器疾患診療実態調査(JROAD)データベースと二次調査に基づく致死性心室性不整脈患者の診断・治療・予後に関する研究
80	不整脈治療科 塗木徳人	18 歳以下の症例に対する Subcutaneous implantable cardioverter-defibrillator(SICD)の有用性と安全性に関する中期成績
81	不整脈治療科 二宮雄一	高血圧を有する心房細動アブレーション後の患者におけるエサキセレノンの心房細動抑制効果を検討する単群パイロット試験
82	不整脈治療科 二宮雄一	心房細動の早期発見への道を拓く唾液内バイオマーカーの探索(科研費:代表)
83	不整脈治療科 二宮雄一	血管老化の早期発見を目指した唾液診断の可能性(科研費:分担)
84	臨床検査科 梅橋功征	化学発光免疫測定法(CLIA 法)における B 型肝炎検査試薬における血漿検体の基礎評価
85	診療放射線科 中間理李加	血管造影装置の線量表示精度管理
86	診療放射線科 久木野豊	経皮的カテーテル心筋焼灼術における患者・術者被ばく線量の推移
87	診療放射線科 宮島隆一	201Tl 心筋血流 SPECT における横隔膜下集積の影響抑制法の検討
88	診療放射線科 宮島隆一	放射線診療における多施設被ばく線量の実態調査と診断参考レベルとの比較
89	診療放射線科 宮島隆一	X線撮影における再撮影の発生状況と要因分析
90	看護部 野内万理子	「関係の質」に関するアンケート調査からみえる職員同士の関係性～「関係の質の向上」を目指して

② 治験実績

(ア) 治験

以下に 2024 年度の治験の実績を示す。

2024 年度（令和 6 年度）治験内容 2024.4～2025.3

	医薬品		医療機器		再生医療		合計
	新規契約	継続契約	新規契約	継続契約	新規契約	継続契約	
治験　第Ⅱ相	1（0）	1（1）	0（0）	0（0）	0（0）	0（0）	2（1）
治験　第Ⅲ相	0（0）	2（2）	0（0）	0（0）	0（0）	0（0）	2（2）
合計	1（0）	3（3）	0（0）	0（0）	0（0）	0（0）	4（3）

（　）内は昨年の実数

実施率（2024 年度に終了した治験）

	契約件数（件）	契約症例・調査数	実施症例・調査票	実施率（%）
治験	1（1）	2（4）	2（4）	100（100）

（　）内は昨年の実数

治験の細目

研究課題名	研究依頼者	責任医師
急性脳梗塞における elezanumab の安全性及び有効性を評価する無作為化、二重盲検、 プラセボ対照、proof of concept 試験	Abbvie 合同会社	松岡秀樹
急性期虚血性脳卒中又は高リスク一過性脳虚血発作後の脳卒中の再発抑制を目的とした経口第 XIa 因子阻害剤 Milvexian の有効性及び安全性を評価する第 3 相，ランダム化，二重盲検，並行群間，プラセボ対照試験（急性期脳卒中）	ヤンセンファーマ株式会社	松岡秀樹
切除したステージ III 又はステージ IV の黒色腫患者を対象としたアジュバント治療における ABP 206 とオプジーボ® (ニボルマブ) の薬物動態の類似性を評価する無作為化二重盲検試験（メラノーマ）	アムジェン/パレクセル	松下　茂人
再発もしくは転移性または切除不能な局所進行の有棘細胞がんを有する日本人患者を対象に MK-3475A の安全性及び有効性を評価する試験	MSD 株式会社	松下　茂人

(イ) 製造販売後調査（新規）

研究課題名	研究依頼者	責任医師
エプキンリ®皮下注　再発又は難治性の大細胞型 B 細胞性リンパ腫及び再発又は難治性の濾胞性リンパ腫　一般使用成績調査（全例調査）	ジェンマブ株式会社	大塚眞紀
オプジーボ点滴静注 20mg・100mg・120mg・240mg、ヤーボイ点滴静注液 20mg・50mg　副作用・感染症詳細調査	小野薬品工業株式会社	青木恵美
レブラミドカプセル 2.5 mg・5 mg及びレナデックス錠 2 mg・4 mg併用療法副作用・感染症詳細調査	ブリストル・マイヤーズスクイブ株式会社	小代　彩
ボイデヤー般使用成績調査（全例調査）	アレクシオンファーマ合同会社	大塚眞紀
オプジーボ®特定使用成績調査〔根治切除不能な進行・再発の上皮系皮膚悪性腫瘍のうち有棘細胞癌以外の病理組織型の患者〕	小野薬品工業株式会社	松下茂人

製造販売後調査（継続）

研究課題名	研究依頼者	責任医師
自家培養表皮ジェイスの先天性巨大色素性母斑に対する使用成績調査	㈱ジャパン・ティッシュ・エンジニアリング	松下茂人
ベスポンサ®点滴静注用 1mg　特定使用成績調査	ファイザー株式会社	原口浩一
ベレキシブル®錠　特定　使用成績調査 再発又は難治性の中枢神経系原発リンパ腫（PCNSL）	小野薬品工業株式会社	魚住公治
サピエン 3（TAV in SAV）　使用成績調査	エドワーズライフサイエンス株式会社	平峯聖久
コララン®特定使用成績調査（洞調律かつ投与開始時の安静時心拍数が 75 回/分以上の慢性心不全：ただし、β 遮断薬を含む慢性心不全の標準的な治療を受けている患者に限る。）	小野薬品工業株式会社	中島　均
コララン®　特定使用成績調査（洞調律かつ投与開始時の安静時心拍数が 75 回/分以上の慢性心不全：ただし、β 遮断薬を含む慢性心不全の標準的な治療を受けている患者に限る。）	小野薬品工業株式会社	東　健作
ビンダケルカプセル　特定使用成績調査　～トランスサイレチン型心アミロイドーシス患者に対する調査～（プロトコール№B3461064）	ファイザー株式会社	薗田正浩
エドルミズ®　特定使用成績調査〔がん悪液質：非小細胞肺癌、胃癌、膵癌、大腸癌〕	小野薬品工業株式会社	魚住公治
ダラキューロ配合皮下注　ベルケイド注射用 3mg　全身性 AL アミロイドーシス患者を対象とした特定使用成績調査	ヤンセンファーマ株式会社	大塚眞紀
ハイヤスタ錠®10mg　再発または難治性の成人 T 細胞白血病リンパ腫(ATL)患者における一般使用成績調査(全例調査)	Meiji Seika ファルマ株式会社	大塚眞紀
エフィエント錠特定使用成績調査-脳梗塞発症リスクが高い虚血性脳血管障害患者-	第一三共株式会社	松岡秀樹
レブラミド®カプセル一般使用成績調査〔再発又は難治性の FL 及び MZL〕	ブリストル・マイヤーズスクイブ株式会社	大塚眞紀
ハイヤスタ錠 10mg 再発又は難治性の末梢性 T 細胞リンパ腫(PTCL)患者における一般使用成績調査（全例調査）	MeijiSeika ファルマ株式会社	大塚眞紀
ソグルーヤ®皮下注 5mg, 10mg　特定使用成績調査 「ソグルーヤ®長期使用に関する特定使用成績調査」	ノボ ノルディスクファーマ株式会社	郡山暢之
アキャルックス点滴静注 250 mg一般使用成績調査（全例調査）切除不能な局所進行又は局所再発の頭頚部癌	楽天メディカル株式会社	西元謙吾

研究課題名	研究依頼者	責任医師
エドワーズ　サピエン 3（TAV in TAV）使用成績調査	エドワーズライフサイエンス株式会社	片岡哲郎
エドワーズ　サピエン 3（TAV in TAV）使用成績調査	エドワーズライフサイエンス株式会社	平峯聖久
サムタス一般使用成績調査（心性浮腫）	大塚製薬株式会社	東　健作
コセルゴ®特定使用成績調査神経線維腫症 1 型における叢状神経線維腫に関する全例調査	アレクシオンファーマ合同会社	松下茂人
エジャイモ点滴静注 1.1g特定使用成績調査＜寒冷凝集素症患者＞	サノフィ株式会社	原口浩一
ゼジューラ特定使用成績調査「卵巣癌」	武田薬品工業株式会社	神尾真樹
エザルミア錠一般使用成績調査	第一三共株式会社	大渡五月
レクビオ皮下注　特定使用成績調査［家族性高コレステロール血症又は高コレステロール血症］	ノバルティスファーマ株式会社	東　健作

治験・受託研究請求額推移

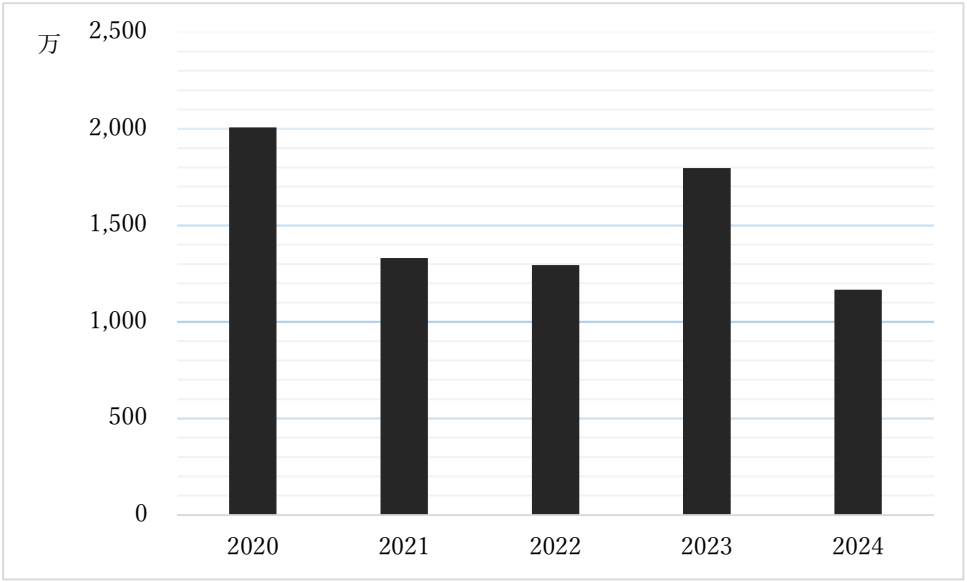

3. 業績報告

① 英文原著論文等

※当院所属として発表されたものに限ります。2024 年度中に Epub (online)で公開された論文も含みます。

■第 1 循環器内科

Kataoka T, Fukunaga K, Hiramine K, Nomoto Y, Matsumoto H, Sonoda K, Okino H, Tagata K, Kumamoto K, Kubota Y, Baba Y, Takasaki K, Nakashima H, Tanaka Y, Tokushige A, Ohishi M.
Two-Year Clinical Outcomes Following SAPIEN 3 20-mm Transcatheter Aortic Valve Implantation in Patients with Symptomatic Severe Aortic Stenosis—Comparison of the Smallest Size Valve against Larger Transcatheter Aortic Valve.
J Transcatheter Valve Ther. 2024;6 (1):24-0001

Michallek F, Nakamura S, Kurita T, Ota H, Nishimiya K, Ogawa R, Shizuka T, **Nakashima H,** Wang YN, Ito T, Sakuma H, Dewey M, Kitagawa K.
Differentiating Macrovascular and Microvascular Ischemia Using Fractal Analysis of Dynamic Myocardial Perfusion Stress-CT.
Invest Radiol. 2024; 59(5): 413-423. (Epub 2023 Oct 9)

Nagasawa N, Nakamura S, Ota H, Ogawa R, **Nakashima H**, Hatori N, Wang Y, Kurita T, Dohi K, Sakuma H, Kitagawa K.
Relationship between microvascular status and diagnostic performance of stress dynamic CT perfusion imaging.
Eur Radiol. 2025; 35(5): 2855-2865. (Epub 2024 Oct 17)

■第 2 循環器内科

Matsumoto H, Ijuin S, Terashi T
Right-side cardiac metastasis of squamous cell carcinoma from oesophagogastric junction cancer.
European Heart Journal - Case Reports. 2024; 8(6): ytae294

■心臓血管外科

Yasumura H, Tao K, Imada R, Yamashita Y, Tateishi N, Arata K, **Kinjo T.**
Pseudoaneurysm formation after embolization of giant arteriovenous malformation of the lower limb associated with Parkes Weber syndrome: A case report and literature review.
Radiol Case Rep. 2024;19(11): 4766-4774.

Yasumura H, Tao K, Imada R, Yamashita Y, Tateishi N, Kinjo T.
Horner's syndrome caused by the first rib fracture sustained during coronary artery bypass grafting: a case report and literature review.
Gen Thorac Cardiovasc Surg Cases. 2024; 3(1): 41.

■脳血管内科

Hamada Y, Matsuoka H, Sato S**, Kawabata Y, Iwamoto K, Ikeda M, Sato T, Takaguchi G,** Takashima H**.**
Combining the deployment of only the distal basket segment of the EMBOTRAP III and an aspiration catheter for M2 occlusions: the ONE-SEG technique.
Front Neurol. 2024; 15: 1424030.

■小児科

Miyazaki A, **Yoshinaga M,** Ogata H, Ito Y, Aoki M, Kubo T, Shinomiya M, Horigome H, Tokuda M, Lin L, Takahashi H, Nagashima M.
An Alternative Approach to Determining Metabolic Syndrome Component Cutoffs in Children and Adolescents Using Segmental Regression Analysis.
Circ Rep. 2024; 6(4): 118-126.

Miyazaki A, **Yoshinaga M**, Shinomiya M, Ogata H.
Letter to the Editor: "An Alternative Approach to Determining Metabolic Syndrome Component Cutoffs in Children and Adolescents Using Segmental Regression Analysis".
Circ Rep. 2024; 6(7): 281-282.

Imamura T, Makiyama T, Ozawa J, Sonoda K, Kato K, Aizawa T, Kashiwa A, Gao J, Huang H, Yamamoto Y, Kohjitani H, Aoki H, Watanabe S, Muraji S, Kojima T, **Yoshinaga M**, Ohno S, Suzuki H, Sumitomo N, Nakagawa Y, Ono K, Horie M, Kimura T.
Sex-specific clinical course of young patients with Brugada syndrome.
Eur Heart J. 2025; 46(13): 1263-1266. (Published 05 February 2025)

Yoshinaga M, Ushinohama H, Sato S, Ohno S, Hata T, Horigome H, Tauchi N, Sumitomo N, Nishihara E, Hirono K, Ichida F, Shiraishi H, Nomura Y, Tsukano S, Ninomiya Y, Yoneyma T, Suzuki H, Takahashi H, Ogata H, Makita N, Shimizu W, Horie M, Nagashima M.
Screening of 1-Month-Old Infants With Prolonged QT Interval and Its Cutoff Value.
Circ J. 2025; 89(6): 826-834. (Epub 2025 Feb 22）

■糖尿病・内分泌内科

Mukai M, Koriyama N, Hirahara R, **Wada K**, Nishio Y.
A Rare Case of Ketosis-Prone Type 2 Diabetes With a Unique Human Leukocyte Antigen (HLA) Profile: Genetic and Metabolic Insights.
Cureus. 2025; 17(1): e77247.（eCollection 2025 Jan）

■消化器内科

Tahata Y, Hikita H, Mochida S, Enomoto N, Kawada N, Ido A, Miki D, Kurosaki M, Yoshiji H, Sakamori R, Kuroda H, Yatsuhashi H, Yamashita T, Hiasa Y, Kato N, Miyaaki H, Ueno Y, Itoh Y, Matsuura K, Takami T, Asahina Y, Suda G, Akuta N, Tateishi R, Nakamoto Y, Kakazu E, Terai S, Shimizu M, Miyazaki M, Nozaki Y, Sobue S, Yano H, Miyaki T, **Moriuchi A**, Hori T, Shirai K, Murai K, Saito Y, Kodama T, Tatsumi T, Yamada T, Takehara T.
Factors involved in gastroesophageal varix-related events in patients with hepatitis C virus-related compensated and decompensated cirrhosis after direct-acting antiviral therapy.
Hepatol Res. 2024. (Epub ahead of print.)

■婦人科

Hasegawa K, Nishio S, Yamamoto K, Fujiwara H, Itagaki H, Nagai T, Takano H, Yamaguchi S, Kudoh A, Suzuki Y, Nakamoto T, Kurosaki A, **Kamio M**, Kato K, Nakamura K, Takehara K, Yahata H, Kobayashi H, Saito M, Fujiwara K.
Tegafur-uracil maintenance chemotherapy post-chemoradiotherapy for cervical cancer: Randomized trial.
Eur J Cancer. 2025; 219:115304.（Epub 2025 Feb 15）

■病理診断科

Goto M, **Nishimoto K**, **Jougasaki Y, Matsuzaki T**, **Tanaka T**, **Nomoto M**.
Heterotopic salivary duct inclusions in Warthin tumor - A cryptic histological finding involved in its pathogenesis.
Pathol Res Pract. 2024; 263:155560. (Epub 2024 Aug 29)

■歯科口腔外科

Takayama H, Yoshimura T, Suzuki H, Hirano Y, Tezuka M, Ishida T, Ishihata K, Amitani M, Amitani H, **Nakamura Y**, Imamura Y, Inui A, Nakamura N.
Comparison between single-muscle evaluation and cross-sectional area muscle evaluation for predicting the prognosis in patients with oral squamous cell carcinoma: a retrospective cohort study.
Front Oncol. 2024; 14: 1336284.

■皮膚腫瘍科

Goto K, Kukita Y, Hishima T, **Matsushita S**, Tsuyuki T, Makihara K, Koga K, Mukumoto S, Honma K.
Primary Cutaneous NUT Carcinoma: Clinicopathologic and Genetic Study of 4 Cases.
Am J Surg Pathol. 2024; 48(8): 942-952. (Epub 2024 May 6)

Fujimura T, Yoshino K, Kato H, Fukushima S, Ishizuki S, Otsuka A, **Matsushita S**, Amagai R, Muto Y, Yamazaki E, Kambayashi Y, Yahata T, Miyata T, Fujisawa Y, Asano Y.
A phase II multicentre study of plasminogen activator inhibitor-1 inhibitor (TM5614) plus nivolumab for treating anti-programmed cell death 1 antibody-refractory malignant melanoma: TM5614-MM trial.
Br J Dermatol. 2024; 191(5): 691-697.

Muto Y, Kambayashi Y, Kato H, Mizuhashi S, Ito T, Maekawa T, Ishizuki S, Uchi H, **Matsushita S**, Yamamoto Y, Yoshino K, Fujisawa Y, Amagai R, Ohuchi K, Hashimoto A, Fukushima S, Asano Y, Fujimura T.
Three-Year Analysis of Adjuvant Therapy in Postoperative Melanoma including Acral and Mucosal Subtypes.
Cancers (Basel). 2024; 16(15): 2755.

Aoki M, **Fujii K**, Yamamura K, **Matsushita S**.
Proportion of Japanese Patients with Multiple Basal Cell Carcinomas: The Effectiveness of Screening.
Journal of Plastic and Reconstructive Surgery. 2024; 2024-0034.

Saito-Sasaki N, Aoki M, **Fujii K**, Yamamura K, Hitaka T, Hirano Y, Nishihara K, Fujino Y, **Matsushita S.**
Age over 90 years is an unfavorable prognostic factor for resectable cutaneous squamous cell carcinoma.
J Dermatol. 2025; 52(1): 183-186. (Epub 2024 Dec 27)

Nishihara K, **Fujii K**, **Aoki M**, **Hirano Y**, **Inoue A**, **Yamamoto S**, **Matsushita S.**
Combination treatment of cultured epithelial autograft and meshed full-thickness skin graft for giant congenital melanocytic nevus.
J Dermatol. 2025; 52(4): e268-e269. (Epub 2025 Jan 16)

Kawamoto H, **Fujii K**, **Aoki M**, **Goto K**, **Ikoma T**, **Tozawa T**, **Iwata M**, **Goto M**, **Nomoto M**, **Matsushita S**.
Ultrasound findings of endocrine mucin-producing sweat gland carcinoma mimicking epidermal cysts: A case series and diagnostic challenges.
J Dermatol. 2025; 52(5): 939-942. (Epub 2025 Mar 7)

Nishihara K, **Fujii K**, **Aoki M**, **Yamamoto S**, **Kawahira S**, **Matsushita S**.
Transurethral resection and oral mucosal grafting for urethral-involved extramammary Paget disease: A function-preserving approach.
J Dermatol. 2025; 52(6): 1094-1097. (Epub 2025 Mar 26)

■救急科

Okuda R, Utsumi S, **Tanaka H**, Takama T, Kakihana Y.
Type III Kounis Syndrome Caused by Iodine Contrast Media After Improvement of Allergic Symptoms.
Cureus. 2024; 16(3): e55514.

■診療放射線科

Hamada K, Fujibuchi T, Arakawa H.
Optimum delineation of skin structure for dose calculation with the linear Boltzmann transport equation algorithm in radiotherapy treatment planning.
Radiol Phys Technol. 2024; 17(4):938-946.（Epub 2024 Sep 9）

Soai Dang Quoc, Fujibuchi T, Arakawa H, **Hamada K**, DongHee Han.
Produced radioactive isotopes, ambient dose equivalent in TrueBeam room with flattening filter (FF) and Flattening Filter Free (FFF) modes: Monte Carlo simulation.
Applied Radiation and Isotopes, 2025; 219: 111704. (Epub 2025 Feb 7)

② 和文原著・著書等

永冨脩二, 伊藤由加, 大野文也, 今田 涼, 山下雄史, 立石直毅, 川津祥和, 金城玉洋
手術部位感染症ハイリスク患者に対する予防的陰圧閉鎖療法
胸部外科. 77(13): 1085-1089, 2024 年 12 月

安村拓人, 峠 幸志, 今田 涼, 山下雄史, 立石直毅, 金城玉洋
IgG4 関連炎症性総腸骨動脈瘤の 1 手術例
脈管学. 64（4）:55-59, 2024 年 7 月

松岡秀樹
心原性脳塞栓症
季刊こまど. 81:16-19, 2024 月 12 月

吉永正夫
第 III 章　症候別・疾患別《各論》 D. 不整脈　4. QT 延長症候群、QT 短縮症候群
小児・成育循環器学改訂第 2 版. 563-569, 2024 年 7 月

森内昭博
新しい脂肪性肝疾患の分類
鹿児島県内科医会報. 56:7-9, 2025 年 1 月

髙取寛之, 塗木健介, 野元三治
口側結腸へ壁内転移をきたした横行結腸癌の1例
臨床外科.79(13): 1427-1432, 2024 年 12 月

弓指里萌, 福西優花, 川原裕史, 神尾真樹
下肢痛を契機にみつかった神経梅毒の一例
鹿児島産科婦人科学会雑誌. 33, 2025 年 3 月

神尾真樹
HSIL に対する円錐切除術とレーザー蒸散術の治療後再発に関する検討
鹿児島産科婦人科学会雑誌. 33, 2025 年 3 月

川原裕史, 弓指里萌, 福西優花, 神尾真樹
子宮摘出後に発症した VAIN 症例の治療経過の検討
鹿児島産科婦人科学会雑誌. 33, 2024 年 4 月

後藤正道, 野上玲子, 岡野美子, 儀同政一, 四津里英, 北島信一, 山口さやか, 阿戸 学, 宮本友司, 高橋健造, 圓純一郎（日本ハンセン病学会・治療指針ワーキンググループ）
ハンセン病治療指針（第4版）
日本ハンセン病学会雑誌. 93（1）:28, 2024 年 4 月

多田亮平，石畑清秀，岐部俊郎，手塚征宏，上栗裕平，木村菜美子，椎木彩乃，大河内孝子，西原一秀，野添悦郎，宮脇正一，中村典史
当科開設後 40 年間の口唇口蓋裂患者における顎矯正手術の臨床統計学的検討
日本口蓋裂学会雑誌. 49(3):209-217，2024 年 11 月

松下茂人
皮弁に必要な顔面の臨床解剖 特集 FLAP!顔面の皮弁術パーフェクトガイド
Visual Dermatology. 23(12):1122-1127，2024 年 11 月

松下茂人
基底細胞癌の切除マージンー日本人と白人の違いー特集:いまこそ update! 皮膚悪性腫瘍の治療 part 1
形成外科. 68(2):127-136，2025 年 2 月

松下茂人，梶原一亨，筒井啓太，平井郁子，前川武雄，前田拓哉，大熊加惠，木村俊寛，小森崇矢，佐藤さゆり，伏間江貴之，森 龍彦，前田達夫，内 博史，古賀弘志，宮垣朝光，中村泰大
皮膚がん診療ガイドライン第 4 版: 乳房外パジェット病診療ガイドライン 2025
日本皮膚科学会ガイドライン. 135(1);1-36, 2025 年 1 月

中尾久美子，青木恵美，戸澤貴久，生駒宗禎，松下茂人
転移性悪性黒色腫の薬物治療中にみられた眼有害事象
鹿児島市医報. 64(3): 16-20, 2025 年 2 月

塗木徳人
鹿児島医療センターでの心臓植込みデバイス抜去の現状
鹿児島市医報. 63(9): 9-11, 2024 年 9 月

二宮雄一
第 2 章ケーススタディ 8.心室細動で救急搬送となった 20 代男性
わかる！読める！心電図ガイド症例解説 Q&A. 58-63, 2024 年 11 月

二宮雄一
バイオマテリアルが拓く低侵襲循環器治療の未来
日本バイオマテリアル学会 学会誌「バイオマテリアルー生体材料ー」. 43(1): 34-37, 2025 年 1 月

末永 亘
がん薬物療法外来—甲状腺がん，甲状腺がん治療におけるレンバチニブ使用患者を例に
薬局. 75(8):1230-1234, 2024 年 7 月

岡村優樹，山口 俊，久保祐子，日野出勇次，梅橋功征，西方菜穂子，馬場善政
Gemella morbillorum による弁破壊を伴った感染性心内膜炎の1例
超音波検査技術. 49(3):237-243，2024 年 6 月

日野出勇次，梅橋功征，中釜美乃里，岡村優樹，原田美里，大迫亮子，久保祐子，西方菜穂子
トランスサイレチン型心アミロイドーシスにおける神経エコー検査の有用性の検討
医学検査. 73(2):215-222, 2024 年 4 月

樋渡まこ，梅橋功征，山口 俊，吉野 歩，高瀬 泉，西方菜穂子
新型コロナウイルス抗原定量検査の臨床的有用性の検討
医学検査. 73(3):460-466，2024 年 7 月

城戸隆宏，野崎加代子，大迫亮子，岡村優樹，久保祐子，日野出勇次，梅橋功征，西方菜穂子
血液検査と腹部超音波検査にて経過を追えたワイル病の 1 症例
医学検査. 73(4): 800-806，2024 年 10 月

宮島隆一
世界の放射線防護関連論文紹介
Association of occupational direct radiation exposure to the hands with longitudinal melanonychia and hand eczema in spine surgeons: a survey by the society for minimally invasive spinal treatment (MIST)
放射線防護部会誌. 24(1):45-50, 2024 年 4 月

宮島隆一
教育講座-放射線防護のアーカイブス 2. 放射線防護体系
日本放射線技術学会雑誌. 80(10):1077-1082, 2024 年 10 月

宮島隆一, 渋谷充, 大井邦治, 市川和幸, 財前誠, 阿南恵吾, 池田敏久, 太田一郎, 松井謙典, 筒井昭詔
X線撮影における再撮影判定基準の標準化や教育による低減効果について
九州国立病院機構 診療放射線技師会誌. №141: 44-47, 2025 年 1 月

大迫朋子
看護現場におけるデータ分析＆活用～DiNQL と上手に付き合おう！
月刊 ナースマネージャー. 26(1):10-15, 2024 年

③ 学会発表

筆頭演者が鹿児島医療センターの職員

＜国際学会＞

Tagata K, Nomoto Y, Tao K, Kataoka T, Ohishi M.
Abrupt cardiac rupture of the patient with ATTR amyloidosis
The American Heart Association`s Scientific Sessions 2024, Chicago, 2024/11/18

Imamura S. Kataoka T, Kubota Y, Kumamoto K, Fukuyado A, Tagata K, Fukunaga K, Chaen H, NinoomiyaY, Takasaki K, Goto J, Matsumoto H, Sonoda K, Baba Y, Hiramine K, Sonoda M, Tanaka Y, Tokushige A, Oishi M.
Mid-term Clinical Outcomes Following SAPIEN 3 20-mm Transcatheter Aortic Valve
Implantation in Patients with Symptomatic Severe Aortic Stenosis
The 89th Annual Scientific Meeting of the Japanese Circulation Society (JCS2025), Yokohama, 2025/03/29

Ijuin S.
Survey for Predictor of Improvement of Mitral Regurgitation Grade after Transcatheter Aortic Valve Replacement in Patients with Severe Aortic Stenosis.
The 89th Annual Scientific Meeting of the Japanese Circulation Society (JCS2025), Yokohama, 2025/03/30

Ijuin S.
Investigation of Nutritional Status before and after MitraClip: a Single-Center Retrospective Study over One Year.
The 89th Annual Scientific Meeting of the Japanese Circulation Society (JCS2025), Yokohama, 2025/03/28

Sato T, Tsuchimochi Y, Hamada Y, Kawabata Y, Iwamoto K, Takaguchi G, Matsuoka H.
Total Small Vessel Disease Score Is Associated With Intraventricular Extension Among Patients With Intracerebral Hemorrhage.
International Stroke Conference, Los Angeles, 2025/02/6

Sato T, Tsuchimochi Y, Hamada Y, Kawabata Y, Iwamoto K, Takaguchi G, Matsuoka H.
Lower High-Density Lipoprotein Cholesterol Level Is Associated With Hematoma Expansion Following Acute Intracerebral Hemorrhage.
International Stroke Conference, Los Angeles, 2025/02/6

Yoshinaga M, Ninomiya Y, Tanaka Y, Kato K, Ohno S, Takahashi H, Ogata H, Nagashima M.
Circadian changes in corrected QT interval in children with long QT syndrome and healthy volunteers.
The 70th Annual Meeting of The Japanese Heart Rhythm Society (JHRS2024), Ishikawa, 2024/07/19

Sasaki-Saito N, Aoki M, Yamamura K, Hitaka T, Hirano Y, Nishihara K, Fujino Y, Matsushita S.
Age over 90 years is an unfavorable prognostic factor for resectable cutaneous squamous cell carcinoma
20th European Association of Dermato-Oncology Congress, Paris, 2024/4/6

Matsushita S.
Surgical Management of EMPD～Anorectal Function Preserving Surgery in Patients with Perianal EMPD～
43rd Annual meeting of the International Society of Dermatologic Surgery, Kaohsiung, 2024/09/15

Matsushita S.
Optimizing Surgical Margins and Reconstruction in skin cancer: Evidence from Japan.
The 30th Korean Society for Dermatologic Surgery Congress, Seoul, 2025/03/15

Ninomiya Y, Kawasoe S, Kubozono T, Sai E, Nuruki N, Enokizono K, Kamada H, Yoshimoto I, Iriki Y, Miyahara H, Tokushige K, Ohishi M.
Smoking cessation is linked to regression of electrocardiographic left ventricular hypertrophy
The American Heart Association's Scientific Sessions 2024, Chicago, 2024/11/18

Ninomiya Y, Kawasoe S, Kubozono T, Sai E, Nuruki N, Enokizono K, Kamada H, Yoshimoto I, Iriki Y, Miyahara H, Tokushige K, Ohishi M.
Smoking cessation is linked to regression of electrocardiographic left ventricular hypertrophy
The 89th Annual Scientific Meeting of the Japanese Circulation Society (JCS2025), Yokohama, 2025/03/28

＜国内学会＞

片岡哲郎, 福永研吾, 田方健人, 隈元健吾, 窪田唯伊, 髙﨑州亜, 平峯聖久, 園田幸一郎, 馬場善政, 大石 充
当院の TAVI 施行患者の 2 年予後の検証
第 345 回日本内科学会九州地方会, 宮崎, 2024 年 5 月 25 日

片岡哲郎
当院のバルーン拡張型 20-mm 人工弁の使用経験
第 13 回ストラクチャークラブ・ジャパン九州支部会, 沖縄, 2024 年 6 月 22 日

福永研吾, 片岡哲郎, 平峯聖久, 馬場善政, 園田幸一郎, 松本洋之, 髙﨑州亜, 野元裕太朗, 沖野秀人, 田方健人, 隈元健吾, 窪田唯伊, 大石 充
カテコラミン依存の LF-LG 重症大動脈弁狭窄症患者に対して ECMO サポート下に TAVI を施行した 1 例
第 136 回日本循環器学会九州地方会, 鹿児島, 2024 年 6 月 29 日

田方健人, 片岡哲郎, 隈元健吾, 窪田唯伊, 沖野秀人, 野元裕太朗, 福永研吾, 髙﨑州亜, 安村拓人, 峠 幸志, 金城玉洋, 大石 充
内視鏡下粘膜剥離術を契機に心アミロイドーシスの診断となった一例
第 136 回日本循環器学会九州地方会, 鹿児島, 2024 年 6 月 29 日

片岡哲郎, 福永研吾, 野元裕太朗, 田方健人, 隈元健吾, 窪田唯伊, 平峯聖久, 園田幸一郎, 松本洋之, 馬場善政, 髙﨑州亜, 大石 充
TAVI 施行患者における 2 年予後の影響因子の検証
第 72 回日本心臓病学会学術集会, 仙台, 2024 年 9 月 29 日

片岡哲郎
診断・治療に苦慮し救命できなかった症例（致死的不整脈、心原生性ショック・呼吸不全）
第 10 回 Pan-Pacific Primary Angioplasty Conference 2024, 東京, 2024 年 11 月 15 日

髙﨑州亜，片岡哲郎，福永研吾，二宮雄一，茶圓秀人，今村春一，田方健人，隈元健吾，福宿 愛，窪田唯伊，大石 充
当院における透析患者の重症大動脈弁狭窄症症例に対する TAVI 治療の短期成績
第 347 回日本内科学会 九州地方会，熊本, 2024 年 11 月 17 日

田方健人，片岡哲郎、隈元健吾、窪田唯伊、福宿 愛、今村春一、福永研吾、茶園秀人、髙﨑州亜，大石 充
左肺動脈に脱落したリードレスペースメーカーを複数のスネアを用いて回収できた一例
第 137 回日本循環器学会九州地方会，別府, 2024 年 12 月 14 日

村山剛大
原因検索により植え込み型除細動器移植を避けられた若年者の QT 短縮症候群による心室細動の一例
第 136 回日本循環器病学会九州地方会，鹿児島, 2024 年 6 月 29 日

中馬洋介
心停止に至った劇症型リンパ球性心筋炎に ECPELLA 管理を行い救命した一例
第 136 回日本循環器病学会九州地方会，鹿児島, 2024 年 10 月 26 日

尾辻良彦
FDG-PET が診断に有効であった右心系腫瘍の一例
第 136 回日本循環器病学会九州地方会，鹿児島, 2024 年 7 月 1 日

永山貴大
腹腔臓器並びに下肢虚血 B 型急性大動脈解離に対して緊急 TEVAR にて救命した症例
第 89 回鹿児島救急医学会学術集会，鹿児島，2024 年 9 月 14 日

村橋 暁
Chain of survival が有効に機能して救命できた高 Ca 血症による QT 間隔短縮が原因の VF survivor の 1 症例
第 89 回鹿児島救急医学会学術集会，鹿児島，2024 年 9 月 14 日

仲田圭秀
アナフィラキシーショック消失後に発症した Kounis 症候群 III 型の 1 例
第 89 回鹿児島救急医学会学術集会，鹿児島，2024 年 9 月 14 日

宇都宮沙代,
運動直後の失神及び呼吸停止に陥った若年者の閉そく性肥大型心筋症の 1 例
第 89 回鹿児島救急医学会学術集会，鹿児島，2024 年 9 月 14 日

原田 聞
Mitral annular disjunction 様に見えた僧帽弁逸脱症に伴う感染性心内膜炎の一例
第 137 回日本循環器学会九州地方会，別府, 2024 年 12 月 14 日

伊集院駿
リードレスペースメーカ植え込み後のペーシング誘発性心筋症についての検討
第 137 回日本循環器学会九州地方会，別府，2024 年 12 月 14 日

宇都宮沙代
左室中隔切除術が奏効した若年者の閉塞性肥大型心筋症の一例
第 137 回日本循環器学会九州地方会，別府，2024 年 12 月 14 日

立石直毅
当院における逆行性 A 型大動脈解離の遠隔成績
第 55 回日本心臓血管外科学会学術総会，下関, 2025 年 2 月 20 日

大野文也
腎動脈上遮断を行った腹部大動脈瘤人工血管置換術の検討
第 55 回日本心臓血管外科学会学術総会，下関, 2025 年 2 月 20 日

濵田祐樹，宮下史生，松岡秀樹，吉留 萌，川畑祐太郎，岩元佳奈，佐藤健朗，髙口 剛，髙嶋 博
CAS に対する Alternative Proximal Protection Method の治療成績
第 40 回日本脳血管内治療学会 九州地方会，福岡，2024 年 8 月 3 日

濵田祐樹, 松岡秀樹, 佐藤慎祐, 吉留 萌, 山中菜央, 川畑祐太郎, 岩元佳奈, 佐藤健朗, 髙口 剛, 髙嶋 博
M2 閉塞に対する EmbotrapIIIの distal basket のみの展開と吸引カテーテルの併用による治療成績
第 5 回日本脳神経内科血管治療学会, 福岡, 2024 年 8 月 23 日

濵田祐樹, 松岡秀樹, 佐藤慎祐, 吉留 萌, 川畑祐太郎, 岩元佳奈, 佐藤健朗, 髙口 剛, 髙嶋 博
M2 閉塞に対する EmbotrapIIIの distal basket のみの展開と吸引カテーテルの併用による治療成績
第 40 回 NPO 法人日本脳神経血管内治療学会総会(JSNET2024), 熊本, 2024 年 11 月 21 日

濵田祐樹, 川畑祐太郎, 岩元佳奈, 佐藤健朗, 髙口 剛, 上野滋登, 樋渡貴昭, 久保文克, 松岡秀樹
CASPER stent を用いた頸動脈ステント留置術の術後 DWI 陽性例の後方視的検討
第 40 回 NPO 法人日本脳神経血管内治療学会総会(JSNET2024), 熊本, 2024 年 11 月 21 日

濵田祐樹, 佐藤健朗, 土持友香, 久木原魁士, 吉留 萌, 山中菜央, 岩元佳奈, 川畑裕太郎, 髙口 剛, 松岡秀樹, 髙嶋 博
心房細動を有する頭蓋内出血患者の特徴や機能学的転帰: 単施設後ろ向きコホート研究
第 50 回日本脳卒中学会学術集会, 大阪, 2025 年 3 月 6 日

濵田祐樹, 久木原魁士, 土持友香, 吉留 萌, 岩元佳奈, 川畑裕太郎, 佐藤健朗, 高口 剛, 松岡秀樹, 髙嶋 博
DOT (Distant Occlusion Tracher)徴候は機械的血栓回収療法において頭蓋内出血に関連する
第 50 回日本脳卒中学会学術集会, 大阪, 2025 年 3 月 6 日

川原弓奈, 濵田祐樹, 川畑裕太郎, 岩元佳奈, 佐藤健朗, 髙口 剛, 松岡秀樹
多発性嚢胞腎に伴う前大脳動脈単独解離を発症した 45 歳女性例
第 247 回日本神経学会九州地方会, 福岡, 2025 年 3 月 15 日

佐藤健朗, 土持友香, 濵田祐樹, 久木原魁士, 川畑裕太郎, 岩元佳奈, 髙口 剛, 松岡秀樹, 髙嶋 博
Total small vessel disease score は脳出血における脳室穿破に関連する
第 50 回日本脳卒中学会学術集会, 大阪, 2025 年 3 月 6 日

佐藤健朗, 土持友香, 濵田祐樹, 久木原魁士, 川畑裕太郎, 岩元佳奈, 髙口 剛, 松岡秀樹, 髙嶋 博
低 HDL コレステロールは急性期脳出血後の血腫拡大に関連する
第 50 回日本脳卒中学会学術集会, 大阪, 2025 年 3 月 6 日

佐藤健朗, 土持友香, 濵田祐樹, 久木原魁士, 川畑裕太郎, 岩元佳奈, 髙口 剛, 松岡秀樹, 髙嶋 博
Fibrosis-4 index と脳出血の予後と血腫量
第 50 回日本脳卒中学会学術集会, 大阪, 2025 年 3 月 6 日

久木原魁士, 佐藤健朗, 土持友香, 濵田祐樹, 川畑裕太郎, 岩元佳奈, 髙口 剛, 松岡秀樹, 髙嶋 博
入院後の便秘は急性期脳出血の予後に関連する
第 50 回日本脳卒中学会学術集会, 大阪, 2025 年 3 月 6 日

土持友香, 佐藤健朗, 久木原魁士, 濵田祐樹, 川畑裕太郎, 岩元佳奈, 髙口 剛, 松岡秀樹, 髙嶋 博
睡眠発症脳出血と脳小血管病の関係
第 50 回日本脳卒中学会学術集会, 大阪, 2025 年 3 月 6 日

吉永正夫, 二宮由美子, 田中裕治, 加藤浩一, 大野聖子, 高橋秀人, 緒方裕光, 長嶋正實
QT 延長症候群患児, 健常児における補正 QT 間隔 (QTc 値) の日内変動に関する研究
第 60 回日本小児循環器学会総会・学術集会, 福岡, 2024 年 7 月 11 日

田中裕治
ウルソ内服でγGTP が低下した限局性結節性過形成を伴うフォンタン手術後の 19 歳女性
第 60 回日本小児循環器学会総会・学術集会, 福岡, 2024 年 7 月 13 日

砂川雄海, 今給黎亮, 久保田知洋, 島子敦史, 田中裕治
アスピリン併用の運動負荷試験でショックとなった食物依存性運動誘発アナフィラキシー
第 187 回小児科学会鹿児島地方会, 鹿児島, 2024 年 10 月 20 日

大渡五月, 小代 彩, 原口浩一, 大塚眞紀
同種移植後に肝臓腫瘤で再発し、シクロスポリンの中止により肝臓腫瘤の縮小を認めた ATL の症例
第 86 回日本血液学会学術集会・学術集会, 京都, 2024 年 10 月 13 日

森内昭博，櫻井一宏，大塚眞紀
当院における HBs 抗原陽性者に対する受診勧奨システムの有用性の検討
第 346 回日本内科学会　球種地方会，久留米　2024 年 8 月 31 日

森内昭博，櫻井一宏，竹中嵩博，千堂一樹，井上和彦，福森　光，井戸章雄
当院における HBs 抗原陽性者に対する受診勧奨システムの有用性
第 124 回日本消化器病学会　九州支部例会，鹿児島, 2024 年 11 月 16 日

東　拓郎，穂原　光，徳留明夫，神尾真樹
診断に DWIBS を利用した子宮体癌の一例
第 76 回日本産科婦人科学会，東京, 2024 年 4 月 20 日

神尾真樹，東　拓郎，弓指里萌，川原裕史，徳留明夫
当院での婦人科癌症例における DWIBS と PET の比較検討
第 66 回日本婦人科腫瘍学会，鹿児島, 2024 年 7 月 19 日

弓指里萌，福西優花，川原裕史，野元三治，神尾真樹
悪性転化と転移の鑑別を要した卵巣腫瘍の一例
第 151 回鹿児島県産科婦人科学会，鹿児島, 2024 年 9 月 21 日

川原裕史，弓指里萌，福西優花，神尾真樹
子宮摘出後の VAIN 症例の検討
第 152 回鹿児島県産科婦人科学会，鹿児島, 2025 年 2 月 1 日

下薗知己，永田　圭，花牟禮豊，積山幸祐
浸潤型蝶形骨同真菌症の 2 症例
第 63 回日本鼻科学会総会，東京, 2024 年 9 月 27 日

下薗知己
当科における副甲状腺手術症例の検討
令和 6 年度鹿児島県地方部会総会，鹿児島，2024 年 6 月 8 日

徳重豪士
マイコプラズマ感染により偽膜性喉頭炎を発症した 1 例
令和 6 年度鹿児島県同門会総会，鹿児島，2025 年 1 月 18 日

今林　徹，牧内祐貴，針持　想，入江良彦，松永　明
当センター集中治療室における心臓血管外科術後症例に対するレミフェンタニル導入への介入
日本心臓血管麻酔学会　第 29 回学術集会，広島, 2024 年 9 月 22 日

後藤正道，野上玲子，岡野美子，儀同政一，四津里英，北島信一，山口さやか，阿戸　学，宮本友司，高橋健造，
圓純一郎（日本ハンセン病学会・治療指針ワーキンググループ）
ハンセン病治療指針の改訂（第 4 版）について
第 97 回日本ハンセン病学会総会，岡山, 2024 年 6 月 14 日

中村康典，大河内孝子，木村菜美子，下田平佳純，福永莉々亜，吉村卓也，手塚征宏，西　恭宏
鹿児島医療センターにおける心臓弁膜症手術患者に対する周術期口腔機能管理
第 21 回日本口腔ケア学会総会・学術大会/第 4 回国際口腔ケア学会総会・学術大会，東京 2024 年 4 月 27 日

中村康典，大河内孝子，福永莉々亜，吉村卓也，手塚征宏，西　恭宏
鹿児島医療センターにおける高齢心臓弁膜症患者に対する周術期口腔機能管理
日本老年歯科医学会第 35 回学術大会，札幌, 2024 年 6 月 29 日

福永莉々亜，大河内孝子，中村康典，西　恭宏
鹿児島医療センターにおける口腔ケアラウンド患者の口腔機能管理についての分析
日本老年歯科医学会第 35 回学術大会，札幌, 2024 年 6 月 29 日

中村康典，大河内孝子，吉村卓也，手塚征宏，野元菜美子，西　恭宏
鹿児島医療センターにおける高齢者の心臓弁膜症手術に対する周術期口腔機能管理の検討
第 78 回 NPO 法人日本口腔科学会学術集会，東京, 2024 年 7 月 20 日

松下茂人
若手皮膚外科医のワークショップ「Take home flaps！」「My favorite flaps」
第 40 回日本皮膚悪性腫瘍学会学術大会，宮崎, 2024 年 5 月 10 日

松下茂人
シンポジウム 4「あざの診断・治療」 黒あざの診断と治療
第 42 回日本美容皮膚科学会総会・学術大会，名古屋（Web）, 2024 年 8 月 30 日

松下茂人
2024 年度西部支部メンター＆メンティー相談会 皮膚外科医への道～組織と個人のためのジョブ・アサインメント～
第 76 回日本皮膚科学会西部支部大会 M&M 相談会，徳島, 2024 年 9 月 7 日

松下茂人
皮膚がん診療における手術療法～コンセプトと私たちに求められる手術手技～
第 77 回日本皮膚科学会西部支部大会，徳島, 2024 年 9 月 8 日

松下茂人
領域横断ワークショップ「会陰部・肛門部腫瘍に対する領域横断的手術」肛囲乳房外パジェット病に対する ESD テクニックを用いた肛門機能温存手術
第 62 回日本癌治療学会学術集会，福岡, 2024 年 10 月 25 日

松下茂人
皮膚がんガイドラインセッション「乳房外パジェット病」
第 42 回日本臨床皮膚外科学会総会・学術大会，川越，2025 年 2 月 22 日

松下茂人
内視鏡を用いた肛門周囲パジェット病の新たな手術アプローチ —私はこうしている
第 42 回日本臨床皮膚外科学会総会・学術大会，川越，2025 年 2 月 22 日

松下茂人
皮膚がん診療のリアル～患者さん一人ひとりに最適な治療を考える～
第 116 回日本皮膚科学会大分地方会，大分，2025 年 3 月 2 日

青木恵美，松下茂人
COVID-19 の流行が皮膚がん患者の受診動機に与えた影響-
第 67 回日本形成外科学会総会・学術集会，神戸, 2024 年 4 月 12 日

青木恵美，西原克彦，山本宗太郎，山村健太郎，小森崇矢，佐々木奈津子，日高太陽，坂本翔一，平野 唯，松下茂人
COVID-19 流行前後での皮膚がん手術件数の推移
第 40 回日本皮膚悪性腫瘍学会学術大会 宮崎, 2024 年 5 月 11 日

青木恵美，岩田昌史，戸澤貴久，河本宏文，生駒宗禎，藤井一恭，松下茂人
超高齢者における皮膚がん治療後の経過観察の重要性
日本皮膚科学会第 197 回鹿児島地方会，鹿児島, 2024 年 6 月 30 日

青木恵美，岩田昌史，戸澤貴文，生駒宗禎，河本宏文，藤井一恭，松下茂人
表皮嚢腫との鑑別を要する疾患の超音波検査所見
第 123 回九州・沖縄形成外科学会総会・学術集会，福岡, 2024 年 7 月 20 日

青木恵美，松下茂人
診断に時間を要した爪部メラノーマの 2 例
第 124 回九州・沖縄形成外科学会学術集会，熊本, 2024 年 10 月 26 日

青木恵美，平野慎悟，岩田昌史，戸澤貴久，生駒宗禎，河本宏文，松下茂人
皮膚腫瘍・皮膚外科を学ぶ若手医師育成のための取り組み
第 198 回日本皮膚科学会鹿児島地方会，鹿児島, 2024 年 12 月 1 日

藤井一恭
T 細胞リンパ腫の治療戦略
第 40 回日本皮膚悪性腫瘍学会，宮崎, 2024 年 5 月 10 日

西原克彦，佐々木奈津子，後藤啓介，平木 翼，吉川周佐，青木恵美，山本宗太郎，藤澤康弘，松下茂人
脂腺細胞様の細胞形態像を呈したアポクリン癌の 2 例
第 40 回日本皮膚悪性腫瘍学会学術大会，宮崎, 2024 年 5 月 10 日

西原克彦，青木恵美，山本宗太郎，川平秀一郎，藤井一恭，藤澤康弘，松下茂人
尿道浸潤を伴う外陰部パジェット病に対する経尿道的切除術を行った 4 症例のまとめ
第 39 回日本皮膚外科学会総会・学術大会，京都, 2024 年 7 月 6 日

西原克彦，青木恵美，佐々木奈津子，山本宗太郎，藤澤康弘，松下茂人
ニボルマブ+イピリムマブ併用療法でサイトカイン放出症候群を発症した直腸原発メラノーマの一例
第 76 回日本皮膚科学会西部支部学術大会，徳島, 2024 年 9 月 7 日

佐々木奈津子，青木恵美，山村健太郎，日高太陽，平野 唯，西原克彦，藤野善久，松下茂人
90 歳以上の超高齢者における有棘細胞癌の予後解析
第 39 回 皮膚外科学会総会・学術大会，京都, 2024 年 7 月 6 日

河本宏文，青木恵美，生駒宗禎，戸澤貴久，岩田昌史，松下茂人
Endocrine Mucin-producing Sweat Gland Carcinoma の 3 例の症例報告
第 410 回 日本皮膚科学会福岡地方会，北九州, 2024 年 9 月 29 日

岩田昌史，大日輝記，松下茂人
pseudolymphomatous folliculitis を疑った 1 例
第 197 回日本皮膚科学会鹿児島地方会，鹿児島, 2024 年 6 月 30 日

古庄正英，安留龍太郎，塗木健介
臍ヘルニア修復術と腹膜透析用カテーテル挿入術を同時に行った一例
第 54 回日本腎臓学会東部学術集会，宇都宮, 2024 年 9 月 28 日

尾辻良彦，古庄正英
Leriche 症候群による発達した体幹壁側副血行路を有する患者に対し腹膜透析用カテーテルを挿入した一例
第 54 回日本腎臓学会東部学術集会，宇都宮, 2024 年 9 月 28 日

二宮雄一
”JOA”(2023)－最多被引用論文はこれだ－
第 70 回日本不整脈心電学会学術集会，金沢, 2024 年 7 月 18 日

諫見圭佑，鳥山陽子，杉尾由希子，馬籠さつき，安庭愛子，松崎 勉
疼痛管理中にケミカルコーピングが疑われた一例
第 17 回緩和医療薬学会年会，東京, 2024 年 5 月 25 日

鳥山陽子，諫見圭佑，杉尾由希子，上之園咲，山形真一
咽頭がんの部位別における制吐剤使用状況の検討
第 17 回緩和医療薬学会年会，東京, 2024 年 5 月 25 日

加茂章弘，笹村真由美，天願博道,東雅也，境井曉，矢口武廣，玉城啓太，山下克也
医療不信に伴いオピオイドを拒否する患者への緩和ケア介入により疼痛緩和が得られた一例
第 17 回緩和医療薬学会年会，東京, 2024 年 5 月 26 日

西村尚芳，山形真一，上之園咲，吉永光辰
調剤プロセスにおけるヒアリハット減少の取り組み－環境調整が効果を示した事例―
第 26 回医療マネジメント学会学術総会，福岡, 2024 年 6 月 21 日

杉尾由希子，山形真一
中規模一般病院でのがん化学療法レジメン監査業務の効率的な教育方法の検討
第 26 回医療マネジメント学会学術総会，福岡, 2024 年 6 月 22 日

西村尚芳，山形真一，吉永光辰，上之園咲，黒田紘生，桑原貴美子，大窪典子
部門内の安全意識を高めることでヒヤリハット発生抑制を得た一方法
第 10 回日本医薬品安全性学会学術大会，新潟, 2024 年 7 月 20 日

杉尾由希子，桑原貴美子，大窪典子，山形真一
ヨード造影剤投与を契機として Kounis 症候群 III 型を発症した一症例
第 83 回九州山口薬学大会，鹿児島, 2024 年 10 月 13 日

上之園咲，今村聖奈，鳥山陽子，杉尾由希子，大窪典子，桑原貴美子，山形真一
アルミノックス療法の実施環境整備と薬剤師の関わり
第 34 回医療薬学会年会，千葉, 2024 年 11 月 2 日

諫見圭佑，鳥山陽子，大渡五月，杉尾由希子，片岡哲郎，大塚眞紀，山形真一
三酸化二ヒ素投与による徐脈性不整脈に対してペースメーカー埋め込み術により自家移植まで行なえた一例
第 34 回医療薬学会年会，千葉, 2024 年 11 月 3 日

末永 亘，五十嵐隆志，山形真一，川﨑敏克
担がん患者における麻薬持続注射自己抜去リスク因子の検討
第 34 回医療薬学会年会，千葉, 2024 年 11 月 4 日

鳥山陽子，諫見圭佑，杉尾由希子，上之園咲，山形真一
咽頭がん CCRT 療法における CDDP 減量理由、再発を含む二次治療移行率に関する検討
第 34 回医療薬学会年会，千葉, 2024 年 11 月 3 日

濵﨑翔平，髙武嘉道，平田亮介，副島啓司，西裕美，塚田寛子，長﨑洋司，橋本雅司
メロペネム供給制限の影響に関する多施設共同後方視的研究
第 72 回日本化学療法学会西日本支部総会，神戸, 2024 年 11 月 15 日

杉尾由希子，桑原貴美子，大窪典子，山形真一
ヨード造影剤投与を契機として Kounis 症候群 III 型を発症した一症例
第 78 回国立病院総合医学会，大阪, 2024 年 11 月 18 日

佐多菜穂子，大窪典子，桑原貴美子，山形真一
入院中薬学ケアにより副作用を軽減した症例について薬剤管理サマリーを用いた病院−薬局間の連携が患者満足度向上につながった一例
第 78 回国立病院総合医学会，大阪, 2024 年 11 月 19 日

草原 智，岡村優樹，大迫亮子，手嶋翔一朗，久保祐子，梅橋功征，安藤諭吉
僧帽弁狭窄を繰り返し左房内に巨大な血栓を多発的に認めた一症例
第 58 回日臨技九州支部医学検査学会，鹿児島, 2024 年 11 月 9 日

手嶋翔一朗，西浦哲哉，藤田寿之，石松 卓，於久幸治
超音波検査が診断形態評価に有用であった頸部仮性動脈瘤の 1 例
第 49 回日本超音波検査学会学術集会，仙台, 2024 年 7 月 19 日

中釜美乃里，原田美里，久保祐子，日野出勇次，梅橋功征，西方菜穂子
軽胸壁心エコー図検査で経過を追えた悪性リンパ腫の一症例
第 49 回日本超音波検査学会学術集会，仙台, 2024 年 7 月 19 日

樋渡まこ，山口 俊，城戸隆宏，吉野 歩，高瀬 泉，梅橋功征，西方菜穂子
喀痰および胃液より M.chelonae を検出した一例
第 73 回日本医学検査学会，金沢，2024 年 5 月 11 日

吉野 歩，江藤裕哉，赤峯未紀，山下咲歩，波野真伍，礒口藍斗，宮川裕司，樋渡まこ，高瀬 泉，梅橋功征，安藤諭吉
機器更新が及ぼす影響に関する考察
第 29 回国立病院臨床検査技師協会九州学会，都城，2024 年 7 月 6 日

吉野 歩
小規模施設のメリット・デメリット ～ 一度は勤務経験をすべき その理由 ～
第 29 回国立病院臨床検査技師協会九州学会，都城, 2024 年 7 月 7 日

吉野 歩，江藤裕哉，赤峯未紀，礒口藍斗，波野真伍，高瀬 泉，城ヶ崎泰代，後藤正道，野元三治
上咽頭に認められた骨髄肉腫の一例
第 29 回国立病院臨床検査技師協会九州学会，都城, 2024 年 7 月 14 日

江藤裕哉，赤峯未紀，山下咲歩，波野真伍，吉野 歩，高瀬 泉，田島直行，梅橋功征，安藤諭吉
肝炎ウイルス陽性をパニック値運用とした効果の評価
第 29 回国立病院臨床検査技師協会九州学会，都城, 2024 年 7 月 7 日

岡村優樹，中釜美乃里，久保祐子，日野出勇次，梅橋功征，西方菜穂子
impending paradoxical embolism を伴う肺動脈血栓塞栓症の一例
日本心エコー図学会、第 35 回学術集会，姫路, 2024 年 4 月 20 日

高山瑞稀，原田美里，中釜美乃里，久保祐子，日野出勇次，梅橋功征，西方菜穂子
超音波検査にて指摘しえた右房内進展を伴う腎細胞癌の 1 症例
第 49 回日本超音波検査学会学術集会、仙台、2024 年 7 月 19 日

池田 光，城戸隆弘，上西菜月，岡村優樹，大迫亮子，宮下恵美，中釜美乃里，手嶋翔一郎，久保祐子，梅橋功征，安藤諭吉
若年性肝硬変症の 1 症例
第 29 回国臨協九州学会，都城, 2024 年 7 月 7 日

Ryuichi Miyajima, Masahiro Mori, Daichi Ideguchi, Tomoko Hitaka, Takemi Watanabe, Satoshi Tateishi
Survey of multicenter exposure doses in diagnostic fluoroscopy and comparison with Japan DRLs 2020
第 80 回日本放射線技術学会総会学術大会、横浜市, 2024 年 4 月 13 日

久木野豊，宮島隆一，濱田圭介，薗田正浩，塗木徳人
経皮的カテーテル心筋焼灼術における患者・術者被ばく線量の推移
第 78 回国立病院総合医学会，大阪, 2024 年 10 月 19 日

小林伊吹，宮島隆一，濱田圭介，市野凌資
画像処理技術を活用した体内留置カテーテル視認性向上の取り組み
第 78 回国立病院総合医学会，大阪, 2024 年 10 月 19 日

宮島隆一，増井飛沙人，大井邦治，渋谷 充，池田敏久，阿南恵吾，松井 謙
X線撮影における再撮影の判定基準の標準化や教育効果について再撮影率の低減は可能か？
第 1 回日本放射線医療技術学術大会，浦添, 2024 年 11 月 1 日

下新原壱成，市野凌資，濱田圭介，宮島隆一，上野 凌
脳血流シンチグラフィにおける 123I-IMP Graph Plot 法の直線回帰式の検討
令和 6 年度九州国立病院機構診療放射線技師会学術大会，熊本, 2024 年 10 月 26 日

中間理李加，久木野豊，宮島隆一，濱田圭介
血管造影装置の線量表示精度管理
令和 6 年度九州国立病院機構診療放射線技師会学術大会，熊本, 2024 年 10 月 26 日

岩元優樹，山口英明，安武 翼，濱田圭介，宮島隆一，阿南恵吾，中村彰吾
多職種で連携した造影剤副作用対応の体制整備について
第 19 回九州放射線医療技術学術大会，宮崎，2024 年 12 月 22 日

日高 優
当院の心筋保護液組成変更における影響についての検討
第 49 回日本体外循環技術医学会九州地方会大会，宮崎, 2024 年 6 月 16 日

日高 優
体外循環における補液について
2024 年度全国国立病院機構臨床工学技士協議会九州支部 学術大会，熊本, 2024 年 9 月 14 日

崎向幸江，花田道代，中之薗妙子，郡山暢之
当院の入院前支援における管理栄養士の活動の現状と課題
第 78 回国立病院総合医学会，大阪，2024 年 10 月 19 日

立宅由佳，栗原美佐子，田代祐子，福迫直美
酸素療法中におけるサージカルマスク装着が患者に与える影響因子
第 77 回国立病院総合医学会，大阪，2024 年 10 月 19 日

澁谷幸子
小児看護学実習経験差が及ぼす子どもの権利擁護実践能力に対する自信度への影響
第 22 回国立病院看護研究学会，横浜，2024 年 12 月 7 日

谷﨑知亜紀
A 病院のエアマットレス管理における現状と課題
第 77 回国立病院総合医学会，大阪，2024 年 10 月 18 日

福島香鈴，前田明歩，五反田栞里，野内万理子
小児科を有する混合病棟における小児患者家族の満足度調査
第 77 回国立病院総合医学会，大阪，2024 年 10 月 18 日

南　真帆，福留美那，阪口美穂，禰占大樹，北原こゆき，原田恵子，福丸美貴，中本　恵
意識障害のある患者のベッドの療養環境を整えるためのアプローチ～シミュレーション，環境ラウンド，環境ラウンドチェックリストを用いて～
日本医療マネジメント学会　第 21 回九州・山口連合大会，佐賀，2024 年 12 月 3 日

中本　恵，加藤崇志，久徳博子，青山綾子，肥後あゆみ，本坊沙織，岩切志織
クラスターが発生した病棟の看護師が看護師長に求める支援
第 77 回国立病院総合医学会，大阪，2024 年 10 月 18 日

今吉弥生，池田智子，中川勇樹，野内万理子，福元京子，福迫直美，野口久美子
ジェネラリストの WE に影響を与える要因
第 55 回日本看護学会学術集会，熊本，2024 年 9 月 28 日

神野　愛，福島紫音，中村敬子，野中美里，溝口　隼，今吉弥生
TAVI を受ける患者・家族の看護に携わる病棟看護師のモチベーションの変化～TAVI に臨む目的や人生における希望の聞き取りを行って～
第 77 回国立病院総合医学会，大阪，2024 年 10 月 18 日

俵積田麻衣，寺田　梢，木佐貫彩果，山形麻里子，中川勇樹
喉頭摘出患者の意思決定支援の関わり～看護師が抱くコミュニケーションの困難さ～
第 55 回日本看護学会学術集会，熊本，2024 年 9 月 29 日

石原由貴，椎原香美，篠崎亜樹子，岩切志織
コロナ禍における面会制限による病棟看護師と介護支援専門員との連携上の課題と支援
日本医療マネジメント学会　第 21 回九州・山口連合大会，佐賀，2024 年 12 月 6 日

田中佑介，谷山凪沙，木下天翔，久保田詳子，本坊沙織
手術室看護師の周手術期の指導に対する「思い」
第 38 回日本手術看護学会年次大会，札幌，2024 年 10 月 20 日

新坂享子，東　健作，田中秀樹
救急科所属の診療看護師は医師のタスク・シフト/シェアに貢献できるか
鹿児島救急医学会学術集会　第 89 回医師部会，鹿児島，2024 年 9 月 14 日

出口喬一
ECPELLA を要した周産期心筋症に対し、診療看護師として治療および看護的視点から多角的に介入した一例
第 137 回日本循環器学会九州地方会，別府，2024 年 12 月 13 日

森山佳奈，永住圭祐，池田美由紀，榎谷小春，加藤崇史，古庄正英
腹膜透析を継続している方が生活の中で大切にしていること
第 30 回日本腹膜透析医学会学術集会・総会，福岡，2024 年 11 月 16 日

四元明江，肥後あゆみ，中川勇樹，大迫朋子，井口麻里
DiNQL を活用した褥瘡対策に向けた取り組み
第 55 回日本看護学会学術集会，熊本，2024 年 9 月 28 日

伊藤由加
診療看護師（NP）が担う開心術後管理にレミフェンタニル導入が与える影響について検討
第 55 回日本心臓血管外科学会学術総会，下関，2025 年 2 月 22 日

筆頭演者が鹿児島医療センターの職員以外

＜国際学会＞

Ishizuka S, Miyamoto Y, Kawakita T, Maeda Y, Goto M, Ato M, Nagae M, Yamasaki S
Mycobacterium leprae reduces immunological “visibility”by deactivating a potent PAMP
The 1st Annual Meeting of the Japanese Cytokine Society，Sapporo, 2024/7/25

＜国内学会＞

戸澤聖也，西 恭宏，山下裕輔，櫻井智章，池田菜緒，原田佳枝，駒走尚大，宮田春香，村上 格，西村正宏，濱野 徹，中村康典
除脂肪量を簡易的体組成として用いるための口腔機能,サルコペニア,フレイルの関連の検討
日本老年歯科医学会第 35 回学術大会，札幌, 2024 年 6 月 29 日

木原成海，木村 菜美子[野元]，大河内孝子，李 光旭，中村典史，神谷 亨
色彩の分離に基づいた 3 次元点群顔データからの口唇領域の抽出
第 43 回日本医用画像工学会大会，東京, 2024 年 8 月 5-7 日

鈴木寛人，平田亮介，津曲恭一，山形真一
ハイリスク薬の注意喚起に対する看護師の意識変化
第 34 回医療薬学会年会，千葉, 2024 年 11 月 3 日

④ 研究会

窪田唯伊
頻脈・皮疹を主訴に入院となり複数診療科連携が必要であった一例
第 1 回城山多職種協働ケースカンファレンス，鹿児島, 2024 年 8 月 2 日

福宿 愛
当院における TAVI(transcatheter aortic valve impantation)施行患者の 2 年後予後の検証
第 11 回鹿児島循環器カンファレンス，鹿児島, 2024 年 10 月 19 日

濵田祐樹
EMBOGUARD の臨床使用経験と ONE-SEG Technique
EMBOTRIP in Kagoshima，鹿児島，2024 年 9 月 13 日

濵田祐樹
LVO 領域の治療
Kyusyu Mechanical Thrombectomy Seminar (KMET)，熊本，2024 年 9 月 27 日

濵田祐樹
TIGERETRIEVER の臨床使用経験
TORA PROJECT，熊本，2024 年 10 月 25 日

濵田祐樹
M1 Strategy from the REACT AIS Registry in Kyusyu
M1 Strategy from the REACT AIS Registry in Kyusyu，福岡，2024 年 12 月 10 日

濵田祐樹
当院における AIS 治療方針
KANEKA　九州 AIS 症例検討会，熊本，2025 年 1 月 17 日

濵田祐樹
当院における AIS 治療方針
第 2 回南九州 AIS セミナー，鹿児島，2025 年 1 月 30 日

佐藤健朗
当院における脳卒中診療の実態
15 回脳血管山峰会研究会，熊本，2024 年 10 月 13 日

川畑裕太郎
PTA を行うか躊躇した Giant cell arteritis related stroke
CN 研究会，福岡，2024 年 6 月 8 日

岩元佳奈
左椎骨動脈解離による延髄外側症候群の症例
第 8 回チェスト，鹿児島，2024 年 12 月 6 日

岩元佳奈
頚動脈ステント留置術後に意識障害が遷延した症例
ARNI Web Seminar，鹿児島，2025 年 01 月 10 日

神尾真樹
働き方改革を意識した開腹手術
第 5 回鹿児島県産婦人科手術懇話会，鹿児島, 2024 年 9 月 6 日

河村英哉，諫見圭介，杉尾由希子，末永 亘，桑原貴美子，山形真一
Infusion reaction 頻度が高いイサツキシマブの投与速度の単位変換ミスによる誤処方の防止策の評価
国立病院薬剤師会宮崎鹿児島地区薬学研究会 2024，都城, 2024 年 10 月 5 日

手嶋翔一朗，池田 光，上西菜月，中釜美乃里，草原 智，城戸隆宏，高山瑞稀，岡村優樹，大迫亮子，下 美里，久保祐子，梅橋功征，安藤諭吉
経胸壁心エコー図検査が有用であった冠動脈瘻の２例
第 12 回 QEC，鹿児島，2024 年 12 月 15 日

城戸隆宏
気腫性胆嚢炎に進展した急性胆嚢炎の 1 症例
第 343 回鹿児島県超音波医学研究会（腹部），鹿児島, 2024 年 7 月 30 日

草原 智，岡村優樹，大迫亮子，手嶋翔一朗，久保祐子，梅橋功征，安藤諭吉
僧帽弁狭窄を繰り返し左房内に巨大な血栓を多発的に認めた一症例
第 346 回鹿児島県超音波医学研究会（循環器），鹿児島, 2024 年 10 月 30 日

吉野 歩，江藤裕哉
症例提示：唾液腺領域
国臨協九州支部病理部門研修会，福岡市（Web），2024 年 6 月 20 日

吉野 歩，江藤裕哉
労働安全衛生規則の変更点と鹿児島医療センター臨床検査科における取組
国臨協九州支部病理部門研修会，福岡市（Web），2024 年 11 月 19 日

江藤裕哉
病理システム導入における妥当性確認の進め方～当院での事例を踏まえて～
国臨協九州支部病理部門研修会，福岡市（Web），2024 年 5 月 23 日

江藤裕哉
当院での肝炎拾い上げ活動の取り組み～肝炎ウイルス検査陽性をパニック値運用とした効果の評価～
令和 6 年度鹿児島県肝炎医療コーディネーター養成講座，鹿児島（Web），2024 年 12 月 1 日

岡村優樹
肝腫瘍の一例
第 345 回鹿児島超音波医学研究会，鹿児島，2024/年 9 月 24 日

岡村優樹，中釜美乃里，手嶋翔一郎，久保祐子，梅橋功征，安藤諭吉
交通外傷後の切迫奇異性塞栓症の一例
第 12 回 QEC，鹿児島，2024 年 12 月 15 日

草原 智，岡村優樹，大迫亮子，手嶋翔一朗，久保祐子，梅橋功征，安藤諭吉
僧帽弁狭窄を繰り返し左房内に巨大な血栓を多発的に認めた一症例
第 347 回鹿児島超音波医学研究会，鹿児島，2024 年 10 月 30 日

大迫亮子
拡張相肥大型心筋症の一例
第 342 回鹿児島超音波医学研究会，鹿児島，2024 年 6 月 26 日

上西菜月
特発性細菌性腹膜炎を合併した非代償性肝硬変の一症例
第 348 回鹿児島超音波医学研究会，鹿児島，2024 年 12 月 10 日

高山瑞稀，原田美里，中釜美乃里，久保祐子，日野出勇次，梅橋功征，西方菜穂子
超音波検査にて発見した右房内進展を伴う腎細胞癌の 1 症例
第 12 回 QEC，鹿児島，2024 年 12 月 15 日

高山瑞稀
経胸壁心エコー図検査にて三尖弁に付着した疣腫を発見しえた1症例
第 349 回鹿児島超音波医学研究会，鹿児島，2025 年 1 月 29 日

池田 光，城戸隆弘，上西菜月，岡村優樹，大迫亮子，宮下恵美，中釜美乃里，手嶋翔一郎，久保祐子，梅橋功征，安藤諭吉
若年性肝硬変症の 1 症例
第 343 回鹿児島県超音波医学研究会（腹部），鹿児島，2024 年 5 月 28 日

上西菜月
膵管内乳頭状粘液性腺癌を超音波検査で指摘しえた一症例
第 351 回鹿児島超音波医学研究会，鹿児島，2025 年 3 月 26 日

小林伊吹，宮島隆一，濱田圭介，市野凌資
画像処理技術を活用した体内留置カテーテル視認性向上の取り組み
令和 6 年度南九州地区研修会，鹿児島 2024 年 9 月 7 日

⑤ 学術講演会

片岡哲郎
心臓突然死から大切な人を救うために
鹿児島医療センター第 11 回心臓・血管病市民公開講座，鹿児島，2024 年 11 月 2 日

茶圓秀人
重症な患者さんの症例報告
鹿児島医療センター第 11 回心臓・血管病市民公開講座，鹿児島, 2024 年 11 月 2 日

石川裕輔
鹿児島における植込み型式人工心臓治療について考える
第 10 回鹿児島救急集中治療研究会，鹿児島, 2024 年 5 月 31 日

伊集院駿
エンレスト開始した後　どうなった
Next stage for ARNI Conference, Web, 2024 年 8 月 20 日

東　健作
ARNI の役割と期待 これまでに分かってきたこと
KAGOSHIMA ARNI MONTH, Web, 2025 年 3 月 4 日

石川裕輔
加護しない両センターでの ATTR-CM 診断について
地域で見る心アミロイドーシスセミナー, Web, 2025 年 3 月 6 日

石川裕輔
心不全診療と高カリウム血症
Heart failure & Hyperkalemia Harmonous seminar, Web, 2025 年 3 月 14 日

東　健作
鹿児島における ACS 二次予防の現状と課題について
Leqvio Web seminar, Web, 2025 年 3 月 14 日

石川裕輔
心不全における F4 導入について ARNi の位置づけ
KAGOSHIMA ARNI MONTH, Web, 2025 年 3 月 25 日

立石直毅
蛇行ネックに対する EVAR
Medallion in West Japan2024，福岡，2024 年 4 月 13 日

立石直毅
VALIANT の使用経験
Medallion in West Japan2024，福岡，2024 年 4 月 13 日

立石直毅
FROZENIX4Brauched 末梢側吻合の工夫
第 57 回日本胸部外科学会九州地方会総会アフタヌーンセミナー，福岡，2024 年 8 月 1 日

立石直毅
FROZENIX4Brauched 末梢側吻合のコツ
JLL Plus(動画コンテンツ)，Web，2024 年 6 月 20 日

立石直毅
FROZENIX4Brauched の使用経験
第 9 回 kyushu Sargical Topics，福岡，2025 年 1 月 18 日

松岡秀樹
鹿児島における脳卒中地域連携と抗凝固療法
脳卒中連携カンファレンス in 鹿児島, WEB, 2024 年 12 月 18 日

松岡秀樹
鹿児島における脳卒中の現状
ALL KAGOSHIMA STROKE CONFERENCE, WEB, 2024 年 9 月 17 日

松岡秀樹
脳卒中プロトコールについて　－新たなスケールをふまえて－
令和 6 年度県下救急担当者会議 鹿児島, 2024 年 12 月 6 日

松岡秀樹
心原性脳塞栓症診療の「いま」と「これから」
脳卒中・心臓病診療の「いま」と「これから」, 鹿児島, 2024 年 10 月 16 日

郡山暢之
SDM カスタマイズド鹿児島　－症例から考えるイメグリミンの位置づけ－
DUAL Seminar in 鹿児島, 鹿児島ハイブリッド型, 2024 年 6 月 27 日

郡山暢之
糖尿病医療学の実践　－スティグマやクリニカルイナーシャの意味を含めて－
第 31 回糖尿病医療連携体制講習会, 鹿児島ハイブリッド型, 2024 年 7 月 16 日

郡山暢之
糖尿病患者の足病変　～病態生理から治療まで～
令和 6 年度 糖尿病重症化予防（フットケア）研修, 鹿児島（WEB）, 2024 年 11 月 7 日

郡山暢之
離島で守る！糖尿病と腎症の重症化予防－保健師と共に地域に根ざしたアプローチ－
令和 6 年度 糖尿病重症化予防に係る人材育成事業研修会, 奄美, 2024 年 12 月 7 日

森内昭博
「令和6年度九州各県内科審査委員懇話会」への参加報告
鹿児島県内科医会（保険診療研修会 鹿児島, 2025 年 2 月 26 日

今林 徹
主治医制集中治療室におけるレミフェンタニル導入への取り組み～当院心臓血管外科術後症例に対する介入～
日本集中治療医学会 第 8 回九州支部学術集会 教育セミナー3【講演 2】, 宮崎, 2024 年 7 月 27 日

松下茂人
皮膚がん啓発について考える
九州・沖縄エリア皮膚悪性腫瘍学術講演会, 鹿児島, 2024 年 11 月 8 日

松下茂人
皮膚がん診療のリアル～患者さん一人ひとりに最適な治療を考える～
Otezla Advance Seminar, 大阪, 2024 年 11 月 21 日

松下茂人
日本人のメラノーマ～患者さん一人ひとりに最適な診療を考える～
第 12 回岡山メラノーマ治療研究会, 岡山, 2024 年 11 月 27 日

青木恵美
有棘細胞癌、メラノーマの診断と治療
2024 年度日本形成外科学会秋季学術講習会, Web, 2024 年 10 月 17 日～2025 年 4 月 15 日

藤井一恭
本邦の皮膚リンパ腫の特徴
京都皮膚科医会学術講演会, Web, 2024 年 5 月 30 日

藤井一恭
皮膚リンパ腫診療の特異性　他の皮膚悪性腫瘍と何が違うのか
皮膚腫瘍セミナー, 大阪, 2024 年 6 月 28 日

塗木徳人
不整脈の薬物療法
第 404 回姶良地区薬剤師研修会, 姶良, 2024 年 10 月 30 日

二宮雄一
心臓突然死とは
第 11 回心臓・血管病市民公開講座，鹿児島, 2024 年 11 月 2 日

梅橋功征
鹿児島医療センターにおける肝炎拾い上げの取り組み
肝炎撲滅のための WEB Seminar, Web, 2024 年 11 月 15 日

久保祐子
当院のタスク・シフト/シェアの現状
第 58 回日臨技九州支部医学検査学会，鹿児島, 2024 年 11 月 9 日

久保祐子
当院のタスク・シフト/シェアへの挑戦
第 13 回国立病院九州医療技術学会，福岡, 2024 年 12 月 7 日

堀上英昭
鹿児島医療センターの IGRT について
鹿児島放射線治療技術研究会，鹿児島（WEB 併用）, 2024 年 8 月 3 日

安武　翼
Avanto Dot から Avanto Fit BioMatrix へ Fit アップグレードを経験して
MAGNETOM 研究会，鹿児島, 2024 年 9 月 29 日

安武　翼
Avanto Dot から Avanto Fit BioMatrix へ Fit アップグレードを経験して
鹿児島地区研修会,鹿児島, 2024 年 10 月 5 日

久木野豊
新しい IVR 装置について
鹿児島地区研修会，鹿児島, 2024 年 10 月 5 日

久木野豊
術前造影 CT を用いた術中透視画像との Fusion（重ね合わせ）により3D 診療支援画像が奏功した事例
令和 6 年度九州国立病院機構診療放射線技師会学術大会，熊本, 2024 年 10 月 26 日

宮島隆一
求められる副診療放射線技師長の役割
令和 6 年度副職場長等管理研修（放射線部門分科会）, Web, 2024 年 9 月 10 日

宮島隆一
放射線検査の外来比率増加への取り組み
全国国立病院診療放射線技師長協議会　勉強会, Web, 2025 年 1 月 21 日

宮島隆一
被ばく管理において診療放射線技師に求められるスキル
第 8 回医療被ばく線量評価実務セミナー，熊本, 2024 年 5 月 25 日

中島麻里
令和 6 年能登半島地震の災害派遣における活動報告
鹿児島救急医学会第 52 回看護部会，鹿児島, 2024 年 9 月 14 日

4. 論文

当院所属で筆頭者として発表された論文を掲載します。

doi: 10.33290/jtvt.oa.24-0001

Original Article

Two-Year Clinical Outcomes Following SAPIEN 3 20-mm Transcatheter Aortic Valve Implantation in Patients with Symptomatic Severe Aortic Stenosis—Comparison of the Smallest Size Valve against Larger Transcatheter Aortic Valve

Tetsuro Kataoka,[1] Kengo Fukunaga,[1] Kiyohisa Hiramine,[1] Yutaro Nomoto,[1] Hiroyuki Matsumoto,[1] Kohichiro Sonoda,[1] Hideto Okino,[1] Kento Tagata,[1] Kengo Kumamoto,[1] Yui Kubota,[1] Yoshimasa Baba,[1] Kunitsugu Takasaki,[1] Hitoshi Nakashima,[1] Yasuhiro Tanaka,[1] Akihiro Tokushige,[2] and Mitsuru Ohishi[3]

[1]*NHO Kagoshima Medical Center, Kagoshima, Kagoshima, Japan*
[2]*Department of Clinical Pharmacology and Therapeutics School of Medicine, University of the Ryukyus, Nakagami-gun, Okinawa, Japan*
[3]*Department of Cardiovascular Medicine and Hypertension, Graduate School of Medical and Dental Sciences, Kagoshima University, Kagoshima, Kagoshima, Japan*

Received: January 11, 2024; Accepted: July 11, 2024

Objective: Transcatheter aortic valve implantation (TAVI) has become a cornerstone treatment for elderly or high-risk surgical patients with symptomatic severe aortic stenosis. The continuous evolution of TAVI techniques and technology has significantly improved its safety and efficacy. This study aims to deepen our understanding of the safety and effectiveness of the smallest size balloon-expanding transcatheter heart valve (BE-THV): SAPIEN 3 20 mm, through extensive utilization at our institution, with the goal of further refining TAVI procedures in the future.
Methods: This retrospective single-center observational study included 456 consecutive patients who underwent TAVI with SAPIEN 3 valves between June 2017 and October 2022. The short-term outcomes, adverse events such as stroke, new pacemaker implantation (PMI), paravalvular leak (PVL), prosthesis-patient mismatch (PPM), 30-day mortality, and 2-year mortality associated with the 20-mm THV were analyzed and compared with those of the 23-mm THV or the 26-/29-mm THV.
Results: The most commonly used THV size was 23 mm, accounting for 55.7% (254 cases), followed by the 26-/29-mm THV at 32.0% (146 cases) and the 20-mm THV at 12.3% (56 cases). There were no instances of new PMI or moderate or severe PVL observed in the 20-mm THV group. The 30-day mortality rate was 1.8% in patients who underwent the 20-mm THV, 1.6% in those with the 23-mm THV, and 0% in those with the 26-/29-mm THV, with no significant difference observed (P = 0.3012). However, the incidence of moderate PPM in patients who underwent the 20-mm THV implantation was 24.1% (13 out of 55), compared to 5.3% in those with the 23-mm THV and 4.3% in those with the 26-/29-mm THV, showing a statistically significant increase (P <0.0001), but severe PPM was not observed in any THV groups. The prevalence of a post-procedural transvalvular mean pressure gradient (MPG) ≥20 mmHg in the 20-mm THV group was higher compared to other size groups (20 mm: 14.3% vs. 23 mm: 2.0% vs 26/29 mm: 1.4%, P <0.0001). There was no significant difference in 2-year all-cause mortality rates (20 mm: 14.3% vs. 23 mm: 11.5% vs. 26/29 mm: 9.7%, P = 0.6491) among the different THV sizes.
Conclusion: The short-term outcomes associated with the 20-mm THV were reasonably satisfactory. While the occurrence of moderate PPM was significantly higher in patients receiving the 20-mm THV compared to other THV sizes, there were no significant differences in the 2-year mortality rate.

Corresponding author: Tetsuro Kataoka. NHO Kagoshima Medical Center, 8-1 Shiroyama-cho, Kagoshima, Kagoshima 892-0848, Japan
Email: kataoka.tetsuro.gt@mail.hosp.go.jp

Keywords: transcatheter aortic valve implantation, balloon-expanding transcatheter heart valve, 2-year mortality, prosthesis–patient mismatch, hemodynamic valve deterioration

Introduction

Transcatheter aortic valve implantation (TAVI) has emerged as a transformative intervention for elderly or high-risk surgical patients afflicted with symptomatic severe aortic stenosis.[1–3] Over the years since its inception, advancements in technique and technology have significantly improved the safety and efficacy of TAVI, making it a widely adopted alternative to surgical aortic valve replacement (SAVR). As TAVI continues to evolve, a critical aspect of its refinement lies in meticulously evaluating and optimizing various procedural elements, including valve size selection, implantation techniques, and postoperative management strategies.

Among the key factors influencing TAVI outcomes, the choice of prosthetic valve size plays a crucial role, particularly in patients with smaller annuli or anatomical complexities. In this context, utilizing the 20-mm balloon-expanding transcatheter heart valve (BE-THV), such as the SAPIEN 3, warrants comprehensive investigation. Despite its smaller size, the 20-mm THV offers potential benefits in specific patient cohorts, yet its efficacy and safety profile necessitate thorough scrutiny, especially given its increasing utilization.

Therefore, this study aims to contribute to the existing literature by providing a detailed analysis of the procedural and postprocedural outcomes associated with the use of the 20-mm THV in TAVI procedures. By evaluating a cohort of patients treated with the SAPIEN 3 20-mm THV at our institution, we seek to elucidate its technical success rate, the incidence of adverse events, and 1- and 2-year mortality. Through this analysis, we aim to shed light on the efficacy, safety, and potential challenges associated with the deployment of the 20-mm THV, thereby informing clinical practice and guiding future advancements in TAVI technology and patient care.

Materials and Methods

This observational cohort study encompasses a series of a total of 500 patients who underwent TAVI at a single institution from June 2017 to October 2022. Written informed consent was obtained from all patients for prospective data acquisition, and the study was approved by the local ethics committee. The eligibility for TAVI, as opposed to SAVR, was determined by the multidisciplinary structural heart team, which included cardiac surgeons and cardiologists, and considered patients with severe symptomatic aortic stenosis.

The patent selection flowchart is shown in **Fig. 1**. Excluded from this analysis were 43 patients (8.6%) who underwent TAVI with a self-expandable transcatheter heart valve (SE-THV) or one patient with a transcatheter aortic valve implanted within surgical aortic valve (TAV in SAV). Baseline characteristics, echocardiographic data, multidetector computed tomography (MDCT) data, procedural data, and clinical outcomes of TAVI patients were gathered and analyzed from our institute database. All 456 patients implanted a SAPIEN 3 THV (Edwards Lifesciences, Irvine, CA, USA); the available THV sizes during the study period were 20, 23, 26, and 29 mm in diameter. The selection of the THV size was based on the valve annulus area measured by MDCT and the anatomical structure of the annulus complex, which was determined by multiple analysts.

A standard follow-up protocol was implemented for all patients, including assessments before discharge (within 7 days after the TAVI procedure), at 30 days, 1 year, and 2 years postprocedure. We compared demographic and clinical characteristics among the following three groups: patients with 20-mm (n = 56), 23-mm (n = 254), and 26- or 29-mm (n = 146) sized valves. Procedural and postprocedural outcomes, including complications, were assessed in accordance with the criteria set forth by the Society of Thoracic Surgeons or Valve Academic Research Consortium 3.[4] Hemodynamic assessment via echocardiography was performed before discharge, at 30 days and 1 year postprocedure. We defined severe prosthesis–patient mismatch (PPM) as an indexed effective orifice area (EOAi) of <0.65 cm^2/m^2 and moderate PPM as an EOAi of ≥ 0.65 cm^2/m^2 and <0.85 cm^2/m^2. Structural valve deterioration (SVD) was characterized by intrinsic permanent changes to the prosthetic valve, encompassing wear and tear, leaflet disruption, frail leaflet, leaflet fibrosis and/or calcification, or strut fracture or deformation. Moderate hemodynamic valve deterioration (HVD) was described as an increase in mean transvalvular gradient ≥10 mmHg, resulting in a mean gradient ≥20 mmHg with a concomitant decrease

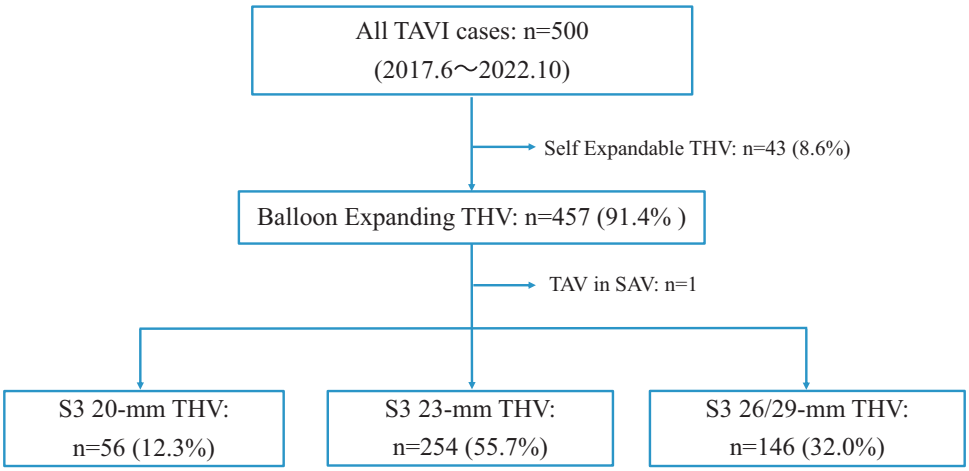

Fig. 1 Study flowchart. TAVI: transcatheter aortic valve implantation; THV: transcatheter heart valve; TAV in SAV: transcatheter aortic valve in the surgical aortic valve; S3: SAPIEN 3

in effective orifice area (EOA) ≥0.3 cm^2 compared with echocardiographic assessment performed 30 days post-procedure, or the new occurrence or increase of ≥1 grade of intra-prosthetic aortic regurgitation (AR) resulting in ≥moderate AR. Severe HVD was defined as an increase in mean transvalvular gradient ≥20 mmHg, resulting in a mean gradient ≥30 mmHg with a concomitant decrease in EOA ≥0.6 cm^2 compared with an echocardiographic assessment performed 30 days postprocedure, or the new occurrence or increase of ≥2 grades of intra-prosthetic AR resulting in ≥moderate AR.

Statistical analysis

Categorical variables are represented as numbers and percentages. Normally distributed continuous variables are expressed as mean ± standard deviation, while non-normally distributed continuous variables are shown as the median along with the interquartile range. We compared categorical variables using the chi-squared test or Fisher's exact test, as appropriate. Continuous variables were analyzed using the Kruskal–Wallis test or analysis of variance, depending on the distribution of the data. We employed the Kaplan–Meier method to create cumulative event curves, which were compared between groups using the log-rank test. A P-value of less than 0.05 was considered statistically significant. All statistical analyses were conducted with JMP Pro (version 16.0; SAS Institute Inc., Cary, NC, USA).

Results

Patient characteristics, clinical history, echocardiographic, and MDCT data at baseline are summarized in **Table 1**. This study included 56 patients with 20-mm THV, 254 patients with 23-mm THV, and 146 patients with 26- or 29-mm THV combined. The 20-mm THV groups exhibited a significantly higher proportion of females (98.2%) compared to other size groups, and they had significantly lower body height (143.6 ± 7.4 cm), body weight (45.2 ± 7.2 kg), body surface area (1.33 ± 0.13 m^2), and body mass index (21.8 ± 2.9 kg/m^2). The 26-/29-mm THV groups had a significantly higher prevalence of prior mitral valve repair or replacement (2.7%), while the Society of Thoracic Surgeons (STS) score (5.37 ± 3.15) was significantly lower.

In the 20-mm THV group, left ventricular diastolic diameter (40.6 ± 3.7 mm) and left ventricular systolic diameter (24.5 ± 3.3 mm) were significantly smaller, while ejection fraction (69.8 ± 8.7%) was higher. Peak flow velocity (PFV; 4.81 ± 0.62 m/s) and mean pressure gradient (MPG; 54.3 ± 15.6 mmHg) across the aortic valve were higher, and the aortic valve area (0.61 ± 0.17 cm^2) was significantly smaller. The annulus diameter (18.8 ± 1.0 mm) and sinus of Valsalva diameter (27.9 ± 3.0 mm) were smaller. Patients in the 26-/29-mm THV group had a higher proportion (6.8%) of the bicuspid valve.

According to the MDCT data, patients with 20-mm THV had significantly smaller measurements in the following parameters compared to other size groups; the annulus area had an average of 311 ± 25 mm^2, with an average perimeter of 64.3 ± 2.7 mm, an average minimum diameter of 17.5 ± 1.3 mm, and an average of the maximum diameter of 22.7 ± 1.3 mm. The Valsalva diameter measured at the right coronary cusp had an average of 25.4 ± 1.8 mm, at the left coronary cusp had

Table 1 Baseline characteristics

	S3 20 mm	S3 23 mm	S3 26 mm/29 mm	P value
Patient characteristics at baseline				
Age, years	84.6 ± 5.0	85.5 ± 4.3	84.5 ± 4.7	0.0702
Female	55 (98.2)	209 (82.3)	37 (25.3)	<0.0001
Body height, cm	143.6 ± 7.4	147.2 ± 7.2	156.3 ± 8.1	<0.0001
Body weight, kg	45.2 ± 7.2	48.8 ± 9.0	56.0 ± 10.2	<0.0001
Body surface area, m^2	1.33 ± 0.13	1.39 ± 0.14	1.54 ± 0.16	<0.0001
Body mass index, kg/m^2	21.8 ± 2.9	22.5 ± 3.6	22.9 ± 3.4	0.1582
Clinical history				
Hypertension	44 (78.6)	205 (80.7)	113 (77.4)	0.7236
Diabetes	12 (21.4)	62 (24.4)	39 (26.7)	0.7230
COPD	8 (14.3)	36 (14.2)	26 (17.8)	0.6070
Atrial fibrillation	11 (19.6)	49 (19.3)	37 (25.3)	0.3450
CAD	9 (16.1)	52 (20.5)	40 (27.6)	0.1292
Prior PCI	7 (12.5)	29 (11.4)	21 (14.4)	0.6887
Prior CABG	0 (0)	7 (2.8)	2 (1.4)	0.3319
PAD	6 (10.7)	29 (11.4)	11 (7.5)	0.4564
Prior MVP/MVR	0 (0)	0 (0)	4 (2.7)	0.0138
Previous stroke	9 (16.1)	42 (16.5)	30 (20.5)	0.5636
eGFR<30ml/min/1.73/m^2	6 (10.7)	23 (9.1)	21 (14.4)	0.2650
Permanent Pacemaker/ICD	5 (8.9)	8 (3.2)	9 (6.2)	0.1239
CRBBB	7 (12.5)	31 (12.2)	14 (9.6)	0.7034
CLBBB	2 (3.6)	7 (2.8)	5 (3.4)	0.9079
MMSE score	23.6 ± 5.3	24.7 ± 5.0	24.6 ± 4.4	0.2961
Clinical Frailty Scale	3.82 ± 0.97	3.78 ± 0.90	3.70 ± 0.98	0.6154
STS score	6.29 ± 3.15	6.34 ± 3.33	5.37 ± 3.15	0.0146
Echocardiographic data at baseline				
LVDd, mm	40.6 ± 3.7	42.8 ± 4.7	46.2 ± 5.7	<0.0001
LVDs, mm	24.5 ± 3.3	26.7 ± 4.9	30.4 ± 6.6	<0.0001
IVSth, mm	12.4 ± 2.5	12.7 ± 2.3	12.8 ± 2.4	0.6292
PWth, mm	11.5 ± 2.2	11.7 ± 2.0	11.9 ± 1.9	0.4439
EF, %	69.8 ± 8.7	67.4 ± 9.8	63.4 ± 11.2	<0.0001
EF<50%	2 (3.6)	14 (5.5)	16 (11.0)	0.0680
SVi<35 ml/m^2	10 (17.9)	45 (17.7)	32 (21.9)	0.5707
Transaortic PFV, m/sec	4.81 ± 0.62	4.58 ± 0.78	4.35 ± 0.69	<0.0001
Transaortic MPG, mmHg	54.3 ± 15.6	50.9 ± 17.9	45.3 ± 14.5	0.0004
AVA, cm^2	0.61 ± 0.17	0.64 ± 0.17	0.72 ± 0.14	<0.0001
AVAi, cm^2/m^2	0.47 ± 0.13	0.46 ± 0.12	0.48 ± 0.10	0.5517
Diameter of annulus, mm	18.8 ± 1.0	19.9 ± 1.4	21.9 ± 1.6	<0.0001
Diameter of Valsalva, mm	27.9 ± 3.0	30.4 ± 2.9	34.7 ± 3.6	<0.0001
Moderate or severe AR	1 (1.8)	10 (3.9)	10 (6.8)	0.2293
Moderate or severe MR	4 (7.1)	12 (4.7)	11 (7.5)	0.4759
Bicuspid AS	2 (3.6)	5 (2.0)	10 (6.8)	0.0460
MDCT data at baseline				
Aortic valve annulus area, mm^2	311 ± 25	379 ± 32	488 ± 56	<0.0001
Aortic valve perimeter, mm	64.3 ± 2.7	70.9 ± 4.6	80.5 ± 4.6	<0.0001
Aortic valve minimum diameter, mm	17.5 ± 1.3	19.2 ± 1.5	21.8 ± 1.5	<0.0001
Aortic valve maximum diameter, mm	22.7 ± 1.3	25.1 ± 1.7	28.5 ± 1.8	<0.0001
Diameter of Valsalva-R, mm	25.4 ± 1.8	28.0 ± 2.2	32.4 ± 3.5	<0.0001
Diameter of Valsalva-L, mm	26.5 ± 2.0	29.0 ± 2.3	33.3 ± 3.4	<0.0001
Diameter of Valsalva-N, mm	26.6 ± 2.3	29.2 ± 2.2	33.5 ± 3.2	<0.0001

Table 1 (Continued)

	S3 20 mm	S3 23 mm	S3 26 mm/29 mm	P value
RCA height, mm	12.9 ± 2.3	14.5 ± 2.4	17.4 ± 2.8	<0.0001
LCA height, mm	11.9 ± 1.8	12.7 ± 1.9	14.6 ± 2.7	<0.0001

Values are expressed mean ± SD or n (%).

AR: aortic regurgitation; AS: aortic stenosis; AVA: aortic valve area; AVAi: indexed aortic valve area; CABG: coronary artery bypass graft; CAD: coronary arterial disease; CLBBB: complete left bundle branch block; COPD: chronic obstructive pulmonary disease; CRBBB: complete right bundle branch block; EF: ejection fraction; eGFR: estimated glomerular filtration rate; ICD: implantable cardioverter defibrillator; IVSth: thickness of interventricular septum; LCA: left coronary artery; LVDd: left ventricular diastolic diameter; LVDs: left ventricular systolic diameter; MDCT: multidetector computed tomography; MMSE: mini mental state examination; MPG: mean pressure gradient; MR: mitral regurgitation; MVP: mitral valvuloplasty; MVR: mitral valve replacement; PAD: peripheral arterial disease; PCI: percutaneous coronary intervention; PFV: peak flow velocity; PWth: thickness of posterior wall; RCA: right coronary artery; STS: Society of Thoracic Surgeons; SVi: stroke volume index

an average of 26.5 ± 2.0 mm, and the non-coronary cusp had an average of 26.6 ± 2.3 mm. The height of the right coronary artery above the annulus averaged 12.9 ± 2.3 mm, while the height of the left coronary artery averaged 11.9 ± 1.8 mm.

Procedural data, follow-up echocardiographic data, and procedural and postprocedural outcomes are demonstrated in **Table 2**. There were no significant differences observed among THV sizes regarding the approach site and method, frequency of pre-dilation, procedural time, or anesthesia time. In the 20-mm THV group, the frequency of post-dilation (75.0%) was significantly higher compared to other size groups (P = 0.0251). There was no significant difference in the frequency of coronary protection procedures performed to prevent coronary occlusion during TAVI among the three groups (P = 0.3589). Echocardiographic data after TAVI were evaluated before discharge at 30 days, and 1 year postoperatively. At all follow-up points, the PFV and MPG at the THV were the highest in the 20-mm THV group compared to other groups, while the EOA and EOAi were the smallest (all P <0.0001). Due to the smaller EOA and EOAi, in the same way, at all follow-up points, the number of cases with a transvalvular MPG ≥20 mmHg was higher in the 20-mm THV group compared to the other groups (all P <0.0001).

Initial outcomes, 30-day outcomes, and 1-year outcomes are detailed in **Table 2**. There was no significant difference in technical success among THV sizes, nor in the conversion to open-heart surgery, the occurrence of coronary obstruction, stroke, new pacemaker implantation (PMI), moderate or severe paravalvular leak (PVL), vascular complications, life-threatening major bleeding and unexpected major bleeding, acute kidney injury, or other major complications. The frequency of moderate PPM at 30 days (24.1%, P <0.0001) was significantly higher in the 20-mm THV group, as was no incidence of severe PPM (0%), leading to significantly lower device success (75.0%, P = 0.0011). However, there was no significant difference in early safety, 30-day mortality, or in-hospital mortality among THV sizes.

At the 1-year follow-up echocardiogram, SVD was not identified; however, three cases resulted in death due to infective endocarditis. Two cases in the 20-mm THV group succumbed to infective endocarditis, which was significantly higher (P = 0.0145) compared to the other groups. Severe HVD was not observed in any group, but moderate HVD was identified in two cases: one in the 20-mm THV group and another in the 23-mm THV group. Due to the smaller EOAi, in the same way, at the time of discharge, both cases were prescribed aspirin monotherapy and were subsequently confirmed to have hypo-attenuated leaflet thickening (HALT) on MDCT, prompting the initiation of anticoagulant therapy. We closely monitored the patients who developed moderate HVD with 20-mm THV during follow-up using both echocardiography and MDCT. As depicted in **Fig. 2**, the patient in the 20-mm THV group exhibited a resolution of HALT and improvement in hemodynamics following the initiation of anticoagulant therapy.

The cumulative incidence curve of all causes of death to 1-year and 2-year follow-up in three groups is shown in **Fig. 3**. The cumulative all-cause mortality at 1 year and 2 years in the 20-mm THV group were 7.1% and 15.4%, respectively. There was no difference in the all-cause mortality when compared with the 23-mm THV

Table 2 Procedural and postprocedural data

	S3 20 mm	S3 23 mm	S3 26 mm/29 mm	P value
Procedural data				
Approach site				
Trans-femoral cutdown	8 (14.0)	28 (11.1)	26 (17.9)	0.1569
Trans-femoral puncture	48 (85.7)	216 (85.4)	116 (80.0)	0.3426
Trans-apical	0 (0)	8 (3.2)	3 (2.1)	0.3584
Trans-subclavian	0 (0)	1 (0.4)	0 (0)	0.6716
Pre-dilation	30 (53.6)	133 (52.3)	81 (55.5)	0.8343
Post-dilation	42 (75.0)	153 (60.2)	79 (54.1)	0.0251
Coronary protection to prevent coronary obstruction	1 (1.8)	1 (0.4)	1 (0.7)	0.3589
Procedure time, min	63.1 ± 31.4	67.2 ± 42.5	64.2 ± 34.1	0.6532
Anesthesia time, min	113.9 ± 41.9	119.8 ± 48.7	115.5 ± 39.5	0.5256
Follow-up echocardiographic data				
Transvalvular PFV before discharge, m/sec	2.57 ± 0.45	2.24 ± 0.38	2.08 ± 0.39	<0.0001
Transvalvular MPG before discharge, mmHg	14.6 ± 5.6	10.8 ± 3.7	9.3 ± 3.5	<0.0001
Transvalvular MPG ≥ 20 mmHg before discharge	8/56 (14.3)	11/54 (2.0)	2/145 (1.4)	<0.0001
EOA before discharge, cm^2	1.40 ± 0.26	1.68 ± 0.32	1.99 ± 0.42	<0.0001
EOAi before discharge, cm^2/m^2	1.14 ± 0.27	1.20 ± 0.25	1.30 ± 0.30	<0.0001
30-day transvalvular PFV, m/sec	2.59 ± 0.46	2.28 ± 0.41	2.04 ± 0.35	<0.0001
30-day transvalvular MPG, mmHg	15.2 ± 5.7	11.3±4.1	8.9 ± 3.2	<0.0001
30-day transvalvular MPG ≥20 mmHg	11/54 (20.4)	8/229 (3.5)	1/140 (0.7)	<0.0001
30-day EOA, cm^2	1.33 ± 0.25	1.63 ± 0.34	1.88 ± 0.39	<0.0001
30-day EOAi, cm^2/m^2	1.01 ± 0.21	1.17 ± 0.25	1.22 ± 0.27	<0.0001
1-year transvalvular PFV, m/sec	2.66 ± 0.35	2.25 ± 0.39	1.98 ± 0.36	<0.0001
1-year transvalvular MPG, mmHg	16.7 ± 5.3	11.1 ± 4.3	8.6 ± 3.3	<0.0001
1-year transvalvular MPG ≥ 20 mmHg	9/44 (20.5)	10/212 (4.7)	1/120 (0.8)	<0.0001
1-year EOA, cm^2	1.33 ± 0.22	1.63 ± 0.34	1.94 ± 0.44	<0.0001
1-year EOAi, cm^2/m^2	0.99 ± 0.17	1.18 ± 0.26	1.25 ± 0.30	<0.0001
Procedural and postprocedural outcomes				
Technical success	53/56 (94.6)	233/254 (91.7)	140/146 (95.9)	0.2512
Conversion to open heart surgery	1/56 (1.8)	2/254 (0.8)	3/146 (2.1)	0.5338
Coronary obstruction	1/56 (1.8)	0/254 (0)	0/146 (0)	0.1228
Stroke	2/56 (3.6)	7/254 (2.8)	3/146 (2.1)	0.8196
New pacemaker implantation	0/56 (0)	6/254 (2.4)	6/146 (4.1)	0.2429
Moderate or severe PVL	0/56 (0)	1/254 (0.4)	1/146 (0.7)	0.7940
Vascular complications	4/56 (7.1)	26/254 (10.2)	9/146 (6.2)	0.3899
Requiring catheter or surgical interventions	1/56 (1.8)	17/254 (6.7)	6/146 (4.1)	0.2479
Acute kidney injury	0/56 (0)	4/254 (1.6)	4/146 (2.8)	0.3899
Life-threatening bleeding and unexpected major bleeding	1/56 (1.8)	9/254 (3.5)	1/146 (0.7)	0.1897
30-day moderate PPM	13/54 (24.1)	12/228 (5.3)	6/140 (4.3)	<0.0001
30-day severe PPM	0/54 (0)	0/228 (0)	0/140 (0)	–
30-day device success VARC	42/56 (75.0)	222/254 (87.4)	137/146 (93.8)	0.0011
30-day early safety VARC	49/56 (87.5)	210/254 (84.7)	124/146 (86.1)	0.8356
30-day mortality	1/56 (1.8)	4/254 (1.6)	0/146 (0)	0.3012
In-hospital mortality	1/56 (1.8)	7/254 (2.8)	1/146 (0.7)	0.3558
Infective endocarditis	2/56 (3.6)	1/254 (0.4)	0/146 (0)	0.0145
One-year SVD VARC	0/44 (0)	0/212 (0)	0/120 (0)	–

Table 2 (Continued)

	S3 20 mm	S3 23 mm	S3 26 mm/29 mm	P value
One-year moderate HVD VARC	1/44 (2.3)	1/212 (0.5)	0/120 (0)	0.2147
One-year severe HVD VARC	0/44 (0)	0/212 (0)	0/120 (0)	–

Values are expressed mean ± SD or n (%).

EOA: effective orifice area; EOAi: indexed effective orifice area; HVD: hemodynamic valve deterioration; MPG: mean pressure gradient; PVL: paravalvular leak; PFV: peak flow velocity; PPM: prosthesis-patients mismatch; SVD: structural valve deterioration; VARC: Valve Academic Research Consortium

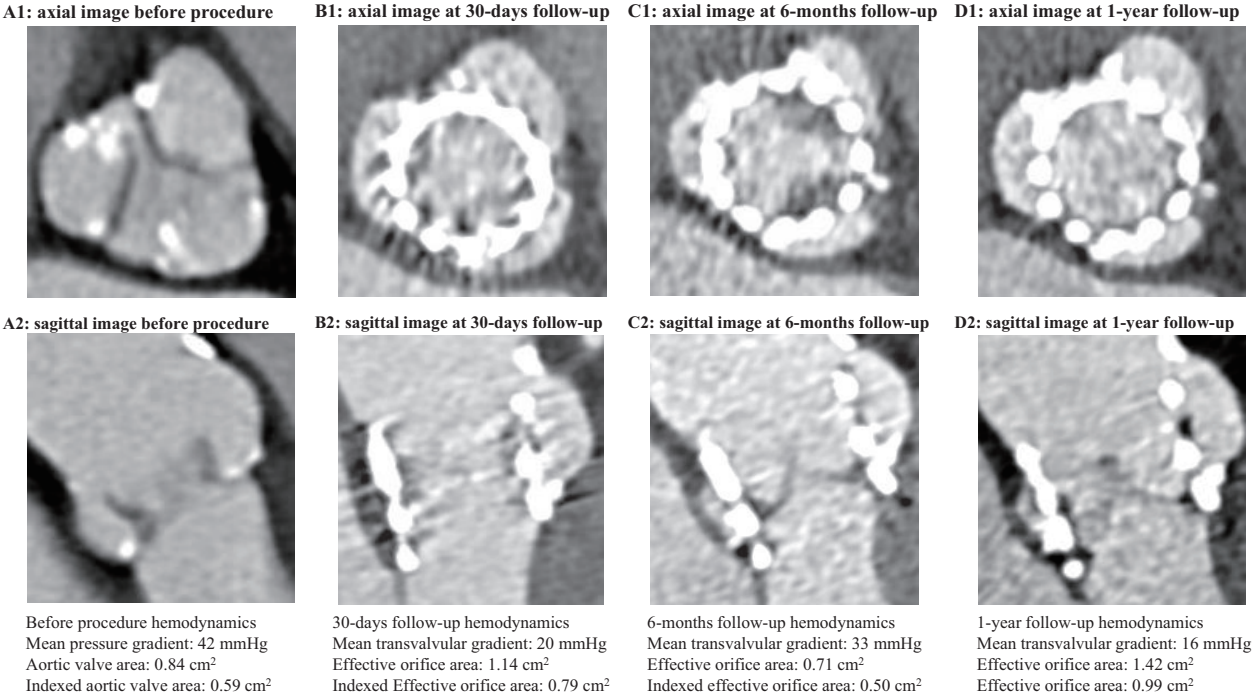

Fig. 2 The case of a 20-mm THV with moderate HVD. Pre-procedure MDCT images of a woman in her 80s with a 20-mm THV (**A1, A2**). At the time of the 30-day assessment on MDCT, the HALT was not evident (**B1, B2**). The HALT was detected in the 20-mm THV patient with moderate HVD (**C1, C2**) at 6-month follow-up. The resolution of HALT and improvement in hemodynamics following 6 months initiation of anticoagulant therapy (**D1, D2**). HALT: hypo-attenuated leaflet thickening; HVD: hemodynamic valve deterioration; MDCT: multidetector computed tomography THV: transcatheter heart valve

group (6.8% and 11.7%), or the 26-/29-mm THV group (5.7% and 10.8%).

Discussion

Since our institution commenced TAVI procedures in 2017, the increasing case volume has led to acceptable levels of technical success, the frequency of stroke, new PMI, and PVL, along with 30-day mortality. These outcomes are consistent with previous reports.[5–8] The 1-year survival rate was similarly satisfactory, and when evaluated for each prosthetic valve size, the outcomes were comparable.

Despite TAVI having a lower incidence of PPM compared with SAVR, it remains a significant concern due to its impact on morbidity and mortality.[9,10] Asian patients, including the Japanese, generally have a smaller physique, resulting in a higher prevalence of small aortic annulus and greater use of the 20-mm THV. The increased usage of the 20-mm THV may contribute to a higher frequency of moderate or severe PPM. Although previous studies suggest that the clinical impact of the elevated PPM frequency is relatively acceptable, the long-term prognosis remains uncertain.[11–13] Notably, our institution's usage rate of 20-mm THV was considerably higher at 12.5% compared to 7.6% in the Japan

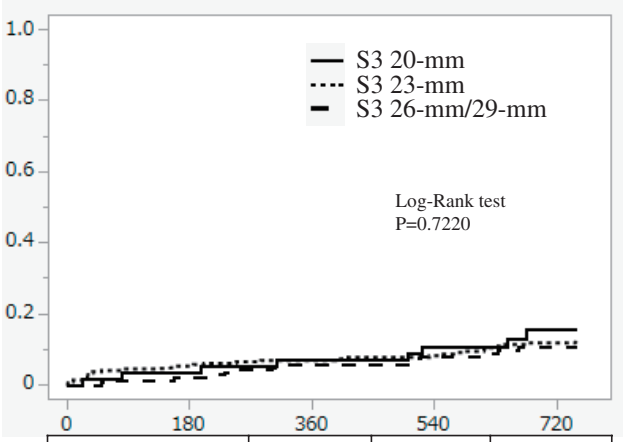

	Baseline	360 days	720 days
S3 20-mm			
Incidence		7.1%	15.4%
No. at risk	56	51	35
S3 23-mm			
Incidence		6.8%	11.7%
No. at risk	253	225	181
S3 26-mm/29-mm			
Incidence		5.7%	10.8%
No. at risk	144	130	89

Fig. 3 Two-year all cause of mortality among THV groups. THV: transcatheter heart valve

Transcatheter Valve Therapies annular report 2023.[14] The incidence rate of 30-day moderate PPM for 20-mm THV was 24.1% (13 cases), significantly higher than for other THV sizes. Efforts were made to perform additional post-dilatation to maximize the EOA and minimize the MPG at THV. However, similar to PPM, the incidence of cases with a postoperative transvalvular MPG ≥20 mmHg was higher in the 20-mm THV group. It is essential to continue monitoring the trend in pressure gradients in the future.

Furthermore, the incidence of moderate HVD at 1-year follow-up was relatively low, with isolated cases observed in the 20-mm and 23-mm THV groups. In both cases, anticoagulant therapy was initiated in response to HALT, with no worsening trend observed under closing monitoring. Given the propensity for hemodynamic deterioration, particularly in patients with 20-mm THV accompanied by PPM and/or follow-up transvalvular MPG ≥20 mmHg experiencing HVD such as HALT, meticulous follow-up will likely remain essential for this group compared to others.

Importantly, while instances of HVD indicating hemodynamic issues or SVD indicating structural issues were infrequent, three cases developed infective endocarditis. Due to advanced age and a high-risk status for surgical intervention, all three patients succumbed to death following conservative treatment with antibiotics. Postoperative follow-up must include patient guidance to prevent infective endocarditis.

If a patient who has received a 20-mm THV reaches a situation where future bioprosthetic valve degeneration progresses, necessitating a transcatheter aortic valve implanted within a transcatheter aortic valve (TAV in TAV), concerns arise regarding achieving an effective EOA with another 20-mm THV. Considering life expectancy and activity levels, the decision to implant a 20-mm THV is crucial and requires careful consideration. During the study period, only the SAPIEN 3 valve was available; however, the improved SAPIEN 3 Ultra RESILIA (SAPIEN 3UR) is now in use. Reports suggest that the SAPIEN 3UR demonstrates better outcomes in terms of PVL, PPM, and transvalvular MPG after TAVI, compared to the SAPIEN 3, and it is anticipated that the performance of the 20-mm THV will be improving in the near future.[15]

Limitations

Primally, a limitation of this study is its observational and retrospective nature conducted at a single institution. There have been periods at our institution when we were unable to use SE-THV due to internal constraints. During such periods, we had to use BE-THV for patients who might not have ideal candidates for them, potentially affecting the occurrence of complications and other factors.

In addition, although we are planning an annual follow-up observation at our institution, it is important to note that many of the patients in our study are elderly, with numerous comorbidities, and are facing a decline in activities of daily living, making it difficult for them to visit the hospital regularly. While we can conduct relatively broad prognosis assessments primarily based on information gathered from primary care physicians, the patients themselves, and their families, we may not be able to perform detailed tracking using echocardiographic examinations. It should be noted the aggregation of data and the analysis of MDCT and echocardiography were not conducted by an independent core laboratory.

Conclusion

The technical success rate and short-term outcomes associated with the 20-mm THV were reasonably satisfactory. While the occurrence of moderate PPM and follow-up transvalvular MPG ≥20 mmHg were significantly higher in patients receiving the 20-mm THV compared to other THV sizes, there were no significant differences in the 2-year mortality rate. Due to its susceptibility to HVD, it appears that longer-term follow-up is necessary.

Acknowledgments

The authors extend their sincere gratitude to the Kagoshima Medical Center Heart Team, whose invaluable collaboration ensures the smooth implementation of routine TAVI procedures.

Author Contributions

The conception and design of the work: Kataoka T. The acquisition and data for the work: Kataoka T, Fukunaga K, Hiramine K, Nomoto Y, Matsumoto H, Sonoda K, Okino H, Tagata K, Kumamoto K, Kubota Y, Baba Y, and Takasaki K. The interpretation of data for the work, revising the work critically for important intellectual content: Kataoka T, Fukunaga K, Hiramine K, Nakashima H, Tanaka Y, Tokushige A, and Ohishi M. Final approval of the version to be published: all authors. Accountability for all aspects of the work: all authors.

Disclosure Statement

All authors do not have conflicts of interest to disclose.

References

1) Leon MB, Smith CR, Mack MJ, et al. Transcatheter aortic-valve implantation for aortic stenosis in patients who cannot undergo surgery. *N Engl J Med* 2010; **363**: 1597–1607.
2) Smith CR, Leon MB, Mack MJ, et al. Transcatheter versus surgical aortic-valve replacement in high-risk patients. *N Engl J Med* 2011; **364**: 2187–2198.
3) Leon MB, Smith CR, Mack MJ, et al. Transcatheter or surgical aortic-valve replacement in intermediate-risk patients. *N Engl J Med* 2016; **374**: 1609–1620.
4) Généreux P, Piazza N, Alu MC, et al. Valve Academic Research Consortium 3: updated endpoint definitions for aortic valve clinical research. *Eur Heart J* 2021; **42**: 1825–1857.
5) Rheude T, Kornhuber K, Pellegrini C, et al. 1-year results after transcatheter aortic valve replacement with balloon-expandable valves. *JACC Cardiovasc Interv* 2021; **14**: 2189–2190.
6) Meguro K, Kumamaru H, Kohsaka S, et al. Transcatheter aortic valve replacement in patients with a small annulus—from the Japanese Nationwide Registry (J-TVT)—. *Circ J* 2021; **85**: 967–976.
7) Cannata S, Gandolfo C, Ribichini F, et al. One-year outcomes after transcatheter aortic valve implantation with the latest-generation SAPIEN balloon expandable valve: the S3U registry. *EuroIntervention* 2023; **18**: 1418–1427.
8) Möllmann H, Kim WH, Kempfert J, et al. Complications of transcatheter aortic valve implantation (TAVI): how to avoid and treat them. *Heart* 2015; **101**: 900–908.
9) Pibarot P, Weissman NJ, Stewart WJ, et al. Incidence and sequelae of prosthesis-patient mismatch in transcatheter versus surgical valve replacement in high-risk patients with severe aortic stenosis: a PARTNER trial cohort-a analysis. *J Am Coll Cardiol* 2014; **64**: 1323–1334.
10) de Agustin JA, Islas F, Jimenez-Quevedo P, et al. Discongruence index-simple indicator to predict prosthesis-patient mismatch after transcatheter aortic valve replacement. *Circ J* 2018; **82**: 2880–2886.
11) Miyasaka M, Tada N, Taguri M, et al. Incidence, predictors, and clinical impact of protsthesis-patient mismatch following transcatheter aortic valve replacement in Asian patients: The OCEAN-TAVI Registry. *JACC Cardiovasc Interv* 2018; **11**: 771–780.
12) Sugiyama K, Mukai K, Watanabe A, et al. Feasibility of SAPIEN 3 20-mm transcatheter heart valve implantation in aortic stenosis patients with a small aortic annulus. *J Transcatheter Valve Ther* 2021; **3**: 7–13.
13) Eng MH, Abbas AE, Hahn RT, et al. Real world outcomes using 20 mm balloon expandable SAPIEN3/ultra valves compared to larger valves (23, 26, 29 mm)-a propensity matched analysis. *Catheter Cardiovasc Interv* 2021; **98**: 1185–1192.
14) JTVT kyogikai. JTVT Annual report at JTVT 2023. https://dx-mice.jp/PMMS_JTVT/U02/U02PreviewPDF (Accessed November 20, 2023)
15) Yamamoto M, Yashima F, Shirai S, et al. Performance and outcomes of the SAPIEN 3 Ultra RESILIA transcatheter heart valve in the OCEAN-TAVI registry. *EuroIntervention* 2024; **20**: 579–590.

ESC European Society of Cardiology
European Heart Journal - Case Reports (2024) **8**, ytae294
https://doi.org/10.1093/ehjcr/ytae294

CARDIOVASCULAR FLASHLIGHT
Adult congenital heart disease

Right-side cardiac metastasis of squamous cell carcinoma from oesophagogastric junction cancer

Hiroyuki Matsumoto [1]*, Shun Ijuin [1], and Toshihiko Terashi[2]

[1]Department of Cardiovascular Medicine, National Hospital Organisation Kagoshima Medical Center: Kokuritsu Byoin Kiko Kagoshima Iryo Center, 8-1, Shiroyama-cho, Kagoshima-shi, Kagoshima 892-0853, Japan; and [2]Department of Cardiovascular Medicine, Kirishima Medical Center, Hayatocho-Matsunaga 3320, Kirishima-shi, Kagoshima 899-5112, Japan

Received 14 May 2024; revised 5 June 2024; accepted 7 June 2024; online publish-ahead-of-print 12 June 2024

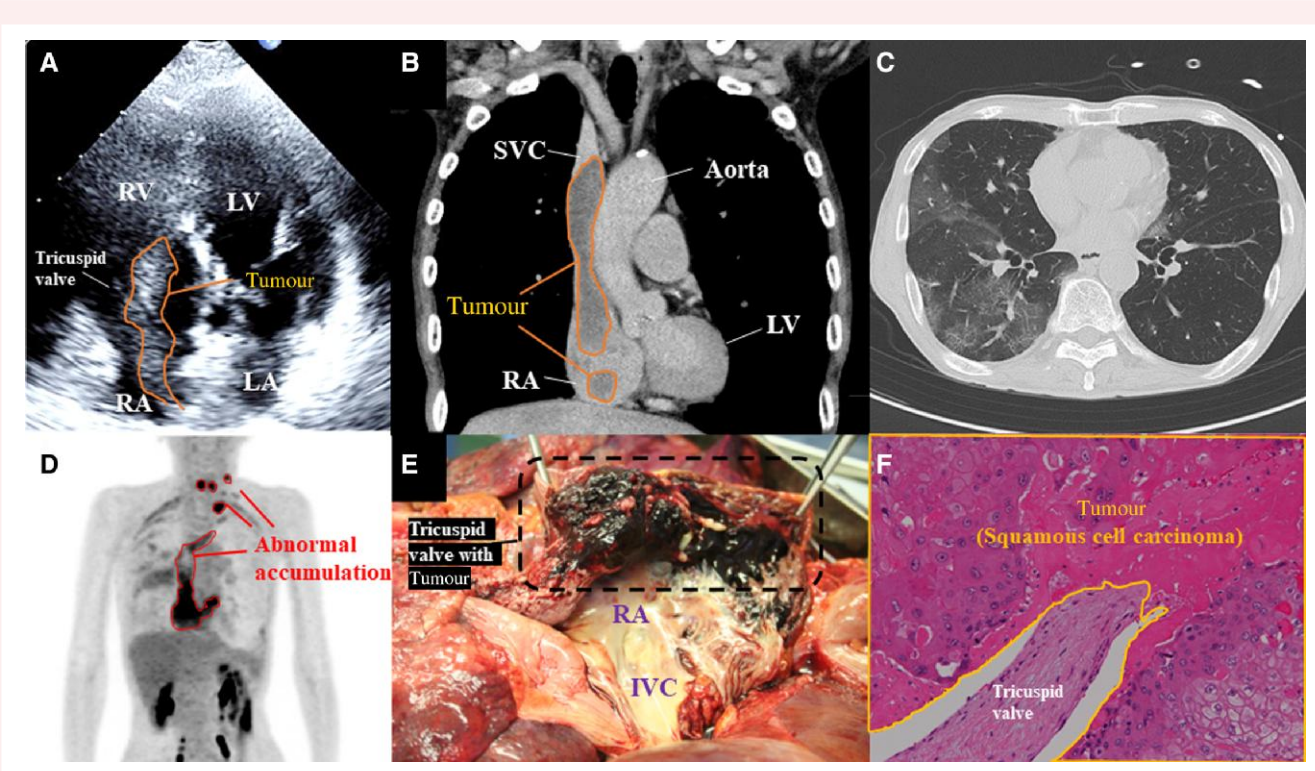

A 74-year-old man was transferred to our hospital for treatment of an intravascular embolus extending from the subclavian vein to the right atrium: that was not dissolved despite 3 months of oral anticoagulant therapy. He had been performed resection of oesophagogastric junction cancer 5 years ago and subsequently undergone post-operative chemotherapy. Although he was asymptomatic, the embolus was incidentally discovered on a follow-up computed tomography (CT). Echocardiography revealed a mobile high-intensity

* Corresponding author. Tel: +81 992231151, Email: iwtbagd.h.ma2mo10@gmail.com
Handling Editor: Jan Henzel

echo extending from the superior vena cava to the right ventricle, which was attached to the tricuspid valve (*Panel A*; Supplementary material online, *Video S1*). Contrast-enhanced CT demonstrated the continuous embolus from the left subclavian vein to the right ventricle (*Panel B*; Supplementary material online, *Video S2*), and diffuse ground-glass opacities were observed in the lung field, suggesting embolization in peripheral arteries of the lungs (*Panel C*). Fluorodeoxyglucose-positron emission tomography demonstrated that abnormal accumulation in the left supraclavicular fossa and cervical lymph nodes and from the left subclavian vein to the right ventricle (*Panel D;* Supplementary material online, *Video S3*), and we diagnosed as tumour embolization. We discussed treatment plans with surgeons. However, a highly invasive surgery involving removal of the left clavicle and subclavian vein was required, and he requested palliative care. Home oxygen therapy was introduced, and he was discharged home. He died 9 days after being discharged. Pathological autopsy revealed tumour embolus extending from the left internal jugular vein to the left and right pulmonary arteries, and histologically, the tumour had characteristics of squamous cell carcinoma (*Panels E* and *F*). This case is a rare case of squamous cell carcinoma in which cancer of the oesophagogastric junction metastasized to right-side cardiac chamber. Fluorodeoxyglucose-positron emission tomography was feasible to differentiate between thrombus and tumours.

Supplementary material

Supplementary material is available at *European Heart Journal – Case Reports* online.

Acknowledgements

The authors thank Masayoshi Tokunaga (pathologist) for his support of this report.

Consent: The authors confirm that written consent for submission and publication of this case report including images and associated text has been obtained from the patient in line with COPE guidelines.

Conflict of interest: None declared.

Funding: None declared.

Data availability

The data underlying this article are available in the article and in its online Supplementary material.

Radiology Case Reports 19 (2024) 4766–4774

Available online at www.sciencedirect.com

ScienceDirect

journal homepage: www.elsevier.com/locate/radcr

Case Report

Pseudoaneurysm formation after embolization of giant arteriovenous malformation of the lower limb associated with Parkes Weber syndrome: A case report and literature review ☆,☆☆

Hiroto Yasumura, MD[a,*], *Koji Tao, MD, PhD*[a,*], *Ryo Imada, MD*[a], *Yushi Yamashita, MD*[a], *Naoki Tateishi, MD*[a], *Kenichi Arata, MD, PhD*[b], *Tamahiro Kinjo, MD, PhD*[a]

[a] *Department of Cardiovascular Surgery, National Hospital Organization Kagoshima Medical Center, Kagoshima, Japan*

[b] *Department of Cardiovascular Surgery, Kagoshima City Hospital, Kagoshima, Japan*

ARTICLE INFO

Article history:
Received 3 May 2024
Revised 18 July 2024
Accepted 21 July 2024

Keywords:
Parkes Weber syndrome
Arteriovenous malformation
Embolization
Pseudoaneurysm
Amputation

ABSTRACT

A 63-year-old woman presented with a giant arteriovenous malformation (AVM) of the lower limbs associated with Parkes Weber syndrome (PWS). The AVM was supplied by 4 branches of the right profunda femoris artery and 4-stage embolization was performed. At 67 years of age, she developed a pseudoaneurysm due to the recanalization of a coiled profunda femoris artery branch arterial aneurysm. We performed re-embolization of the coiled profunda femoris artery and observed its shrinkage, but 2 months later, the pseudoaneurysm began to expand again, having a fatal course. This case indicates that battles against giant AVM-associated PWS follow a long and convoluted path. We present this case with reviewing 15 previously reported cases to improve our management of PWS.

Introduction

Parkes Weber syndrome (PWS) is a rare genetic disease that manifests as red skin lesions, high-flow arteriovenous malformations (AVMs), and hypertrophy of the unilateral limb [1]. AVM is a progressive disease with manifestations ranging from the Schobinger classification of quiescence stage (I) to decompensation stage (IV) ([2], Table 1). Patients with AVM require invasive treatment after transitioning to the symp-

☆ Competing Interests: The authors declare that they have no known competing financial interests or personal relationships that could have appeared to influence the work reported in this paper.

☆☆ Acknowledgments: We thank radiologist Hidefumi Mimura, MD, PhD, for advising us on the re-embolization strategy for the profunda femoris artery aneurysm. We would also like to thank the radiologists Junichi Ideue, MD, PhD, and Kentaro Akune, MD, for performing the challenging re-embolization.

* Corresponding author.
E-mail address: hiroto1331255@yahoo.co.jp (H. Yasumura).

https://doi.org/10.1016/j.radcr.2024.07.117

Table 1 – Schobinger's classification.

Stage	Clinical features
I (Quiescence period)	May or may not have vascular skin stain, warmth of the affected tissues, and arteriovenous shunts can be detected by Doppler ultrasound. The arteriovenous malformation is present but causes no clinical symptoms
II (Expansion period)	Stage I plus enlargement, pulsations, palpable thrill, audible bruit, and enlarged arterialized tortuous/tense veins
III (Destruction period)	Stage II plus dystrophic skin changes, skin ulcerations that can be nonhealing, bleeding from ulcerated skin or mucosal surfaces, overt tissue necrosis, and lytic lesions of bone may occur
IV (Decompensation period)	Stage III plus congestive cardiac failure with increased cardiac output, abnormally lowered peripheral vascular resistance, and venous hypertension secondary to tissue and skin changes

tomatic stage. Embolization may be a safe and effective option for high-flow AVMs [3]. However, some unsuccessful cases have been reported and reports on the long-term follow-up after embolization are sparse. In this report, we present a patient with PWS whose staged embolization failed and resulted in an uncontrollable pseudoaneurysm. While true aneurysm has distended vascular wall, pseudoaneurysm has disrupted vascular wall and surrounding fibrous tissue wall. Moreover, we review 15 previously reported cases to improve our understanding of the management of PWS.

Case presentation

A 63-year-old woman (height, 147 cm; weight, 46.5 kg) with a history of subarachnoid hemorrhage (SAH) had pain in the right thigh and popliteal fossa during walking. She had hypertrophy in the right thigh since childhood and found a varicose vein a few years ago. The patient's family history was unremarkable. She consulted a physician, and contrast-enhanced CT revealed a giant AVM in the right thigh (Figs. 1A-E). The right common and external iliac artery was tortuous and dilated, and both superficial femoral arteries were hypoplastic. Ankle brachial index was 0.78 at the right leg and 1.09 at the left leg. She was then referred to a hospital specializing in AVM. The Schobinger classification was stage III and she was diagnosed with PWS based on clinical features. Angiography showed that 4 branches (B1–B4) of the right profunda femoris artery, and superior and inferior gluteal arteries formed the AVM (Figs. 2A-C). The B2 branch had a small saccular arterial aneurysm at its origin. The AVM was a dilated fistula between multiple feeding arteries and draining veins, and was categorized as a type IIIb arteriovenous fistula according to Cho's classification [4]. Staged embolization was planned, and 3 months after the angiography, the first embolization was performed for the distal B1–B4 with n-butyl-2- cyanoacrylate (NBCA) plus ethiodized oil (Figs. 3A-H). Six months later, a second embolization was performed for B1 with NBCA and ethiodized oil. Furthermore, 6 months later, when she was 65 years old, the third embolization was performed for B4 with NBCA plus ethiodized oil (Figs. 4A and B) and for a saccular B2 arterial aneurysm (20×17×27 mm) with Target® XXL360 coils (Stryker, Michigan, U.S.A.) (24 mm×50 cm×2) and NBCA plus ethiodized oil (Figs. 4C and D). Complete occlusion of the aneurysm was confirmed. Seven months later, a fourth embolization was performed for a superior gluteal artery branch, using NBCA plus ethiodized oil. The other superior gluteal artery branches had low flow, and the inferior gluteal artery was difficult to embolize selectively. Embolization from the proximal profunda femoris artery was performed with NBCA plus ethiodized oil for finishing. Regular MRI follow-up 6 months later did not reveal any complications or more enlarged AVM.

At 66 years of age, she was transferred to our hospital with sudden swelling of her right thigh, edema of her right lower leg, and difficulty walking. Physical examination revealed that her right thigh was twice as large as her left thigh and had red skin lesions (Fig. 5A). The enlarged right thigh was also pulsating and hot. Her vital signs were within the normal limits.

Admission laboratory testing revealed a wide range of abnormalities, as follows: white blood cell and platelet counts, and hemoglobin level at 9330/μL, 71,000/μL, and 5.0 g/dL, respectively. The levels of the fibrin/fibrinogen degradation products were 106.1 μg/mL. The patient was diagnosed with disseminated intravascular coagulation (DIC). The blood urine nitrogen, serum creatinine, and C-reactive protein levels were 63.0 mg/dL, 3.30 mg/dL, and 14.32 mg/dL, respectively.

Contrast-enhanced computed tomography (CT) revealed a giant aneurysm (97×71×154 mm) adjacent to the embolization coils in the right thigh (Figs. 5B and C). Ultrasonography of the limb arteries revealed a to-and-fro blood waveform via a 5-mm channel between the giant aneurysm and the coiled B2 arterial aneurysm, suggesting that the giant aneurysm was a pseudoaneurysm (Fig. 5D). Chest X-ray revealed a cardiothoracic ratio of 0.60 and echocardiography revealed dilated ventricles.

The patient first received conservative therapy to improve her general condition, which consisted of bed rest, hydration, blood transfusion, compression of the enlarged right thigh, and elevation of the right lower limbs. Profunda femoris artery angiography revealed high flow, with contrast pooling in the giant aneurysm (Fig. 5E). Because the aneurysm had enlarged rapidly, we concluded that the coiled B2 arterial aneurysm had recanalized, ruptured, and generated a giant pseudoaneurysm in which red blood cells, platelets, and coagulation factors were consumed, leading to DIC.

She was conservatively managed in our hospital for 1 week, but the skin on her right thigh was tighter. CT showed further enlargement of the pseudoaneurysm (113 × 85 × 175 mm) and the diameter of the right thigh was 216 × 248 mm. We concluded that vascular surgical procedures would

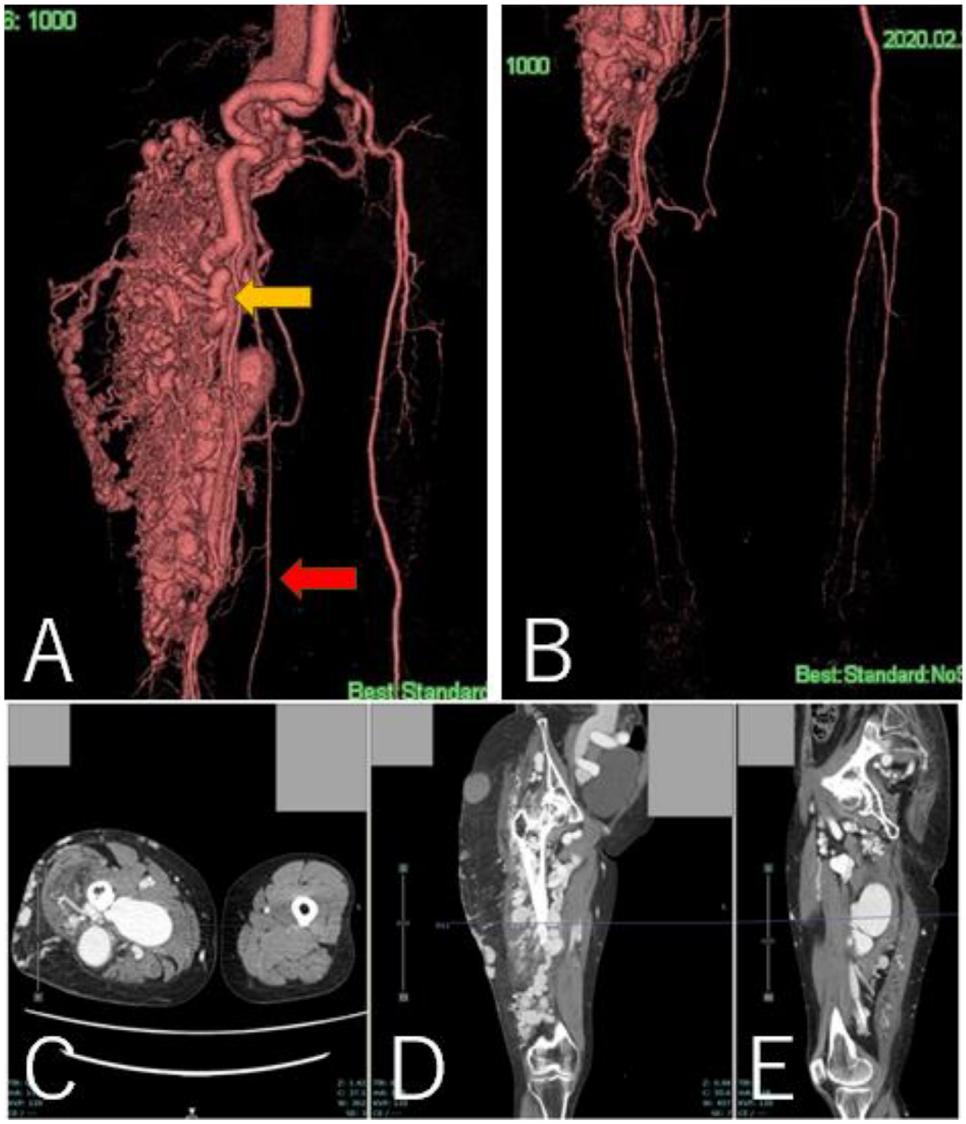

Fig. 1 – 3D-CT angiography and multi-planar reconstruction of a giant arteriovenous malformation (AVM).(A) The feeding vessels included 4 branches from the right profunda femoris artery and the right superior and inferior gluteal arteries. One of the profunda femoris artery branches had a saccular arterial aneurysm (orange arrow, 20 x 17 x 27 mm). The right superficial femoral artery was hypoplastic and was not involved in the AVM (red arrow).(B) The giant AVM was located only in the right femoral region.(C) Axial view. (D) Coronal view. (E) Sagittal view.

not control bleeding after incision of the pseudoaneurysm. The patient subsequently underwent re-embolization of the coiled B2 arterial aneurysm via the left femoral artery. The right profunda femoris artery flow was rapid, necessitating the use of 11 Target ® XXL360 coils(24 mm × 50 cm × 4, 22 mm × 50 cm × 4, 20 mm × 50 cm × 1, 16 mm × 50 cm × 1, 10 mm × 50 cm × 1)and 1 Interlock® (Boston Scientific, Massachusetts, U.S.A.) coil 14 mm × 50 cm (Fig. 6A). Digital subtraction angiography revealed that the contrast agent was not visible in the giant pseudoaneurysm after the procedure (Fig. 6B). The pulsation in the right thigh disappeared. One week after the procedure, platelet counts and hemoglobin levels recovered to 261,000/μL and 9.1g/dL, respectively. Contrast-enhanced CT revealed shrinkage of the giant pseudoaneurysm (119 × 65 × 173 mm) and the diameter of the right thigh (201 × 225 mm). Ultrasonography also revealed the absence of blood flow into the re-embolized B2 arterial aneurysm and a giant pseudoaneurysm. The patient was discharged to her referring hospital 14 days after the procedure. However, 2 months after the transference, the right thigh began to swell and involved skin ulceration. CT revealed an expanded pseudoaneurysm (131 × 107 × 180 mm, Figs. 7A and B). She was given the option of an additional procedure but chose conservative therapy. The ulcerated right thigh was applied with KALTOSTAT® Alginate Dressing (Convatec, New Jersey, USA) and was compressed. The ulcerated wound involved oozing and severe bacterial infection, and 7 months after the transference she died.

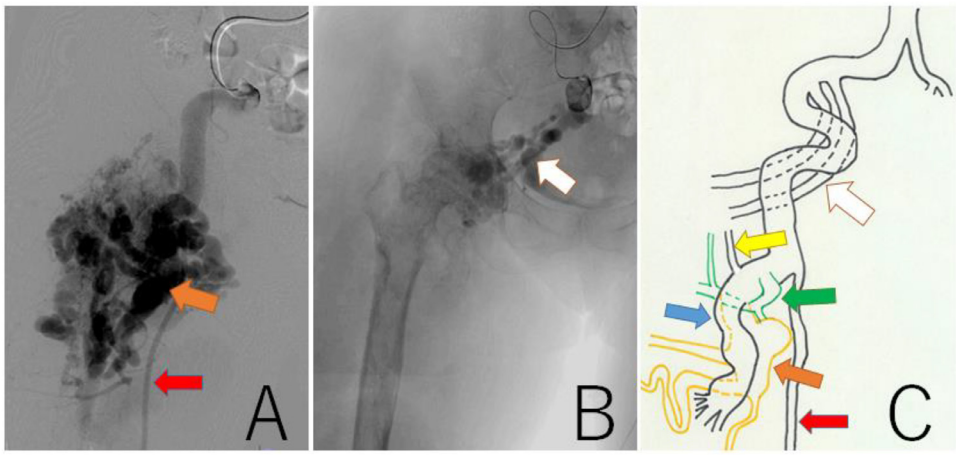

Fig. 2 – Findings of angiography and a scheme of AVM feeders. (A) Angiography from the external iliac artery showed that profunda femoris artery branches (B1-B4) were high flow feeders of the AVM. The B2 branch had a small saccular arterial aneurysm at its origin (orange arrow). The superficial femoral artery (red arrow) was hypoplastic. (B) Angiography from the inferior gluteal arteries (white arrow). (C) The AVM included 4 branches (B1: blue arrow, B2: orange arrow, B3: green arrow, B4: yellow arrow) of the profunda femoris artery, and superior and inferior gluteal arteries (white arrow).The red arrow is superficial femoral artery.

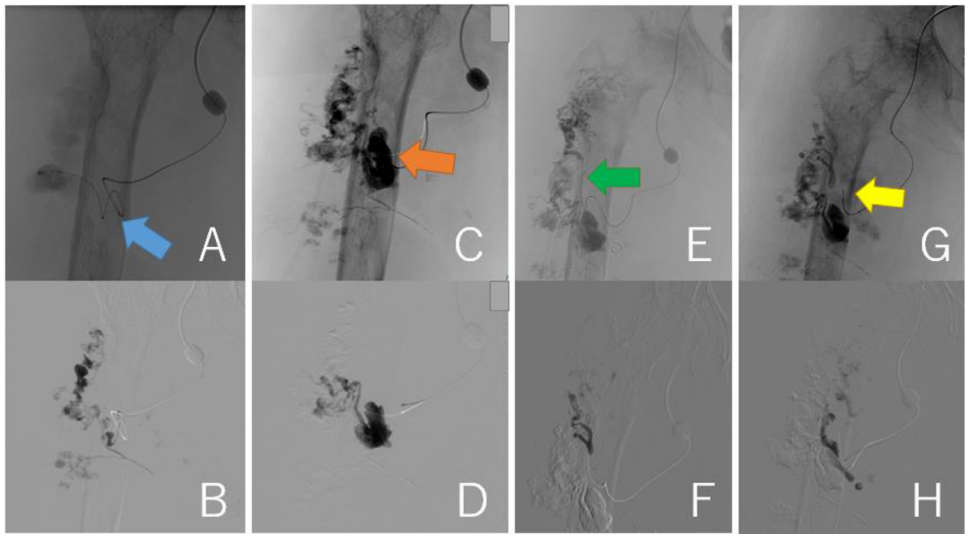

Fig. 3 – Findings of the first embolization with n-butyl-2- cyanoacrylate plus ethiodized oil. (A, B) B1 (blue arrow) was embolized. (C, D) B2 (orange arrow) was embolized. (E, F) B3 (green arrow) was embolized.(G, H) B4 (yellow arrow) was embolized.

Discussion

PWS often occurs sporadically and is associated with loss-of-function mutations in the *RASA1* gene [5], which encodes the p120-Ras GAP protein responsible for controlling cellular proliferation and differentiation [6]. The *RASA1* gene is also associated with cerebral AVMs [4], and spinal AVMs are associated with PWS [7]. The patient's past SAH was not caused by a cerebral AVM but by a posterior communicating internal carotid artery aneurysm. A skin biopsy of the affected limb could have revealed a pathogenic variant of *RASA1* [8]; however, this was not performed in this patient.

In Japan, giant AVM in a limb has been designated by the Ministry of Health, Labour, and Welfare as an "intractable disease." The estimated number of Japanese patients with giant AVM in a limb is 700 [9] and the Japanese prevalence rate is 0.56 patients per 100,000 people. Therefore, we searched PubMed for case reports of giant AVM associated with PWS to improve our understanding. We found 15 case reports and 15 clinical cases stage III and IV of Shobinger's classification when we searched with the terms "(Parkes Weber Syndrome)"

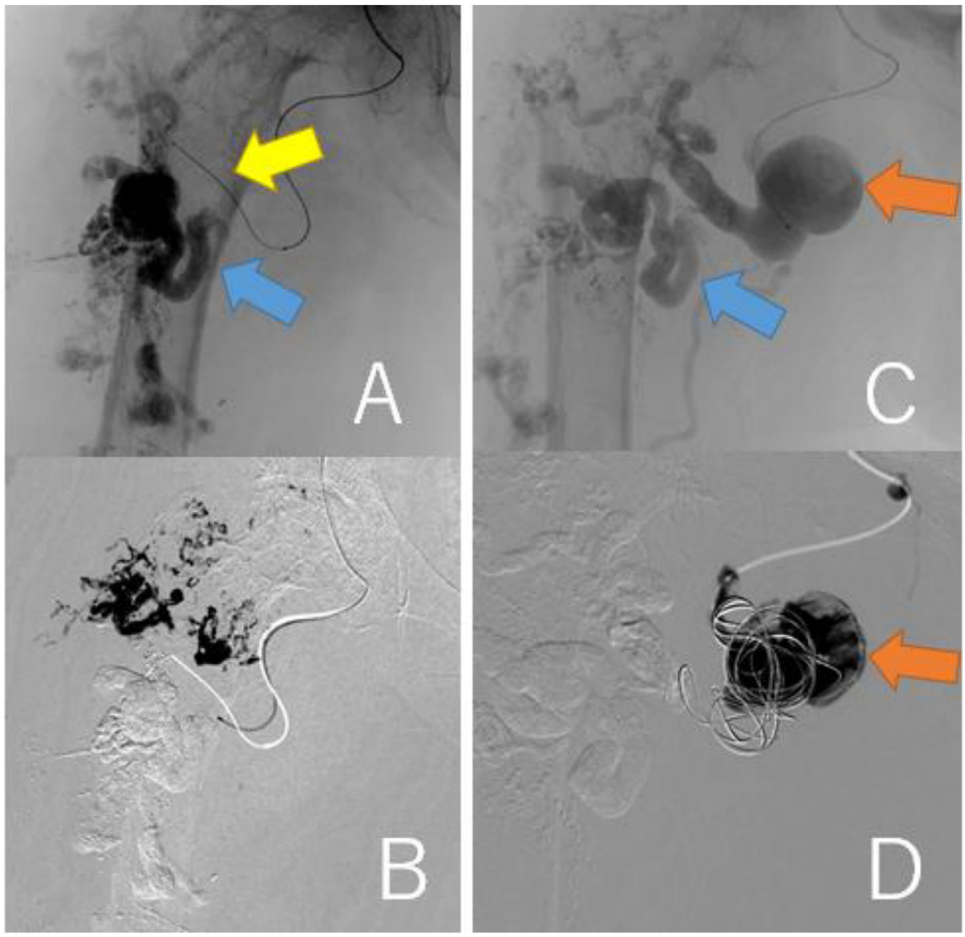

Fig. 4 – Findings of the third embolization. (A, B) B4 (yellow arrow) was embolized with NBCA plus ethiodized oil. Blue arrow represents B1. (C, D) A saccular B2 arterial aneurysm (20 × 17 × 27 mm, orange arrow) was embolized with Target® XXL360 coils (Stryker, Michigan, U.S.A.) (24 mm × 50 cm × 2) and NBCA plus ethiodized oil.

(Table 2). The number of female patients was almost equal to the number of male patients (7 female cases and 8 male cases). In 2 cases [19,23] stage IV AVM was observed in the neonate. The most common AVM site was the lower limb (11 lower limb cases and 4 upper limb cases), and no bilateral lesions were reported. Embolization [12,13,16,19–21,24] was the most common therapy for giant AVM, but it was not effective in more than half cases [13,16,21,24].

PWS is a progressive disease with a poor prognosis. Therefore, multidisciplinary therapy is needed for the management of giant AVM. Patients in the quiescent stage (I) or expansion stage (II) of the Schobinger clinical classification have fewer symptoms and are often treated conservatively with bed rest, elevation, and compression of the affected limb. In contrast, patients in the destructive stage (III) and decompensation stage (IV) have severe and life-threatening conditions, and invasive treatments such as sclerotherapy, embolization of the feeding arteries and draining veins [3], and major amputation or disarticulation of the affected limb [15] are required. During embolization, the feeding arteries should be occluded distally close to the shunt and not proximal to the shunt. Otherwise, the shunt may remain patent, and collateral recruitment may develop into a shunt. Thus, embolization should be as selective as possible for shunts where the feeding arteries and drainage veins are abnormally connected. Amputation should be considered in cases of unsuccessful embolization. Amputation of the limb affected by a giant AVM can cause massive hemorrhage. Ismail [25] and Young [26] employed partial cardiopulmonary bypass to minimize hemorrhage.

Reports of pseudoaneurysm formation after coil embolization and persistent pseudoaneurysm are few. Pathological dilated vascular wall [24] of AVM or radial force of coils might induce recanalization of coiled aneurysm. The unleashed edge of coil might disrupt the fragile vascular wall, leading to rapid growth of pseudoaneurysm. Moreover, collateral vessels or migration of the embolized coils might help develop persistent pseudoaneurysm [27]. Pseudoaneurysm can be diagnosed by ultrasound. A swirling pattern inside the false lumen by the color-flow image, and ‘‘to-and-fro’’ waveform at the communicating point between the native vessel and the false lumen are characteristic of pseudoaneurysm [28]. Contrast enhanced CT can distinguish pseudoaneurysm from ruptured aneurysm. While the contrast increases and changes its shape in the active bleeding, pseudoaneurysm maintains its shape on delayed phase. Moreover, pseudoaneurysm may not always fill with contrast due to the presence of thrombus [29].

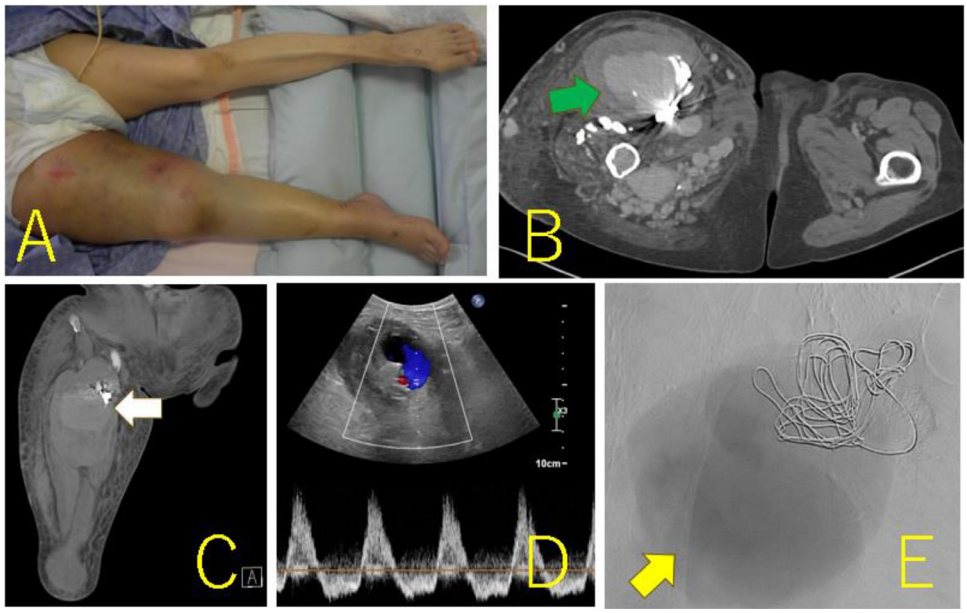

Fig. 5 – The photograph and imaging findings on admission to our hospital. (A) The right thigh was swollen, was twice as large as the left leg, and had red skin lesions. (B, C) Axial (B) and coronal (C) contrast-enhanced computed tomography revealing a giant aneurysm (green and white arrows) (97 x 71 x 154 mm) next to the coils. (D) Ultrasonography of the limb arteries shows a to-and-fro waveform between the giant aneurysm and the coiled B2 arterial aneurysm, suggesting that the giant aneurysm was a pseudoaneurysm. (E) Digital subtraction angiography image showing the pooling of the contrast agent in the giant pseudoaneurysm (yellow arrow).

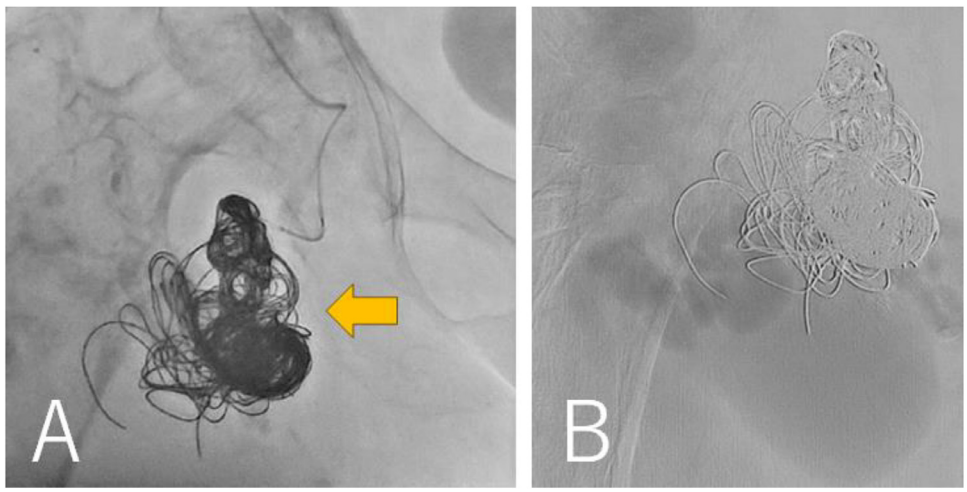

Fig. 6 – Findings during the latest embolization procedure. (A) The coiled B2 arterial aneurysm was embolized with additional 12 coils (orange arrow). (B) Digital subtraction angiography showed that the blood flow into the pseudoaneurysm disappeared.

Our patient's giant AVM was fed by the profunda femoris artery and superior and inferior gluteal arteries, and invaded the right ischial bone. If this patient had wished for an additional procedure, re-embolization would not have controlled the life-threatening giant pseudoaneurysm again, so we would have proceeded to perform an orthopedic procedure as a last resort. In this case transfemoral amputation and hip disarticulation are challenging because the pseudoaneurysm is located proximal to the pelvis and the procedure involves complex vascular ligation techniques with massive hemorrhage. Therefore, we would have performed transpelvic hemi-amputation (hemipelvectomy). This procedure is invasive and technically demanding, but it can ligate the unilateral common iliac artery and vein safer [30] and eradicate both the pseudoaneurysm and giant AVM.

Herein, we describe a rare case of pseudoaneurysm formation after embolization of a giant AVM of the lower limb associated with PWS. Embolization may be a safer and more ef-

Table 2 – Summary of 15 reported cases of a giant AVM associated with Parkes Weber syndrome.

Author, country	Age/Sex	AVM Site	Previous AVM treatments	Symptoms and conditions	Treatments	Outcomes
Yamamoto, Japan [10]	23/M	Right lower leg	-	Lower leg fracture	Cast immobilization	Union of the fractures at 2 years and 3 months after injury.
Dubrey, U.K. [11]	21/F	Right thign and leg	Surgical interventions	Skin bleeding	Compressive therapy	Unknown
Plasencia, U.S.A. [12]	37/M	Right upper arm	-	Skin ulcer	Embolization	Uneventful, but long term follow-up is unknown
Yahata, Japan [13]	23/M	Left leg	Embolization	Limb ischemia and skin ulcer	Amputation	Uneventful more than 2.5 years
Stefanov-Kiuri, Spain [14]	77/F	Left forearm	-	Skin ulcer	Compressive therapy and local wound care	Unknown
Kondapavuluri, India [15]	32/F	Right leg	-	Skin bleeding ulcer	Disarticulation	Unknown
Espitia, France [16]	61/M	Left thigh	-	Heart failure	Embolization	Death at day 40
Chagas, Brazil [17]	21/F	Left leg	Surgical intervention	Skin ulcer, joint pain and claudication	Compressive therapy	Uneventful, but long term follow-up is unknown
Sharma, India [18]	17/M	Left thigh to leg	-	Skin plaques, varicose veins and erosions	Compressive therapy and topical emollients	Improvement after 1 month of follow-up
Anzina, Latvia [19]	Neonate /F	Left scapula and shoulder	-	Heart failure	Embolization of AVM and occ|usion of PDA	Stable at the age of 16 months.
Zhao, China [20]	18/F	Right leg	-	Hypertrophic stains	Embolization	No sign of recurrence 2 years after the procedure
Acar, Turkey [21]	15/M	Left upper arm	Embolization	Heart failure	Implantation of covered stents	Recurrence of heart failure 6 months after the intervention
Patel, U.S.A. [22]	20/F	Left thigh	-	Pain of the thigh	Analgesics	Unknown
Peñalver, U.S.A. [23]	Neonate/ M	Left upper arm	-	Heart failure	Surgical banding	Improvement over the course of several months.
Yamamoto, Japan [24]	51/M	Right buttock and pelvis	Surgical ligation and embolization	Heart failure	Embolization	Death 1.5 years later
Present case, Japan	67/F	Right thigh	Embolization	Sudden swelling of the thigh and walking difficulty	Embolization of the aneurysm next to a pseudoaneurysm	Re-expansinon of the pseudoaneurysm 2 months after embolization

AVM, arteriovenous malformation; PDA, Patent ductus arteriosus.

fective option than surgery for high-flow AVMs [3] in terms of pain reduction and ulcer healing. However, as shown in Table 2, the effectiveness of embolization may be temporary. Repeated interventions are generally required for PWS, and strategies against PWS follow long and convoluted paths. The pathological findings of AVMs reveal that the malformed arterial wall consists of heterogeneous elastic fibers [31], indicating the possibility that AVMs and aneurysms can enlarge over time, even after embolization. When embolization of a giant AVM is ineffective, amputation and disarticulation of the affected limb should be considered as an eradication therapy.

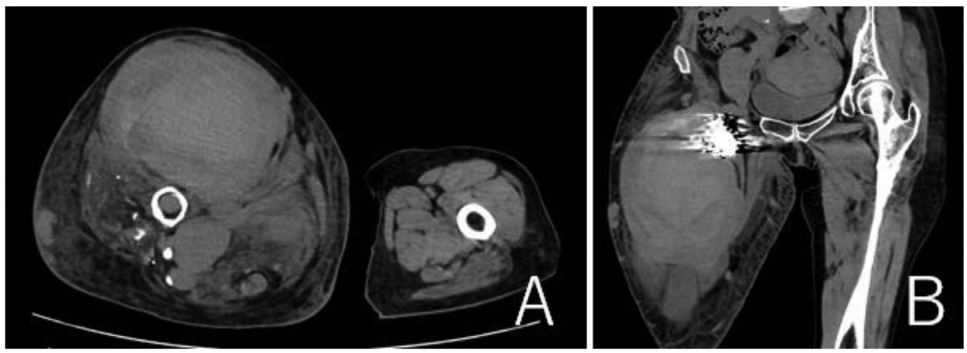

Fig. 7 – Findings of CT 2 month after discharge. (A, B) CT revealed more expanded pseudoaneurysm (131 x 107 x 180 mm).

Conclusion

The treatment of a giant AVM of the lower limb associated with Parks follows a long and convoluted path. When embolization is ineffective, an orthopedic procedure should be considered.

Author contributions

Study conception: HY
Data collection: HY
Writing: HY, KT, TK
Critical review and revision: All authors.
Final approval of the article: All authors.
Accountability for all aspects of the work: All authors.

Patient consent

The patient's identity was protected, and informed consent was obtained from the patient for the publication of this report.

REFERENCES

[1] Weber P. Angioma-formation in connection with hypertrophy of limbs and hemi-hypertrophy. Brit J Dermatol 1907;19:231–5.
[2] Gilbert P, Dubois J, Giroux MF, Soulez G. New treatment approaches to arteriovenous malformations. Semin Intervent Radiol 2017;34(3):258–71. doi:10.1055/s-0037-1604299.
[3] Ornelas-Flores MC, Rojas-Reyna GA, Hinojosa-Gutiérrez CG, Leo SG. Endovascular management of a complex high-flow lower limb arteriovenous malformation: case report and literature review. Cir Cir 2021;89(S1):14–19. doi:10.24875/CIRU.20000802.
[4] Cho SK, Do YS, Shin SW, Kim DI, Kim YW, Park KB, et al. Arteriovenous malformations of the body and extremities: analysis of therapeutic outcomes and approaches according to a modified angiographic classification. J Endovasc Ther 2006;13(4):527–38. doi:10.1583/05-1769.1.
[5] Boon LM, Mulliken JB, Vikkula M. RASA1: variable phenotype with capillary and arteriovenous malformations. Curr Opin Genet Dev 2005;15(3):265–9. doi:10.1016/j.gde.2005.03.004.
[6] Girón-Vallejo O, López-Gutiérrez JC, Fernández-Pineda I. Diagnosis and treatment of Parkes Weber syndrome: a review of 10 consecutive patients. Ann Vasc Surg 2013;27(6):820–5. doi:10.1016/j.avsg.2013.01.001.
[7] Li ZF, Li Q, Xu Y, Hong B, Huang QH, Liu JM. Spinal arteriovenous malformation associated with Parkes Weber syndrome: report of two cases and literature review. World Neurosurg 2017;107:1043.e7–1043.e13. doi:10.1016/j.wneu.2017.06.080.
[8] Flores Daboub JA, Grimmer JF, Frigerio A, Wooderchak-Donahue W, Arnold R, Szymanski J, et al. Parkes Weber syndrome associated with two somatic pathogenic variants in RASA1. Cold Spring Harb Mol Case Stud 2020;6(4):a005256 25. doi:10.1101/mcs.a005256.
[9] Japan Intractable Diseases Information Center. https://www.nanbyou.or.jp/entry/4630 (Accessed July 17, 2024.)
[10] Yamamoto H, Muneta T, Asahina S, Furuya K, Suzuki K. Lower leg fracture with Parkes-Weber syndrome complicated by disseminated intravascular coagulation. J Orthop Trauma 1995;9(5):449–52. doi:10.1097/00005131-199505000-00016.
[11] Dubrey SW, Hillson R, Dahdal M. High output heart failure caused by extensive arteriovenous malformation: problems and pregnancy. BMJ Case Rep 2009;2009 bcr07.2008.0546. doi:10.1136/bcr.07.2008.0546.
[12] Plasencia AR, Santillan A. Giant arteriovenous fistula in Parkes Weber syndrome. J Vasc Surg 2014;60(1):233. doi:10.1016/j.jvs.2013.08.041.
[13] Yahata T, Takeuchi A, Yoshida S, Tsuchiya H. Distinctive features of stump volume change in a fresh lower limb amputee with Parkes-Weber syndrome. BMJ Case Rep 2014;21:bcr2014206315 2014. doi:10.1136/bcr-2014-206315.
[14] Stefanov-Kiuri S, Fernandez-Heredero A. Images in clinical medicine. Parkes Weber syndrome. N Engl J Med 2014;371(22):2114 27. doi:10.1056/NEJMicm1312948.
[15] Kondapavuluri BK, Bharadwaj RN, Shaikh S, Chand A, Chaturvedi V. Parkes weber syndrome involving right lower limb: a case report. Indian J Surg 2015;77(Suppl 1):130–4. doi:10.1007/s12262-014-1201-8.
[16] Espitia O, Connault J, Hamidou MA. A rare case of worsening of Parkes-Weber syndrome with development of POEMS syndrome. Br J Haematol 2016;175(4):558. doi:10.1111/bjh.14318.
[17] Chagas CAA, Pires LAS, Babinski MA, Leite TFO. Klippel-Trenaunay and Parkes-Weber syndromes: two case

reports. J Vasc Bras 2017;16(4):320–4. doi:10.1590/1677-5449.005417.
[18] Sharma R, Gupta M, Thakur S, Gupta A. Parkes Weber syndrome presenting as Stewart-Bluefarb acroangiodermatitis. BMJ Case Rep 2019;12(3):e227793. doi:10.1136/bcr-2018-227793.
[19] Auzina L, Skuja E, Janis Safranovs T, Ozolins V, Kidikas H, Taurina G, et al. A giant arteriovenous malformation and fistula in a newborn with Parkes Weber syndrome. Case Report. Acta Med Litu 2020;27(2):90–9. doi:10.15388/Amed.2020.27.2.7.
[20] Zhao Q, Liu L, Liao Z, Pan Y, Liu J, Jiang X. Ethanol combined with coil embolisation for the treatment of arteriovenous malformations in a patient with Parkes Weber syndrome. Ann R Coll Surg Engl 2020;102(3):e54–6. doi:10.1308/rcsann.2019.0146.
[21] Acar Z, Kırış A, Bektaş H, Erden T. Short- and mid-term effects of covered stent implantation on extremity findings and heart failure in Parkes Weber syndrome: a case report. Eur Heart J Case Rep 2020;4(2):1–4. doi:10.1093/ehjcr/ytaa046.
[22] Patel R, Durant EJ, Freed R. Parkes-Weber syndrome in the emergency department. BMJ Case Rep 2021;14(9):e241649. doi:10.1136/bcr-2021-241649.
[23] Peñalver JM, Bennett JT, Nelson Z, Bly RA, Perkins JA, Bull CV, et al. Computational fluid dynamics modeling aiding surgical planning in a toddler with Parkes Weber syndrome. J Pediatr Surg Case Rep 2021;66:101780. doi:10.1016/j.epsc.2021.101780.
[24] Yamamoto H, Makiuchi M, Itamoto C, Hata H. An autopsy case of Parkes-Weber syndrome with high-output heart failure: hemodynamic alterations following treatment for arteriovenous fistulas. J Cardiol Cases 2022;26(2):118–21. doi:10.1016/j.jccase.2022.03.017.
[25] Ismail MS, Sharaf I, Thambidorai CR, Zainal A, Somasundaram S, Adeeb S, et al. Cardiopulmonary bypass in surgery for complex-combined vascular malformation of the lower limb: case report. Pediatr Surg Int 2005;21(5):392–5. doi:10.1007/s00383-005-1367-z.
[26] Lee YO, Hong SW. Treatment of large arteriovenous malformation in right lower limb. Korean J Thorac Cardiovasc Surg 2014;47(1):66–70. doi:10.5090/kjtcs.2014.47.1.66.
[27] Mann AJ, Rueda M, Azar F, Ramseyer M, Lottenberg L, Borrego R. Persistent pseudoaneurysm after non-operative management of a Grade 4 liver injury. Trauma Case Rep. 2023;48:100946. doi:10.1016/j.tcr.2023.100946.
[28] Corvino A, Catalano O, de Magistris G, Corvino F, Giurazza F, Raffaella N, et al. Usefulness of doppler techniques in the diagnosis of peripheral iatrogenic pseudoaneurysms secondary to minimally invasive interventional and surgical procedures: imaging findings and diagnostic performance study. J Ultrasound 2020;23(4):563–73. doi:10.1007/s40477-020-00475-6.
[29] Corvino F, Giurazza F, Ierardi AM, Lucatelli P, Basile A, Corvino A, et al. Splenic artery pseudoaneurysms: the role of ce-CT for diagnosis and treatment planning. Diagnostics (Basel) 2022;12(4):1012. doi:10.3390/diagnostics12041012.
[30] Ohta M, Masuda M, Wada H. A case-report of the voluminous chondrosarcoma in the pelvis removed by hemipelvectomy. Orthoped Traumatol; 18:17-20. https://www.jstage.jst.go.jp/article/nishiseisai1951/18/1/18_1_17/_article/-char/ja/(Accessed July 17, 2024.)
[31] Hori Y, Morii E, Hirose K. Important points for the new standards of diagnosis for vascular anomalies. Jpn J Diagn Pathol 2022;39:247–54. https://mol.medicalonline.jp/library/journal/download?GoodsID=cd9jjodp/2022/003904/001&name=0247-0254j&UserID=1100004887-01&base=jamas_pdf Accessed July 17, 2024.

Yasumura *et al.*
General Thoracic and Cardiovascular Surgery Cases (2024) 3:41
https://doi.org/10.1186/s44215-024-00166-2

General Thoracic and Cardiovascular Surgery Cases

CASE REPORT

Open Access

Horner's syndrome caused by the first rib fracture sustained during coronary artery bypass grafting: a case report and literature review

Hiroto Yasumura[1*], Koji Tao[1], Ryo Imada[1], Yushi Yamashita[1], Naoki Tateishi[1] and Tamahiro Kinjo[1]

Abstract

Background Horner's syndrome is a rare complication of cardiovascular surgery. A bone fragment and hematoma due to rib fracture after cardiac surgery may cause injury to the brachial nerve plexus and sympathetic nerve trunk, leading to neurologic disorders and Horner's syndrome. However, few reports have revealed the etiology of Horner's syndrome after cardiovascular surgery based on imaging. Herein we present a case in which a plain CT scan confirmed the etiology of Horner's syndrome after coronary artery bypass grafting (CABG), reviewing 139 CABG cases retrospectively in our hospital and 6 case reports of Horner's syndrome associated with cardiovascular surgery.

Case presentation A 69-year-old woman with a history of percutaneous coronary intervention and total abdominal hysterectomy with bilateral salpingo-oophorectomy had chest pain on exertion. Coronary angiography showed severe triple vessel disease. She underwent off-pump coronary artery bypass grafting (CABG). A median sternotomy was performed, and the split sternums were widened using a sternal retractor. The bilateral internal thoracic arteries were harvested. A triple CABG was performed. She had left shoulder pain after surgery. She complained of anhidrosis involving the left face and hyperhidrosis involving the right face from postoperative day (POD) 6. Left ptosis and blurry vision appeared after discharge from the hospital, for which she saw a neurologist in our hospital on POD 48. Miosis could not be clearly confirmed. She was diagnosed with Horner's syndrome. A plain CT scan revealed displaced fractures of the bilateral first ribs and left second rib. The bone fragment of the left first rib head was displaced 3 mm anteriorly compared to the left first rib head before surgery, which suggested that the fragment affected the stellate ganglion in the sympathetic trunk. The patient had regular follow-up evaluations. The anhidrosis persisted, but the ptosis improved, and the miosis was not confirmed at the 6-month follow-up evaluation.

Conclusions We should recognize that Horner's syndrome is one of the complications of cardiovascular surgery, especially CABG. Fracture of the first rib head with a displaced bone fracture was shown to be a contributor to ipsilateral Horner's syndrome. When symptoms of Horner's syndrome and other neurologic symptoms are noted after open heart surgery, a plain CT examination should be obtained.

Keywords Horner's syndrome, Rib fracture, Open heart surgery, Coronary artery bypass grafting

*Correspondence:
Hiroto Yasumura
hiroto1331255@yahoo.co.jp
[1] Department of Cardiovascular Surgery, Kagoshima Medical Center, 8-1, Shiroyamacho, Kagoshima, Kagoshima 892-0853, Japan

Background

Horner's syndrome is a rare complication of cardiovascular surgery. The triad of Horner's syndrome is ptosis, miosis, and anhidrosis, which leads to a lower aesthetic, visual, and hygienic quality of life [1]. The mean force of

median sternotomy is a remarkably forceful procedure, requiring forces from 150 to 300 N ($kg \cdot m/s^2$) in corpses [2] and leading to rib fracture. A bone fragment and hematoma due to rib fracture may cause injury to the sympathetic nerve trunk and brachial nerve plexus [3, 4], leading to Horner's syndrome and other neurologic disorders. However, few reports have revealed the etiology based on imaging. Herein we present a case in which a plain CT scan confirmed the etiology of Horner's syndrome after coronary artery bypass grafting (CABG), reviewing 139 CABG cases retrospectively in our hospital and 6 case reports of Horner's syndrome associated with cardiovascular surgery.

Case presentation

A 69-year-old woman with a history of percutaneous coronary intervention and a total abdominal hysterectomy with bilateral salpingo-oophorectomy had chest pain on exertion. Coronary angiography showed severe triple vessel disease. The SYNTAX score was 30, which favored CABG over percutaneous coronary intervention. She underwent off-pump CABG without anti-platelet respite. A pillow was placed under the back adjacent to the shoulder bones. A median sternotomy was performed, and the split sternums were widened using a sternal retractor (IMR15-710-J; Getinge, Gothenburg, Sweden) (Fig. 1A, B). Bilateral internal thoracic arteries (ITAs) were harvested with a Harmonic® scalpel (Johnson and Johnson, NJ, USA). A saphenous vein graft was also harvested. A triple CABG was performed. The respirator was withdrawn on postoperative day (POD) 1. Her recovery was uneventful, but she complained of left shoulder pain after the surgery. She also had anhidrosis involving the left face and hyperhidrosis involving the right face from POD 6. The pain persisted and was treated with acetaminophen. The patient had such a severe allergy to a contrast agent that myocardial scintigraphy was substituted for a postoperative coronary CT. A plain CT and MRI were not performed. The patient was discharged on POD 16. After discharge, in addition to anhidrosis involving the left face, left ptosis and blurry vision appeared, for which she saw a neurologist in our hospital on POD 48 (Fig. 2A). Miosis could not be clearly confirmed. She was diagnosed with Horner's syndrome. A head MRI revealed no lesions around the medulla oblongata. The symptoms persisted and a plain CT scan on POD 76 revealed displaced fractures of the bilateral first ribs and left second rib (Fig. 2B), which were thought to be caused by rib retraction during the CABG. The bone fragment of the left first rib head was displaced 3 mm anteriorly compared to the left first rib head before surgery (Fig. 2C), which suggested that the fragment affected the stellate ganglion in the sympathetic trunk. The patient had regular follow-up evaluations. At the 6-month follow-up evaluation, the anhidrosis persisted, but the ptosis and blurry vision improved, and the miosis was not confirmed.

To elucidate the relationship between Horner's syndrome and the first rib fracture due to CABG using ITA in our hospital, we retrospectively researched 139 patients who underwent CABG using an ITA from January 2022 to February 2024 who were followed by coronary or plain CT scans within 2 months after CABG (Table 1). In all cases, the same sternal retractor (IMR15-710-J) was used. The bilateral ITAs, LITA, and RITA were used in 91, 44, and 4 patients, respectively. The types of rib fractures were categorized as displaced or non-displaced (infraction fracture), and the sites of rib fractures were divided into the head, neck, tubercle, and body. Among all patients who sustained rib fractures, no patient sustained more than one fracture per rib. Among 95 patients in whom the RITA was used, 31 (32.6%) patients sustained a right first rib fracture, and among 135 patients in whom the LITA was used, 37 (27.4%) patients sustained a left first rib fracture. Of both ribs, a

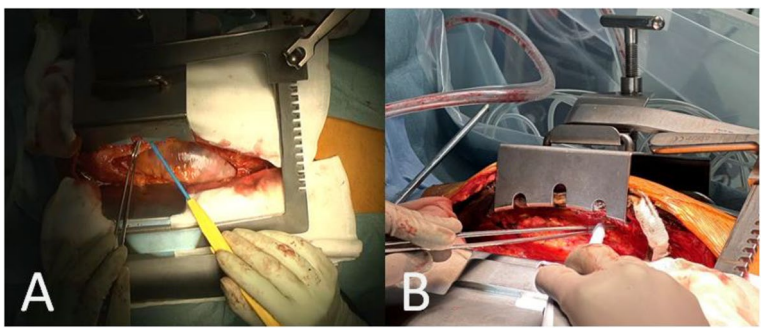

Fig. 1 Finding of LITA harvesting (These are pictures of reference and irrelevant to the patient described herein). **A** A median sternotomy was performed and the split sternums were widened using a sternal retractor (IMR15-710-J; Getinge, Gothenburg, Sweden). The maximum chest opening width of this retractor is 130 mm. This is a picture of reference and irrelevant to the patient described herein. **B** Rib retraction can be adjusted by a screw. The maximum movement range of the screw is 70 mm

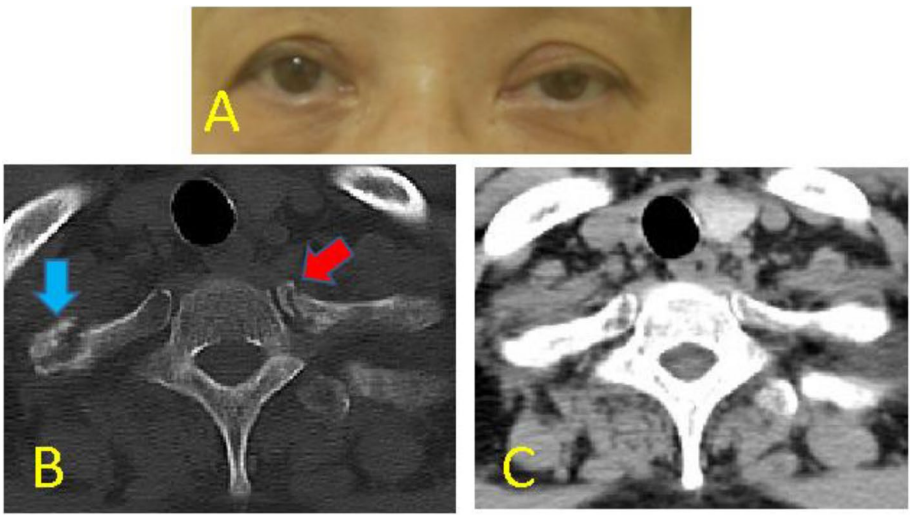

Fig. 2 Findings before and after CABG. **A** Left ptosis appeared after discharge and she was diagnosed with Horner's syndrome on postoperative day (POD) 48. **B** Plain CT scan on POD 76 revealed displaced fractures of the right first rib neck (blue arrow) and the left first rib head (red arrow). **C** Plain CT scan before CABG. Compared to this image, the bone fragment of the left first rib head (**B**, red arrow) was shown to be displaced 3 mm anteriorly, which suggested that the fragment affected the stellate ganglion in the sympathetic trunk

Table 1 The first rib fracture after CABG using the ITA in our hospital (2022.1∼2024.2)

			Right				Left			
	Harvested ITA		95				135			
	Site		Head	Neck	Tubercle	Body	Head	Neck	Tubercle	Body
First rib fracture	Type	Displaced	0	0	1	1	1 (this case)	0	0	8
		Non-displaced (infraction)	3	10	0	16	4	5	6	13
	Total		31				37			

ITA Internal thoracic artery

fracture of rib body was most frequent (right, 54.8%; left, 56.8%). Although 8 (5.8%) of 139 patients sustained the first rib head fracture, only the patient described herein (0.72%) developed Horner's syndrome.

Discussion

Horner's syndrome results from damage to the ipsilateral oculosympathetic pathway. Lung, breast, and mediastinum tumors, as well as neck injuries may cause the syndrome due to direct compression of the oculosympathetic pathway [5]. However, cardiovascular surgery can also cause Horner's syndrome. Only six case reports [1, 6–10] of Horner's syndrome due to cardiovascular surgery were identified on a search of the literature (Table 2), which may in part be because the symptoms of Horner's syndrome do not always appear simultaneously and are sometimes too mild to be noticed. Left-sided Horner's syndrome was attributed to CABG in three cases [1, 6, 10] and the current case, and left lateral thoracotomy operation in two case [7, 8]. In most cases, the firstly recognized Horner's symptom was ptosis and the onset day was within 2 days after the operation. Generally speaking, Horner's syndrome caused by trauma is immediately diagnosed after a traumatic event, but the symptoms can be shown in a delayed manner [11], as in the current case. In some cases, the symptoms resolved spontaneously or with medication.

A sternal retractor, especially one for harvesting the ITAs, can cause rib fractures. Kimura [12] reported up to five fractures of the left upper rib after CABG using the left ITA (LITA). Rib retraction for harvesting ITAs after a median sternotomy exerts leverage on ribs like a nail puller. Specifically, the rib tubercle, split sternum, and rib head are the fulcrum, point of force, and point of action, respectively (Fig. 3). The rib head and neck are fixed by the costovertebral joint and costotransverse ligament, respectively. A sternal retractor for ITA harvesting is often placed at an upper position across the sternal angle. Forceful retraction during harvesting an ITA can exert excessive work according to the principle of leverage,

Table 2 Case reports of Horner's syndrome caused by cardiovascular surgery

Author and year of publication	Age (years)	Sex (M/F)	Affected side	Surgery	Incision	Used ITA	The first symptom and the onset day	Findings on radiology	Treatment and course
Imamaki et al. in 2006 [1]	70	F	Left	Off-pump CABG	Median sternotomy	BITA	Ptosis on POD2	No data	Spontaneous remission 1 month after the surgery
Murakami et al. in 2007 [6]	77	F	Left	MAP + CABG	Median sternotomy	LITA	Ptosis, miosis, and enophthalmos on POD2	Fracture of left 1st rib on chest X-ray	Spontaneous remission 6 months after the surgery
Tsuchiya et al. in 2013 [7]	0 (1 month)	F	Left	PA banding + PDA closure	Left lateral thoracotomy	No use	Ptosis just after the operation	No data	Transconjunctival resection of Muller muscle 1.5 years after the surgery
Nasser et al. in 2015 [8]	0 (9 months)	F	Left	Division of vascular ring	Left lateral thoracotomy	No use	Ptosis, miosis, and enophthalmos on POD2	No data	No remission 7 days after the surgery
Aslankurt et al. in 2021 [9]	9	M	Right	VSD, aortic and mitral valve repair	Median sternotomy	No use	Ptosis on unknown day	No data	No remission 4 months after the surgery
Gopinath et al. in 2021 [10]	56	M	Left	CABG	Median sternotomy	No data	Unknown symptom on POD1	Infraction fracture of left 1st rib head on CT	Remission with Anti-immflammatories and steroids
This case in 2024	69	F	Left	Off-pump CABG	Median sternotomy	BITA	Anhidrosis on POD6	Displaced fracture of 1st rib and left 2nd rib on plain CT	Anhidrosis remained, but ptosis improved 6 months after the surgery

CABG Coronary artery bypass grafting, *MAP* Mitral annuloplasty, *PA* Pulmonary artery, *PDA* Patent ductus arteriosus, *ITA* Internal thoracic artery, *BITAs* Bilateral internal thoracic arteries

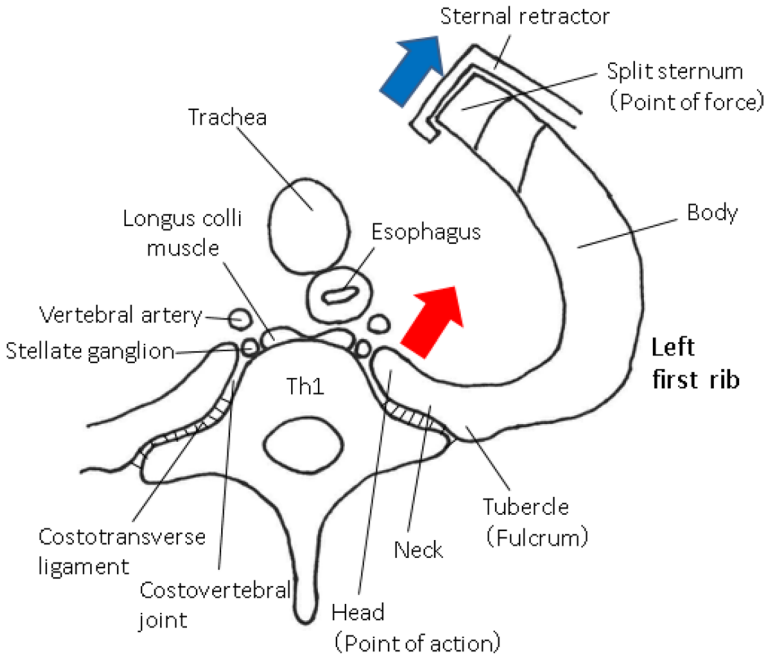

Fig. 3 Schema for the mechanism underlying rib fracture. Forceful retraction (blue arrow) can exert excessive work according to the principle of leverage (red arrow), leading to a fracture at the point of action (rib head). If the rib is fragile, the power of excessive retraction may be conducted to the point of action, resulting in disruption of the leverage principle and fracture between the fulcrum (rib tubercle) and point of force (split sternum)

leading to fracture of the point of action (head of the first rib). If the rib is fragile, the power of excessive retraction may focus on the point of action, resulting in disruption of the principle of leverage and a fracture between the fulcrum (rib tubercle) and the point of force (split sternum). The rib fracture on CABG will incur more bleeding because perioperative anti-platelet drug therapy is a cornerstone of CABG. A displaced fracture and the ensuing bleeding could lead to injury of the surrounding organs and a hemothorax.

A dislocation fracture of the costovertebral joint has been reported to cause injury to the intercostal artery and azygos vein, leading to a hematoma [13]. In the same way, a bone fragment of the first rib and subsequent hematoma is considered to directly or indirectly compress brachial nerve plexus and stellate ganglion [3, 4, 12] (Fig. 4). The stellate ganglion, which is a second-order neuron of the oculosympathetic pathway, is located on the ventral surface of the first rib head [14] (Fig. 3). The left stellate ganglion is more densely surrounded than the right ganglion by the vertebral artery, esophagus, longus colli muscle, vertebral body, and left rib head, which might explain why Horner's syndrome occurs more often on the left side after open heart surgery. In addition, the LITA is used more frequently than the right ITA (RITA) during CABG for its good patency.

Horner's syndrome complicates all open heart surgery in 0.6–1.7% of cases [3, 16–18] and 0.2–7.7% of CABG cases [19–21]. We retrospectively reviewed 139 CABG cases, among which 8 patients (5.8%) sustained the first rib head fracture (Table 1). Among those 8 patients, only the patient with displaced fracture described herein (0.72%) developed Horner's syndrome, and the other 7 patients with non-displaced fracture (infraction fracture) did not develop Horner's syndrome. This can not only graphically but also statistically prove that the displaced bone fracture of the first rib head and the ensuing inflammation and hematoma directly compress or injure the left stellate ganglion and lead to Horner's syndrome.

Horner syndrome after cardiovascular surgery may be a self-limiting complication based on the outcomes of 7 patients (Table 2), including the patient described herein. This finding can be in part because the inflammation and hematoma surrounding the fracture improved over time and the injured neuron recovered spontaneously. However, we should take Horner syndrome into account as a preventable complication. Minimum sternal widening and careful manipulation of a sternal retractor may prevent iatrogenic Horner's syndrome [6]. The incidence of first rib fractures due to median sternotomy has been reported to decrease when the sternal retractor is placed at a lower position [3].

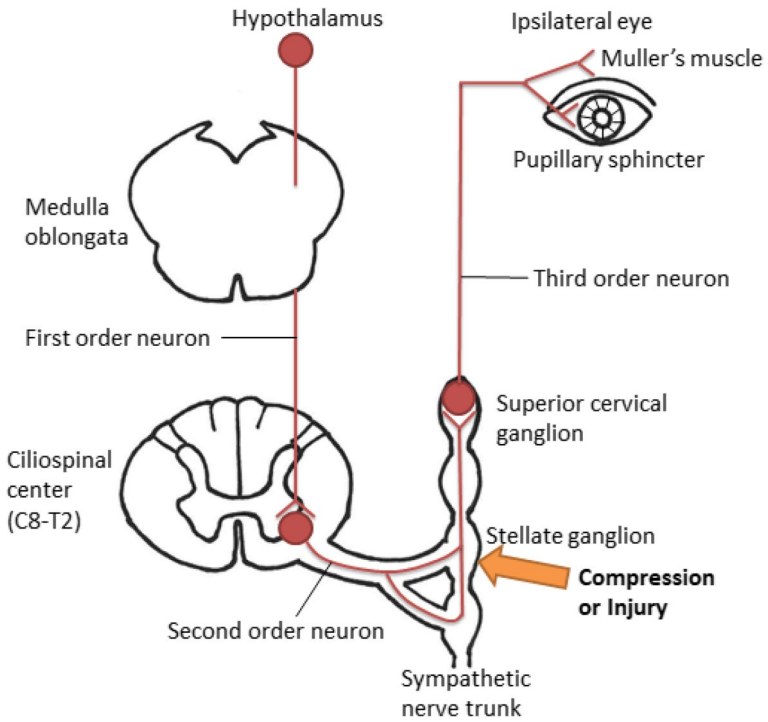

Fig. 4 Schema involving the mechanism underlying Horner's syndrome due to fracture of the first rib head. A bone fragment of the first rib head and subsequent hematoma can compress or injure the stellate ganglion (orange arrow), which is a second-order neuron of the oculosympathetic pathway, leading to Horner's syndrome. Copyright© 2011, Medic Media. Reproduced with permission from Institute for Health Care Information Sciences ed. *Medical Disease: An Illustrated Reference Guide. vol. 7 Neurology and Neurosurgery*. 1st ed. Tokyo, Japan: Medic Media; 2011 [15]

From the viewpoints of the retraction blade, a sternal retractor for harvesting the ITAs is mainly divided into two types: Takedown pattern retractor and French pattern retractor (Fig. 5). There are no reports comparing the two retractors in the literature. A sternal retractor can be equipped with foil load sensors to measure the force distribution over the retractor blades [2]. Therefore, further research for the relation among retraction force, chest opening width, harvesting time, and orthopedic and neurological complications for each retractor is expected, which may lead to a decrease in the complications by retractors.

Conclusion

We should recognize that Horner's syndrome is one of the complications of cardiovascular surgery, especially CABG. Fracture of the first rib head with a displaced bone fracture is a contributor to ipsilateral Horner's syndrome. When symptoms of Horner's syndrome and other neurologic symptoms are noted after cardiovascular surgery, a plain CT examination should be obtained.

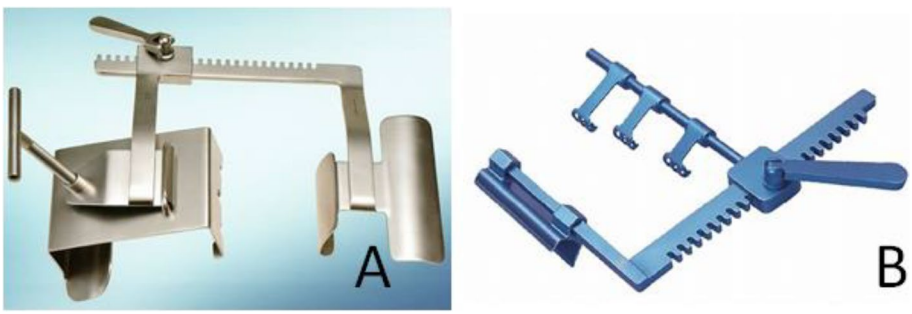

Fig. 5 Two types of sternal retractor for harvesting the ITAs. **A** Takedown pattern retractor (IMR15-710-J; Getinge, Gothenburg, Sweden). **B** French pattern retractor (SCT70026 Sternal-IMA Retractor, M A Corporation, Chiba, Japan)

Abbreviations

CABG	Coronary artery bypass grafting
PCI	Percutaneous coronary intervention
ITA	Internal thoracic artery
POD	Postoperative day
LITA	Left internal thoracic artery
RITAs	Right internal thoracic arteries

Acknowledgements
We would like to thank cardiologist Kento Tagata for the perioperative examination and treatment, and orthopedist Hisashi Sameshima for image diagnosis.

Authors' contributions
T.K., K.T., and H.Y. performed the cardiac surgery. H.Y. drafted the manuscript. K.T. and T.K. supervised manuscript preparation. All authors contributed to patient treatment. All the authors read and approved the final manuscript.

Funding
There are no sources of funding.

Availability of data and materials
There are no additional data to disclose.

Declarations

Ethics approval and consent to participate
Not applicable.

Consent for publication
Informed consent was obtained from the patient for publication of this case report and accompanying images.

Competing interests
The authors declare that they have no competing interests.

Received: 20 April 2024 Accepted: 30 August 2024
Published online: 10 September 2024

References

1. Imamaki M, Ishida A, Shimura H, et al. A case complicated with Horner's syndrome after off-pump coronary artery bypass. Ann Thorac Cardiovasc Surg. 2006;12(2):113–5.
2. Aigner P, Eskandary F, Schlöglhofer T, et al. Sternal force distribution during median sternotomy retraction. J Thorac Cardiovasc Surg. 2013;146(6):1381–6.
3. Vander Salm TJ, Cereda JM, Cutler BS. Brachial plexus injury following median sternotomy. J Thorac Cardiovasc Surg. 1980;80:447–52.
4. Grocott HP, Clark JA, Homi HM, et al. "Other" neurologic complications after cardiac surgery. Semin Cardiothorac Vasc Anesth. 2004;8:213–26.
5. Kanagalingam S, Miller NR. Horner syndrome: clinical perspectives. Eye Brain. 2015;10(7):35–46.
6. Murakami T, Kato H, Makino Y. A case of Homer's syndrome after coronary artery bypass graft surgery. Jpn J Cardiovasc Surg. 2007;36(5):273–6.
7. Tsuchiya A, Sakurai H, Tsuzuki K. Horner syndrome following cardiac surgery in a child. Jpn J Clin Ophthalmol. 2013;67(5):755–7.
8. Nasser BA, Mesned A, Moazamy YE, et al. Horner's syndrome after paediatric cardiac surgery: case report and review of the literature. Cardiol Young. 2015;25(3):569–72.
9. Aslankurt M, Aslan L. Horner's syndrome secondary to heart surgery in a pediatric patient. Saudi J Ophthalmol. 2020;34(4):303–5.
10. Gopinath P, Seetharaman C, Senthilkumar E, et al. Postoperative Horner's syndrome following CABG - an unusual complication: case report. Eurorad; 2021. Case 17545. https://www.eurorad.org/case/17545. Accessed 4 Sep 2024.
11. Ryu S, Won S, Lee SY, et al. Delayed Horner's syndrome after multiple penetrating stab injury of the neck. Ear Nose Throat J. 2022:1455613221125920. https://journals.sagepub.com/doi/epub/10.1177/01455613221125920. Accessed 4 Sep 2024.
12. Kimura M, Yoshimura H, Kohara N. Lower trunk brachial plexopathy due to hematoma following median sternotomy: a case report. Rinsho Shinkeigaku. 2020;60(11):758–61.
13. Takizawa K, Suzuki S, Ito S, et al. Vascular injury associated with fracture dislocation of a left costovertebral joint–a case of traumatic subcostohemiazygos fistula. Nippon Igaku Hoshasen Gakkai Zasshi. 1988;25(48):579–83.
14. Totoki T, Morimoto M, Taniguchi Y, et al. Anatomy of the stellate ganglion. J Jpn Soc Pain Clin. 1994;1:3–11.
15. Institute for Health Care Information Sciences, ed. Medical disease: an illustrated reference guide. vol. 7. In: Neurology and neurosurgery. 1st ed. Tokyo: Medic Media; 2011. p. 208.
16. Benecke R, Klingelhofer J, Rieke H, et al. Manifestations and course of brachial plexus injury following median sternotomy. Nervenarzt. 1988;59:388–92.
17. Rieke H, Benecke R, DeVivie ER, et al. Brachial plexus lesions following cardiac surgery with median sternotomy and cannulation of the internal jugular vein. J Cardiothorac Anesth. 1989;3:286–9.
18. Vahl CF, Carl I, Muller-Vahl H, et al. Brachial plexus injury after cardiac surgery. The role of internal mammary artery preparation: a prospective study on 1000 consecutive patients. J Thorac Cardiovasc Surg. 1991;102:724–9.
19. Lederman RJ, Breuer AC, Hanson MR, et al. Peripheral nervous system complications of coronary artery bypass graft surgery. Ann Neurol. 1982;12:297–301.
20. Shaw PJ, Bates D, Cartlidge NE, et al. Neuroophthalmological complications of coronary artery bypass graft surgery. Acta Neurol Scand. 1987;76:1–7.
21. Barbut D, Gold JP, Heinemann MH, et al. Horner's syndrome after coronary artery bypass surgery. Neurology. 1996;46:181–4.

Publisher's Note

frontiers | Frontiers in Neurology

TYPE Original Research
PUBLISHED 27 August 2024
DOI 10.3389/fneur.2024.1424030

OPEN ACCESS

EDITED BY
Lukas Meyer,
University Medical Center
Hamburg-Eppendorf, Germany

REVIEWED BY
Gabriel Broocks,
Medical School Hamburg, Germany
Chao Zhou,
Nanjing University, China

*CORRESPONDENCE
Yuki Hamada
✉ sunamushi.elmonkichi@gmail.com

RECEIVED 08 May 2024
ACCEPTED 14 August 2024
PUBLISHED 27 August 2024

CITATION
Hamada Y, Matsuoka H, Sato S, Kawabata Y, Iwamoto K, Ikeda M, Sato T, Takaguchi G and Takashima H (2024) Combining the deployment of only the distal basket segment of the EMBOTRAP III and an aspiration catheter for M2 occlusions: the ONE-SEG technique.
Front. Neurol. 15:1424030.
doi: 10.3389/fneur.2024.1424030

Combining the deployment of only the distal basket segment of the EMBOTRAP III and an aspiration catheter for M2 occlusions: the ONE-SEG technique

Yuki Hamada[1]*, Hideki Matsuoka[1], Shinsuke Sato[2,3], Yutaro Kawabata[1], Kana Iwamoto[1], Mei Ikeda[1], Takeo Sato[1], Go Takaguchi[1] and Hiroshi Takashima[4]

[1]Department of Strokology, Stroke Center, National Hospital Organization Kagoshima Medical Center, Kagoshima, Japan, [2]Department of Neurosurgery, St. Luke's International Hospital, Tokyo, Japan, [3]Department of Neuroendovascular Therapy, St. Luke's International Hospital, Tokyo, Japan, [4]Department of Neurology and Geriatrics, Kagoshima University Graduate School of Medical and Dental Sciences, Kagoshima, Japan

Background: Endovascular therapy (EVT) for distal medium vessel occlusions requires prioritizing effectiveness and safety. We developed a technique combining the deployment of only the distal basket segment of the EMBOTRAP III and an aspiration catheter (AC) for M2 occlusions, called the "ONE-SEG technique," and evaluated its clinical and technical impacts.

Methods: This was a retrospective review of 30 consecutive patients with M2 segment middle cerebral artery occlusion treated using the ONE-SEG technique. This method involves deploying the EMBOTRAP III through a microcatheter in only one segment and guiding the AC to the M2 origin or distal M1. The rates of final-pass expanded thrombolysis in cerebral infarction (eTICI) scores of 2c/3 or 2b/2c/3, safety (symptomatic intracranial hemorrhage [sICH]), and clinical outcomes (modified Rankin Scale [mRS] score 0–2, 0–3 at 90 days, and mortality at 90 days) were evaluated.

Results: Of the 30 cases, 36.7% were female, and the mean age was 75.6 ± 11.0 years. The ONE-SEG technique was used for 17 cases (56.7%, median NIHSS 10 [5–15.5]) with primary M2 occlusion and 13 cases (43.3%, median NIHSS 20 [14–22.5]) with secondary M2 occlusion after proximal thrombus removal. The successful final reperfusion rate (eTICI 2b/2c/3) was 90% overall (27/30 cases). One case (3.3%) developed sICH with secondary M2 occlusion. At 3 months, mRS scores 0–2 were seen in 64.7% of patients with primary M2 occlusion (11/17 cases) and in 23.1% (3/13 cases) with secondary M2 occlusion.

Conclusion: EVT using the ONE-SEG technique appears to be safe and effective for M2 occlusion.

KEYWORDS

thrombectomy, stroke, M2 occlusion, intervention, MeVO, DMVOs

Introduction

The effectiveness and safety of endovascular therapy (EVT) for large vessel occlusion (LVO) in the anterior circulation have been established, and it is now considered standard treatment (1–5). However, questions still remain regarding the efficacy and safety of EVT for peripheral cerebral artery occlusions such as medium vessel occlusions (MeVOs), which account for 25–40% of all acute ischemic stroke cases (6). This is believed to be due to the challenges of medium cerebral artery occlusion treatment, since peripheral vessels are narrow, tortuous, and fragile, increasing the risk of bleeding complications associated with EVT. A meta-analysis of EVT for M2 occlusion by the HERMES collaboration reported modified thrombolysis in cerebral infarction (mTICI) 2b/3 in 58.2% and no symptomatic intracranial hemorrhage (ICH), but a mortality rate of 11.9% (7). Furthermore, a review of EVT for distal medium vessel occlusions (DMVOs) by Biljin et al. found mTICI 2b/3 in 77%, a symptomatic ICH rate of 5.7%, and a subarachnoid hemorrhage (SAH) rate of 8.3% (8), demonstrating a considerable risk of bleeding complications. Meanwhile, the TOPMOST registry suggested the potential benefit of EVT compared with best medical treatment with respect to early neurological improvement of P2 or P3 occlusions and reported a symptomatic ICH rate of 4.3% (9). Thus, for MeVOs and DMVOs, treatment prioritizing both effectiveness and safety is required.

Recently, evidence regarding the efficacy and safety of EVT for MeVOs and DMVOs has been increasing. Devices such as Tigertriever 13 (Rapid Medical, Yoqneam, Israel) (10), Mindframe Capture low profile (LP) device (Medtronic, Minneapolis, MN, USA) (11), Aperio (Acandis, Pforzheim, Germany) (12), Catch View mini (Catch View; Balt, Montmorency, France) (13), pREset LITE (phenoxGmbH, Bochum, Germany) (14), among others, have shown promising results for MeVO and DMVO treatment. This is presumed to be due to the improved performance and evolution of recent stent retrievers (SRs) and aspiration catheters (ACs), allowing devices to reach more peripheral vessels and achieve a good efficacy and safety profile.

However, there is a growing number of reports demonstrating safe and effective outcomes for MeVO or DMVO treatment by using modified existing SRs and ACs. Techniques such as the BEMP technique (15) and distal combined technique (16) are examples. In addition, results for the effectiveness and safety of semi-deployment of SRs for DMVO patients have also been reported (17). The EMBOTRAP III (CERENOVUS, Johnson & Johnson Medical Devices, Irvine, CA, USA) is an SR with a structure divided into five segments, designed to have a high thrombus capture rate and minimal resistance to the vessel. Its distal segment, called the distal basket, has a finely designed mesh at the tip, potentially capturing thrombi within it. This design, being only one segment, reduces the amount of metal deployed within the vessel and minimizes friction between the SR and the vessel wall, potentially contributing to fewer bleeding complications. A thrombectomy technique using only the distal basket segment of the EMBOTRAP III and an AC for M2, named the ONE-SEG technique, was evaluated, and the outcomes and technical parameters, such as hemorrhagic complications, SAHs, and spasm, of MCA M2 occlusion thrombectomy are reported.

Subjects and methods

Study design

This was a retrospective, cohort study. Data were extracted from the stroke database of our facility for patients who underwent EVT from April 2014 to March 2024. The retrospective selection criteria were as follows: (1) acute ischemic stroke (AIS) with a confirmed M2 occlusion on initial magnetic resonance imaging (MRI), or AIS with LVO treated with EVT, with distal occlusion; (2) National Institutes of Health Stroke Scale (NIHSS) score ≥ 1; (3) time from symptom onset to puncture of less than 24 h; and (4) EVT performed using the EMBOTRAP III device with the ONE-SEG technique. In addition, no definition has been established regarding whether M2 occlusion is LVO, MeVO, or DMVO. For convenience, M2 occlusion was not classified as LVO (which included the internal carotid artery or M1) in this paper, but as MeVO. This retrospective study was approved by the local ethics committee.

Embotrap III

The EMBOTRAP III reperfusion device is a dual-structure segmented SR designed to capture a wide range of thrombus compositions and adhere to the vessel wall during retrieval. The main design difference lies in the presence of closed-cell inner channels within the outer cage and distal mesh of closed cells at the tip, known as the distal basket. This design feature is expected to result in a high rate of successful revascularization in EVT (18). Whereas the distal basket is primarily designed to prevent distal embolization of thrombi, each basket is equipped with gaps called inlet windows to capture thrombi within the cage, including the distal basket, allowing for thrombus capture. An overview of the distal basket of EMBOTRAP III is shown in Figure 1.

Interventional protocol with the ONE-SEG technique

The thrombectomy procedure was performed using the Siemens ARTIS zee biplane angiography system (Siemens, Erlangen, Germany) under local anesthesia. Cerebral digital subtraction angiography (DSA) and EVT were performed via right femoral artery puncture in all cases. A balloon-guiding catheter (BGC) was placed in the internal carotid artery on the occlusion side using either an 8-Fr Optimo (Tokai Medical Products Inc., Aichi, Japan) or an 8-Fr Emboguard (CERENOVUS, Johnson & Johnson Medical Devices).

The ONE-SEG technique was performed in all cases using the EMBOTRAP III device in combination with an AC. First, a 0.021-inch microcatheter, Phenom21 (Medtronic, Minneapolis, MN, USA), was placed distally to the occluded vessel. The Phenom21 was advanced as distally as possible from the occlusion site to facilitate entry of the thrombus into the inlet window of the distal basket of the EMBOTRAP III. While attempting to advance the AC as far as possible to M2, if difficulty was encountered due to vessel tortuosity or size, it was positioned at the distal M1 for standby. AC size was selected by measuring the diameter of the occluded vessel in the frontal and

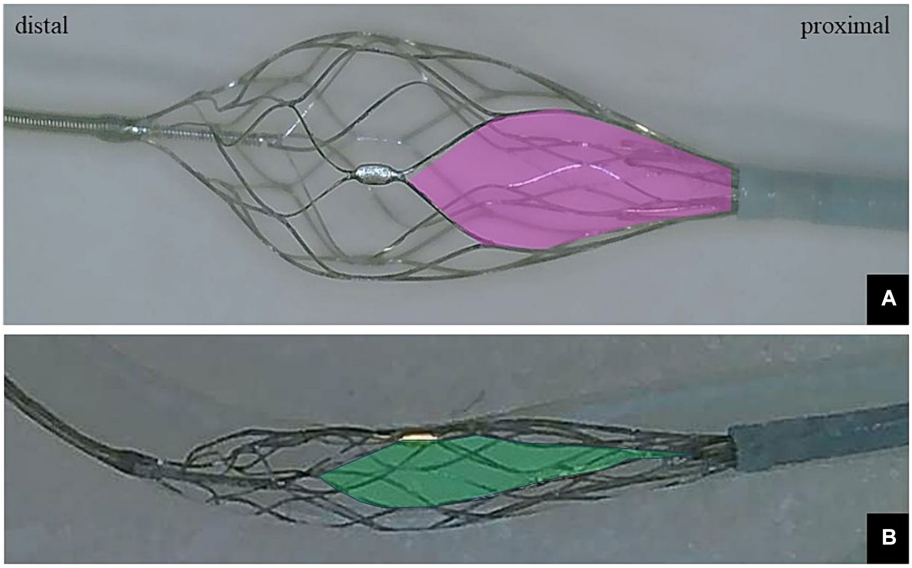

FIGURE 1
(A) Photograph showing only the distal basket of the EMBOTRAP III deployed. The inlet window (pink area) of the distal basket is designed to capture fragmentable thrombus. **(B)** Only the distal basket of the EMBOTRAP III is deployed in a vascular model that mimics a 2-mm-diameter M2. Compared to the inlet window in **(A)**, the inlet window (green area) in **(B)** extends in the long-axis direction.

lateral views on baseline angiography. Subsequently, only the distal basket of the EMBOTRAP III was deployed. As a guideline for deployment under fluoroscopy, deployment was performed up to the second marker from the tip. Next, aspiration was started using a commercially available aspiration pump via the AC. If the AC could be advanced to M2, the EMBOTRAP III was slowly pulled back and withdrawn into the AC. If the AC could only be advanced to the distal M1, both the AC and the EMBOTRAP III were pulled back to M1, and then the EMBOTRAP III was withdrawn into the AC. Figures 2, 3 show an example of the ONE-SEG technique in action, and Figure 4 shows the steps of the ONE-SEG technique with illustrations.

Clinical factors

Baseline clinical characteristics were collected for the following variables: sex, age, pre-stroke modified Rankin Scale (mRS) score, medical history (hypertension, dyslipidaemia, diabetes mellitus, current smoking, ischemic stroke, atrial fibrillation), admission systolic blood pressure, baseline NIHSS score, initial symptoms such as motor hemiparesis, sensory disturbance, and aphasia, baseline Alberta Stroke Program Early CT Score (ASPECTS) on diffusion-weighted imaging (DWI), time parameters (onset-to-door time, door-to-puncture time, puncture-to-recanalization time), treatment profile (intravenous thrombolysis), presentation type due to vascular occlusion (isolated M2 occlusion, tandem occlusion, multi-vessel M2 occlusion), M2 occlusion location (proximal, distal), M2 type (dominant, codominant, non-dominant), M2 division (superior, inferior, intermediate), M2 vessel diameter, type of AC used, and stroke etiology mechanism.

M2 definition

The MCA M2 segment is defined as the vessel from the bifurcation/branching of the middle cerebral artery (MCA) to the circular sulcus of the insula (19, 20). The proximal M2 is defined as the horizontal M2 segment within 1 cm from the bifurcation/branching of the MCA, and the distal M2 is defined as the Sylvian M2 segment from the bifurcation/branching to the circular sulcus of the insula (7, 20, 21). M2 dominance is defined as the M2 branch having a larger diameter than other branches or when the retrograde flow disturbance due to the occluded M2 branch is greater than 50% of the same MCA territory. Occluded vessels were considered co-dominant only when the diameters of the distal and proximal branches were equal, and the associated perfusion deficit was less than 50% of the MCA territory (22). Occlusions were classified based on their clinical scenarios: isolated M2 occlusion, tandem occlusion, or multi-vessel M2 occlusion. Tandem occlusion was defined as simultaneous large vessel/proximal occlusion with M2 occlusion. Multi-vessel M2 occlusion was defined as occlusion of the M2 superior trunk and M2 inferior trunk of the MCA on the same side.

Outcomes

Technical outcomes were defined as achieving expanded Thrombolysis in Cerebral Infarction (eTICI) scores (23) of 2c/3 and 2b/2c/3 in the target M2 segment. Safety outcomes included the presence of any parenchymal hematoma (PH) [PH type 1 or 2] based on hemorrhagic transformation criteria from the ECASS (24), any intracerebral hemorrhage (ICH), symptomatic ICH (defined as any ICH including those with an increase from the baseline NIHSS score ≥ 4 points based on ECASS II criteria), subarachnoid hemorrhage (SAH) (diffuse or focal within the territory of treated artery occlusion), extravasation (defined as extravascular leakage of contrast media), degree of spasm (defined as any degree of spasm in treated vessels), embolization to the same or different territory after thrombectomy, active perfusion deficits, and 90-day mortality. Imaging evaluation of ICH and SAH was done on day 1 with head

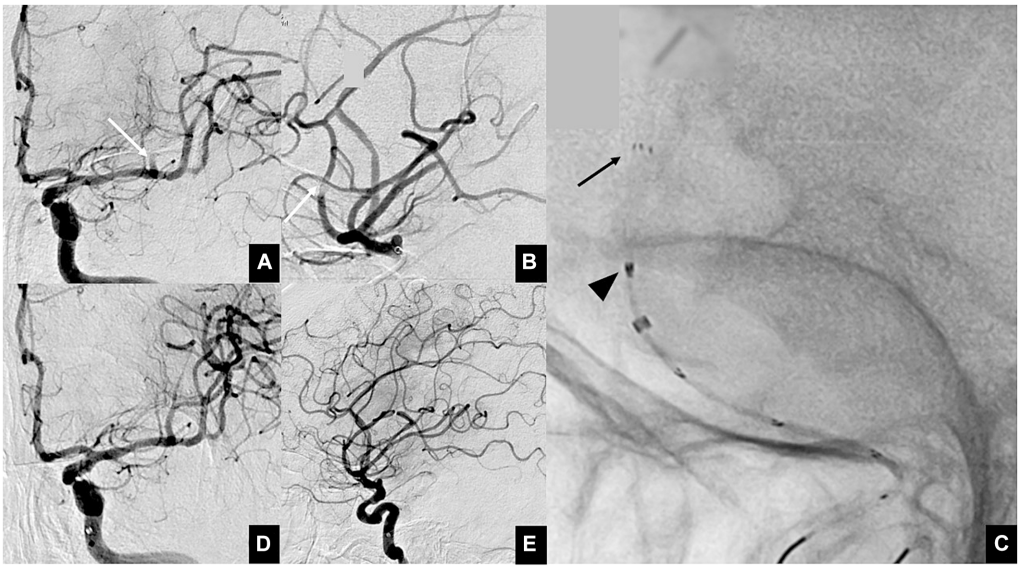

FIGURE 2
Illustrative cases of the ONE-SEG technique using an EMBOTRAP III to remove a clot. **(A)** Anterior view and **(B)** lateral view of multiple M2 occlusions. Thrombectomy is performed on the superior branch (white arrow). **(C)** Photograph showing the EMBOTRAP III deployed in a one-segment configuration (black arrow). As a guide for fluoroscopic deployment, deployment is performed up to the second marker from the tip (black arrowhead). **(D,E)** Final angiographic images, anterior view **(D)** and lateral view **(E)**, after reperfusion.

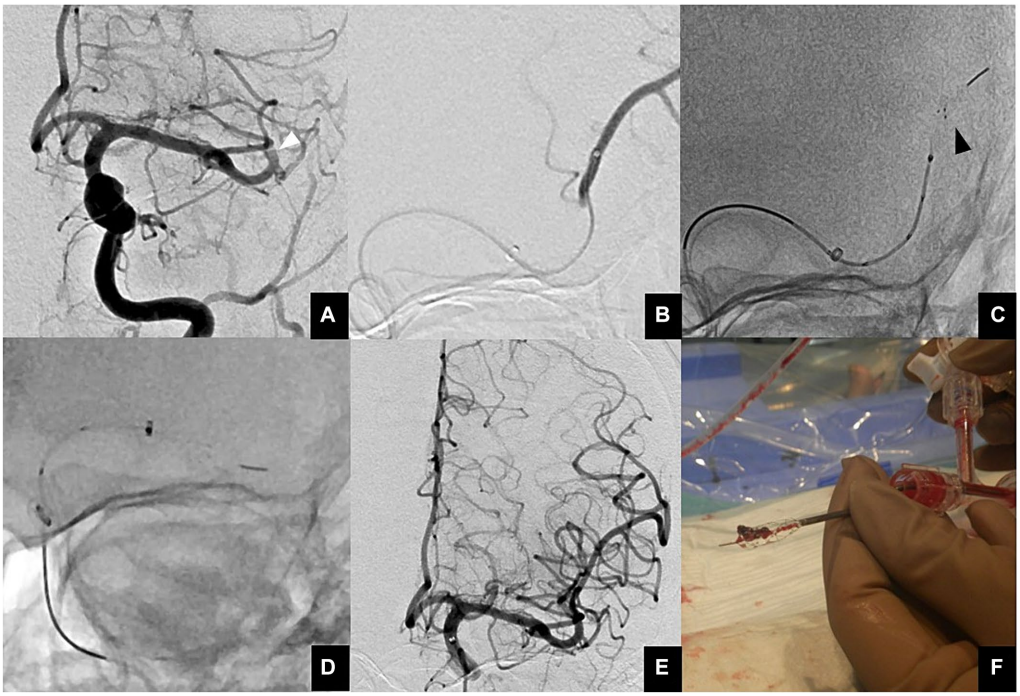

FIGURE 3
(A) Anterior view of a proximal M2 occlusion (white arrowhead). **(B)** A microcatheter is guided distal to a thrombus using a microguidewire. Then, contrast injection is performed to ensure that the tip of the microcatheter is beyond the thrombus. **(C)** The EMBOTRAP III is subsequently deployed in a one-segment configuration (black arrowhead). As a guide for fluoroscopic deployment, deployment is performed up to the second marker from the tip. **(D)** Since the AC cannot advance to M2, both the AC and EMBOTRAP III distal basket are pulled back to M1, and then the distal basket is pulled back into the AC. **(E)** Final angiographic image after reperfusion. **(F)** Actual thrombus retrieved within the distal basket using the ONE-SEG technique.

CT. Functional outcomes were defined as good (rate of mRS scores 0–2) at discharge or at 90 days, or relatively good (mRS scores of 0–3). Patients were analyzed together and then separately based on the EVT approach: ONE-SEG technique for patients with primary M2 occlusion or ONE-SEG technique for patients with secondary M2 occlusion after proximal thrombectomy with another technique.

Statistical methods

Statistical analysis was performed using JMP version 15 (SAS Institute, Cary, NC, USA). Continuous variables, including treatment-related time, NIHSS, DWI-ASPECTS, and mRS score, are presented as median [interquartile range (IQR)] values, and non-continuous variables are reported as proportions. Ages are shown as mean and standard deviation values.

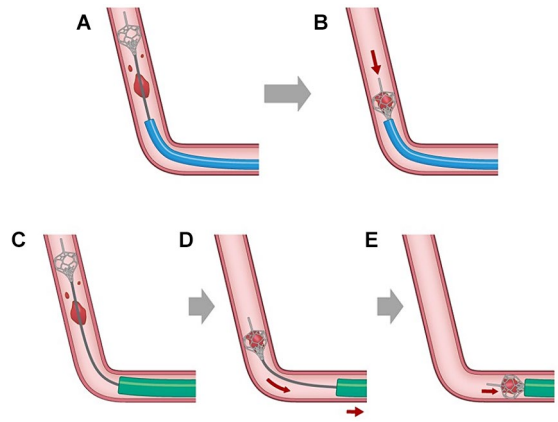

FIGURE 4
Illustration demonstrating clot retrieval using the ONE-SEG technique with the EMBOTRAP III. The balloon of the guiding catheter with a balloon is inflated to preclude flow from the internal carotid artery beforehand. **(A,B)** When the aspiration catheter (AC) can be navigated to the M2, a 0.021-inch microcatheter is guided distally using a microguidewire into the occluded vessel. Subsequently, only the distal basket of the EMBOTRAP III is deployed, with fluoroscopy guidance to ensure deployment up to the second marker from the tip. Then, aspiration is started using the AC, followed by slowly pulling and retracting the EMBOTRAP III into the AC. **(C–E)** When the AC can be navigated only to the M1 distal, similar to the approach in **(A,B)**, the distal basket of the EMBOTRAP III is deployed from the distal end of the clot. Subsequently, both the AC and the EMBOTRAP III are pulled linearly to the M1, followed by retracting the EMBOTRAP III into the AC.

Results

The flowchart of the study is provided in Figure 5. From a retrospective stroke registry, 262 patients diagnosed with AIS within 24 h of onset between April 2014 and March 2024 were included. Of them, 72 patients underwent EVT for M2 occlusion; 30 were treated using the ONE-SEG technique, including 17 with primary M2 occlusion and 13 with secondary M2 occlusion.

Baseline characteristics

Results are presented in Table 1. Overall, there were 11 females (36.7%), and the average age was 75.6 ± 11.0 years. The median NIHSS score was 14 (IQR: 5.8–21.3) for all patients, 10 (5–15.5) for primary M2 occlusion, and 20 (14–22.5) for secondary M2 occlusion, indicating lower neurological severity in primary M2 occlusion cases. Motor hemiparesis was present in 26/30 (86.7%) overall, with sensory disturbance in 17/30 (56.7%). Only sensory disturbance was seen in 0%. Aphasia, which is considered to be functionally important, was seen in 18/30 (60.0%) overall. The DWI-ASPECTS was 8 (IQR: 6–9) overall, 8 (8–9.5) for primary M2 occlusion, and 6 (5–8) for secondary M2 occlusion, suggesting a more extensive infarct in secondary M2 occlusion cases. The median time from symptom onset-to-door was 107 (IQR: 65–356) minutes, median time from door-to-puncture was 68 (55–85) minutes, and median time from puncture-to-reperfusion was 59

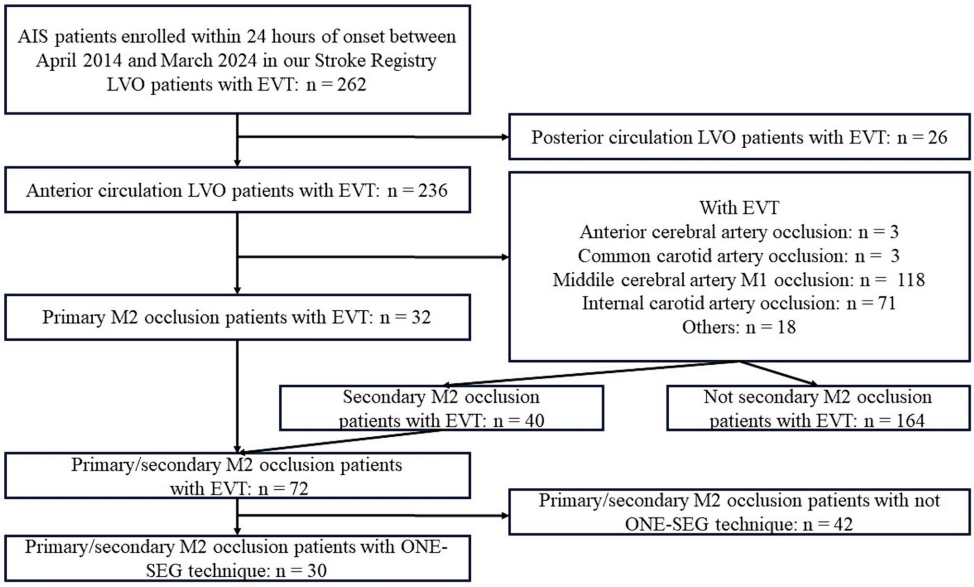

FIGURE 5
Study flowchart. AIS, acute ischemic stroke; ACA, anterior cerebral artery; CCA, common carotid artery; EVT, endovascular therapy; ICA, internal carotid artery; MCA, middle cerebral artery.

10.3389/fneur.2024.1424030

TABLE 1 Baseline characteristics of primary/secondary M2 patients treated with the ONE-SEG technique.

	All	Primary M2	Secondary M2
Number of patients, n (%)	**30 (100)**	**17 (56.7)**	**13 (43.3)**
Baseline characteristic			
Age, y (mean ± SD)	75.6 ± 11.0	74.9 ± 12.8	76.6 ± 8.6
Female, *n* (%)	11 (36.7)	7 (41.2)	4 (30.8)
Prestroke mRS score, median (IQR)	0 (0–0.25)	0 (0–0)	0 (0–3)
Hypertension, *n* (%)	23 (76.7)	13 (76.5)	10 (76.9)
Dyslipidaemia, *n* (%)	9 (30)	6 (35.3)	3 (23.1)
Diabetes mellitus, *n* (%)	8 (26.7)	4 (23.5)	4 (30.8)
Current smoking, *n* (%)	8 (26.7)	6 (35.3)	2 (15.4)
Ischemic stroke, *n* (%)	4 (13.3)	2 (11.8)	2 (15.4)
Atrial fibrillation, *n* (%)	22 (73.3)	12 (70.6)	10 (76.9)
Systolic blood pressure on admission, mmHg (IQR)	168 (153–178)	166 (145–184)	168 (161–178)
Baseline NIHSS score, median (IQR)	14 (5.8–21.3)	10 (5–15.5)	20 (14–22.5)
Motor hemiparesis, *n* (%)	26 (86.7)	14 (82.4)	12 (92.3)
Sensory disturbance, *n* (%)	17 (56.7)	8 (47.1)	9 (69.2)
Aphasia, *n* (%)	18 (60.0)	8 (47.1)	10 (76.9)
Baseline DWI ASPECTS score, median (IQR)	8 (6–9)	8 (8–9.5)	6 (5–8)
Intravenous alteplase, *n* (%)	13 (43.3)	10 (58.8)	3 (23.1)
Time parameters			
Onset-to-Door time, min (IQR)	107 (65–356)	78 (54–243)	197 (78–663)
Door-to-Puncture time, min (IQR)	68 (55–85)	71 (56–84)	62 (55–86)
Puncture-to-Recanalization time, min (IQR)	59 (40–78)	56 (34–72)	67 (45–108)

Data are presented as number (%) or median (interquartile range) values. Ages are shown as mean and standard deviation values. ASPECTS, Alberta Stroke Program Early Computed Tomographic Score; DWI, diffusion-weighted imaging NIHSS, National Institutes of Health Stroke Scale. ONE-SEG technique, combining the deployment of only the distal basket segment of the EMBOTRAP III and aspiration catheter. Bold values in Primary M2, M2 occlusion that occurred de novo; Secondary M2, M2 occlusion from occlusion of a large vessel due to migration or fragmentation of a thrombus.

(40–78) minutes. For primary M2 occlusion cases, the median time from puncture-to-reperfusion was 56 (34–72) minutes.

Intravenous alteplase was used in 13 patients (43.3%), with a higher rate observed in primary M2 occlusion cases (10/17, 58.8%) than in secondary M2 occlusion cases (3/13, 23.1%).

The following points are presented in Table 2. BGC was used in all cases. As for the ACs, mid-sized catheters including 3MAX (Penumbra, Alameda, CA, USA) (2 cases, 6.7%), 4MAX (Penumbra) (4 cases, 13.3%), and 5Fr SOFIA (MicroVention Terumo, Aliso Viejo, CA, USA) (1 case, 3.3%) were used, along with large-sized catheters such as CAT60 (Stryker Neurovascular, Fremont, CA, USA) (1 case, 3.3%), RED62 (Penumbra) (2 cases, 6.7%), REACT68 (Medtronic, Minneapolis, MN, USA) (7 cases, 23.3%), REACT71 (Medtronic) (12 cases, 40%), and 6Fr Esperance Distal Access Catheter 0.071″ (Wallaby, Shanghai, China) (1 case, 3.3%). Of the occlusion patterns, solitary M2 occlusion accounted for 23/30 cases (76.7%). Tandem occlusion was absent, but multi-vessel M2 occlusion was observed in 7/30 cases (23.3%), although EVT was not performed for non-eloquent occlusion sites. Regarding the location of M2 occlusion, proximal and distal M2 occlusions were observed in 15/30 cases (50%) each. A dominant upper or lower branch was observed in 19/30 cases (63.3%), whereas co-dominance of M2 branches was observed in 11/30 cases (36.7%) in patients with M2 occlusion, with primary M2 in 35.3% and secondary M2 in 38.5%. Non-dominant M2 accounted for 0% throughout this study.

Functional outcomes

Of the 30 patients, 6 (20%) achieved eTICI score 2c/3 on the first pass, and 12 (40%) achieved eTICI score 2b/2c/3 on the first pass. A final eTICI score of 2c/3 was achieved in 22 patients (73.3%), whereas a final eTICI score of 2b/2c/3 was obtained in 27 patients (90%). The median (IQR) number of passes for primary M2 occlusion was 2 (1–3). For secondary M2 occlusion, considering the first attempt after the occlusion changed due to the preceding technique as the 1st pass, the median (IQR) number of passes was 2 (1–2.5).

Technical parameters

Regarding safety and efficacy outcomes, there were a total of 5 cases of ICH, with 3/5 cases (17.7%) occurring in primary M2 occlusion and 2/5 cases (15.4%) in secondary M2 occlusion cases. Symptomatic ICH occurred in 1 case (3.3%) overall, in a case of secondary M2 occlusion. PH occurred in 2 cases (6.7%) overall, all of which were observed in secondary M2 occlusion cases. Embolization to the same territory after thrombectomy for proximal occlusion was observed in 1 case (3.3%) overall, in a primary M2 occlusion case. Spasm was observed in 1/30 cases (3.3%) overall, in a primary M2 occlusion case. SAH, extravasation, and embolization to different territories were not observed.

10.3389/fneur.2024.1424030

TABLE 2 Baseline angiographic type and stroke etiology of primary/secondary M2 patients treated with the ONE-SEG technique.

	All	Primary M2	Secondary M2
Number of patients, n (%)	**30 (100)**	**17 (56.7)**	**13 (43.3)**
Angiographic type of presentation (by vessel)			
Isolated M2 occlusion, *n* (%)	23 (76.7)	12 (70.6)	11 (84.6)
Tandem M2 occlusion, *n* (%)	0 (0)	0 (0)	0 (0)
Multi-vessel M2 occlusion, *n* (%)	7 (23.3)	5 (29.4)	2 (15.4)
Vessel diameter of M2, median, (IQR) mm	2.0 (1.8–2.2)	2.0 (1.9–2.3)	2.0 (1.8–2.1)
M2 occlusion site			
Proximal M2, *n* (%)	15 (50)	10 (58.8)	5 (38.5)
Distal M2, *n* (%)	15 (50)	7 (41.2)	8 (61.5)
M2 division			
Superior M2, *n* (%)	16 (53.3)	8 (47.1)	8 (61.5)
Inferior M2, *n* (%)	14 (46.7)	8 (47.1)	6 (46.2)
Intermediate M2, *n* (%)	0 (0)	0 (0)	0 (0)
M2 type			
Dominant M2, *n* (%)	19 (63.3)	11 (64.7)	8 (61.5)
Co-dominant M2, *n* (%)	11 (36.7)	6 (35.3)	5 (38.5)
Non-dominant M2, *n* (%)	0 (0)	0 (0)	0 (0)
Aspiration catheter			
3MAX, *n* (%)	2 (6.7)	1 (5.9)	1 (7.7)
4MAX, *n* (%)	4 (13.3)	2 (11.8)	2 (15.4)
5Fr SOFIA, *n* (%)	1 (3.3)	1 (5.9)	0 (0)
CAT60, *n* (%)	1 (3.3)	1 (5.9)	0 (0)
RED62, *n* (%)	2 (6.7)	2 (11.8)	0 (0)
REACT68, *n* (%)	7 (23.3)	4 (23.5)	3 (23.1)
REACT71, *n* (%)	12 (40)	5 (29.4)	7 (53.9)
6Fr Esperance, *n* (%)	1 (3.3)	1 (5.9)	0 (0)
Etiology			
Cardioembolic, *n* (%)	25 (83.3)	16 (94.1)	9 (69.2)
Large artery atherosclerosis, *n* (%)	4 (13.3)	3 (5.9)	3 (23.1)
Undetermined, *n* (%)	1 (3.3)	0 (0)	1 (7.7)

Data are presented as number (%) or median (interquartile range) values. Bold values in Primary M2, M2 occlusion that occurred de novo; Secondary M2, M2 occlusion from occlusion of a large vessel due to migration or fragmentation of a thrombus.

The rate of good outcomes (mRS score 0–2) at discharge was 43.3% overall (13/30 patients), and at 3 months, it was 46.7% (14/30 patients). The rate of relatively good outcomes (mRS score 0–3) was 60% (18/30 patients) at discharge and 73.3% (22/30 patients) at 3 months. Two patients with a history of severe heart failure died. Outcomes of M2 patients treated with the ONE-SEG technique are summarized in Table 3.

Discussion

Clinical outcomes and technical parameters

In this retrospective study, the ONE-SEG technique for M2 occlusion appeared to be safe and effective, both for primary and secondary M2 occlusions. In this selected small series of patients, the clinical outcomes seemed encouraging, with functional independence at 3 months observed in 13 of 30 patients overall (46.7%), with 11 of 17 patients (64.7%) with primary M2 occlusion achieving functional independence at 3 months. In contrast, only 3 of 13 patients (23.1%) with secondary M2 occlusion achieved functional independence at 3 months, but the mRS score 0–3 rate was 53.9% (7/13). This discrepancy may be attributed to the fact that patients with secondary M2 occlusion had higher baseline NIHSS scores (median 20 vs. 10), lower baseline DWI-ASPECTS values (median 6 vs. 8), and delayed onset-to-door times (median 197 vs. 78 min), which were believed to have affected the outcomes. There were only 2 deaths (6.7%), which is similar to previous reports and may suggest the clinical benefits and safety of the ONE-SEG technique for M2 occlusion. Symptomatic ICH was observed in 1 case (3.3%), and PH was observed in 2 cases (6.7%), all in cases of secondary M2 occlusion. SAH, extravasation, and spasm

10.3389/fneur.2024.1424030

TABLE 3 Outcomes of primary/secondary M2 patients treated with the ONE-SEG technique.

	All	Primary M2	Secondary M2
Number of patients, n (%)	**30 (100)**	**17 (56.7)**	**13 (43.3)**
Outcome			
Procedural outcome			
Number of passes, median (IQR)	2 (1–3)	2 (1–3)	2 (1–2.5)
First-pass eTICI score 2c/3, *n* (%)	6 (20)	3 (17.7)	3 (23.1)
First-pass eTICI score 2b/2c/3, *n* (%)	12 (40)	7 (41.2)	5 (38.5)
Final eTICI score 2c/3, *n* (%)	22 (73.3)	12 (70.6)	10 (70.9)
Final eTICI score 2b/2c/3, *n* (%)	27 (90)	15 (88.2)	12 (92.3)
Safety outcome			
Any ICH, *n* (%)	5 (16.7)	3 (17.7)	2 (15.4)
Symptomatic ICH, *n* (%)	1 (3.3)	0 (0)	1 (7.7)
Parenchymal hematoma, *n* (%)	2 (6.7)	0 (0)	2 (15.4)
Subarachnoid hemorrhage, *n* (%)	0 (0)	0 (0)	0 (0)
Extravasation, *n* (%)	0 (0)	0 (0)	0 (0)
Spasm, *n* (%)	1 (3.3)	1 (5.9)	0 (0)
Embolization to distal territory, *n* (%)	1 (3.3)	1 (5.9)	0 (0)
Embolization to new territory, *n* (%)	0 (0)	0 (0)	0 (0)
Mortality at 90 days, *n* (%)	2 (6.7)	1 (5.9)	1 (7.7)
Efficacy outcome			
mRS score at discharge, median (IQR)	3 (1–4)	2 (0.5–3)	4 (3–4.5)
mRS score 0–2 at discharge, *n* (%)	13 (43.3)	11 (64.7)	2 (15.4)
mRS score 0–3 at discharge, *n* (%)	18 (60)	14 (82.4)	4 (30.8)
mRS score at 3 months, median (IQR)	3 (1–4)	1 (0–3)	3 (2.5–4.5)
mRS score 0–2 at 3 months, *n* (%)	14 (46.7)	11 (64.7)	3 (23.1)
mRS score 0–3 at 3 months, *n* (%)	22 (73.3)	15 (88.2)	7 (53.9)

Data are presented as number (%) or median (interquartile range) values.
eTICI, expanded Thrombolysis in Cerebral Infarction; ICH, intracranial hemorrhage; mRS, modified Rankin Scale; ONE-SEG technique, combining the deployment of only the distal basket segment of the EMBOTRAP III and aspiration catheter. Bold values in Primary M2, M2 occlusion that occurred de novo; Secondary M2, M2 occlusion from occlusion of a large vessel due to migration or fragmentation of a thrombus.

were not observed. Kurre et al. (14) described their experience using the pREset LITE device in patients with extensive occlusions, achieving a successful reperfusion rate (modified TICI 2b/3) of 70%, with a low rate of vasospasm (5.6%), similar to the low incidence of spasm observed in the present study (3.3%). Kühn et al. (25) used the 3 mm × 20 mm Trevo XP ProVue (Baby Trevo, Stryker Neurovascular, Fremont, CA, USA), achieving successful reperfusion in 85.7% (TICI grade 2b/3) of cases without observed vascular damage, rupture, or significant vasospasm. These results are believed to minimize stress on the vessel wall and reinforce the clinical safety of the ONE-SEG technique.

Radiological outcomes

Of all M2 patients treated with the ONE-SEG technique, effective reperfusion with final eTICI 2b/3 was achieved in 27 of 30 cases (90%). Comparing baseline characteristics and angiographic and clinical outcomes of M2 occlusion patients treated with the ONE-SEG technique with other series focusing on DMVO, they appeared similar. Guenego et al. (10) used the Tigertriever 13 in DMVO patients, reporting an overall effective reperfusion rate (modified TICI 2b/3) of 94% (91% for primary DMVO, 100% for secondary DMVO) and good clinical outcomes (mRS score 0–2 at 3 months) of 65% (55% for primary DMVO, 83% for secondary DMVO). In addition, Dobrocky et al. (11) used the Mindframe Capture LP device for M2 occlusions, achieving a successful reperfusion rate (modified TICI 2b/3) of 74% and good clinical outcomes (mRS score 0–2 at 3 months) in 65% of cases. Hofmeister et al. (13) used a different device, the CatchMini, resulting in a successful reperfusion (good capillary reperfusion) rate of 78% and good clinical outcomes (mRS score ≤ 2) in 82.4% of cases.

Procedural concepts

The ONE-SEG technique relies primarily on a combined technique using both an SR and an AC. Though various effective techniques have been reported as combined techniques for LVO (26–28), reports specifically focusing on techniques limited to DMVO are scarce (15, 16). The ONE-SEG technique is divided into two methods based on whether the AC can be advanced to the M2 segment or only to the distal M1 segment. This is to align the vector of traction of the

SR with the aspiration port of the AC. If the AC can only be advanced to the distal M1 segment, there will be a misalignment of the aforementioned axis, potentially leading to clot loss when retracting the SR into the AC. Therefore, both devices are initially lowered to the M1 segment of the MCA, which is anatomically closer to a straight line, before retracting the SR into the AC. This method is believed to prevent a decrease in thrombus retrieval efficiency.

In addition, the structure of the EMBOTRAP III is unique compared to other SRs. The distal basket of the EMBOTRAP III has an inlet window, a gap designed into the distal basket. Compared to the previous EMBOTRAP II, the mesh at the tip of the distal basket has become finer, and the gap of the inlet window has been slightly expanded in the EMBOTRAP III. Whereas the diameter of the M2 vessel is reported to be 1.4–2.3 mm (29), when deploying the device in narrow vessels for a one-segment expansion, the gap of the inlet window expands further. This structure facilitates the capture of thrombi even in small-diameter vessels and contributes to preventing distal embolization of thrombi. It is believed that this feature contributes to the successful incorporation of clot retrieval during one-segment expansion. This may explain the relatively high rate of final eTICI 2b/2c/3 observed in the present study. Furthermore, one-segment expansion reduces friction of the SR, leading to decreased bending, stretching, and twisting of small tortuous distal vessels, which is expected to prevent damage during withdrawal of penetrating branches.

Strengths and pitfalls of the ONE-SEG technique

One of the strengths of the ONE-SEG technique is its ability to perform reperfusion procedures safely and effectively even in relatively tortuous vessels branching from the superior trunk or similar small bends, with minimal friction and resistance to the vessel during traction. Since only one of the five segments of the EMBOTRAP III is deployed, the metal contact area with the vessel is minimized, reducing the traction force on the vessel during SR retrieval and contributing to a decreased risk of penetrating branch withdrawal injury or vessel dissection. Another strength is the simplicity of the technique compared with other combined techniques, which is believed to have minimal impact on the delay in puncture-to-reperfusion time. Furthermore, the EMBOTRAP III has a 4-mm flexible distal marker at the tip, which allows for advancement in tortuous vessels with minimal risk of vessel damage and enables deployment while pushing out during one-segment expansion. The authors have not seen vessel damage during push-out expansion in tortuous segments, indicating an advantage in that even non-experts can perform this technique safely.

However, there are several pitfalls to this technique. When there is a large amount of thrombus, there may be limitations to the occupied volume of the distal basket, and it may not be possible to retrieve all thrombi in one pass. Therefore, it is recommended that the procedure be performed in multiple passes rather than insisting on reperfusion in one pass, especially when there is a large amount of thrombus. The median number of passes in ONE-SEG technique was two. In addition, it has been reported that it may be difficult to achieve successful reperfusion in cases of firm clot (30). It should also be noted that, depending on the location of the thrombus (e.g., on the convex or concave side of the vessel), there may be difficulty in effectively capturing it with the inlet window of the distal basket. Thus, achieving reliable retrieval may also be challenging with this technique.

Limitations

There are several limitations to this study. First, it was a single-arm study with a small sample size of 30 cases. Second, the ONE-SEG technique using the EMBOTRAP III cannot be compared to techniques using other devices, including simple SR techniques, AC, or the combined use of stent retriever techniques. Third, the lack of a formal protocol for device selection may introduce bias by not measuring variables not captured for the ONE-SEG technique for distal occlusion thrombectomy. Fourth, the inclusion criteria of NIHSS score $\geq$ 1 point and within 24 h of onset may overestimate the efficacy of EVT for M2 occlusions. Fifth, the present study included M2 occlusion cases with an NIHSS score $\geq$ 1. However, the efficacy of EVT for mild symptoms with an NIHSS score $\leq$ 5 has not been demonstrated. For MeVO cases, though intravenous rt-PA therapy may be effective, the comparative benefit of monotherapy versus combination therapy with EVT in cases with mild symptoms remains unclear. Sixth, although this procedure is based on the premise of a combined technique, it is considered to be safe and easy to perform even for first-time students of thromboprophylaxis because of its low intraoperative complications. However, its widespread adoption depends on medical infrastructure, expertise, and patient choice. Continued research and education are essential to increase its accessibility and impact. Finally, due to insurance issues, careful consideration of the costs associated with device use is necessary. However, despite these limitations, the present results are encouraging, and further research is warranted.

Conclusion

Using the ONE-SEG technique for thrombus extraction appears to be safe and effective for M2 occlusions, classified as MeVOs. Clinical outcomes, including high rates of successful reperfusion and minimal hemorrhagic complications, align with those observed in patients with proximal occlusions. However, larger cohort studies are needed to verify its clinical benefits.

Data availability statement

The original contributions presented in the study are included in the article/supplementary material, further inquiries can be directed to the corresponding author.

Ethics statement

The studies involving humans were approved by the Kagoshima Medical Center Ethics Review Committee. The studies were conducted in accordance with the local legislation and institutional requirements. Written informed consent for participation was not required from the participants or the participants' legal guardians/

next of kin in accordance with the national legislation and institutional requirements.

Author contributions

YH: Investigation, Methodology, Writing – original draft, Conceptualization, Data curation, Formal analysis, Resources, Visualization. HM: Investigation, Methodology, Project administration, Supervision, Validation, Writing – review & editing. SS: Investigation, Methodology, Supervision, Validation, Writing – review & editing. YK: Investigation, Writing – review & editing. KI: Investigation, Writing – review & editing. MI: Investigation, Methodology, Supervision, Writing – review & editing. TS: Investigation, Project administration, Writing – review & editing. GT: Data curation, Investigation, Writing – review & editing. HT: Supervision, Validation, Writing – review & editing.

Funding

The author(s) declare no financial support was received for the research, authorship, and/or publication of this article.

Acknowledgments

The authors would like to thank Luba Wolchuk from Forte Science Communications (https://www.forte-science.co.jp) for editing a draft of this manuscript and medical fig. (https://medicaleducation.co.jp) for illustrating Figure 4 of this manuscript.

Conflict of interest

The authors declare that the research was conducted in the absence of any commercial or financial relationships that could be construed as a potential conflict of interest.

Publisher's note

References

1. Berkhemer OA, Fransen PSS, Beumer D, van den Berg LA, Lingsma HF, Yoo AJ, et al. A randomized trial of intraarterial treatment for acute ischemic stroke. *N Engl J Med*. (2015) 372:11–20. doi: 10.1056/NEJMoa1411587

2. Goyal M, Demchuk AM, Menon BK, Eesa M, Rempel JL, Thornton J, et al. Randomized assessment of rapid endovascular treatment of ischemic stroke. *N Engl J Med*. (2015) 372:1019–30. doi: 10.1056/NEJMoa1414905

3. Saver JL, Goyal M, Bonafe A, Diener HC, Levy EI, Pereira VM, et al. Stent-retriever thrombectomy after intravenous t-PA vs. t-PA alone in stroke. *N Engl J Med*. (2015) 372:2285–95. doi: 10.1056/NEJMoa1415061

4. Jovin TG, Chamorro A, Cobo E, de Miquel MA, Molina CA, Rovira A, et al. Thrombectomy within 8 hours after symptom onset in ischemic stroke. *N Engl J Med*. (2015) 372:2296–306. doi: 10.1056/NEJMoa1503780

5. Campbell BCV, Mitchell PJ, Kleinig TJ, Dewey HM, Churilov L, Yassi N, et al. Endovascular therapy for ischemic stroke with perfusion-imaging selection. *N Engl J Med*. (2015) 372:1009–18. doi: 10.1056/NEJMoa1414792

6. Saver JL, Chapot R, Agid R, Hassan AE, Jadhav AP, Liebeskind DS, et al. Thrombectomy for distal, medium vessel occlusions: a consensus statement on present knowledge and promising directions. *Stroke*. (2020) 51:2872–84. doi: 10.1161/STROKEAHA.120.028956

7. Menon BK, Hill MD, Davalos A, Roos YBWEM, Campbell BCV, Dippel DWJ, et al. Efficacy of endovascular thrombectomy in patients with M2 segment middle cerebral artery occlusions: meta-analysis of data from the HERMES collaboration. *J Neurointerv Surg*. (2019) 11:1065–9. doi: 10.1136/neurintsurg-2018-014678

8. Bilgin C, Hardy N, Hutchison K. First-line thrombectomy strategy for distal and medium vessel occlusions: a systematic review. *J Neurointerv Surg*. (2023) 15:539–46. doi: 10.1136/jnis-2022-019344

9. Meyer L, Stracke CP, Jungi N, Wallocha M, Broocks G, Sporns PB, et al. Thrombectomy for primary distal posterior cerebral artery occlusion stroke: the topmost study. *JAMA Neurol*. (2021) 78:434–44. doi: 10.1001/jamaneurol.2021.0001

10. Guenego A, Mine B, Bonnet T. Thrombectomy for distal medium vessel occlusion with a new generation of Stentretriever (Tigertriever 13). *Interv Neuroradiol*. (2022) 28:444–54. doi: 10.1177/15910199211039926

11. Dobrocky T, Bellwald S, Kurmann R, Piechowiak EI, Kaesmacher J, Mosimann PJ, et al. Stent retriever thrombectomy with mindframe capture LP in isolated M2 occlusions. *Clin Neuroradiol*. (2020) 30:51–8. doi: 10.1007/s00062-018-0739-4

12. Kaschner M, Lichtenstein T, Weiss D, Turowski B, Goertz L, Kluner C, et al. The new fully radiopaque Aperio hybrid stent retriever: efficient and safe? An early multicenter experience. *World Neurosurg*. (2020) 141:e278–88. doi: 10.1016/j.wneu.2020.05.104

13. Hofmeister J, Kulcsar Z, Bernava G, Pellaton A, Yilmaz H, Erceg G, et al. The catch Mini stent retriever for mechanical thrombectomy in distal intracranial occlusions. *J Neuroradiol*. (2018) 45:305–9. doi: 10.1016/j.neurad.2018.01.051

14. Kurre W, Aguilar-Pérez M, Martinez-Moreno R, Schmid E, Bäzner H, Henkes H. Stent retriever thrombectomy of small caliber intracranial vessels using pREset LITE: safety and efficacy. *Clin Neuroradiol*. (2017) 27:351–60. doi: 10.1007/s00062-016-0497-0

15. Haussen DC, al-Bayati A, Eby B, Ravindran K, Rodrigues G, Frankel M, et al. Blind exchange with mini-pinning technique for distal occlusion thrombectomy. *J Neurointerv Surg*. (2020) 12:392–5. doi: 10.1136/neurintsurg-2019-015205

16. Miura M, Shindo S, Nakajima M, Namitome S, Wada K, Nagao Y, et al. Stent retriever-assisted continuous aspiration for distal intracranial vessel embolectomy: the distal combined technique. *World Neurosurg*. (2019) 131:e495–502. doi: 10.1016/j.wneu.2019.07.202

17. Wan Y, Yang IH, Orru E. Endovascular thrombectomy for distal occlusion using a semi-deployed Stentriever: report of 2 cases and technical note. *Neurointervention*. (2019) 14:137–41. doi: 10.5469/neuroint.2019.00143

18. Zaidat OO, Bozorgchami H, Ribó M, Saver JL, Mattle HP, Chapot R, et al. Primary results of the multicenter ARISE II study (analysis of revascularization in ischemic stroke with EmboTrap). *Stroke*. (2018) 49:1107–15. doi: 10.1161/STROKEAHA.117.020125

19. Fischer E. Die Lageabweichungen der vorderen Hirnarterieim Gefassbild. *Zentralblatt Fur Neurochirurgie*. (1938) 3:300–12.

20. Goyal M, Ospel JM, Menon BK, Hill MD. MeVO: the next frontier? *J Neurointerv Surg*. (2020) 12:545–7. doi: 10.1136/neurintsurg-2020-015807

21. Ospel JM, Menon BK, Demchuk AM, Almekhlafi MA, Kashani N, Mayank A, et al. Clinical course of acute ischemic stroke due to medium vessel occlusion with and without intravenous alteplase treatment. *Stroke*. (2020) 51:3232–40. doi: 10.1161/STROKEAHA.120.030227

22. Compagne KCJ, Van Der Sluijs PM, Van Den Wijngaard IR, Roozenbeek B, Mulder MJHL, van Zwam WH, et al. Endovascular treatment: the role of dominant caliber M2 segment occlusion in ischemic stroke. *Stroke*. (2019) 50:419–27. doi: 10.1161/STROKEAHA.118.023117

23. Liebeskind DS, Bracard S, Guillemin F, Jahan R, Jovin TG, Majoie CB, et al. eTICI reperfusion: defining success in endovascular stroke therapy. *J Neurointerv Surg*. (2019) 11:433–8. doi: 10.1136/neurintsurg-2018-014127

24. Hacke W, Kaste M, Fieschi C, von Kummer R, Davalos A, Meier D, et al. Randomised double-blind placebo-controlled trial of thrombolytic therapy with intravenous alteplase in acute ischaemic stroke (ECASS II). Second European-Australasian acute stroke study investigators. *Lancet*. (1998) 352:1245–51. doi: 10.1016/S0140-6736(98)08020-9

25. Kuhn AL, Wakhloo AK, Lozano JD, Massari F, De Macedo Rodrigues K, Marosfoi MG, et al. Two-year single-center experience with the "Baby Trevo" stent retriever for mechanical thrombectomy in acute ischemic stroke. *J Neurointerv Surg*. (2017) 9:541–6. doi: 10.1136/neurintsurg-2016-012454

26. Maus V, Behme D, Kabbasch C, Borggrefe J, Tsogkas I, Nikoubashman O, et al. Maximizing first-pass complete reperfusion with SAVE. *Clin Neuroradiol*. (2018) 28:327–38. doi: 10.1007/s00062-017-0566-z

27. Massari F, Henninger N, Lozano JD, Patel A, Kuhn AL, Howk M, et al. ARTS (aspiration-retriever technique for stroke): initial clinical experience. *Interv Neuroradiol*. (2016) 22:325–32. doi: 10.1177/1591019916632369

28. McTaggart RA, Tung EL, Yaghi S. Continuous aspiration prior to intracranial vascular embolectomy (CAPTIVE): a technique which improves outcomes. *J Neurointerv Surg*. (2017) 9:1154–9. doi: 10.1136/neurintsurg-2016-012838

29. Umansky F, Juarez SM, Dujovny M, Ausman JI, Diaz FG, Gomes F, et al. Microsurgical anatomy of the proximal segment of the middle cerebral artery. *J Neurosurg*. (1984) 61:458–67. doi: 10.3171/jns.1984.61.3.0458

30. Duffy S, McCarthy R, Farrell M. Per-pass analysis of thrombus composition in patients with acute ischemic stroke undergoing mechanical thrombectomy. *Stroke*. (2019) 50:1156–63. doi: 10.1161/STROKEAHA.118.023419

Circulation Journal
Circ J 2025; 89: 826–834
doi:10.1253/circj.CJ-24-0148

ORIGINAL ARTICLE

Screening of 1-Month-Old Infants With Prolonged QT Interval and Its Cutoff Value

Masao Yoshinaga, MD, PhD; Hiroya Ushinohama, MD, PhD; Seiichi Sato, MD, PhD; Seiko Ohno, MD, PhD; Tadayoshi Hata, MD, PhD; Hitoshi Horigome, MD, PhD; Nobuo Tauchi, MD, PhD; Naokata Sumitomo, MD, PhD; Eiki Nishihara, MD; Keiichi Hirono, MD, PhD; Fukiko Ichida, MD, PhD; Hirohiko Shiraishi, MD, PhD; Yuichi Nomura, MD, PhD; Shinya Tsukano, MD; Yumiko Ninomiya, MD; Tatsuya Yoneyma; Hiroshi Suzuki, MD, PhD; Hideto Takahashi, PhD; Hiromitsu Ogata, PhD; Naomasa Makita, MD, PhD; Wataru Shimizu, MD, PhD; Minoru Horie, MD, PhD; Masami Nagashima, MD, PhD

Background: The prevalence of congenital long QT syndrome (LQTS) (1:2,000) is based on genetic testing and ECG data, but the prevalence of electrocardiographically determined prolonged corrected QT interval (pQTc) in infants is unclear.

Methods and Results: Subjects were 10,282 1-month-old infants who participated in 2 prospective ECG screening studies performed in 2010–2011 and 2014–2016. Infants with a QTc ≥0.45 using Bazett's formula [QTc(B)] at 1-month medical checks were re-examined. pQTc was defined as QTc ≥0.46 on 2 different ECGs in early infancy. Infants with QTc ≥0.50 or progressive prolongation of QTc to 0.50 were defined as at high risk. The prevalence of infants with a pQTc was 11/10,282 (1:935; 95% confidence interval, 1:588–1:2,283). Five infants were diagnosed as at high risk, and all infants had an abrupt increase in QTc(B) values in early infancy, mostly at 6–11 weeks after birth and when medication was started. No infants with a pQTc experienced LQTS-related symptoms. Statistical analysis showed that a cutoff QTc(B) ≥0.45 was optimal for screening infants with a pQTc.

Conclusions: The prevalence of ECG-determined pQTc is approximately 1:1,000. An abrupt increase in QTc(B) values occurs in infants at high risk, mostly at 6–11 weeks after birth. A cutoff QTc(B) value ≥0.45 may be appropriate for 1-month-old screening in this population.

Key Words: Cutoff values; Infants; Neonatal screening; Prevalence; Prolonged QT interval

Congenital long QT syndrome (LQTS) is a genetic disorder that is characterized by delayed repolarization and a long QT interval on 12-lead ECG.[1,2] The hallmark of LQTS is syncope or sudden death due to torsade de pointes.[1,2] Sudden infant death syndrome (SIDS) is one of the major causes of death in infancy, with the highest peak at 75 days of life.[3] SIDS is multifactorial in origin, but a previous study showed that the odds ratio for SIDS in infants with a prolonged corrected QT interval by Bazett's formula [QTc(B)] was 41.3.[4] The period of the

Received February 20, 2024; revised manuscript received December 12, 2024; accepted December 23, 2024; J-STAGE Advance Publication released online February 22, 2025 Time for primary review: 19 days

Department of Pediatrics, NHO Kagoshima Medical Center, Kagoshima (M.Y., Y. Ninomiya); Orange Medical and Welfare Center for Severe Motor and Intellectual Disabilities, Kagoshima (M.Y.); Pediatric Cardiology, Ohori Children's Clinic, Fukuoka (H.U.); Division of Pediatric Cardiology & Pediatric Intensive Care Unit, Okinawa Prefectural Nanbu Medical Center & Children's Medical Center, Okinawa (S.S.); Medical Genome Center (S.O.), Omics Research Center (N.M.), National Cerebral and Cardiovascular Center, Osaka; Fujita Health University, Graduate School of Health Science, Aichi (T.H.); Department of Child Health, Graduate School of Comprehensive Human Sciences, University of Tsukuba, Ibaraki (H.H.); Aichi Saiseikai Rehabilitation Hospital, Nagoya (N.T., M.N.); Department of Pediatric Cardiology, Saitama Medical University International Medical Center, Saitama (N.S.); Pediatric Cardiology and Neonatology, Ogaki Municipal Hospital, Gifu (E.N.); Department of Pediatrics, Toyama University Graduate School of Medicine, Toyama (K.H.); Department of Pediatrics, Sanno Hospital, Tokyo (F.I.); International Pediatric Center Josai Hospital, Ibaraki (H. Shiraishi); Department of Pediatrics, Kagoshima City Hospital, Kagoshima (Y. Nomura); Department of Pediatrics, Niigata City General Hospital, Niigata (S.T.); Fukuda Denshi Co., Ltd., Tokyo (T.Y.); Uonuma Institute of Community Medicine, Niigata University Medical and Dental Hospital, Niigata (H. Suzuki); Graduate School of Environmental Information, Teikyo Heisei University, Tokyo (H.T.); Graduate School of Kagawa Nutrition University, Kagawa (H.O.); Department of Cardiology, Sapporo Teishinkai Hospital, Sapporo (N.M.); Department of Cardiovascular Medicine, Graduate School of Medicine, Nippon Medical School, Tokyo (W.S.); and Department of Cardiovascular Medicine, Shiga University of Medical Science, Shiga (M.H.), Japan

(Footnote continued the next page.)

highest peak of SIDS[3] and the highest prevalence of unexpected sudden infant death (1–3 months of age)[5] correspond to the period of the highest QTc values (6–11 weeks after birth) in the healthy general population.[6]

Population-based neonatal screening remains controversial.[7–10] However, prospective studies on the prevalence of LQTS that were performed in Italy (44,596 infants),[11] Japan (4,319 infants),[12] Germany (2,251 infants),[13] and Spain (685 infants)[14] showed that no infants with congenital LQTS or with a prolonged corrected QT interval (pQTc) showed LQTS-related symptoms,[11–14] including sudden death with interventional medication. Those studies suggest that ECG screening can identify most infants with a pQTc and that it is an effective preventive measure for sudden infant death in those with a pQTc.

The prevalence of congenital LQTS is approximately 1:2,000 when the diagnosis is based on the combination of QT interval and genetic testing.[11] The prevalence of infants with a pQTc can differ according to the definition of pQTc. However, the prevalence of QT prolongation determined by ECG in infancy is not well known, and screening cutoff values for infant pQTc is still under investigation. In previous studies, ECG recordings were repeated when the initial QTc(B) was >450 ms (or ≥450 ms).[11,12] A recent study of 5,000 neonatal ECGs, including 17 infants with LQTS-causing pathogenic variants, showed that an appropriate cutoff value of QTc(B) for infants was 460 ms,[15] although subsequent studies still used the cutoff value of 450 ms.[13,14] The cutoff value of 460 ms should be applied to other ethnic groups that include a relatively large number of participants.

The first study of ECG screening was performed in 4,319 1-month-old infants in Japan.[12] A second prospective study of ECG screening was performed in 6,006 1-month-old infants, and 10,325 infants were prospectively screened. The present study aimed to determine the prevalence of infants with a pQTc and identify those at high risk, as well as determining the cutoff QTc(B) values for screening infants with a pQTc in this population.

Methods

Subjects

Prospective ECG screenings were performed twice at 1-month medical checks. The first study was conducted in 16 maternity institutes in 8 areas in Japan between July 2010 and March 2011. Details of this study were described in a previous report.[12] The second study was performed in 14 maternity institutes in 8 areas (Kagoshima, Fukuoka, Nagoya, Toyoake, Ogaki, Tsukuba, Toyama, and Niigata) between September 2014 and February 2016. The parents were asked to participate in these studies at the time of discharge from the maternity institutes. A total of 10,325 infants, including 4,319 and 6,006 infants in the first and second studies, respectively, participated at the time of the 1-month medical check after obtaining written informed consent from the parents. The procedures in this study were performed in accordance with the Declaration of Helsinki. We obtained permission to use and analyze these data from the Ethics Committee of the NHO Kagoshima Medical Center (Approval nos. 22-3, 26-7, and 2020-45).

Analysis of ECGs and Measurement of the QT Interval

The 12-lead ECGs were recorded at a speed of 25 mm/s using a FCP-series recorder (FCP-4700, -7431, -7541, -8221, and -8800; Fukuda Denshi, Tokyo, Japan). The ECGs were initially read in each center, and a written report was sent to the parents of each participant. All QT/RR data for the present study were re-measured by 1 author (M.Y.). The QT intervals of 3 consecutive beats were manually measured using the tangent method from the onset of the Q wave to the end of the T wave in lead V_5 or lead II.

Correction of the QT Interval in Infants and School-Age Children

The exponent k in the formula of (QTc)=(QT interval)/(RR interval)^k that minimizes the effect of heart rate in infants was shown to be 0.43 in a Japanese population[6] or 0.467 in an Italian population.[15] The k value was also determined for the present population and calculated by simple regression analysis using the log-transformed QT interval as the dependent variable and the log-transformed RR interval as the independent variable. All 3 QT/RR data of the subjects were used in the calculation, which revealed that the k value was 0.449 for the present population. The k values for these 3 populations (0.430 for Japanese infants, 0.467 for Italian neonates, and 0.449 for infants at 1-month medical check in the present study) were closer to that calculated by Bazett's formula (k=1/2 or 0.500) than that calculated by Fridericia's formula (k=1/3 or 0.333). We used Bazett's formula to correct the QT interval in the present study because the difference in k values between population studies and Bazett's formula was smaller than that between those and Fridericia's formula. We also wanted to compare the cutoff value of the present study with that of Stramba-Badiale et al. who used Bazett's formula.[15] In the follow-up ECGs of infants at school age, the QTc by Fridericia's formula [QTc(F)] was also used.[16]

Screening and Follow-up Strategies

The algorithm for screening and follow-up strategies is shown in **Supplementary Figure 1**. Infants who showed a QTc(B) ≥0.45 were reexamined. Infants who showed a QTc ≥0.45 and <0.46 were reexamined 2–3 weeks later, and those who showed a QTc ≥0.46 were reexamined within 2 or 3 weeks. After that, they were reexamined based on the judgement of the doctors. Infants were diagnosed as having a pQTc when they showed a QTc(B) value ≥460 ms on 2 different standard 12-lead ECGs[8] during the follow-up, because the QT interval lengthens physiologically and temporarily during early infancy, particularly within few weeks after birth.[9,13] Infants who were diagnosed as pQTc were followed for at least 1 year after birth, and subsequently followed based on the judgement of the doctors. Infants who fulfilled 1 of the following 3 criteria were diagnosed as at high risk and medication was initiated: (1) presence of symptoms; (2) presence of QT prolongation, with a QTc(B) ≥0.50[17] or a progressive prolongation

Mailing address: Masao Yoshinaga, MD, PhD, Department of Pediatrics, NHO Kagoshima Medical Center, 8-1 Shiroyama-cho, Kagoshima, Kagoshima 892-0853, Japan. email: myoshi330@yahoo.co.jp

ISSN-1346-9843

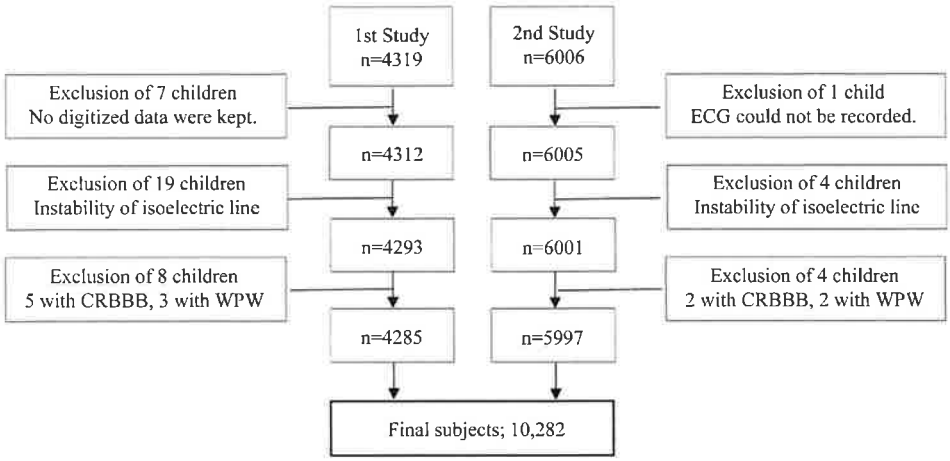

Figure 1. Flow chart of the participants and final subjects in the present study.

Table 1. Characteristics of the Infant Subjects

	1st study	2nd study	P value	Total
No of participants	4,285	5,997		10,282
Male/female*	2,150/2,041	3,017/2,978	0.33	5,167/5,019
Gestational age (weeks)†	(1,547) 39.2±1.3	(5,980) 39.3±1.3	0.11	(7,527) 39.2±1.3
Birth weight (g)†	(1,549) 3,008±381	(5,982) 3,026±382	0.21	(7,531) 3,022±382
QT interval (ms)	254±17	253±17	0.26	254±17
RR interval (ms)	381±39	379±40	0.002	380±40
Heart rate (bpm)	159±16	160±17	<0.001	160±16
QTc(B) values (ms)	412±19	413±19	0.02	412±19

*Sex was not described in 96 infants (94 and 2 infants in the 1st and 2nd studies, respectively). †Data of gestational age and birth weight were not mandatory in the first study. QTc(B), QT interval corrected by Bazett's formula.

of QTc(B) to 0.50 including a QTc(B) on Holter recordings[17–20] during sleeping; and (3) presence of both QT prolongation and a family history of LQTS with symptoms. No infants fulfilled the criterion of (1) or (3). Therefore, we used the second criterion for at high risk in the present study.

In this study, a β-blocker alone or the co-administration of a β-blocker and mexiletine was used for treatment. The reason for this administration is that, in a nation-wide study in Japan, patients with LQTS who showed life-threatening arrhythmia in the perinatal period and whose mutations were determined were mostly those with LQTS type 2 (LQT2) or LQTS type 3 (LQT3).[21] In this Japanese series, a β-blocker and mexiletine were co-administered to 7 of 11 infants with LQT2 and to all 7 infants with LQT3.[21] The clinical course of these patients was favorable.

Familial Study and Genetic Testing

In the first and second studies, thorough familial ECG recording and/or genetic testing was not mandatory. Therefore, the conducting of familial ECG screening and/or genetic testing was based on the judgment of the doctors.

Genetic testing was performed after obtaining written informed consent. In the first study, screening of causative genes for LQTS type 1 (LQT1) to LQT3 and types 5–7 (*KCNQ1*, *KCNH2*, *SCN5A*, *KCNE1*, *KCNE2*, and *KCNJ2*) was performed by polymerase chain reaction and direct DNA sequencing.[19] Genes that were related to inherited arrhythmia syndrome, including LQTS, catecholaminergic polymorphic ventricular tachycardia, and Brugada syndrome, were retrospectively screened for in infants at high risk or those whose parents asked for it. The test was performed by a targeted gene sequencing method using the HaloPlex Target Enrichment System (Agilent Technology, Santa Clara, CA, USA) and the MiSeq system (Illumina, San Diego, CA, USA). Detected variants were confirmed using Sanger's method.[22]

Presence or Absence of Symptoms (e.g., Cardiac Arrest and Sudden Death) During Infancy

The maternity institutes that collaborated with the present study were asked to provide any information on the health condition of infants who participated in the study. Additionally, 1 year after screening, questionnaires were sent to parents to ask the following: infant's present health condition, and the presence or absence of syncope, convulsion, diseases, aborted cardiac arrest, or death.[23]

Statistical Analysis

Differences in mean values were examined using Student's

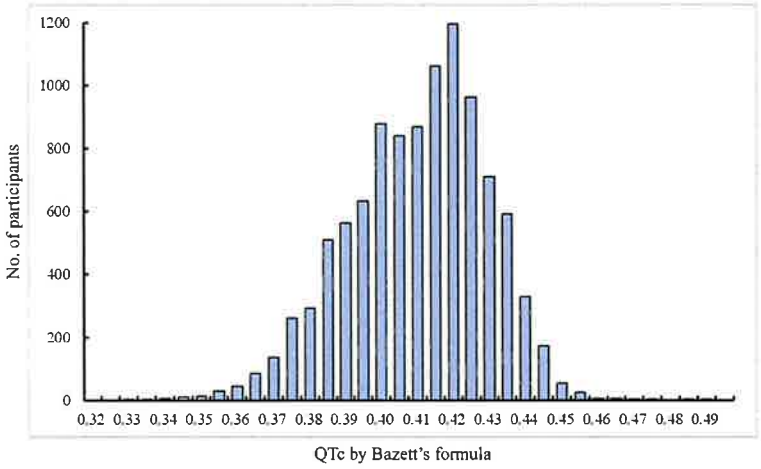

Figure 2. Distribution of QTc(B) of infants at their 1-month medical check. QTc(B), QT interval corrected by Bazett's formula.

Table 2. Characteristics of High-Risk Infants With Prolonged QT Interval

Case no.	Age at sequencing (days)	QTc(B) at screening (ms)	Age at 1st visit (days)	Start of medication (days)	Pharmacotherapy		Cessation of therapy (mg/kg/day)	Last visit (years) (days or months)	Genetic testing by a targeted gene method (refer to the text)
					Propranolol (mg/kg/day)	Mexiletine			
1	34	474	46	52	0.71	3.6	92 days[a]	1.1	Performed but not determined
2	31	492	37	65	0.94	3.1	14 months	13.2	*KCNH2*-L1022PfsTer35
3	29	469	51	53	1.90	4.5	16 months	8.8	Performed but not determined
4	32	450	57	98	1.59	(–)	21 months	2.0	Performed but not determined
5	32	456	62	175	1.86	(–)	18 months	8.3	Performed but not determined

[a]In case 1, mild liver dysfunction (AST/ALT=67/50) appeared after starting medication (before medication, AST/ALT=36/18). The infant was followed without medication at 1-month intervals till 6 months old and at a 3- or 4-month intervals till 1 year old. QTc(B), QT interval corrected by Bazett's formula.

t-test. To determine the optimal cutoff QTc(B) value, Youden's index and the distance between the point (0,1) and the receiver-operating characteristic curve plots were used.[24] For the analysis, QTc(B) values at 1-month medical check were used. Statistical analysis was performed using IBM® SPSS® Statistics Version 23.0 (IBM Japan, Ltd., Tokyo, Japan). A two-tailed probability value <0.05 was considered statistically significant.

Results

Participants

Of 10,325 participants, 34 and 9 infants' ECGs in the first and second studies, respectively, were excluded (**Figure 1**). Finally, ECGs from 10,282 infants were analyzed. ECGs of 12 infants with few ventricular premature contractions, 16 with few supraventricular premature contractions, and 2 with a small ventricular septal defect were included. Among 5 infants with Wolf-Parkinson-White syndrome who were excluded from the analysis, 1 had left ventricular non-compaction and experienced supraventricular tachycardia.[12]

There were significant differences in the QT interval, RR interval, heart rate, and QTc(B) values between the first and second studies (all $P<0.05$, **Table 1**). However, the differences were small, and may have been due to the large number of participants.

The frequency distribution of the QTc(B) values of infants at a 1-month medical check is summarized in **Supplementary Table 1** and **Figure 2**.

Infants With QT Prolongation and Their ECG Findings

A total of 11 infants showed a QTc(B) value ≥460 ms on 2 different ECGs during early follow-up. The prevalence of a pQTc was 4/4,285 (1:1,080) and 7/5,997 (1:857) infants in the first and second studies, respectively. The total prevalence of a pQTc was 11/10,282 infants (1:935; 95% confidence interval, 1:588 to 1:2,283). The distribution of the QTc(B) intervals of the infants is shown in **Supplementary Table 1**. Of these infants, 5 were diagnosed as being at high risk and medication was started (**Table 2**). The prevalence of infants at high risk was 2/4,285 (1:2,143) and 3/5,997 (1:1,999) infants in the first and the second studies, respectively. The total prevalence of infants at high risk was

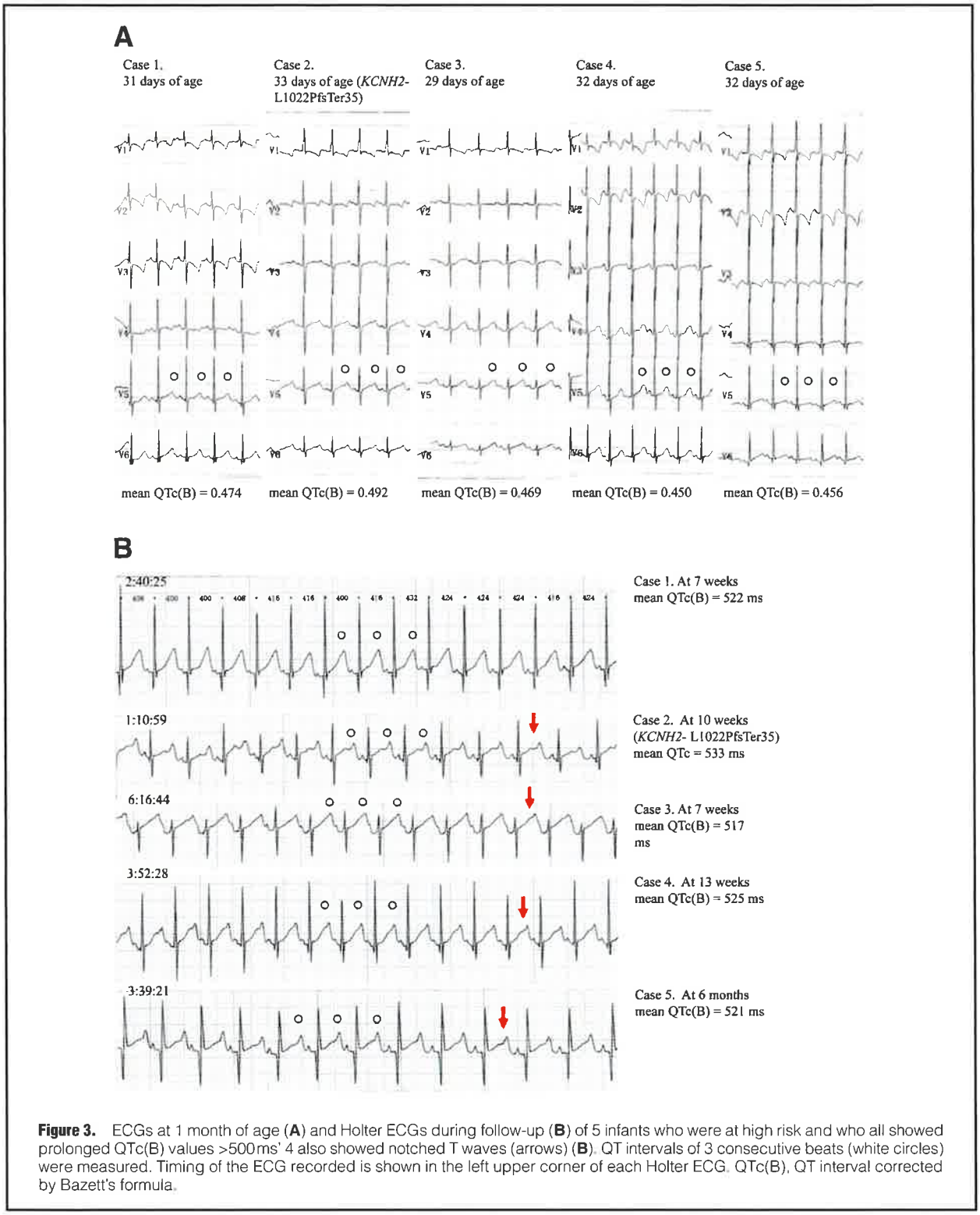

Figure 3. ECGs at 1 month of age (**A**) and Holter ECGs during follow-up (**B**) of 5 infants who were at high risk and who all showed prolonged QTc(B) values >500 ms' 4 also showed notched T waves (arrows) (**B**). QT intervals of 3 consecutive beats (white circles) were measured. Timing of the ECG recorded is shown in the left upper corner of each Holter ECG. QTc(B), QT interval corrected by Bazett's formula.

5/10,282 infants (1 : 2,056; 95% confidence interval, 1 : 1,095 to 1 : 16,666). No infants with a pQTc, including those at high risk, experienced LQTS-related symptoms. Genetic testing was performed for all 5 infants at high risk, and showed 1 *KCNH2* mutation (c.3065 delT, p.L1022PfsTer35) in these 5 high-risk infants.

The resting ECGs of the 5 infants at high risk showed that the peak of the T waves was present in the latter half of the T wave (**Figure 3A**). Additionally, all 5 infants showed prolonged QTc(B) values that exceeded 500 ms, and 4 of

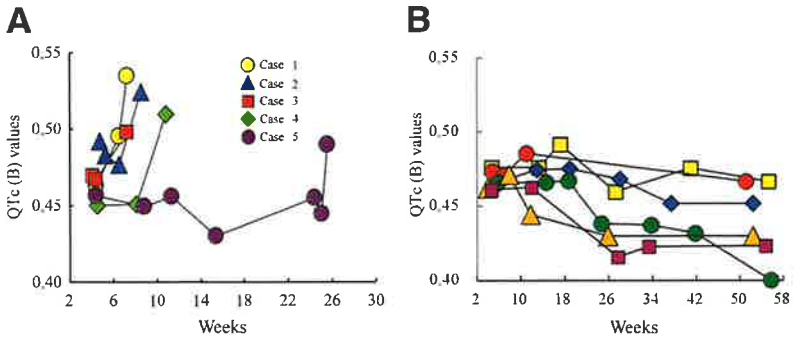

Figure 4. Changes in QTc(B) values in infants who were (**A**) at high risk and (**B**) not at high risk. Four of five infants who were at high risk showed an abrupt increase in QTc(B) values between 6 and 11 weeks after birth, and one infant showed an increase in QTc(B) values at 5 months of age (**A**). Infants who were not at high risk showed a plateau or a decrease in QTc(B) values during infancy (**B**). QTc(B), QT interval corrected by Bazett's formula.

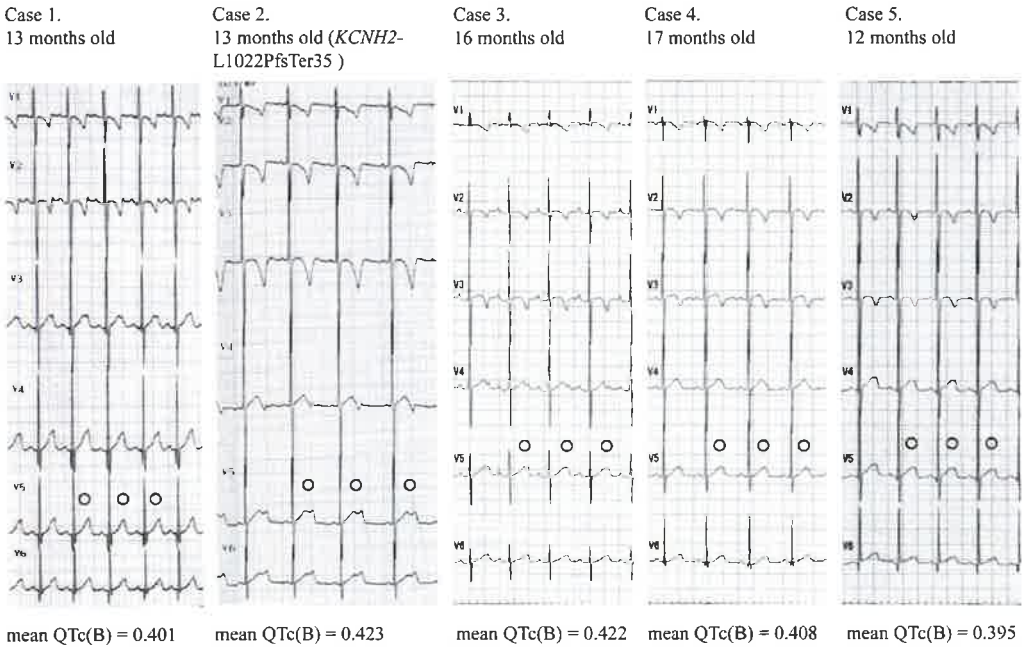

Figure 5. ECGs after 1 year of age of the 5 infants who were at high risk. All showed a decrease in QTc(B) values to <0.45. QT intervals of 3 consecutive beats (white circles) were measured. QTc(B), QT interval corrected by Bazett's formula.

them also showed notched T waves on their Holter ECGs (**Figure 3B**). The infants at high risk showed an abrupt increase in their QTc(B) between 6 and 11 weeks after birth, except for 1 who showed an abrupt increase at 5 months (**Figure 4A**). Case 5 was followed up repeatedly, although he sometimes showed normal QTc(B) values (<0.45) because he showed prominent notched T waves during the follow-up. Infants who were not at high risk showed a plateau or a decrease during infancy (**Figure 4B**).

Follow-up of 5 Infants at High Risk

All 5 infants at high risk showed a decrease in their QTc(B) values to <0.45 by 1–1.5 years of life (**Figure 5**) and medications were stopped (**Table 2**). Cases 1 and 2 dropped out of the study after stopping medication. Case 2 was screened again through a school-based screening program at 12 years of age owing to the presence of notched T waves from leads V2 through V6 and a QTc(B) of 0.465 (**Supplementary Figure 2A**). His Holter ECG on the day of the hospital visit showed extremely prolonged QTc(B) values and medication was restarted (**Supplementary Figure 2B,C**). He was not screened through the screening program at 6 years of age. Unfortunately, his ECG at this age was missing. Cases 3 and 5 were followed from 1 year through 8 years of age; their QTc(B) values did not increase on resting 12-lead ECGs (0.416 and 0.356, respectively, at 8 years of age). Case 4's medication was stopped at 21 months old. Her family moved out of the study area when she was 24 months old and her present QTc(B) value is unclear.

Out-of-Hospital Cardiac Arrest (OHCA) at <1 Year

Among all participants, 5 infants experienced OHCA. The

Table 3. Sensitivity, Specificity, Predictive Values, and Calculation for the Optimal Cutoff Point of QTc(B) Using Youden's Index and the ROC Curve

QTc(B)	Sensitivity	Specificity	PPV	NPV	Youden's index	Distance[a]
0.45	1.0000	0.9915	0.1122	1.0000	0.9915	0.0001
0.46	0.7273	0.9991	0.4706	0.9997	0.7264	0.2727
0.47	0.2727	0.9999	1.0000	0.9992	0.2726	0.7273
0.48	0.0909	1.0000	1.0000	0.9990	0.0909	0.9091

Youden's index denotes (sensitivity+specificity−1). The largest is the best value. [a]Distance denotes the shortest distance between the point (0,1) and ROC plot, calculated as $\{(1-\text{sensitivity})^2+(1-\text{specificity})^2\}^{0.5}$. The smallest is the best value. NPV, negative predictive value; PPV, positive predictive value; QTc(B), QT interval corrected by Bazett's formula; ROC, receiver-operating characteristic.

participating researchers in the present study obtained information about these OHCAs from the collaborating maternity institutes. Of them, 4 infants died, 3 of unknown etiology, and 1 of suffocation (**Supplementary Table 2**). All 5 infants showed a QTc(B) value <0.43 at a 1-month medical check, suggesting that the cause of their OHCA was probably not due to prolonged QT intervals.

Cutoff QTc(B) Values for ECG Screening at 1 Month of Life

To assess the diagnostic performance of each QTc(B) value in identifying the 11 infants with a pQTc, sensitivity, specificity, predictive values, Youden's index, and the distance between the point (0,1) and receiver-operating characteristic curve plot were determined (**Table 3, Supplementary Figure 3**). Youden's index and the distance showed that a cutoff QTc(B) value ≥0.45 was appropriate for screening infants with a pQTc for this population.

Discussion

The present study showed that the prevalence of infants with a pQTc and that of infants at high risk were approximately 1:1,000 and 1:2,000, respectively. Importantly, all 5 infants at high risk in the present study showed an abrupt increase in QTc(B) during early infancy, mostly between 6 and 11 weeks after birth. This time corresponds to the period of the highest values of QTc in the healthy general population and to the highest peak of sudden unexpected infant death. The cutoff QTc(B) value for screening infants with a pQTc was 0.45.

The prevalence of congenital LQTS was 1:2,000 in a previous cohort study with a large number of infants, and the data were mainly based on genetic testing in addition to ECG findings.[11] The present study showed that the prevalence of a pQTc was 1:935 when infants with a pQTc were defined as those whose QTc(B) was ≥0.46 on 2 different ECGs in early infancy. This prevalence is not high. A previous study in Italy showed that the prevalence of a QTc(B) ≥0.46 at least once between 15 and 25 days of life was 1:730 (59/43,080).[11] Another study showed that the probability of diagnosing LQTS was 1:988 in subjects aged 12 years according to the criteria of the Expert Consensus Statement of the Heart Rhythm Society, the European Heart Rhythm Association, and the Asia Pacific Heart Rhythm Society.[25] These data indicate that the prevalence of a QTc(B) ≥0.46 at multiple times during early infancy may be approximately 1:1,000.

Well-known diagnostic criteria for LQTS were published in 1993.[26] Thereafter, a QTc(B) criterion ≥450 ms has been used in the clinical setting for many years with a minor change (a QTc(B) at 4 min of recovery from an exercise stress test) in 2013.[1] In 2018, Stramba-Badiale et al. reported that a cut-off QTc(B) value of 460 ms was best for neonatal screening[15] using 5,000 ECGs from a cohort of 44,596 healthy neonates.[11] There were no neonates with congenital LQTS whose QTc(B) values were <460 ms in their cohort, and thus this cutoff point was suitable for their population. In the present study, 2 infants showed a QTc(B) between 450 and 460 at a 1-month medical check-up (**Table 2**), and they showed a QTc(B) ≥0.46 on 2 different ECGs during follow-up. We believe that the cutoff value of 450 ms should also be used for neonatal screening, at least in Japan, as a well-known diagnostic criterion for LQTS. Researchers who want to perform neonatal screening are unlikely to choose the criterion of a QTc(B) ≥440 ms because the criterion of a QTc(B) ≥450 ms has been used to diagnose LQTS for many years, and the criterion of a QTc(B) ≥440 ms would screen many infants (598/10,282, 5.82% in the present study). Therefore, the criterion of a QTc(B) ≥450 appears to be best for neonatal screening. All 4 studies that performed neonatal screenings used the screening criterion of a QTc(B) >450 ms or ≥450 ms.[11–14] Finally, it should be stated that the premise of the definition of pQTc was that a QTc(B) value should be ≥450 ms on initial screening, and that this was not a study that examined the validity of values <450 ms, but was a comparison with ≥460 ms.

A definition for infants at a high risk of aborted cardiac arrest or sudden death has not been established. Therefore, concluding that infant ECG screening contributes to the eventual prevention of sudden death is difficult. Regarding risk stratification of patients with LQTS, Priori et al. classified patients with LQTS on the basis of the probability of a first cardiac event (syncope, aborted cardiac arrest, or sudden cardiac death) before 40 years of age and before therapy, and defined a probability ≥50% as "the high risk group".[17] One of their criteria of "the high risk group" was a QTc(B) of ≥500 ms.[17] Hobbs et al. determined risk factors for aborted cardiac arrest or sudden cardiac death during adolescence, and found that a QTc(B) ≥530 ms was associated with a higher risk (adjusted hazard ratio, 2.3; 95% confidence interval, 1.6–3.3; P<0.001) than those who had a shorter QTc(B).[27] We also used a QTc(B) ≥500 ms to represent a high risk. Of the 5 infants at high risk, in case 2 there was a QTc(B) ≥530 ms including on Holter ECG (**Figure 3B**). He was rescreened thorough a school-based screening program at 12 years of age. His Holter ECG on the day of revisiting hospital showed a QTc of 567 ms by both Bazett's and Fridericia's formulae (**Supplementary Figure 2B**). This infant might have had strong potential for

aborted cardiac arrest or sudden death, and he might have had a lower risk of life-threatening events with medication. The number of infants in the present study was 10,282. Therefore, this study suggests that life-threatening events could be prevented in 1 of 10,000 infants.

All 5 infants at high risk in the present study showed an abrupt increase in QTc(B) during early infancy. Of them, 4 showed an increase in QTc(B) between 6 and 11 weeks of life, which corresponds to the period of the highest QTc values (6–11 weeks after birth) during infancy in the healthy general population.[6] This finding indicates that infants with a pQTc should be followed carefully during this time. Another infant showed an abrupt increase in QTc(B) at 25 weeks (5 months) of age, which suggests that infants with a pQTc may have an abrupt increase in QTc(B) values during the early half of infancy.

To implement population-based ECG screening, several issues need to be solved. (1) The number of cardiologists who are familiar with infant ECGs. Accurate measurement of the QT interval, even by cardiologists, may be difficult.[10] Consequently, the distribution of QT intervals from different groups of clinicians is dissimilar.[10] (2) Another concern is insufficient time to perform any sort of intervention from the time of ECG screening to the peak of unexpected sudden infant death at 1 or 3 months.[5] A system with artificial intelligence-assisted ECG analysis might improve accurate measurement of the QT interval,[28] and such as system might also help screen abnormal T wave morphologies, which are characteristic of LQTS, and were also shown in the present study. (3) Creation of follow-up systems, including authorized cardiovascular institutions and psychosocial assistance to follow-up, are also required.

Study Limitations

Genetic testing was not mandatory. We aimed to screen infants with a pQTc to prevent them from experiencing LQTS-related symptoms and identify the prevalence of an ECG-determined pQTc. However, currently, genetic testing using next-generation sequencing is becoming increasingly available. Thorough genetic testing for infants with a pQTc will help determine their precise background, although genetic variants determined by next-generation sequencing technologies should be carefully interpreted.[29,30]

Conclusions

There should be awareness of the genetically determined prevalence of LQTS (1 : 2,000) and ECG-determined prevalence of a pQTc in infants (≈1 : 1,000). In this study, all 5 infants at high risk showed an abrupt increase in QTc(B) during early infancy, mostly between 6 and 11 weeks after birth, which corresponds to the period of the highest values of corrected QT interval in the healthy general population and to the highest peak of sudden unexpected infant death. The QTc(B) cutoff value for screening infants with a pQTc might be 0.45 in this population, and the 0.45 value in this study is for screening for the present definition of pQTc, but not for screening of high-risk infants.

Acknowledgments

We are grateful to the many physicians and nurses in the 16 maternity institutes who contributed to this study and to the parents of the 10,325 infants who agreed to participate in this study. We express our gratitude to the Ministry of Health, Labour and Welfare of Japan for their funding of this study. We thank Ellen Knapp, PhD, from Edanz Group (www.edanzediting.com/ac) for editing a draft of this manuscript.

Sources of Funding

This work was supported by a Health and Labour Sciences Research Grant from the Ministry of Health, Labour and Welfare of Japan (H22-032, H24-033, H26-002, and H29-055).

Disclosures

W.S. is a member of the *Circulation Journal*'s Editorial Team.

References

1. Schwartz PJ, Ackerman MJ. The long QT syndrome: A transatlantic clinical approach to diagnosis and therapy. *Eur Heart J* 2013; **34:** 3109–3116.
2. Schwartz PJ, Ackerman MJ, George AL Jr, Wilde AA. Impact of genetics on the clinical management of channelopathies. *J Am Coll Cardiol* 2013; **62:** 169–180.
3. Guntheroth WG, Spiers PS. The triple risk hypotheses in sudden infant death syndrome. *Pediatrics* 2002; **110:** e64.
4. Schwartz PJ, Stramba-Badiale M, Segantini A, Austoni P, Bosi G, Giorgetti R, et al. Prolongation of the QT interval and the sudden infant death syndrome. *N Engl J Med* 1998; **338:** 1709–1714.
5. Lavista Ferres JM, Anderson TM, Johnston R, Ramirez JM, Mitchell EA. Distinct populations of sudden unexpected infant death based on age. *Pediatrics* 2020; **145:** e20191637.
6. Yoshinaga M, Kato Y, Nomura Y, Hazeki D, Yasuda T, Takahashi K, et al. The QT intervals in infancy and time for infantile ECG screening for long QT syndrome. *J Arrhythmia* 2011; **27:** 193–201.
7. Quaglini S, Rognoni C, Spazzolini C, Priori SG, Mannarino S, Schwartz PJ. Cost-effectiveness of neonatal ECG screening for the long QT syndrome. *Eur Heart J* 2006; **27:** 1824–1832.
8. Saul JP, Schwartz PJ, Ackerman MJ, Triedman JK. Rationale and objectives for ECG screening in infancy. *Heart Rhythm* 2014; **11:** 2316–2321.
9. Schwartz PJ, Montemerlo M, Facchini M, Salice P, Rosti D, Poggio G, et al. The QT interval throughout the first 6 months of life: A prospective study. *Circulation* 1982; **66:** 496–501.
10. Skinner JR, Van Hare GF. Routine ECG screening in infancy and early childhood should not be performed. *Heart Rhythm* 2014; **11:** 2322–2327.
11. Schwartz PJ, Stramba-Badiale M, Crotti L, Pedrazzini M, Besana A, Bosi G, et al. Prevalence of the congenital long-QT syndrome. *Circulation* 2009; **120:** 1761–1767.
12. Yoshinaga M, Ushinohama H, Sato S, Tauchi N, Horigome H, Takahashi H, et al. Electrocardiographic screening of 1-month-old infants for identifying prolonged QT intervals. *Circ Arrhythm Electrophysiol* 2013; **6:** 932–938.
13. Simma A, Potapow A, Brandstetter S, Michel H, Melter M, Seelbach-Göbel B, et al. Electrocardiographic screening in the first days of life for diagnosing long QT syndrome: Findings from a birth cohort study in Germany. *Neonatology* 2020; **117:** 756–763.
14. Sarquella-Brugada G, García-Algar O, Zambrano MD, Fernández-Falgueres A, Sailer S, Cesar S, et al. Early identification of prolonged QT interval for prevention of sudden infant death. *Front Pediatr* 2021; **9:** 704580.
15. Stramba-Badiale M, Karnad DR, Goulene KM, Panicker GK, Dagradi F, Spazzolini C, et al. For neonatal ECG screening there is no reason to relinquish old Bazett's correction. *Eur Heart J* 2018; **39:** 2888–2895.
16. Sumitomo N, Baba R, Doi S, Higaki T, Horigome H, Ichida F, et al. Guidelines for heart disease screening in schools (JCS 2016/JSPCCS 2016): Digest version. *Circ J* 2018; **82:** 2385–2444.
17. Priori SG, Schwartz PJ, Napolitano C, Bloise R, Ronchetti E, Grillo M, et al. Risk stratification in the long-QT syndrome. *N Engl J Med* 2003; **348:** 1866–1874.
18. Yoshinaga M, Kucho Y, Ushinohama H, Ishikawa Y, Ohno S, Ogata H. Autonomic function and QT interval during nighttime sleep in infant long QT syndrome. *Circ J* 2018; **82:** 2152–2159.
19. Yoshinaga M, Ninomiya Y, Tanaka Y, Fukuyama M, Kato K, Ohno S, et al. Holter electrocardiographic approach to predicting outcomes of pediatric patients with long QT syndrome. *Circ J* 2024; **88:** 1176–1184.
20. Shimamoto K, Aiba T. How can we evaluate arrhythmic risk in children with long QT syndrome? *Circ J* 2024; **88:** 1185–1186.
21. Horigome H, Nagashima M, Sumitomo N, Yoshinaga M.

Ushinohama H, Iwamoto M, et al. Clinical characteristics and genetic background of congenital long QT syndrome diagnosed in fetal, neonatal and infantile life: A nation-wide questionnaire survey in Japan. *Circ Arrhythm Electrophysiol* 2010; **3:** 10–17.
22. Sanger F, Nicklen S, Coulson AR. DNA sequencing with chain-terminating inhibitors. *Proc Natl Acad Sci USA* 1977; **74:** 5463–5467.
23. Hirabayashi M, Yoshinaga M, Nomura Y, Ushinohama U, Sato S, Tauchi T, et al. Environmental risk factors for sudden infant death syndrome in Japan. *Eur J Pediatr* 2016; **175:** 1921–1926.
24. Perkins NJ, Schisterman EF. The inconsistency of "optimal" cutpoints obtained using two criteria based on the receiver operating characteristic curve. *Am J Epidemiol* 2006; **163:** 670–675.
25. Yoshinaga M, Kucho Y, Nishibatake M, Ogata H, Nomura Y. Probability of diagnosing long QT syndrome in children and adolescents according to the criteria of the HRS/EHRA/APHRS expert consensus statement. *Eur Heart J* 2016; **37:** 2490–2497.
26. Schwartz PJ, Moss AJ, Vincent GM, Crampton RS. Diagnostic criteria for the long QT syndrome: An update. *Circulation* 1993; **88:** 782–784.
27. Hobbs JB, Peterson DR, Moss AJ, McNitt S, Zareba W, Goldenberg I, et al. Risk of aborted cardiac arrest or sudden cardiac death during adolescence in the long-QT syndrome. *JAMA* 2006; **296:** 1249–1254.
28. Pass RH, Fisher JD. Neonatal ECG screening and QT correction: The march towards consistency and accuracy. *Eur Heart J* 2018; **39:** 2896–2897.
29. Giudicessi JR, Roden DM, Wilde AAM, Ackerman MJ. Classification and reporting of potentially proarrhythmic common genetic variation in long QT syndrome genetic testing. *Circulation* 2018; **137:** 619–630.
30. Adler A, Novelli V, Amin AS, Abiusi E, Care M, Nannenberg EA, et al. Evidence-based reappraisal of genes reported to cause congenital long QT syndrome. *Circulation* 2020; **141:** 418–428.

Supplementary Files

Please find supplementary file(s);
https://doi.org/10.1253/circj.CJ-24-0148

Cureus
Part of SPRINGER NATURE

Open Access Case Report

A Rare Case of Ketosis-Prone Type 2 Diabetes With a Unique Human Leukocyte Antigen (HLA) Profile: Genetic and Metabolic Insights

Mai Mukai [1], Nobuyuki Koriyama [1], Ryotaro Hirahara [1], Kanako Wada [1], Yoshihiko Nishio [2]

1. Diabetes and Endocrine Medicine, National Hospital Organization (NHO) Kagoshima Medical Center, Kagoshima, JPN 2. Diabetes and Endocrine Medicine, Kagoshima University, Kagoshima, JPN

Corresponding author: Nobuyuki Koriyama, koriyama.nobuyuki.wm@mail.hosp.go.jp

Review began 01/01/2025
Review ended 01/06/2025
Published 01/10/2025

DOI: 10.7759/cureus.77247

Abstract

This report describes the case of a 21-year-old man with ketosis-prone type 2 diabetes (KPD), highlighting the genetic and metabolic factors influencing disease progression. The patient presented with diabetic ketoacidosis and demonstrated rapid insulin secretory recovery, allowing early discontinuation of insulin. Genetic analysis revealed human leukocyte antigen (HLA)-DRB1*15:01 and DRB1*09:01 haplotypes, suggesting a role of immune factors typically associated with type 1 diabetes in the pathogenesis of KPD. Metabolic factors, evidenced by prolonged ketone clearance, further underscore the complexity of KPD. These findings contribute to a growing understanding of KPD as a unique subtype of diabetes, reinforcing the importance of personalized, genetically informed management approaches for optimal care.

Categories: Endocrinology/Diabetes/Metabolism, Internal Medicine
Keywords: diabetic ketoacidosis, hla gene haplotype, ketosis-prone diabetes, type 1 diabetes, type 2 diabetes

Introduction

In 1987, Winter et al. offered the first description of young, obese individuals with type 2 diabetes (T2D) who developed diabetic ketoacidosis (DKA) without apparent triggers [1]. These individuals experienced recurrent episodes of DKA or ketosis but showed marked recovery of insulin secretion within a few months, allowing insulin withdrawal. This atypical form of T2D, termed ketosis-prone T2D (KPD), was initially thought to be prevalent mainly among African-American populations [2], but recent studies have increasingly reported cases in Asian populations [3]. KPD is predominantly observed in young, obese men with a family history of diabetes [4]. The pathology is often triggered by stress [5] or weight gain [6] and develops suddenly with ketosis or ketoacidosis [6]. It is inferred that understanding and responding to the characteristics of KPD is crucial for improving long-term glycemic control status and managing the risk of complications, while education based on these characteristics will also contribute to improving patient self-management skills. Genetic studies have shown a distinct human leukocyte antigen (HLA) profile for KPD, with a significantly lower prevalence of the type 1 diabetes (T1D)-susceptible haplotype HLA-DRB1*09:01 and a higher prevalence of the protective haplotypes HLA-DRB1*15:01 and/or HLA-DRB1*15:02 [7]. Here, we present a rare case of KPD with both HLA-DRB1*09:01 and HLA-DRB1*15:01.

Case Presentation

A 21-year-old man presented to a family doctor with a two-week history of thirst, polydipsia, polyuria, and significant weight loss (9 kg). He had a history of ureteral stones and a family history of T2D; his father, who had T2D, had died of myocardial infarction. The patient presented with a blood glucose level of 460 mg/dL and ketonuria (4+), prompting referral to our department. On admission, DKA was confirmed based on a glycohemoglobin A1c (HbA1c) level of 14.0% and a serum total ketone level of 10,101 µmol/L. Arterial blood gas analysis showed a pH of 7.296, arterial partial pressure of carbon dioxide at 28 mmHg, arterial partial pressure of oxygen at 104.8 mmHg, bicarbonate ions (HCO3-) at 13.4 mmol/L, base excess of -11.1 mmol/L, and anion gap of 24.90 mmol/L, indicating metabolic acidosis with a high anion gap and respiratory compensation (Table *1*).

	Laboratory test	Value		Reference range
Urinalysis	Protein	(+)	-	-
	Glucose	(4+)	-	-
	Ketone bodies	(4+)	-	-
Peripheral blood	WBC	8240	/µL	3300-8600
	RBC	595	$\times 10^4$/µL	435-555

How to cite this article
Mukai M, Koriyama N, Hirahara R, et al. (January 10, 2025) A Rare Case of Ketosis-Prone Type 2 Diabetes With a Unique Human Leukocyte Antigen (HLA) Profile: Genetic and Metabolic Insights. Cureus 17(1): e77247. DOI 10.7759/cureus.77247

	Hb	17.5	g/dL	13.7-16.8
	PLT	333	$\times 10^4/\mu L$	158-348
Biochemistry	AST	32	U/L	13-30
	ALT	73	U/L	10-42
	LDH	173	U/L	124-222
	ALP	117	U/L	38-113
	γ-GTP	65	U/L	13-64
	T. Bil	0.56	mg/dL	0.40-1.50
	chE	553	U/L	240-486
	AMY	69	mg/dL	44-132
	CK	105	U/L	59-248
	Alb	5.03	g/dL	4.10-5.10
	Na	136	mmol/L	138-145
	K	4	mmol/L	3.6-4.8
	Cl	98	mmol/L	101-108
	Ca	9.7	mg/dL	8.8-10.1
	IP	2.7	mg/dL	2.7-4.6
	Mg	2.1	mg/dL	1.8-2.3
	BUN	10.7	mg/dL	8.0-20.0
	Cr	0.7	mg/dL	0.65-1.07
	eGFR	113.8	mL/min/1.73 m^2	>60
	UA	8.9	mg/dL	3.7-7.8
	CRP	0.18	mg/dL	0.00-0.14
	TG	207	mg/dL	0.00-0.14
	LDL	218	mg/dL	65-163
	HDL	36	mg/dL	38-90
Arterial blood gas	pH	7.296	-	7.350-7.450
	$PaCO_2$	28.1	mmHg	35.0-45.0
	PaO_2	104.8	mmHg	83.0-108.0
	HCO_3^-	13.4	mmol/L	22.0-28.0
	BE	-11.1	mmol/L	-2 - +2
	AG	24.9	mmol/L	10.0-14.0

TABLE 1: Laboratory findings

WBC: white blood cells, RBC: red blood cells, Hb: hemoglobin, PLT: platelets, AST: aspartate aminotransferase, ALT: alanine aminotransferase, LDH: lactate dehydrogenase, ALP: alkaline phosphatase, γ-GTP: γ-glutamyltransferase, T.Bil: total bilirubin, chE: cholinesterase, AMY: amylase, CK: creatine kinase, Alb: albumin, Na: sodium, K: potassium, Cl: chloride, Ca: calcium, IP: inorganic phosphorus, Mg: magnesium, BUN: blood urea nitrogen, Cr: creatinine, eGFR: estimated glomerular filtration rate, UA: uric acid, CRP: C-reactive protein, TG: triglycerides, LDL: low-density lipoprotein cholesterol, HDL: high-density lipoprotein cholesterol, PaCO2: arterial partial pressure of carbon dioxide, PaO2: arterial partial pressure of oxygen, HCO3-: bicarbonate ion, BE: base excess, AG: anion gap

Height was 167.8 cm, weight was 70.6 kg, body mass index (BMI) was 25.1 kg/m², blood pressure was 148/82 mmHg, and heart rate was 122 beats/min. Body temperature was 37.1°C, respiratory rate was 16 breaths/min, and peripheral oxygen saturation on pulse oximetry was 97.0%. No other physical abnormalities or complications were identified.

Fasting serum C-peptide immunoreactivity (CPR) (2.19 ng/mL) and a CPR index (CPI: calculated as fasting serum CPR/fasting plasma glucose × 100) of 0.6 indicated significantly reduced endogenous insulin secretion. Results for islet autoantibodies were negative (Table 2).

Laboratory test	Value		Reference range
GADA	<5.0	U/mL	<5.0
IA-2A	<0.6	U/mL	<0.6
IAA	<0.4	U/mL	<0.4
ICA	Negative (<1.25)	JDF units	Negative (<1.25)
ZnT8A	<10.0	U/mL	<10.0
TgA	<10.0	IU/mL	<19.0
TPOA	2.5	IU/mL	<3.0
FT4	0.98	ng/dL	0.78-1.48
TSH	1.021	μU/mL	0.610-4.230
FPG at onset	357	mg/dL	73-109
HbA1c at onset	14.3	%	4.9-6.0
IRI at onset	6.3	μU/mL	5.0-10.0
Fasting CPR at onset	2.19	ng/mL	0.61-2.09
Fasting CPI at onset	0.6	-	1.03-2.17
24-h UCPR at onset	18.7	μg/day	29.2-167.0
TK at onset	10101	μmol/L	<130
3HBA at onset	7602	μmol/L	<85
AA at onset	2499	μmol/L	<55
Fasting CPR on day 8	2	ng/mL	0.61-2.09
Fasting CPI on day 8	1.6	-	1.03-2.17
24-h UCPR on day 12	70.2	μg/day	29.2-167.0
ΔCPR in glucagon tolerance test on day 15	1.82	ng/mL	>1.0

TABLE 2: Endocrinological laboratory findings

GADA: anti-glutamic acid decarboxylase antibody, IA-2A: anti-insulinoma-associated protein-2 antibody, IAA: anti-insulin autoantibody, ICA: islet cell antibody, ZnT8A: zinc transporter 8 antibody, TgA: anti-thyroglobulin antibody, TPOA: anti-thyroperoxidase antibody, FT4: free thyroxine, TSH: thyroid-stimulating hormone, FPG: fasting plasma glucose, HbA1c: glycohemoglobin A1c, IRI: immunoreactive insulin, CPR: C-peptide immunoreactivity, CPI: CPR index, 24-h UCPR: 24-h urinary CPR, TK: total ketone bodies, 3HBA: 3-hydroxybutyric acid, AA: acetoacetic acid

ΔCPR: calculated by subtracting pre-load CPR from post-load CPR; GADA, IA2A, and ZnT8: measured by enzyme-linked immunosorbent assay; ICA: measured by an indirect method with immunofluorescent antibody; TgA and TPOA: measured by electrochemiluminescent immunoassay

The HLA haplotypes were A*02:01, DRB1*09:01-DQB1*03:03, and DRB1*15:01-DQB1*06:02. A*02:0 has been reported to be involved in pancreatic β-cell dysfunction7. DRB1*09:01-DQB1*03:03 is reportedly associated with T1D susceptibility, whereas DRB1*15:01-DQB1*06:02 is reportedly associated with T1D resistance. These findings suggested the presence of a unique KPD profile-related immune gene (Table 3).

	Allele	Allele
A	02:01:01	26:03:01
B	15:01:01	39:01
C	03:03:01	07:02:01
DRB1	09:01:02	15:01
	DR9	DR15
DPB1	02:01:02	-
	or	
	02:01:02	141:01
	or	
	141:01	-
DQB1	03:03:02	06:02:01

TABLE 3: HLA genotyping

HLA: human leukocyte antigen

The patient was treated with insulin lispro and degludec, along with saline infusion, transitioning to dextrose by day 2. Insulin requirements peaked on days 8 and 9 and were tapered as metformin was introduced on day 11. During this period, blood glucose levels remained within 140-270 mg/dL (Figure *1*), and urinary ketones became negative on day 10. On day 16, insulin was discontinued, and the patient was discharged. Four weeks later, HbA1c had improved to 8.0% with a lower metformin dose, stabilizing at 5% by week 8 (Figure *1*). CPI on day 8 was 1.6, urinary CPR on day 12 had significantly recovered from 18.7 to 70.2 µg/day, and ΔCPR in the glucagon tolerance test performed on day 15 was 1.82 ng/mL (Table *2*).

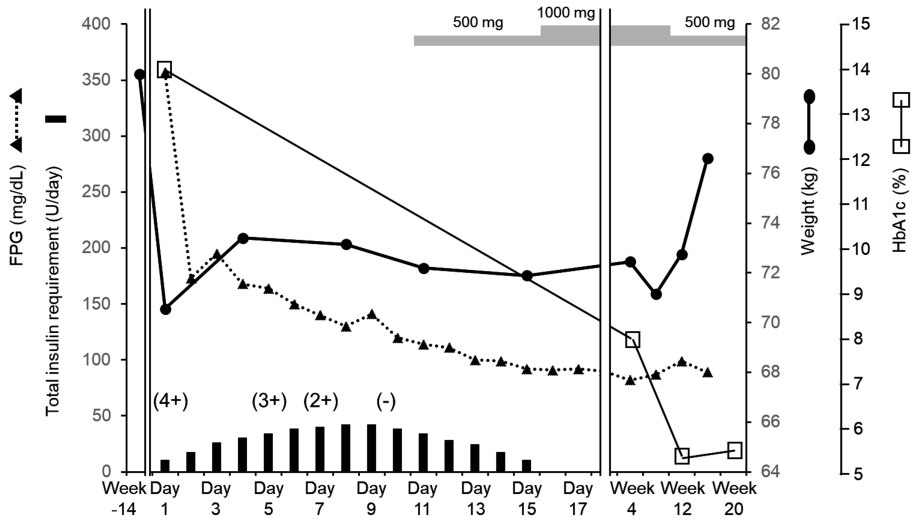

FIGURE 1: Clinical course of the patient

The bar graph at the bottom depicts the total daily insulin requirement. The dashed line with closed triangles indicates fasting blood glucose levels, while the thick solid line with closed circles shows body weight. The thin solid line with open squares denotes HbA1c levels. Values within parentheses with "+" or "-" signs indicate changes in urinary ketone levels over time. Gray-shaded bars at the top represent the dosage of metformin administered during the observation period.

HbA1c: glycohemoglobin A1c

Discussion

The patient was a young, obese male with a family history of T2D on the paternal side, and hyperglycemia was initially noted at the onset of DKA. Insulin secretory capacity recovered quickly after initiating treatment, allowing early discontinuation of insulin therapy. Given these characteristics, KPD was diagnosed. In cases initially resembling T1D, endogenous insulin secretion can sometimes improve, so considering the possibility of KPD is important in such presentations. According to some reports, KPD often recurs within two years after remission, with biguanides being effective in extending the remission period [4]. Consequently, metformin therapy was initiated for this patient, who achieved good glycemic control with an HbA1c of 5.3% at 12 weeks (Figure *1*). However, repeated episodes of DKA may lower the body weight threshold for onset and progressively impair insulin secretion. Therefore, weight gain trends in this patient will need to be monitored closely (Figure *1*).

KPD can be classified into four categories based on different diagnostic criteria: the American Diabetes Association (ADA) classification, the modified ADA classification, the BMI classification, and the Aβ classification [8]. The Aβ classification system divides patients into four subgroups according to the presence or absence of islet autoantibodies and β-cell function: antibody present with function absent (A+β-), antibody present with function present (A+β+), antibody absent with function absent (A-β-), and antibody absent with function present (A-β+) [8]. This classification system has clinical relevance, providing insights into glycemic control and insulin dependency status, thus serving as a valuable tool in both clinical and research settings. The Aβ classification of this case was A-β+.

Interestingly, Satomura et al. reported that approximately 36.4% of A-β+ KPD cases exhibit specific immunoreactivity to the insulin B chain amino acids 9-23-related peptide (B:9-23rPep), which is associated with interferon γ and reflects disease activity in T1D [7]. Detection rates of this immunoreactivity have been reported as 38.1% in acute-onset T1D and 8% in T2D, suggesting a potential role in the pathogenesis of T1D [7]. These findings and reports indicating reduced insulin secretion over time in KPD (A-β+) [6] support the hypothesis that KPD may represent a subtype of T1D with overlapping features.

In Japanese populations, the typical T1D susceptibility haplotypes are DRB1*0405-DQB1*0401, DRB1*0901-DQB1*0303, and DRB1*0802-DQB1*0302, while the typical resistance haplotypes are DRB1*1501-DQB1*0602 and DRB1*1502-DQB1*0601 [9]. Resistant alleles are known to be dominant over susceptibility alleles with respect to the development of T1D [10]. Genetically, about 60% of KPD patients possess HLA-DR3 or HLA-DR4 haplotypes associated with T1D susceptibility [11]. Approximately 30% show DRB1*15:01 or DRB1*15:02, representing HLA haplotypes associated with T1D resistance, and 50% carry A*02:01 or A24:02, which are linked to pancreatic β-cell dysfunction. The genotypes in this patient included HLA-DRB1*15:01 and DRB1*09:01, a T1D susceptibility haplotype, and A*02:01 (Table *2*). Although the pathogenesis of KPD remains unclear, this genetic information suggests that both the genetic background and immune response mechanisms seen in T1D could also be involved in KPD onset and activity. Major histocompatibility complex II of the T1D resistance haplotype reportedly presents islet antigens (suppressive antigens) to regulatory T cells (Tregs), thereby promoting the production of anti-inflammatory cytokines such as interleukin 10 and suppressing the activity of autoreactive islet-responsive T cells [12]. The T1D resistance haplotype is speculated to contribute to pancreatic β-cell protection in KPD by promoting specific Treg activation and suppressing autoreactive T cells. Further research would be extremely beneficial in elucidating the cellular pathways that promote the onset and progression of organ-specific autoimmune diseases such as T1D or clarifying how to induce tolerance.

In KPD, (1) leucine catabolism is enhanced; (2) α-glutamate accumulates due to a kinetic defect in ketoglutarate dehydrogenase; (3) anaplerosis of glucose carbon for the tricarboxylic acid (TCA) cycle is blunted; and (4) impaired peripheral oxidation of ketone bodies, which depends on the TCA cycle, has been reported [13]. In this case, the relatively prolonged duration of 10 days required for ketone clearance suggests a role of metabolic factors in the pathophysiology of KPD (Figure *1*). Other reports have linked KPD to glucose toxicity [14], reduced glucose-6-phosphate dehydrogenase activity [15], and inadequate glucagon inhibition following glucose loading [16]. These observations suggest a complex metabolic profile for KPD, likely involving genetic abnormalities in metabolism-related enzymes. Further research is needed to clarify these pathways' roles and identify potential therapeutic targets.

Conclusions

This case highlights the unique genetic and metabolic characteristics of KPD, contributing to our understanding of its pathogenesis and clinical management. The rapid recovery of insulin secretion and subsequent discontinuation of insulin in this patient, alongside his specific HLA haplotypes (HLA-DRB1*15:01 and DRB1*09:01), underscore the potential influence of genetic background and immune response on KPD. In addition, the extended duration required for ketone clearance suggests an underlying metabolic complexity, possibly related to abnormalities in ketone metabolism and amino acid pathways. These findings reinforce the notion that KPD may represent a distinct subtype of diabetes, potentially overlapping with T1D in terms of genetic and immunological profiles. Ongoing genetic and immunological studies are essential to fully elucidate the mechanisms underlying KPD and to inform targeted therapeutic strategies. Further, longitudinal monitoring of glycemic control and weight gain is crucial, as recurrence is

common, and weight fluctuations may affect insulin secretion capacity over time. This case adds valuable insights into the nuanced management of KPD, emphasizing a need for tailored therapeutic approaches in light of complex interplays between genetic, immunologic, and metabolic factors.

Additional Information

Author Contributions

All authors have reviewed the final version to be published and agreed to be accountable for all aspects of the work.

Concept and design: Nobuyuki Koriyama, Ryotaro Hirahara, Kanako Wada, Yoshihiko Nishio

Acquisition, analysis, or interpretation of data: Nobuyuki Koriyama, Mai Mukai

Drafting of the manuscript: Nobuyuki Koriyama, Mai Mukai

Critical review of the manuscript for important intellectual content: Nobuyuki Koriyama, Ryotaro Hirahara, Kanako Wada, Yoshihiko Nishio

Supervision: Nobuyuki Koriyama, Yoshihiko Nishio

Disclosures

Human subjects: Consent for treatment and open access publication was obtained or waived by all participants in this study. **Conflicts of interest:** In compliance with the ICMJE uniform disclosure form, all authors declare the following: **Payment/services info:** All authors have declared that no financial support was received from any organization for the submitted work. **Financial relationships:** All authors have declared that they have no financial relationships at present or within the previous three years with any organizations that might have an interest in the submitted work. **Other relationships:** All authors have declared that there are no other relationships or activities that could appear to have influenced the submitted work.

References

1. Winter WE, Maclaren NK, Riley WJ, Clarke DW, Kappy MS, Spillar RP: Maturity-onset diabetes of youth in black Americans. N Engl J Med. 1987, 316:285-91. 10.1056/NEJM198702053160601
2. Vellanki P, Umpierrez GE: Diabetic ketoacidosis: a common debut of diabetes among African Americans with type 2 diabetes. Endocr Pract. 2017, 23:971-8. 10.4158/EP161679.RA
3. Gupta RD, Ramachandran R, Gangadhara P, et al.: Clinical characteristics, beta-cell dysfunction and treatment outcomes in patients with A-β+ Ketosis-Prone Diabetes (KPD): The first identified cohort amongst Asian Indians. J Diabetes Complications. 2017, 31:1401-7. 10.1016/j.jdiacomp.2017.06.008
4. Umpierrez GE, Smiley D, Kitabchi AE: Narrative review: ketosis-prone type 2 diabetes mellitus . Ann Intern Med. 2006, 144:350-7. 10.7326/0003-4819-144-5-200603070-00011
5. Small C, Egan AM, Elhadi EM, O'Reilly MW, Cunningham A, Finucane FM: Diabetic ketoacidosis: a challenging diabetes phenotype. Endocrinol Diabetes Metab Case Rep. 2017, 2017:109. 10.1530/EDM-16-0109
6. Satomura A, Oikawa Y, Haisa A, Inoue I, Noda M, Shimada A: Bodyweight threshold for sudden onset of ketosis might exist in ketosis-prone type 2 diabetes patients. J Diabetes Investig. 2020, 11:499-501. 10.1111/jdi.13120
7. Satomura A, Oikawa Y, Haisa A, Suzuki S, Nakanishi S, Katsuki T, Shimada A: Clinical significance of insulin peptide-specific interferon-γ-related immune responses in ketosis-prone type 2 diabetes. J Clin Endocrinol Metab. 2022, 107:2124-32. 10.1210/clinem/dgab912
8. Maldonado M, Hampe CS, Gaur LK, et al.: Ketosis-prone diabetes: dissection of a heterogeneous syndrome using an immunogenetic and beta-cell functional classification, prospective analysis, and clinical outcomes. J Clin Endocrinol Metab. 2003, 88:5090-8. 10.1210/jc.2003-030180
9. Kawabata Y, Ikegami H, Kawaguchi Y, et al.: Asian-specific HLA haplotypes reveal heterogeneity of the contribution of HLA-DR and -DQ haplotypes to susceptibility to type 1 diabetes. Diabetes. 2002, 51:545-51. 10.2337/diabetes.51.2.545
10. Kawabata Y, Ikegami H, Awata T, et al.: Differential association of HLA with three subtypes of type 1 diabetes: fulminant, slowly progressive and acute-onset. Diabetologia. 2009, 52:2513-21. 10.1007/s00125-009-1539-9
11. Banerji MA, Chaiken RL, Huey H, et al.: GAD antibody negative NIDDM in adult black subjects with diabetic ketoacidosis and increased frequency of human leukocyte antigen DR3 and DR4. Flatbush diabetes. Diabetes. 1994, 43:741-5. 10.2337/diab.43.6.741
12. Choukem SP, Sobngwi E, Boudou P, et al.: β- and α-cell dysfunctions in africans with ketosis-prone atypical diabetes during near-normoglycemic remission. Diabetes Care. 2013, 36:118-23. 10.2337/dc12-0798
13. Mitchell AM, Michels AW: Self-antigens targeted by regulatory T cells in type 1 diabetes . Int J Mol Sci. 2022, 23:3155. 10.3390/ijms23063155
14. Patel SG, Hsu JW, Jahoor F, et al.: Pathogenesis of A^{-}β^{+} ketosis-prone diabetes . Diabetes. 2013, 62:912-22. 10.2337/db12-0624
15. Gosmanov AR, Smiley D, Robalino G, Siqueira JM, Peng L, Kitabchi AE, Umpierrez GE: Effects of intravenous

glucose load on insulin secretion in patients with ketosis-prone diabetes during near-normoglycemia remission. Diabetes Care. 2010, 33:854-60. 10.2337/dc09-1687

16. Sobngwi E, Gautier JF, Kevorkian JP, et al.: High prevalence of glucose-6-phosphate dehydrogenase deficiency without gene mutation suggests a novel genetic mechanism predisposing to ketosis-prone diabetes. J Clin Endocrinol Metab. 2005, 90:4446-51. 10.1210/jc.2004-2545

Pathology - Research and Practice 263 (2024) 155560

Contents lists available at ScienceDirect

Pathology - Research and Practice

journal homepage: www.elsevier.com/locate/prp

Heterotopic salivary duct inclusions in Warthin tumor – A cryptic histological finding involved in its pathogenesis

Masamichi Goto [a, *, 1], Kengo Nishimoto [b], Yasuyo Jougasaki [a], Tsutomu Matsuzaki [b], Tomonori Tanaka [b], Mitsuharu Nomoto [a]

[a] Department of Pathology, NHO Kagoshima Medical Center, Kagoshima, Japan
[b] Department of Otorhinolaryngology, NHO Kagoshima Medical Center, Kagoshima, Japan

ARTICLE INFO

Keywords:
Warthin tumor
Pathogenesis
Lymph node
Ectopic salivary duct
Smoking

ABSTRACT

Warthin tumor (WT) is the second most common benign parotid gland tumor after pleomorphic adenoma. WT is characterized by cystic and papillary proliferation of a two-layered oncocytic epithelium supported by lymphoid tissue. Heterotopic salivary duct inclusions (SDIs) are frequently observed in lymph nodes (LNs) of WT (SDI/LNs), and are thought to be the origin of WT. If this is true, SDIs should also persist in the lymphoid tissue of WT itself (SDI/WT), as a missing link between SDIs and WTs, but studies of this issue are limited. From 2008–2023, 138 WT cases were surgically excised at our hospital. SDI/LNs and SDI/WTs were histologically examined. Of 100 WT cases with LNs, SDI/LNs were observed in 67 cases (67 %). SDI/WTs were detected in 114 of 138 cases (82.6 %), including 107 of 127 smokers (84.3 %) and 7 of 11 never-smokers (63.6 %). SDI/WTs were located mainly in the subcapsular lymphoid tissue and often surrounded by a fibrous coat resembling salivary excretory ducts. This study revealed a high incidence of SDIs in WT itself, strongly supporting the theory that WT develops from heterotopic salivary ducts.

1. Introduction

Warthin tumor (WT) is a benign neoplasm of the parotid gland characterized by cystic and papillary proliferation of a two-layered oncocytic epithelium supported by lymphoid tissue [1]. WT was reported by Albrecht and Arzt as "Papilläre Cystadenome in Lymphdrüsen" in 1910 [2]. In 1929, Warthin described two parotid tumors named "papillary cystadenoma lymphomatosum" that had a ciliated respiratory epithelium with lymphoid stroma [3]. Given the current understanding of the tumor, this description does not exactly match WT, but this tumor is still referred to as Warthin tumor.

There are two major hypotheses for the pathogenesis of WT. Since heterotopic salivary duct inclusions (SDIs) are frequently observed in lymph nodes (LNs) of the parotid region [4], WT may arise from the oncocytic component of this ectopic tissue (SDI/LNs). This theory is widely accepted, but it has also been suggested that tumors can induce tumor-associated lymphoid proliferation [5]. If the first theory is true, persistent heterotopic salivary ducts (SDIs) should also be observed in lymphoid tissue of WT itself, at least in some lesions, but few studies of this issue have been performed. In Albrecht and Arzt's historical paper, Fig. 1 clearly illustrates such a structure [2]. Recently, Sakamoto et al. showed that non-oncocytic excretory duct-type salivary inclusions transform into oncocytic epithelial components of WT [6].

With this background, we sought to identify SDIs in WT in this study. Since smoking is a known risk factor for WT, we also examined the influence of smoking on SDIs.

2. Materials and methods

All cases of WT with a surgically excised parotid gland were retrieved from the database of the Department of Otorhinolaryngology, National Hospital Organization (NHO) Kagoshima Medical Center, Kagoshima from April 2008 to June 2023. Among these cases, those with a recorded smoking status were reviewed pathologically.

* Correspondence to: Department of Pathology, NHO Kagoshima Medical Center, 8-1 Shiroyama-cho, Kagoshima 892-0853, Japan.
E-mail addresses: masagoto@po4.synapse.ne.jp (M. Goto), nishimoto.kengo.gy@mail.hosp.go.jp (K. Nishimoto), jogasaki.yasuyo.vm@mail.hosp.go.jp (Y. Jougasaki), matsuzaki.tsutomu.qv@mail.hosp.go.jp (T. Matsuzaki), tanaka.tomonori.uf@mail.hosp.go.jp (T. Tanaka), nomoto.mitsuharu.sh@mail.hosp.go.jp (M. Nomoto).
[1] ORCID ID0000–0003-0943–4115

https://doi.org/10.1016/j.prp.2024.155560
Received 10 June 2024; Received in revised form 15 August 2024; Accepted 23 August 2024
Available online 29 August 2024

WT was diagnosed using the criteria of the World Health Organization [1]. WT was diagnosed regardless of the lesion size. SDI/LNs were defined as ectopic salivary ducts in the LN parenchyma [4]. Ducts admixed with adipose tissue at the hilum of the LN were excluded. Eosinophilic (oncocytic) change was recorded if present. SDI/WTs were defined as non-oncocytic ectopic salivary ducts within lymphoid tissue of WT. Ducts within the fibrous capsule were excluded. Some LNs showed proliferation of oncocytic epithelium resembling WT. These cases were defined as WT if the area of oncocytic epithelium was ≥50 % of the lesion.

Age, gender, left or right side, number of lesions, and smoking status were obtained from clinical records. Cases with LNs, cases with SDI/LNs, cases with oncocytic SDI/LNs, number of LNs, number of LNs with SDIs, cases with SDI/WTs, number of lesions with SDI/WTs, and cases with squamous metaplasia in WT were histologically evaluated by hematoxylin and eosin staining.

2.1. Statistics

Data were analyzed using the R computing environment (EZR) [7]. Nonparametric tests of group differences were performed by Fisher exact test (two-tailed) or Mann-Whitney U test (two-tailed). A p-value < 0.05 was considered to be statistically significant.

2.2. Ethical considerations

This study was approved by the Ethical Committee of NHO Kagoshima Medical Center (accession number 2023–10).

3. Results

From April 2008 to June 2023, 182 WT cases were treated by surgical excision from the parotid gland. Smoking status was recorded in 138 of these cases. Current smokers (n=104) and ex-smokers (n=23) were collectively classified as smokers (n=127), and persons with no smoking history as never-smokers (n=11). The main results of the study are summarized in Table 1. In the present study, 138 cases with known smoking status were analyzed. The mean age of WT cases (n=138) was 64.4 years ± 7.7 (median 65, range 41–81) and the male-to-female ratio was 7.1/1. Ten cases (7.2 %) had bilateral lesions, 38 (27.5 %) had multiple lesions, and 4 (2.9 %) had recurrence. Of the 38 cases with multiple lesions, 28 had two lesions and 10 had ≥3 lesions. The mean size of WT (n=138) was 34.3 ± 14.1 mm (median 33 mm, range 7–80 mm) in largest diameter.

Representative photomicrographs of SDI/LNs are shown in Fig. 1a-c, and those of SDI/WTs are shown in Fig. 1d-j. A single LN (Fig. 1a) at higher magnification (Fig. 1b) showed multiple SDI/LNs (blue arrowheads) surrounded by thin fibrous tissue. Oncocytic SDI/LN (pink arrowhead) and non-oncocytic SDI/LN (blue arrowhead) in another LN are shown in Fig. 1c. WT with non-oncocytic SDI/WTs in lymphoid tissue (Fig. 1d) is shown at higher magnification (Fig. 1e) to show the SDI/WTs (yellow arrowheads). A blood vessel (*) resembling the duct was also present. A WT with SDI/WTs (Fig. 1f-h) had both non-oncocytic SDI/WTs (yellow arrowheads) (Fig. 1g, h) and an oncocytic duct (red arrowhead) (Fig. 1h). The latter was not counted as a SDI/WT. Another WT with non-oncocytic and oncocytic SDI/WTs is shown in Figs. 1i and 1j. Here, the oncocytic ducts (red arrowheads) were in transition with the epithelial component of WT (black arrowhead). Most SDI/WTs were located close to capsules of WT and were often surrounded by a layer of fibrous tissue (Fig. 1g). These SDI/WTs were easily overlooked at low magnification.

As shown in Table 1, 100 of 138 WT cases had LNs within or around the salivary glands. Among them, SDI/LNs were observed in 67 cases (67.0 %). Oncocytic SDI/LNs were present in 21 of 100 WT cases (21.0 %), and similar rates were found in smokers (19/93, 20.4 %) and never-smokers (2/7, 28.5 %). The mean number of LNs per WT case was 2.41. Among all LNs examined, SDI/LNs were observed in 100 of 333 LNs (30.0 %). A comparison of the SDI/LNs incidence by age group did not reveal a consistent trend (3/6 in 40 s, 14/22 in 50 s, 28/40 in 60 s, 13/20 in 70 s, and 3/3 in 80 s).

Table 1
Heterotopic salivary ducts in lymph nodes and Warthin tumors of the parotid gland.

Item	Warthin tumor			
	Total	Smoking status	Smokers*	Never-smokers
Number of cases	182	138	127	11
Gender				
Male	155	121	114	7
Female	27	17	13	4
Male/Female	5.7/1	7.1/1	8.8/1	1.8/1
Age				
Range	41–81	41–81	41–81	64–74
Mean + Standard deviation	65.1 + 7.8	64.4 + 7.7	63.8 + 7.6	70.3 + 5.5
Median	66	65	65	73
Location				
Left only	90	70	64	6
Right only	76	58	53	5
Bilateral	16	10	10	0
Number of lesions				
Single lesion	138	100	89	11
Multiple lesions	44	38	38	0
Total number of lesions	NE	198	187	11
Recurrence	4	4	4	0
Lymph nodes and SDI/LNs				
Cases with lymph nodes	NE	100/138 (72.5 %)	93/127 (73.2 %)	7/11 (63.6 %)
Cases with salivary duct inclusions (SDI/LNs)	NE	**67/100 (67.0 %)**	61/93 (65.6 %)	6/7 (85.7 %)
Cases with oncocytic heterotopic salivary ducts (SDI/LNs)	NE	21/100 (21.0 %)	19/93 (20.4 %)	2/7 (28.5 %)
Number of lymph nodes/case	NE	2.41	2.47	1.73
Lymph nodes with salivary duct inclusions (SDI/LNs)	NE	100/333 (30.0 %)	90/314 (28.7 %)	7/19 (36.8 %)
Warthin tumors and SDI/WTs				
Cases with heterotopic salivary ducts in the tumor (SDI/WTs)	NE	**114/138 (82.6 %)**	107/127 (84.3 %)	7/11 (63.6 %)
Number of WT lesions/case	NE	1.43	1.47	1.00
Lesions with heterotopic salivary ducts in the tumor (SDI/WTs)	NE	152/198 (76.8 %)	145/187 (77.5 %)	7/11 (63.6 %)
Cases with squamous metaplasia in the tumor	NE	19/138 (13.8 %)	15/127 (11.8 %)	4/11 (36.4 %)

NE, not evaluated
* Smokers include current smokers and ex-smokers.

SDI/WTs were found in lymphoid tissue of WT in 114/138 cases (82.6 %). The rate of SDI/WTs did not differ significantly between smokers (107/127 (84.3 %)) and never-smokers (7/11 (63.6 %)). A comparison of the SDI/WTs incidence by tumor size did not reveal a consistent trend, and SDI was observed in every size of WT (3/4 in 1–10 mm, 14/18 in 11–20 mm, 32/42 in 21–30 mm, 31/35 in 31–40 mm, 20/24 in 41–50 mm, 10/10 in 51–60 mm, 2/2 in 61–70 mm, and 2/3 in 71–80 mm). The mean number of WT lesions per WT cases was 1.43. Among all WT lesions examined, SDI/WTs were observed in 152/198 lesions (76.8 %).

The position of SDI/WT in the pathogenesis of WT is shown in Fig. 2. Ordinary LNs (Fig. 2A), LNs with SDI (Fig. 2B), oncocytic SDIs (Fig. 2C), and WT (Fig. 2E) have been described previously. The results of this study allow WT with SDIs (Fig. 2D) to be inserted between Fig. 2B/C and Fig. 2E.

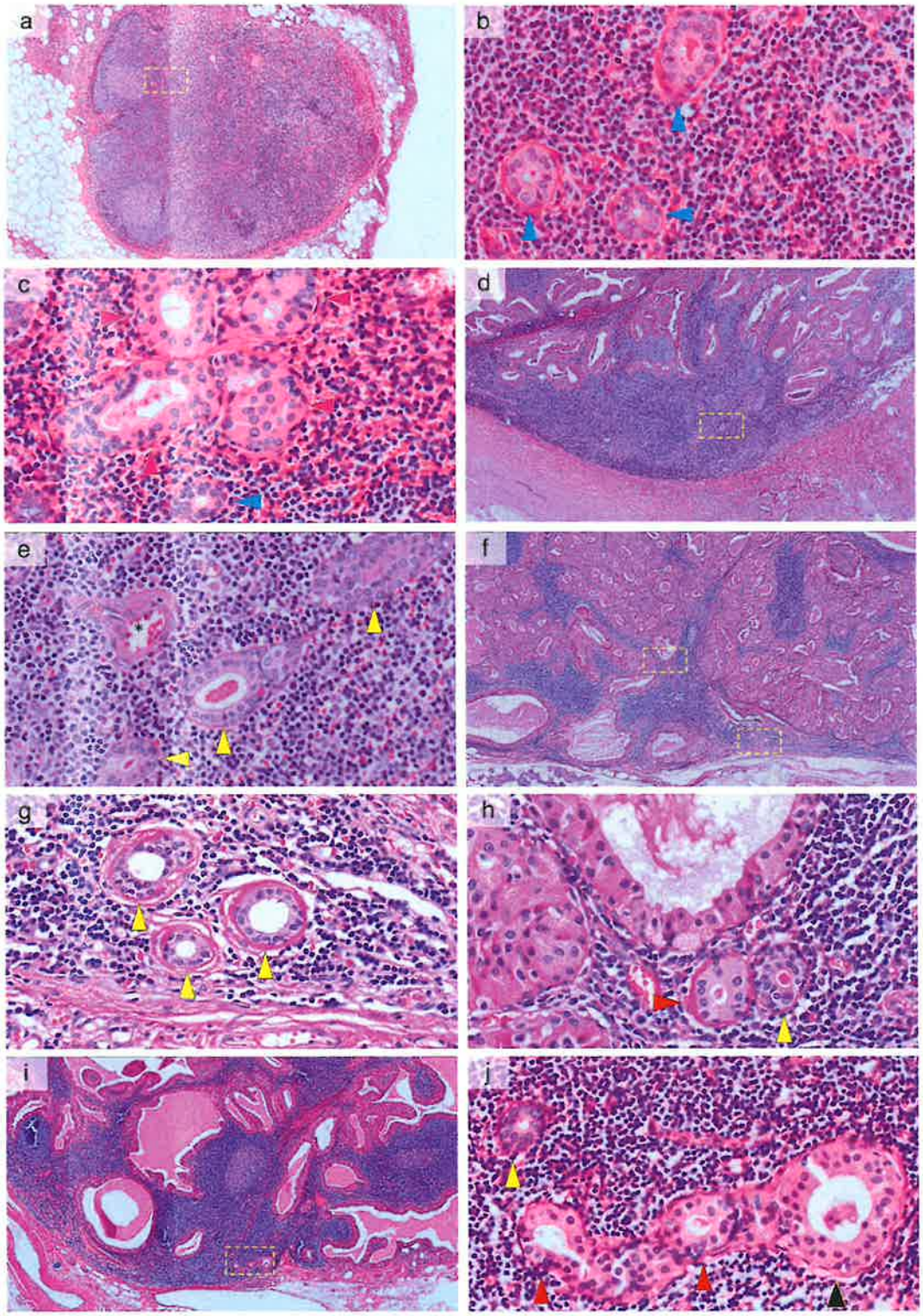

Fig. 1. Histopathology of heterotopic salivary duct inclusions in lymph nodes (SDI/LNs) and Warthin tumors (SDI/WTs). (a) Lymph node with SDI/LNs. (b) SDI/LNs (blue arrowheads) surrounded by thin fibrous tissue. (c) Oncocytic SDI/LN (pink arrowhead) and SDI/LN (blue arrowhead) in another lymph node. (d) Warthin tumor with SDI/WTs. (e) Non-oncocytic SDI/WTs (yellow arrowheads). A blood vessel (*) is also present. (f) Warthin tumor with SDI/WTs. (g) Non-oncocytic SDI/WTs (yellow arrowheads) surrounded by thin fibrous tissue. (h) A non-oncocytic SDI/WT (yellow arrowhead) and an oncocytic duct (red arrowhead). The latter was excluded from this study. (i) Warthin tumor with SDI/WTs. (j) A non-oncocytic SDI/WT (yellow arrowhead), oncocytic ducts (red arrowheads) and epithelial component of WT (black arrowhead). (a-j) Hematoxylin and eosin staining. Magnification (Objective lens) a, d, f, i, 4x; b, c, e, g, h, j, 40x.

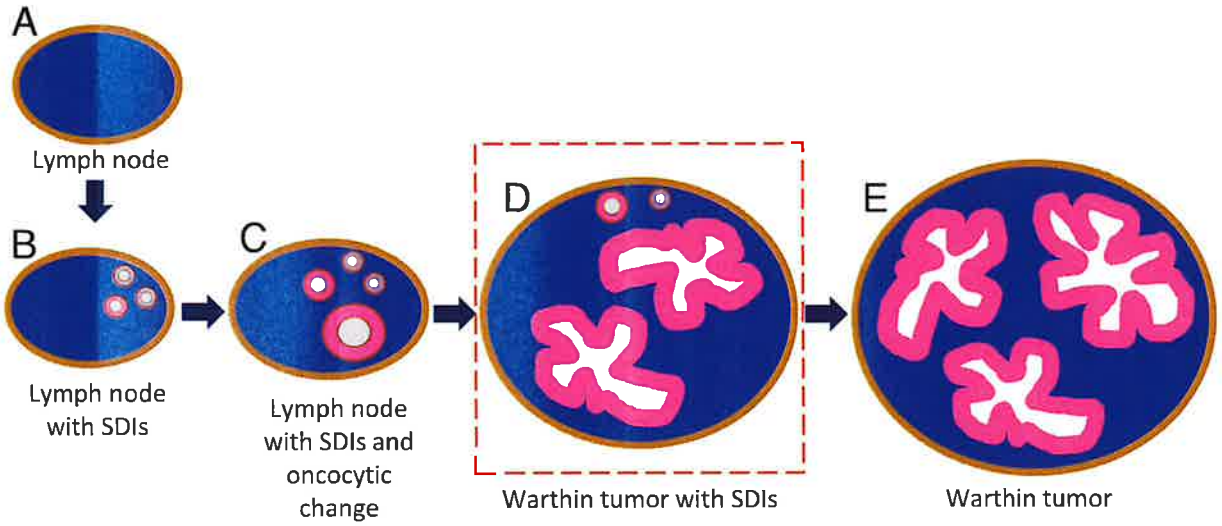

Fig. 2. Hypothesis for the pathogenesis of Warthin tumor. (A) Normal lymph node. (B) Lymph node with heterotopic salivary duct inclusions (SDI/LNs). (C) Oncocytic change of SDI. (D) Warthin tumor with persistent heterotopic salivary ducts (SDI/WTs). (E) Warthin tumor without SDIs. In this study, (D), the missing link, was common (82.6 %) in Warthin tumor.

4. Discussion

The age and gender distributions of WT in the present study were similar to those in previous studies [8,9]. In this study, 7.2 % of WT cases were bilateral, 27.5 % were multiple, and 7.2 % had three or more lesions. The recurrence rate was 2.9 %. In Maiorano et al. [8], 6.5 % of WT cases were bilateral and 20.5 % were multifocal, consistent with our data.

The ducts of the major salivary glands consist of intercalated, striated, and excretory (interlobular) ducts located from the acini to the oral cavity [10]. The striated duct has a bright eosinophilic (oncocytic) columnar epithelium due to rich mitochondria and invagination of the deep cell membrane. The excretory duct is surrounded by a fibrous coat of collagen and elastic fibers. As the epithelium of WT is oncocytic, the striated duct is suspected to be the origin of WT [11]. In the lymphoid stroma of WT, oncocytic ducts were also frequently observed, but were sometimes similar or in transition with the epithelial component of WT; therefore, we did not count oncocytic ducts in WT as SDI/WTs. Instead, non-oncocytic ducts in WT were often surrounded by fibrous coats, which resembled excretory ducts, as shown in an immunohistochemical study [6].

Heterotopic salivary tissue, especially ducts, is often present in parotid LNs, which are of fetal origin and appear by the 2nd month of gestation [10]. In the present study, SDI/LNs were observed irrespective of age, which supports the developmental origin of SDIs. These ducts have commonly been thought to be the origin of WT [2,12]. We have shown that SDIs are frequent in LNs in WT cases (67.0 %), supporting this theory. Cope et al. also found that 71.7 % of WT cases had SDIs [4], which is consistent with our current results. One difference between the two studies is the incidence of SDI/LNs based on the number of LNs. In our study, 107/333 (32.1 %) of WT LNs had SDIs, while Cope et al. found rates of 85/383 (22 %) [4]. This may mainly be due to the number of LNs examined per case: 2.41 for WT in this study, and 6.13 for WT in Cope et al. The difference may also be caused by the different definitions of WT: "an aggregate of lymphoid tissue >1 cm in greatest dimension containing proliferating oncocytic epithelium" in Cope et al. [4], whereas we diagnosed WT irrespective of the lesion size because the greatest dimension of WT was $\leq$10 mm in four cases.

Smoking is an important risk factor for WT. In a case-control study in the 1980s in Canada, smokers had an eight times higher risk of developing WT compared to non-smokers [13]. In a nationwide case-control study in Israel, the risk (odds ratio) for WT was 15.3 times in ever cigarette smokers [14]. In the present study, 127/138 (92.0 %) of WT cases were smokers (including ex-smokers), which also implies that smoking is a risk factor for WT. Oncocytic change of SDI/LNs was frequent in WT, suggesting a possible role of smoking in oncocytic change. Cope et al. have observed that 45.7 % of WT subjects with nodal tissue had oncocytic inclusions, compared with 5.8 % of pleomorphic adenoma subjects. They showed oncocytic inclusions were significantly associated with smoking in a multivariate model [4]. Lewis et al. demonstrated mitochondrial DNA damage in 2.5 % of WT and 0.1 % of normal parotid glands by fluorescent in situ hybridization and polymerase chain reaction studies [15]. The DNA deletion was significantly higher in oncocytic tumor cells. However, in the present study oncocytic SDI/LNs were found in both smokers (20.4 %) and never-smokers (28.5 %) in WT, which suggests that smoking is not directly associated with the incidence of SDI/LNs.

In this study, we used the terms SDI not only in LNs (SDI/LNs) but also in WT itself (SDI/WTs). Oncocytic ducts were included in SDI/LNs, but excluded from SDI/WTs, because it was sometimes difficult to distinguish the epithelial component of WT from the heterotopic oncocytic salivary duct in WT. There was a gradual transition from LNs with SDIs and small WT, and non-oncocytic salivary ducts were a common finding in established WT (82.6 %). Therefore, we assume that SDI/LNs and SDI/WTs are essentially identical.

In a molecular analysis, Honda et al. [16] showed the polyclonal nature of the epithelial component of WT, suggesting that WT is a non-neoplastic tumor-like condition. Low molecular weight cytokeratin, revealed by Cam5.2 immunohistochemistry, is a marker of extrafollicular reticulum cells found only in true LNs. McLean-Holden and Bishop [17] showed that lymphoid tissue in WT is positive for Cam5.2, which strongly supports the theory that WT arises from SDIs. In contrast to these studies, we performed a simple histological examination of WT specimens, but identified SDI/WTs at a high frequency.

The role of SDI/WTs in the pathogenesis of WT is summarized in Fig. 2. LNs with SDIs (Fig. 2B), oncocytic SDIs (Fig. 2C), and WTs (Fig. 2E) have been widely studied. In this study, we have added WT with SDIs (Fig. 2D) to fill the missing link between Fig. 2B/C and Fig. 2E. In conclusion, a high incidence of SDI in WT itself proven in our study strongly supports the theory that WT develops from ectopic salivary ducts.

Disclosure statement

The authors declare no conflicts of interest associated with this study.

CRediT authorship contribution statement

Yasuyo Jougasaki: Writing – review & editing, Investigation. **Tsutomu Matsuzaki:** Resources. **Tomonori Tanaka:** Resources. **Mitsuharu Nomoto:** Writing – review & editing, Investigation, Conceptualization. **Masamichi Goto:** Writing – original draft, Project administration, Conceptualization. **Kengo Nishimoto:** Resources, Investigation.

Declaration of Competing Interest

The authors have no competing interests to disclose.

References

[1] R.H.W. Simpson, W.C. Faquin, S. Di Palma, S. Pasricha, Warthin tumour, in: A. Skalova, M.D. Hyrcza, R. Mehrotra (Eds.), WHO Classif. Head Neck Tumours (5th Ed., 2024: pp. 173–175.
[2] H. Albrecht, L. Arzt, Beiträge zur Frage der Gewebsrevirrung, Papillare cystadenome in lymphdrüsen, Frankf. Z. Pathol. 4 (1910) 47–69.
[3] A.S. Warthin, Papillary cystadenoma lymphomatosum: a rare teratoid of the parotid region, J. Cancer Res. 13 (1929) 116–125, https://doi.org/10.1158/jcr.1929.116.
[4] W. Cope, C. Naugler, S.M. Taylor, J. Trites, R.D. Hart, M.J. Bullock, The association of warthin tumor with salivary ductal inclusions in intra and periparotid lymph nodes, Head. Neck Pathol. 8 (2014) 73–76, https://doi.org/10.1007/s12105-013-0477-5.
[5] P.L. Auclair, Tumor-associated lymphoid proliferation in the parotid gland: A potential diagnostic pitfall, Oral. Surg. Oral. Med. Oral. Pathol. 77 (1994) 19–26, https://doi.org/10.1016/S0030-4220(06)80102-7.
[6] S. Sakamoto, F. Ide, M. Hoshino, M. Nishimura, K. Kusama, K. Kikuchi, A new insight into the histogenesis and morphogenesis of Warthin tumour: significance of intranodal excretory duct inclusions, Histopathology 82 (2023) 789–791, https://doi.org/10.1111/his.14866.
[7] Y. Kanda, Investigation of the freely available easy-to-use software "EZR" for medical statistics, Bone Marrow Transpl. 48 (2013) 452–458, https://doi.org/10.1038/bmt.2012.244.
[8] E. Maiorano, L. Lo Muzio, G. Favia, A. Piattelli, Warthin's tumour: A study of 78 cases with emphasis on bilaterality, multifocality and association with other malignancies, Oral. Oncol. 38 (2002) 35–40, https://doi.org/10.1016/S1368-8375(01)00019-7.
[9] A. Teymoortash, Y. Krasnewicz, J.A. Werner, Clinical features of cystadenolymphoma (Warthin's tumor) of the parotid gland: a retrospective comparative study of 96 cases, Oral. Oncol. 42 (2006) 569–573, https://doi.org/10.1016/j.oraloncology.2005.10.017.
[10] F. Martinez-Madrigal, Major Salivary Glands, 5th ed., in: S. Mills (Ed.), Histol. Pathol., 5th Ed, Wolters Kluwer, 2019, pp. 440–466, 5th ed.
[11] A. Teymoortash, J.A. Werner, Tissue that has lost its track: Warthin's tumour, Virchows Arch. 446 (2005) 585–588, https://doi.org/10.1007/s00428-005-1276-5.
[12] A. Teymoortash, J.A. Werner, R. Moll, Is Warthin's tumour of the parotid gland a lymph node disease? Histopathology 59 (2011) 143–145, https://doi.org/10.1111/j.1365-2559.2011.03891.x.
[13] C.A. Kotwall, Smoking as an etiologic factor in the development of Warthin's tumor of the parotid gland, Am. J. Surg. 164 (1992) 646–647, https://doi.org/10.1016/S0002-9610(05)80725-1.
[14] S. Sadetzki, B. Oberman, L. Mandelzweig, A. Chetrit, T. Ben-Tal, A. Jarus-Hakak, S. Duvdevani, E. Cardis, M. Wolf, Smoking and risk of parotid gland tumors: a nationwide case-control study, Cancer 112 (2008) 1974–1982, https://doi.org/10.1002/cncr.23393.
[15] P. Lewis, P. Baxter, A. Paul Griffiths, J. Parry, D. Skibinski, Detection of damage to the mitochondrial genome in the oncocytic cells of Warthin's tumour, J. Pathol. 191 (2000) 274–281.
[16] K. Honda, K. Kashima, T. Daa, S. Yokoyama, I. Nakayama, Clonal analysis of the epithelial component of Warthin's tumor, Hum. Pathol. 31 (2000) 1377–1380, https://doi.org/10.1053/hupa.2000.19449.
[17] A.C. McLean-Holden, J.A. Bishop, Low molecular weight cytokeratin immunohistochemistry reveals that most salivary gland warthin tumors and lymphadenomas arise in intraparotid lymph nodes, Head. Neck Pathol. 15 (2021) 438–442, https://doi.org/10.1007/s12105-020-01215-2.

JPRS Journal of Plastic and Reconstructive Surgery
https://doi.org/10.53045/jprs.2024-0034
https://j-prs.jp/index.html

Brief Report

Proportion of Japanese Patients with Multiple Basal Cell Carcinomas: The Effectiveness of Screening

Megumi Aoki[1)], Kazuyasu Fujii[1)], Kentaro Yamamura[1)2)] and Shigeto Matsushita[1)]

1) Department of Dermato-Oncology/Dermatology, NHO Kagoshima Medical Center, Kagoshima, Japan
2) Department of Dermatology, Kyoto University Hospital, Kyoto, Japan

Abstract
Basal cell carcinoma (BCC) usually occurs as a solitary lesion but occasionally presents as multiple lesions. The proportion of multiple BCCs is 5.9%-7.1% in Asian patients. We conducted BCC screening in April 2021, focusing on the presence or absence of multiple lesions. Patients examined between April 2021 and March 2022 (161 lesions in 136 patients) were classified as the screening group (SG) and those examined between April 2020 and March 2021 (111 lesions in 103 patients) were classified as the non-screening group (NSG). The proportion of patients with multiple BCCs was significantly higher in the SG than in the NSG (15.4% and 6.8%, p = 0.04). We provisionally classified the head and neck gaze region into the 'central region' and 'peripheral region' based on gaze patterns. In the SG, the proportion of lesions in the peripheral region was higher in patients with multiple BCCs (32.6%) than in patients with a solitary BCC (14.8%). We speculate that we missed recognizing tumours in different areas, especially peripheral areas of the head and neck. Our results indicate that the increase in multiple lesion cases through screening occurred owing to more conscious observation of different regions, especially head and neck regions, thereby overcoming human gaze patterns.

Keywords
Asian, multiple basal cell carcinoma, gaze behaviour, screening, skin cancer

J Plast Recontr Surg 2025; 4(3): 169-172
https://doi.org/10.53045/jprs.2024-0034

Introduction

Basal cell carcinoma (BCC) is the most common skin cancer, and its incidence is increasing worldwide[1)]. It usually occurs as a solitary lesion but occasionally presents as multiple lesions. Racial differences have been reported in the proportion of patients with BCC who have another BCC, ranging from 30% to 45% in Caucasians[2,3)] and from 5.9% to 7.1% in Asians[4-7)].

In April 2021, the Japan Clinical Oncology Group/Dermatologic Oncology Group (JCOG/DOG) started the prospective clinical trial JCOG2005 for head and neck BCC[8)]. Since the key inclusion criterion was isolated head and neck BCC, our rigorous check for multiple lesions gave the impression that the frequency of multiple BCC was higher than previously reported. Therefore, we conducted this retrospective study to clarify the frequency and characteristics of Japanese patients with multiple BCCs.

Methods

This retrospective study included Japanese patients with BCCs treated at our hospital between April 2020 and March 2022. Patients with xeroderma pigmentosum or nevoid BCC syndrome were excluded. As we started BCC screening focusing on the presence of multiple lesions in April 2021, patients examined between April 2021 and March 2022 were classified into the screening group (SG) and those examined between April 2020 and March 2021 were classified into the non-screening group (NSG). When the first BCC was confirmed, we also checked for any additional BCC. During the screening, dermoscopy was used for observation, and biopsies were performed as needed. A full-body tumour screening was conducted without removing undergarments, unless the patient was aware of a lesion in an area covered by undergarments. All patients were examined by the same three dermato-oncologists (one board-certified plastic surgeon and

Corresponding author: Shigeto Matsushita, shigeto0302@gmail.com
Received: June 12, 2024, Accepted: August 21, 2024, Advance Publication by J-STAGE: November 8, 2024

two board-certified dermatologists). Each patient was seen by one dermato-oncologists. Clinical information was obtained from medical records, including patient age, tumour location, tumour diameter, number of tumours, and histopathological pattern. Although there is no definition of gaze pattern for dermato-oncologists, we provisionally classified the head and neck gaze region into the 'central region' and 'peripheral region' based on behavioural patterns in routine practice (**Figure 1**). The central region was defined as surrounded by the bilateral upper edges of the eyebrow, lateral edge of the masseter muscle, and lower edge of the mandible. The peripheral region was defined as other regions of the head and neck. We assessed the distribution of tumour location in patients with multiple BCCs: the central and peripheral regions of the head and neck, whole trunk, and upper and lower extremities.

This study was approved by the Institutional Review Board and Human Research Ethics Committee of our institution (2022-3) and performed in accordance with the ethical guidelines of the 1975 Declaration of Helsinki (revised in 2013). The requirement for written informed consent was waived because this study retrospectively analysed anonymized patient data.

Continuous data are summarized as means and standard deviations; categorical variations are summarized as numbers and proportions (%). Categorical data were compared using chi-square and Fisher's exact tests. Continuous variables were compared using Student's *t*-test. Statistical analyses were performed using EZR version 1.36 (Saitama Medical Center, Jichi Medical University, Shimotsuke-shi, Japan; www.jichi.ac.jp/saitama-sct/SaitamaHP.files/statmedEN.html).

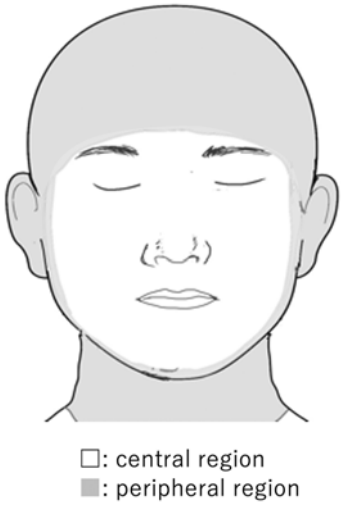

Figure 1. Provisional classification for gaze patterns head and neck region in dermato-oncologist. The 'central region' was defined as the region surrounded by the bilateral upper edge of the eyebrow, lateral edge of the masseter muscle, and lower edge of the mandible (white area of the head and neck). The 'peripheral region' was defined as other regions in the head and neck (grey area).

Results

Patient characteristics

In total, 239 patients, 136 in the SG and 103 in the NSG, were treated during the study period (**Table 1**). No significant differences were found between the two groups with respect to sex and age. In the SG, 115 (84.6%) patients had a single lesion and 21 (15.4%) had two or more lesions. In the NSG, 96 (93.2%) patients had a single lesion and 7 (6.8%) had two or more lesions; the difference between groups was significant (p = 0.04).

Tumour characteristics

The total number of tumours in the SG and NSG groups was 161 and 111, respectively (**Table 2**). Out of 161 lesions in the SG, 160 were diagnosed as BCC through histopathological examination. In the remaining case, the lesion was diagnosed as BCC via dermoscopy, but treatment was not pursued due to the exacerbation of a comorbid condition. The tumour diameter was 11.3 ± 7.9 mm and 9.9 ± 6.1 mm in the SG and NSG, respectively, with no significance between the groups (p = 0.14; **Table 1**). Approximately 70% of BCCs were located in the central region of the head and neck in both SG and NSG. In patients with multiple BCCs in the SG, the proportions of lesions in the peripheral region of the head and neck (32.6%) and whole trunk (13.0%) were higher than those in patients with solitary BCC (14.8%, 6.1%, respectively; p = 0.003; **Table 2**). **Figure 2**

Table 1. Patient Characteristics.

	Total	Screening group	Non-screening group	p
No. of patients	239	136	103	
No. of tumours	272	161	111	
Sex				0.77
Female, n (%)	118 (49.4)	66 (48.6)	52 (50.5)	
Male, n (%)	121 (50.6)	70 (51.4)	51 (49.5)	
Age (years) means ± SD	75.5 ± 12.5	75.6 ± 13.4	75.3 ± 11.1	0.83
Solitary BCC, n (%)	211 (88.3)	115 (84.6)	96 (93.2)	0.04
Multiple BCC, n (%)	28 (11.7)	21 (15.4)	7 (6.8)	
Diameter, mm	10.7 ± 7.3	11.3 ± 7.9	9.9 ± 6.1	0.14

BCC, basal cell carcinoma

Table 2. Anatomical Location and Histopathology of 272 BCC Lesions Developing in 239 Patients.

	Screening group				Non-screening group			
	Total n=161 (%)	Solitary BCC n=115 (%)	Multiple BCC n=46 (%)	p	Total n=111 (%)	Solitary BCC n=96 (%)	Multiple BCC n=15 (%)	p
Anatomical location								
Central region of the head and neck	111 (69.9)	87 (75.6)	24 (52.2)	0.003	79 (71.2)	67 (69.8)	12 (80.0)	0.06
Peripheral region of the head and neck	32 (19.9)	17 (14.8)	15 (32.6)		20 (18.0)	20 (20.8)	0 (0.0)	
Whole trunk	13 (8.1)	7 (6.1)	6 (13.0)		7 (6.3)	4 (4.2)	3 (20.0)	
Upper extremities	4 (2.5)	4 (3.5)	0 (0.0)		3 (2.7)	3 (3.1)	0 (0.0)	
Lower extremities	1 (0.6)	0 (0.0)	1 (2.2)		2 (1.8)	2 (2.1)	0 (0.0)	
Histologic pattern								
Nodular	92 (57.1)	72 (62.6)	20 (43.5)	<0.001	63 (56.8)	54 (56.2)	9 (60.0)	0.92
Superficial	12 (7.5)	2 (1.7)	10 (21.7)		14 (12.6)	13 (13.5)	1 (6.7)	
Micronodular	15 (9.3)	10 (8.7)	5 (10.9)		8 (7.2)	7 (7.3)	1 (6.7)	
Infiltrating	9 (5.6)	7 (6.1)	2 (4.3)		3 (2.7)	3 (3.1)	0 (0.0)	
Morphoeic	0 (0.0)	0 (0.0)	0 (0.0)		0 (0.0)	0 (0.0)	0 (0.0)	
Mixed	29 (18.0)	24 (20.9)	5 (10.9)		23 (20.7)	19 (19.7)	4 (26.6)	
Unknown	4 (2.5)	0 (0.0)	4 (8.7)		0 (0.0)	0 (0.0)	0 (0.0)	

BCC, basal cell carcinoma

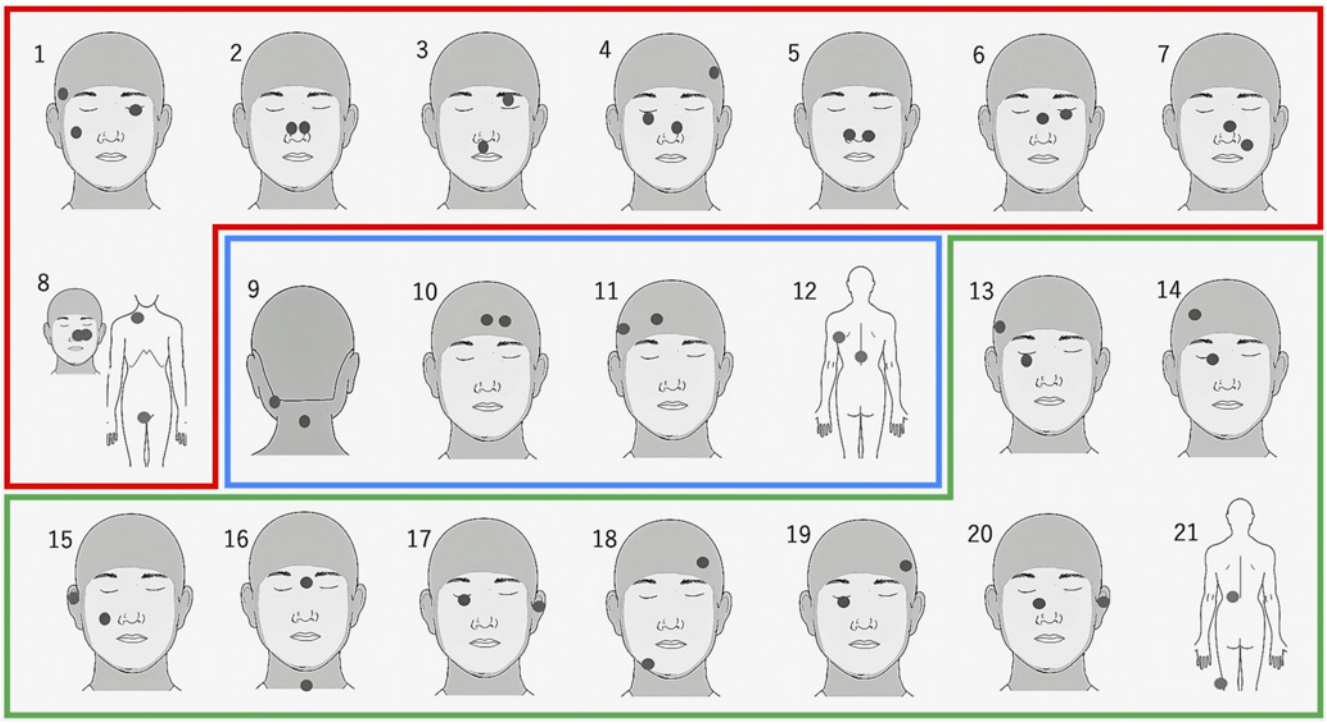

Figure 2. Tumour location in patients with multiple BCCs in the screening group.
Plotting schema of tumour location in patients with multiple BCCs in the screening group and provisional classification for gaze patterns of dermato-oncologist in head and neck region. Tumour sites are plotted by black dots (n = 46 in 21 patients). Group A (cases 1–8, red frame) had multiple lesions, including two lesions in the central region of the head and neck. Group B (cases 9–12, blue frame) had multiple lesions in the same region, the peripheral region of the head and neck or the whole trunk region. Group C (cases 13–21, green frame) had multiple lesions in different regions.

shows a plot of tumour location in patients with multiple BCCs in the SG. Groups A+B (12/136, 8.8%) had at least two tumours in the same region. Nodular BCC was the most common histological pattern in both groups, followed by mixed, micronodular, superficial, and infiltrating patterns. The proportion of superficial patterns in the SG was significantly higher in the multiple BCC group than in the solitary BCC group ($p < 0.001$).

Discussion

The frequency of multiple BCCs in Asians has been re-

ported to be lower than that of Caucasians. Indeed, the frequency of multiple BCCs in Asians at our institution before we initiated this study was similar to previous reports of the frequency of multiple BCCs in Asians. However, in this study, the frequency of multiple BCCs increased even though the duration and number of patients enrolled were similar and the examining physicians were the same.

We hypothesized that the gaze pattern was the cause for not identifying other lesions. Ishii et al. reported that casual observers gazing at paralyzed and normal faces direct most attention to the central triangular region, including the eyes, nose, and mouth regions[9]. Cai et al. reported that viewers with increased experience in cosmetic surgery focus more quickly on areas of interest relevant to facelifts, such as the cheeks, chin, and neck, and have a more evenly distributed gaze pattern across the face[10]. Previous reports on multiple BCCs did not describe the observer's gaze pattern. We provisionally classified the head and neck gaze region into the 'central' and 'peripheral' regions. In patients with multiple BCCs in the SG, the proportion of lesions in the peripheral region of the head and neck (32.6%) and whole trunk (13.0%) was higher than that in patients with a solitary BCC. Eight and four patients (8.8%, group A+B) in the SG had two BCCs in the same region (**Figure 2**), which was similar to previous reports[4-7]. Our results indicate that the increase in multiple lesion cases through screening occurred owing to more conscious observation of different regions, especially head and neck regions, thereby overcoming human gaze patterns. Early detection of other lesions benefits patients because a few millimetres difference in BCC in the head and neck can affect reconstructive surgery.

The higher proportion of superficial patterns in patients with multiple BCCs in the SG may be due to the difficulty in identifying superficial BCCs with clinical features such as pigmented macules. In patients with a single BCC, physicians should conduct a full-body screening to check for additional BCCs at other sites. If it is difficult to perform a full-body screening on all patients with BCC in routine clinical practice, patients and their families should be made aware that the proportion of multiple BCCs is higher than that in previous reports[4-7].

Although this was a single-centre study with a short observation period of 2 years, the researchers found that the frequency of multiple BCC was higher than previously assumed in the Japanese population. Whether the frequency of multiple BCCs in Japanese is higher than previously assumed requires further large-scale epidemiological studies. We must examine this region more carefully.

Acknowledgments: This study was supported in part by the National Cancer Center Research and Development Fund (2023-J-03).

Author Contributions: MA wrote the manuscript. SM and KY supervised the study. SM and KF critically reviewed the manuscript and supervised the whole study process.

Conflicts of Interest: There are no conflicts of interest.

Ethical Approval: This study was approved by the Institutional Review Board and Human Research Ethics Committee of our institution (2022-3) and performed in accordance with the ethical guidelines of the 1975 Declaration of Helsinki (revised in 2013).

Consent to Participate: The requirement for written informed consent was waived because this study retrospectively analysed anonymized patient data.

References

1. Lomas A, Leonardi-Bee J, Bath-Hextall F. A systematic review of worldwide incidence of nonmelanoma skin cancer. Br J Dermatol. 2012 May;166(5):1069−80.
2. Marghoob A, Kopf AW, Bart RS, et al. Risk of another basal cell carcinoma developing after treatment of a basal cell carcinoma. J Am Acad Dermatol. 1993 Jan;28(1):22−8.
3. Flohil SC, Koljenovic S, Haas ERM, et al. Cumulative risks and rates of subsequent basal cell carcinomas in the Netherlands. Br J Dermatol. 2011 Oct;165(4):874−81.
4. Adachi K, Yoshida Y, Noma H, et al. Characteristics of multiple basal cell carcinomas: The first study on Japanese patients. J Dermatol. 2018 Oct;45(10):1187−90.
5. Li CL, Chen YC, Yang KC, et al. Different histopathologic profiles and outcomes between sun-exposed BCC and non-sun-exposed BCC. Sci Rep. 2020 Apr;10:7387.
6. Ishii Y, Sakaino M, Fujisawa Y, et al. [A nationwide survey of basal cell carcinoma in Japan]. Skin Cancer. 2013;28(2):205−11. Japanese.
7. Murata Y, Kumano K, Takai T, et al. [Multiple basal cell carcinoma trend to develop on the ipsi-lateral side of the body]. Jpn J Dermatol. 2012;122:2487−93. Japanese.
8. Nakamura Y, Sano Y, Kataoka T, et al. Confirmatory trial of narrower side margin excision for head and neck basal cell carcinoma in the Japanese (East Asian) population: JCOG2005 (J-BASE-MARGIN). J Clin Oncol. 2022 Jun;40(16 Suppl):TPS9604.
9. Ishii L, Dey J, Boahene KD, et al. The social distraction of facial paralysis: Objective measurement of social attention using eye-tracking. Laryngoscope. 2016 Feb;126(2):334−9.
10. Cai LZ, Kwong JW, Azad AD, et al. Where do we look? Assessing gaze patterns in cosmetic face-lift surgery with eye tracking technology. Plast Reconstr Surg. 2019 Jul;144(1):63−70.

Received: 23 September 2024 | Accepted: 31 October 2024

DOI: 10.1111/1346-8138.17551

THE JOURNAL OF DERMATOLOGY

CONCISE COMMUNICATION

Age over 90 years is an unfavorable prognostic factor for resectable cutaneous squamous cell carcinoma

Natsuko Saito-Sasaki[1,2] | Megumi Aoki[1] | Kazuyasu Fujii[1] | Kentaro Yamamura[1] | Taiyo Hitaka[1] | Yui Hirano[1] | Katsuhiko Nishihara[1] | Yoshihisa Fujino[3] | Shigeto Matsushita[1]

[1]Department of Dermato-Oncology, NHO Kagoshima Medical Center, Kagoshima, Japan

[2]Department of Dermatology, University of Occupational and Environmental Health, Kitakyusyu, Japan

[3]Department of Environmental Epidemiology, Institute of Industrial Ecological Science, University of Occupational and Environmental Health, Kitakyusyu, Japan

Correspondence
Shigeto Matsushita, Department of Dermato-Oncology, NHO Kagoshima Medical Center 8-1, Shiroyama-cyo, Kagoshima-City 892-0853, Kagoshima, Japan.
Email: shigeto0302@gmail.com

Abstract

The rapid aging of the population has led to an increase in the number of cutaneous squamous cell carcinoma (cSCC) cases among the older population. However, the characteristics of these cases remain unclear. In this study, we aimed to identify the problem by analyzing the clinical characteristics of patients with cSCC aged 90 years and over. In this retrospective study, we analyzed the characteristics of patients aged >90 years with regard to gender, risk factors for cSCC, and disease course, using data from 316 patients with cSCC who underwent surgery at the Kagoshima Medical Centre between October 2014 and September 2022. Patients were separated into two groups based on age: those aged ≥90 years (104 patients) and those aged <90 years (212 patients). Regarding the National Comprehensive Cancer Network risk classification, there was no difference between groups. Univariate, multivariate, and Cox analyses of relapse-free survival of patients in both groups indicated that the recurrence risk was significantly high among those aged ≥90 years. Patients aged ≥90 years were at higher risk for recurrence, suggesting a need for closer follow-up than that for patients aged <90 years.

KEYWORDS
cutaneous squamous cell carcinoma, epidemiologynonagenarianolder-oldrecurrence

1 | INTRODUCTION

The incidence of cutaneous squamous cell carcinoma (cSCC) in Japan has risen sharply in recent years,[1] particularly in the older population. The majority of cSCC cases are caused by long-term ultraviolet radiation exposure,[2] which explains why the risk and incidence of cSCC increase with age.[3] With the rapid aging of the population, the number of cSCC cases among older patients aged >90 years is expected to further increase in the future. However, the characteristics of cSCC in this population are largely unknown.

According to the current cSCC guidelines, age is not considered a risk factor for cSCC.[4–6] For example, in the National Comprehensive Cancer Network (NCCN) guidelines,[4] the risk classification of localized cSCCs is based on the tumor location or size, clinical tumor boundaries, primary or recurrent tumor status, immunosuppression, previous irradiation sites or chronic inflammatory processes, tumor growth rate, neurologic manifestations, and histologic features.

Herein, we investigated the clinical characteristics and prognoses of patients with cSCC occurring in patients aged >90 years. This study aimed to identify the features of cSCC occurring in this patient population to facilitate better assessment of treatment strategies.

2 | METHODS

2.1 | Patient population

A total of 316 patients who underwent surgery as initial treatment for cSCC at the Division of Dermato-Oncology of Kagoshima Medical Center between October 2014 and September 2022 were

enrolled in this study. The medical and surgical records of the patients were retrospectively reviewed. All patient data were de-identified. Patients were excluded from the study if they had only in situ disease, including Bowen's disease or actinic keratosis, and had missing clinical information. The depth of the excision was determined by preoperative ultrasonography, computed tomography, and magnetic resonance imaging if a deeper tumor invasion depth was expected. In deciding on the surgical procedure, the patient's overall condition, including mental state and presence of dementia, was considered, but the patient's age was not.

2.2 | Evaluation criteria

Clinical characteristics such as age, sex, risk factors, histologic differentiation, and history of taking immunosuppressive drugs were extracted. All tumors were confirmed as cSCC by pathologists and classified according to the tumor-node-metastasis classification of the Union for International Cancer Control (eighth edition). Risk classification was assessed according to the updated NCCN guidelines.[4] The patients were followed up at our hospital or referred to dermatologic clinics. Reffered patiens were contacted to collect the patients' data following the surgical course.

2.3 | Statistical analysis

Univariate and multivariate analyses of recurrence-free survival and the log-rank test were performed using STATA. Recurrence-free survival was calculated from the date of the initial surgery to the date of the first recurrence or the latest contact with the patient using the Cox proportional hazards model. Multivariate comparisons were performed using the Cox proportional hazards model.

2.4 | Study approval

This retrospective, nonrandomized, observational study using existing data was reviewed and approved by the Institutional Review Board of the Kagoshima Medical Center in accordance with the Declaration of Helsinki. Because this was a retrospective cohort study, the opt-out method of obtaining informed consent was used.

3 | RESULTS

The clinical data of 316 patients included in this study are summarized in Table 1. The age distribution of the patients ranged from 45 to 101 years. Among the participants of this study, 212 (67.1%) were aged <90 years and 104 (32.9%) were aged ≥90 years. There were more women aged 90 years or older, reflecting the longer life expectancy of women than that of men. Additionally, there were fewer patients taking immunosuppressive drugs in the group aged ≥90 years. While there were no significant differences in the NCCN

TABLE 1 Cutaneous squamous cell carcinoma occurrence according to age groups.

	Age category (years)		
	≥90	<90	
Variable	*n* = 104 (%)	*n* = 212 (%)	*p*
Age (years)			
Median (IQR)	93.0 (90.5–96.0)	83.0 (77.0–87.0)	<0.001
Sex			
Male	40 (38.5)	130 (61.3)	<0.001
Female	64 (61.5)	82 (38.7)	
Location			
Head and neck	84 (80.8)	141 (66.5)	0.051
Extremity	16 (15.4)	62 (29.2)	
Trunk	2 (1.9)	6 (2.8)	
Genitals	2 (1.9)	3 (1.4)	
History of taking immunosuppression drugs			
Yes	11 (10.6)	43 (20.3)	0.031
No	93 (89.5)	169 (79.7)	
Risk classification (NCCN)			
Low risk and high risk	63 (60.6)	141 (66.5)	0.3
Very high risk	41 (39.4)	71 (33.5)	
Invasion level beyond fat			
Yes	12 (11.5)	8 (3.8)	0.008
No	92 (88.5)	204 (96.2)	
Perineural or lymphovascular involvement			
Yes	15 (14.4)	18 (8.5)	0.11
No	89 (85.6)	194 (91.5)	
Surgical margin			
5–10 mm	29 (27.9)	35 (16.5)	0.018
Narrower margin (<5 mm)	75 (72.1)	177 (83.5)	
Surgical margin			
Negative	98 (94.2)	201 (94.8)	0.83
Positive	6 (5.8)	11 (5.2)	
Tumor size (mm)			
Median	18	16	0.12
IQR	12.25–28.75	10.75–25	
Minimum	5	2	
Maximum	90	110	
Tumor thickness (mm)			
Median	4.5	3.8	0.842
IQR	2.9–7.5	2.3–6.8	
Minimum	0.5	0.3	
Maximum	18	36	

Abbreviations: IQR, interquartile range; NCCN, National Comprehensive Cancer Network.

TABLE 2 Recurrence-free survival of patients with cutaneous squamous cell carcinoma.

	Age <90 years	Age ≥90 years	*P*
Observation period (days)			
Median	579.6	283.5	
IQR	190.5–818.0	61.5–396.0	
Number of recurrences (local:distant)	12 (6:6)	13 (8:5)	
Recurrence rate (1000 person-years)	29.70	129.79	
Univariate analysis HR (95% CI)	1	6.68 (2.76–16.20)	<0.001
Multivariate analysis HR (95% CI)	1	8.79 (3.33–23.20)	<0.001

Abbreviations: CI, confidence interval; HR, hazard ratio; IQR, interquartile range.

risk classifications between the groups, those aged ≥90 years had significantly more patients with cSCC tumor invasion beyond the subcutaneous fat ($P=0.008$). This may reflect the delay in accessing clinics and the progression of cSCCs in those aged ≥90 years. While the patients in the group aged ≥90 years were subject to standard surgical margin resection, the surgical margin tended to be wider (≥5 mm) in those aged ≥90 years ($P=0.018$). To examine the impact of age (≥90 vs <90 years) on the recurrence of patients with cSCC, the tumor recurrence rates were evaluated using the Cox analysis. According to the univariate analysis, individuals aged ≥90 years had significantly worse recurrence-free survival rates. Furthermore, according to the multivariate analysis including clinical factors such as sex, surgical margins, invasion level beyond the subcutaneous fat, risk classification (NCCN), perineural or lymphovascular involvement, history of taking immunosuppression drugs, and surgical margins (positive or negative), the hazard ratio of patients aged ≥90 years was significantly higher than that of patients aged <90 years. These findings demonstrate that age ≥ 90 years is an independent prognostic factor for cSCC (Table 2).

4 | DISCUSSION

The key conclusion of this study is that patients over 90 years of age had a higher rate of cSCC recurrence than did patients under 90. The NCCN risk classification does not include aging, hence there has never been any evidence linking it to cSCC recurrence. It is unclear if cancer recurrence rates are higher in elderly people, especially those who are very old, than in younger patients. Regarding rectal cancer, younger patients typically present with more advanced disease and have a higher recurrence rate, but their stage-specific survival rates are similar to those of older patients.[7] In non-small-cell lung cancer, overall survival is shorter in older patients, but recurrence rates are similar across age groups.[8] The recurrence rate and mortality rate for breast cancer vary.[9–11] These reports suggest that age can be an important factor in cancer recurrence and survival, but the impact of age varies depending on the type of cancer and other disease characteristics.

The frequency of taking immunosuppressants was higher in patients under 90 years old than in those over 90 years old. Although immunosuppressants are associated with an increased risk of skin cancer, in the very old population other risks such as accumulated DNA damage may be more likely to cause the development of skin cancer. Previous research has shown that tumors in patients aged 75 years and over tend to be larger, poorly differentiated, and deeply invasive.[12] However, in this study, only the level of invasion differed between the patient groups aged 90 years and over and those aged under 90 years. The underlying cause of the high recurrence rate of cSCC in patients aged 90 and over observed in this study is not entirely clear; however, it may be associated with the accumulation of DNA damage and the propensity for deeper tumor invasion.

Patients in their 90s accounted for 33% of all patients in this study. This is clearly high given the proportion of the population by age. According to a population survey in Kagoshima Prefecture, the population in their 90s only accounts for approximately 10% of the population aged 70 years and above.[13] This is reflected in the cancer statistics by site for 2019 on the Japanese Ministry of Health, Labour and Welfare website, which shows that while the overall cancer incidence rate peaks at age 90 years and gradually declines, the skin cancer incidence rate shows a further increasing trend even at age 90 years and older.[14] Furthermore, the incidence of cSCC has been reported to be increasing, although it is unclear whether this is due to an increase in the incidence or an increase in the number of diagnoses following advances in diagnostic techniques.

In conclusion, cSCC in patients over 90 years of age has a high recurrence rate, even when treated like that in patients under 90 years of age. Accordingly, patients over 90 years of age require careful postoperative follow-up with recurrence in mind.

CONFLICT OF INTEREST STATEMENT

The authors declare no conflicts of interest.

ORCID

Natsuko Saito-Sasaki https://orcid.org/0000-0001-6122-8429
Kazuyasu Fujii https://orcid.org/0000-0002-6482-8953
Kentaro Yamamura https://orcid.org/0000-0003-1614-591X
Yui Hirano https://orcid.org/0000-0001-8204-1997
Katsuhiko Nishihara https://orcid.org/0000-0002-3801-4278
Shigeto Matsushita https://orcid.org/0000-0003-2001-5341

REFERENCES

1. Umezono Y, Sato Y, Noto M, Yamada K, Noguchi N, Hasunuma N, et al. Incidence rate of cutaneous squamous cell carcinoma is rapidly increasing in Akita prefecture: urgent alert for super-aged society. J Dermatol. 2019;46:259–62.
2. Young AR, Claveau J, Rossi AB. Ultraviolet radiation and the skin: photobiology and sunscreen photoprotection. J Am Acad Dermatol. 2017;76:100–9.
3. Green AC, Olsen CM. Cutaneous squamous cell carcinoma: an epidemiological review. Br J Dermatol. 2017;177:373–81.
4. NCCN Clinical Practice Guidelines in Oncology (NCCN Guidelines®). Squamous Cell Skin Cancer. Available from: chrome-extension://efaidnbmnnnibpcajpcglclefindmkaj/https://www.nccn.org/professionals/physician_gls/pdf/squamous.pdf
5. Stratigos AJ, Garbe C, Dessinioti C, Lebbe C, van Akkooi A, Bataille V, et al. European consensus-based interdisciplinary guideline for invasive cutaneous squamous cell carcinoma. Part 1: diagnostics and prevention-update 2023. Eur J Cancer. 2023;193:113251.
6. Ansai SI, Umebayashi Y, Katsumata N, Kato H, Kadono T, Takai T, et al. Squamous cell carcinoma guidelines Committee of the Japanese Skin Cancer Society. Japanese dermatological association guidelines: outlines of guidelines for cutaneous squamous cell carcinoma 2020. J Dermatol. 2021;48:288–311.
7. You YN, Dozois EJ, Boardman LA, Aakre J, Huebner M, Larson DW. Young-onset rectal cancer: presentation, pattern of care and long-term oncologic outcomes compared to a matched older-onset cohort. Ann Surg Oncol. 2011;18:2469–76.
8. Goodgame B, Viswanathan A, Zoole J, Gao F, Miller CR, Subramanian J, et al. Risk of recurrence of resected stage I non-small cell lung cancer in elderly patients as compared with younger patients. J Thorac Oncol. 2009;4:1370–4.
9. Samman S, Cornacchi SD, Foster G, Thabane L, Thomson S, Lovrics O, et al. A population-based study of treatment patterns, 10-year recurrence and breast cancer-specific mortality in a cohort of elderly patients with breast cancer. Am J Surg. 2021;222:361–7.
10. Bollet MA, Sigal-Zafrani B, Mazeau V, Savignoni A, de la Rochefordière A, Vincent-Salomon A, et al. Age remains the first prognostic factor for loco-regional breast cancer recurrence in young (<40 years) women treated with breast conserving surgery first. Radiother Oncol. 2007;82:272–80.
11. Dufour O, Houvenaeghel G, Classe JM, Cohen M, Faure C, Mazouni C, et al. Early breast cancer in women aged 35 years or younger: a large national multicenter French population-based case control-matched analysis. Breast. 2023;68:163–72.
12. Leus AJG, Haisma MS, Terra JB, Diercks GFH, Van Kester MS, Halmos GB, et al. Age-related differences in tumour characteristics and prognostic factors for disease progression in cutaneous squamous cell carcinoma of the head and neck. Acta Derm Venereol. 2022;102:adv00652.
13. Annual report (Population by age etc.) Kagoshima Prefecture. Available from: https://www.pref.kagoshima.jp/ac09/tokei/bunya/jinko/jinkouidoutyousa/nennpou.html
14. Cancer Information Service NCC-t, Japan. Cancer Statistics.: National Cancer Registry, Ministry of Health, Labour and Welfare, National Cancer Institute; [Cancer Information Service, National Cancer Cen- ter, Japan. National Cancer Registry, Ministry of Health, Labour and Welfare, National Cancer Institute]. Available from: https://ganjoho.jp/reg_stat/statistics/data/dl/index.html#a14

How to cite this article: Saito-Sasaki N, Aoki M, Fujii K, Yamamura K, Hitaka T, Hirano Y, et al. Age over 90 years is an unfavorable prognostic factor for resectable cutaneous squamous cell carcinoma. J Dermatol. 2025;52:183–186. https://doi.org/10.1111/1346-8138.17551

Received: 29 August 2024 | Accepted: 15 October 2024

DOI: 10.1111/1346-8138.17529

THE JOURNAL OF DERMATOLOGY

LETTER TO THE EDITOR

Combination treatment of cultured epithelial autograft and meshed full-thickness skin graft for giant congenital melanocytic nevus

Dear Editor,

A 7-day-old girl was referred to our clinic for circumferential pigmented lesions on the trunk, pubic groin, and left thigh and was diagnosed as a case of congenital giant melanocytic nevus (GCMN). Considering the risk of carcinogenesis and cosmetic concerns, we opted for early surgical intervention. At 16 months of age, she underwent volume reduction surgery for the left thigh lesion and skin harvesting from the right inguinal region for cultured epidermal autograft (CEA) transplantation. Subsequent excision of the residual lesion and CEA transplantation were performed at 23 months of age (Figure 1a–c). Because of the extensive size of her lesions, a single method of covering was insufficient. After obtaining written consent from her family, three different CEA coverage methods were employed: (i) upper medial lesion excision with CEA, (ii) lower medial lesion excision with CEA and 3:1 full-thickness skin graft (FTSG) mesh, and (iii) lower medial lesion excision with CEA and 3:1 split-thickness skin graft (STSG) mesh. The lesions repaired with CEA alone were resected at the level of the mid dermis, while lesions repaired with

FIGURE 1 Clinical findings of (a) the patient's left thigh preoperatively, (b) after congenital giant melanocytic nevus (GCMN) resection, and (c) after reconstruction. Areas marked A, B, and C represent the areas repaired with cultured epidermal autograft (CEA) alone, CEA with full-thickness skin graft (FTSG), and CEA with split-thickness skin graft (STSG), respectively. (d, e) One and a half years postoperatively, areas repaired with CEA alone exhibited recurrent nevi, whereas areas repaired with CEA and STSG showed prominent scarring, which was subsequently excised. (f) Five years postoperatively, the areas repaired with CEA and FTSG remained cosmetically satisfactory. The scarred region following repair with CEA and STSG (Area C in [c]) was excised at the level of the middle layer of adipose tissue, resulting in a linear scar at the margins of the lesion.

The Journal of Dermatology

CEA and the FTSG mesh or CEA and the STSG mesh were resected at a deeper level, leaving a subcutaneous vascular network. The FTSG mesh was harvested from her right inguinal region, while the STSG mesh, with a thickness of 10/1000 inches, was harvested from her back. One year postoperatively, her lower medial lesions healed more favorably with slight scarring compared to the lateral and upper medial lesions (Figure 1d,e). The lateral area covered with CEA and STSG was later excised due to scarring, severe itching, and disfigurement. The areas covered with CEA and FTSG remain in favorable condition on assessment 5 years' postoperatively (Figure 1f).

Because of potential cosmetic problems, early excision is recommended for GCMN, which often requires extensive reconstruction for larger skin defects. Traditionally used for skin defects due to severe burns, CEA has emerged as a promising treatment option for GCMN skin defects. Two methods have been reported when using CEA following nevus curettage for GCMN: CEA application alone or CEA application in combination with meshed STSG.[1,2] However, both methods can lead to cosmetic issues such as pigmentation and hypertrophic scarring, respectively. In our study, similar results were observed in areas repaired with CEA alone or CEA with STSG. Conversely, areas repaired using CEA with FTSG exhibited excellent prognosis with minimal scar formation. Compared to STSG, FTSG demonstrates superior cosmetic outcomes, although this is limited by their viability.[3] This advantage is attributable to the retention of the subcutaneous plexus, which stabilizes blood flow to the graft and allows mesenchymal stem cell proliferation,[4] thereby inhibiting scar formation and promoting wound healing.

To the best of our knowledge, this is the first study to report the potential benefits of retaining the subdermal vascular plexus and using CEA in conjunction with meshed FTSG for GCMN repair. Despite limitations in harvested skin size, this approach offers a valuable option for GCMN treatment with excellent cosmetic outcomes.

CONFLICT OF INTEREST STATEMENT

None declared.

INFORMED CONSENT

Written informed consent was obtained from the patient's family for publication of the case details.

Katsuhiko Nishihara
Kazuyasu Fujii
Megumi Aoki
Yui Hirano
Akiha Inoue
Sotaro Yamamoto
Shigeto Matsushita

Department of Dermato-Oncology/Dermatology, NHO Kagoshima Medical Center, Kagoshima, Japan

Correspondence
Kazuyasu Fujii, Department of Dermato-Oncology/Dermatology, NHO Kagoshima Medical Center, Kagoshima, Japan.
Email: k7597938@kadai.jp

ORCID

Katsuhiko Nishihara https://orcid.org/0000-0002-3801-4278
Kazuyasu Fujii https://orcid.org/0000-0002-6482-8953
Yui Hirano https://orcid.org/0000-0001-8204-1997
Sotaro Yamamoto https://orcid.org/0009-0003-8617-6444
Shigeto Matsushita https://orcid.org/0000-0003-2001-5341

REFERENCES

1. Shoji-Pietraszkiewicz A, Sakamoto M, Katsube M, Ogino S, Tsuge I, Yamanaka H, et al. Treatment of giant congenital melanocytic nevi with cultured epithelial autografts: clinical and histopathological analysis. Regen Ther. 2021;18:1–6.
2. Im S, Yamanaka H, Tsuge I, Katsube M, Sakamoto M, Morimoto N. A case of Giant congenital melanocytic nevus treated with combination therapy of autologous mesh-skin grafts and cultured epithelial autografts. Plast Reconstr Surg Glob Open. 2021;9:e3613.
3. Saleki M, Noor MA, Hurt P, Abul A. Full-thickness skin graft versus Split-thickness skin graft for radial forearm free flap transfer in Oral cavity reconstruction: a systematic review and meta-analysis. Cureus. 2023;15:e49279.
4. Jeon YK, Jang YH, Yoo DR, Kim SN, Lee SK, Nam MJ. Mesenchymal stem cells' interaction with skin: wound-healing effect on fibroblast cells and skin tissue. Wound Repair Regen. 2010;18:655–61.

Received: 8 December 2024 | Accepted: 22 February 2025

DOI: 10.1111/1346-8138.17694

THE JOURNAL OF DERMATOLOGY

CONCISE COMMUNICATION

Ultrasound findings of endocrine mucin-producing sweat gland carcinoma mimicking epidermal cysts: A case series and diagnostic challenges

Hirofumi Kawamoto[1] | Kazuyasu Fujii[1] | Megumi Aoki[1] | Keisuke Goto[1] | Tokiyoshi Ikoma[1] | Takahisa Tozawa[1] | Masashi Iwata[1] | Masamichi Goto[2] | Mitsuharu Nomoto[2] | Shigeto Matsushita[1]

[1]Department of Dermato-Oncology, NHO Kagoshima Medical Center, Kagoshima, Japan

[2]Department of Pathology, NHO Kagoshima Medical Center, Kagoshima, Japan

Correspondence
Kazuyasu Fujii, Department of Dermato-Oncology, NHO Kagoshima Medical Center, Kagoshima, Japan.
Email: k7597938@kadai.jp

Abstract

Endocrine mucin-producing sweat gland carcinoma (EMPSGC) is an uncommon, low-grade, malignant tumor that predominantly affects older patients and is often located around the eyelids. Diagnosing EMPSGC is challenging because of its clinical and imaging similarities to benign lesions such as epidermal cysts. This report presents two cases of EMPSGC with ultrasound features resembling benign cystic lesions that were initially considered in the differential diagnosis. For both cases, ultrasound imaging revealed hypoechoic masses with posterior acoustic enhancement and peritumoral vascularity, which are frequently associated with epidermal cysts. However, a histopathological analysis confirmed the diagnosis of EMPSGC demonstrating solid and papillary structures with mucin pools and neuroendocrine differentiation. These cases highlight the potential for misdiagnosis using preoperative imaging because ultrasound can obscure malignancy. Enhanced posterior echoes likely stem from mucin deposits within the tumor, thus underscoring the need for an early biopsy and histological analysis when atypical findings are observed. Additionally, Doppler ultrasound detected a peritumoral blood flow, which may suggest malignancy; however, benign lesions may exhibit similar vascularity. Further accumulation of cases is necessary to determine whether peritumoral vascularity is a distinguishing characteristic of EMPSGC. This report emphasizes the importance of recognizing EMPSGC's mimicry of benign lesions on ultrasound, particularly in cosmetically sensitive areas. An accurate diagnosis of EMPSGC requires imaging, histopathology, and immunohistochemical staining because misinterpretation may delay appropriate treatment and increase the risk of recurrence.

KEYWORDS
adnexal and skin appendage, diagnostic imaging, differential diagnosis, facial neoplasms, ultrasonography

1 | INTRODUCTION

Endocrine mucin-producing sweat gland carcinoma (EMPSGC) is a rare, low-grade, malignant tumor that primarily affects older individuals and predominantly occurs around the eyelids. Histologically, EMPSGC comprises solid and papillary structures with cells exhibiting neuroendocrine features. An immunohistochemical analysis is essential to confirming its diagnosis, as evidenced by the expression of markers such as synaptophysin, chromogranin, and hormone receptors that help differentiate EMPSGC from other adnexal tumors,

including benign entities such as epidermal cysts or malignant sweat gland carcinomas.[1] The rarity of EMPSGC and its clinical and morphological similarities to benign lesions, such as epidermal cysts, often lead to diagnostic challenges.[2]

Ultrasound is widely used to evaluate soft tissue lesions because it is a non-invasive, rapid, and cost-effective modality that provides detailed anatomical information and allows the assessment of lesion vascularity.[3] Although ultrasound is useful for assessing all areas of the body, it is particularly useful for assessing cosmetically and functionally important areas (such as the periorbital region) that require accurate imaging to enable appropriate clinical decision-making. Ultrasound significantly improves preoperative diagnostic accuracy when evaluating subcutaneous benign lesions, particularly lipomas and epidermal cysts. However, the ability of ultrasound alone to determine a definitive diagnosis,[4] and the existence of overlapping imaging features, can further complicate the differential diagnosis. The ultrasound findings of EMPSGC have not been reported because such cases are rare. We performed ultrasound imaging using a FUJIFILM-FCI-X HFL25xp linear probe (Fujifilm; central frequency, 9 MHz; effective frequency range, 6–13 MHz). This report describes the characteristics of EMPSGC that mimic those of epidermal cysts on ultrasound.

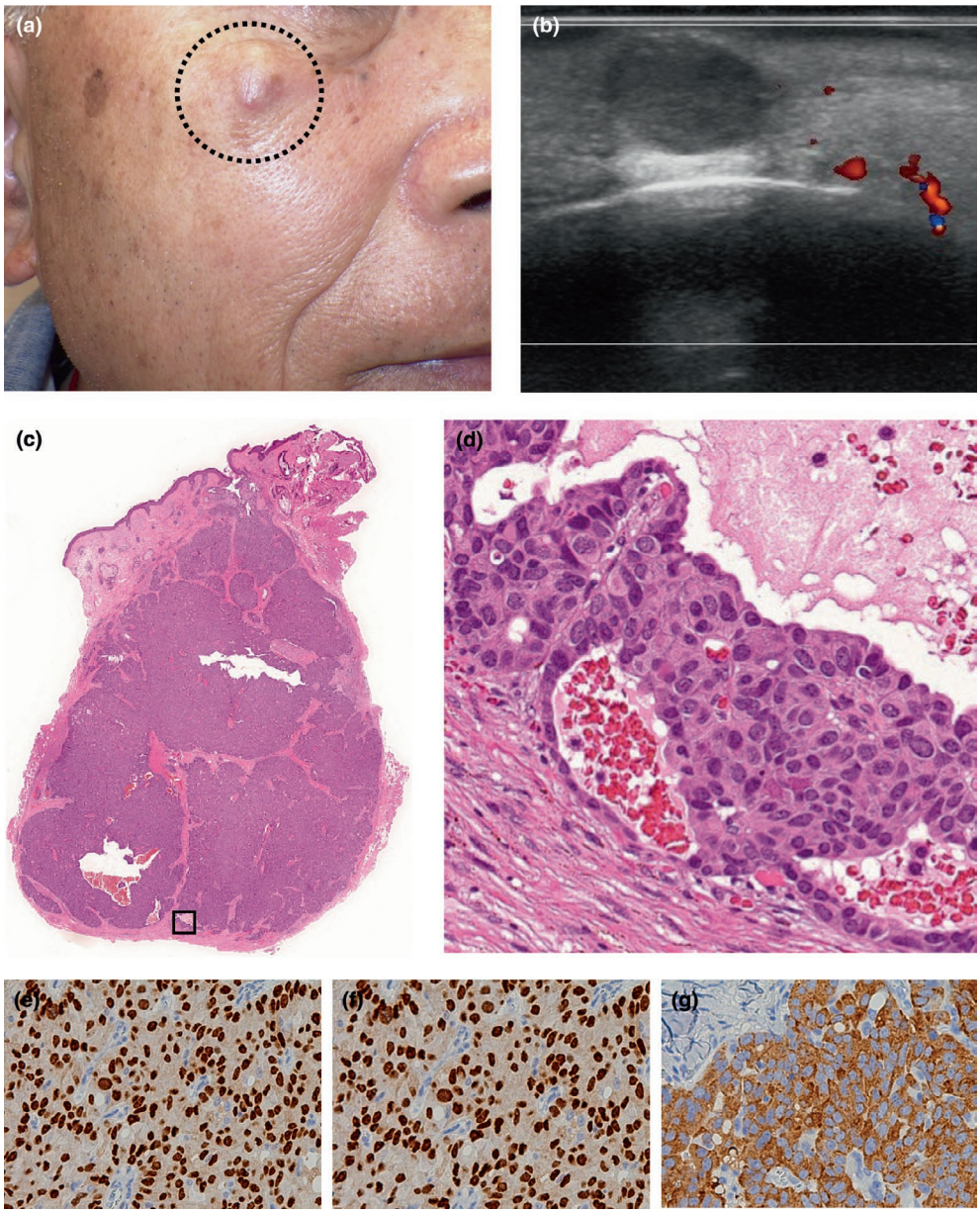

FIGURE 1 Clinical findings, ultrasound image, and pathological findings of case 1. (a) A 1-cm-diameter nodule with a normal color is observed on the right cheek. (b) Doppler ultrasound image of the nodule. (c) Histopathological findings of the tumor (hematoxylin and eosin staining, orginal magnification ×6.5) and (d) original magnification ×400. (e) Immunostaining images of estrogen receptor, (f) progesterone receptor, and (g) synaptophysin (original magnification ×400).

THE JOURNAL OF DERMATOLOGY

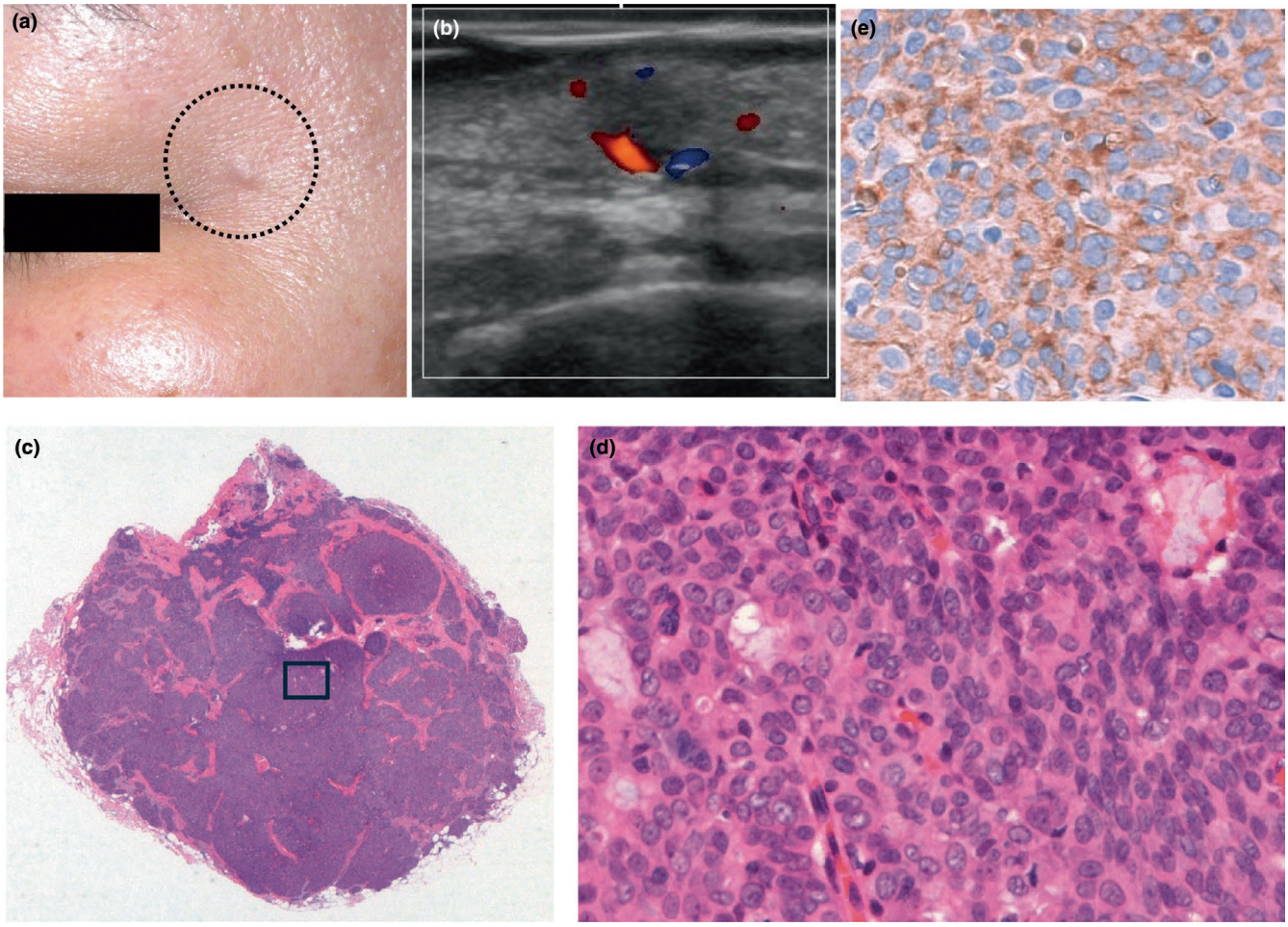

FIGURE 2 Clinical findings, ultrasound image, and pathological findings of case 2. (a) A nodule is observed on the left cheek. (b) Doppler ultrasound image of the nodule. (c) Histopathological findings of the tumor (hematoxylin and eosin staining, original magnification ×12.5 and (d) original magnification ×400. (e) Immunostaining image of synaptophysin (original magnification ×400).

2 | CASE REPORTS

2.1 | Case 1

A man in his 70s presented to our clinic with a gradually increasing subcutaneous mass on the right cheek that he had noticed 4 months earlier. The initial examination revealed a slightly reddish, 1-cm mass with a smooth elevated surface on the right cheek (Figure 1a). The mass was mobile over the underlying tissue. Ultrasound imaging demonstrated an approximately 9-×5-mm, well-defined, oval, hypoechoic mass within the dermis. Internal debris was visualized as echogenic linear reflections, and the lateral borders appeared unclear. Notable posterior acoustic enhancement and mild lateral acoustic shadowing were observed. A color Doppler analysis revealed vascular signals in the surrounding tissue (Figure 1b). The mass, which was suspected to be an epidermal cyst, was excised. Histologically, a well-defined, non-encapsulated, solid tumor that was continuous with a portion of the epidermis and proliferated throughout the dermis was observed (Figure 1c,d). The tumor cells had large round-to-oval nuclei with prominent nucleoli, and their cytoplasm ranged from eosinophilic to amphophilic and appeared round or spindle-shaped. The cells proliferated in a sheet-like pattern and formed tubular structures. At the periphery, the tumor exhibited invasive growth and the formation of small nests. Numerous mitotic figures were also observed. Immunohistopathological findings indicated that the tumor cells were positive for estrogen receptor, progesterone receptor, synaptophysin (Figure 1e–g), insulinoma-associated protein 1, and cytokeratin 7. EMPSGC was diagnosed, and the patient underwent extended resection because part of the lateral margin was positive. Six months after the second surgery, no evidence of tumor recurrence was observed.

2.2 | Case 2

A woman in her 50s presented to our clinic with a small, non-tender nodule on her left upper eyelid that she had noticed 1 year previously. The nodule was firm, mobile, and had a diameter of approximately 5 mm (Figure 2a). Ultrasound imaging revealed a 5-mm hypoechoic lesion with unclear boundaries and heterogeneous internal echoes in the subcutaneous tissue. Posterior acoustic enhancement and mild lateral acoustic shadowing were observed. Color Doppler imaging detected vascular signals adjacent to and along the tumor boundary, which appeared unclear. These findings as well as the mobility and characteristics of the lesion

initially suggested a cyst or pilomatricoma (Figure 2b). The tumor was excised under local anesthesia and exhibited solid mucinous nests with neuroendocrine differentiation (Figure 2c,d). An immunohistochemical examination indicated positive staining for synaptophysin, thus confirming the diagnosis of EMPSGC (Figure 2e). The patient subsequently underwent a second surgery to ensure complete excision with a 3-mm margin around the previous surgical site. No signs of recurrence were observed during regular follow-up for more than 4 years after surgery.

3 | DISCUSSION

Hypoechoic masses with posterior acoustic enhancement and lateral shadowing observed during ultrasound imaging of subcutaneous tumors are often recognized as characteristic features of epidermal cysts. These sonographic characteristics are non-specific. Similar findings were observed in our cases; however, the histopathological examination indicated a diagnosis of EMPSGC. Although the findings in our cases may be better explained by the high cell density of the tumor that resulted in hypoechoic masses with posterior acoustic enhancement and lateral shadows, mucin deposition is a characteristic feature of EMPSGC that should be considered a factor that contributes to the appearance of this tumor type on ultrasound.[5] Even though mucin was less pronounced in our cases, its potential influence on enhanced posterior echoes cannot be entirely excluded. Additionally, ultrasound findings such as unclear lateral boundaries are worth noting because they may occur in epidermal cysts with certain phases or conditions.[6] These characteristics could contribute to diagnostic challenges when differentiating benign lesions, such as epidermal cysts, from malignancies. Therefore, integrating imaging with histopathological analyses is important for interpretating these findings and ensuring timely and appropriate treatment.

Another notable characteristic of the ultrasound findings of these cases was the presence of blood flow surrounding the tumor. In particular, case 2 demonstrated blood flow adjacent to the tumor. The presence of blood flow around a subcutaneous mass on Doppler ultrasound may suggest malignancy. The blood flow of malignant tumors is generally more extensive than that of benign masses[7,8] because of tumor-induced angiogenesis. Although vascular signals on Doppler ultrasound are sensitive and specific for malignancy, they are not definitive markers because benign lesions can also exhibit high vascularity.[9] Yamanaka et al.[10] reported that benign cutaneous tumors, such as inflammatory epidermal cysts, pilomatricomas, and palmoplantar fibromatoses, also exhibited vascular signals in 25% of cases. In the present cases, blood flow was observed around the tumor, but not within it. Additionally, the face is a highly vascularized area. Therefore, whether the presence of peritumoral blood flow on Doppler ultrasound is a characteristic feature of EMPSGC requires further accumulation of cases.

In conclusion, this case report highlights the diagnostic challenges of EMPSGC caused by its rarity as well as the similarities of EMPSGC to benign lesions such as epidermal cysts on ultrasound. Hypoechoic regions with posterior acoustic enhancement observed with EMPSGC can mimic benign cysts, leading to potential misdiagnoses. Although Doppler ultrasound images showing abundant peritumoral vascularity may suggest malignancy, it cannot be considered definitive. Ultrasound is a valuable and non-invasive diagnostic method used to assess subcutaneous tumors, especially those in cosmetically sensitive and functionally important areas; however, its limitations should be acknowledged. Consideration of the possibility of malignancies such as EMPSGC during clinical evaluations is essential, particularly for periocular tumors presenting with cyst-like features resembling epidermal cysts.

CONFLICT OF INTEREST STATEMENT

None declared.

CONSENT

Written informed consent was obtained from the patients for publication of their case details.

ORCID

Kazuyasu Fujii https://orcid.org/0000-0002-6482-8953
Keisuke Goto https://orcid.org/0000-0002-4165-1809
Shigeto Matsushita https://orcid.org/0000-0003-2001-5341

REFERENCES

1. Qin H, Moore RF, Ho CY, Eshleman J, Eberhart CG, Cuda J. Endocrine mucin-producing sweat gland carcinoma: a study of 11 cases with molecular analysis. J Cutan Pathol. 2018;45:681–7.
2. Zembowicz A, Garcia CF, Tannous ZS, Mihm MC, Koerner F, Pilch BZ. Endocrine mucin-producing sweat gland carcinoma: twelve new cases suggest that it is a precursor of some invasive mucinous carcinomas. Am J Surg Pathol. 2005;29:1330–9.
3. Kuwano Y, Ishizaki K, Watanabe R, Nanko H. Efficacy of diagnostic ultrasonography of lipomas, epidermal cysts, and ganglions. Arch Dermatol. 2009;145:761–4.
4. Greenall CJ, Jones JL, Jones AV, Drage NA, Bhatia S, Hourihan MD. Solitary fibrous tumour of the cheek: an unusual presentation of a rare soft tissue tumour. Ultrasound. 2014;22:236–9.
5. Kaoku S, Konishi E, Fujimoto Y, Tohno E, Shiina T, Kondo K, et al. Sonographic and pathologic image analysis of pure mucinous carcinoma of the breast. Ultrasound Med Biol. 2013;39:1158–67.
6. Wortsman X. Ultrasound of common non-vascular benign cutaneous lesions. In: Wortsman X, editor. Atlas of dermatologic ultrasound. Cham: Springer International Publishing; 2018. p. 35–83.
7. Hughes BR, Black D, Srivastava A, Dalziel K, Marks R. Comparison of techniques for the non-invasive assessment of skin tumours. Clin Exp Dermatol. 1987;12:108–11.
8. Giovagnorio F, Andreoli C, De Cicco ML. Color doppler sonography of focal lesions of the skin and subcutaneous tissue. J Ultrasound Med. 1999;18:89–93.
9. Scotto di Santolo M, Sagnelli M, Mancini M, Scalvenzi M, Delfino M, Schonauer F, et al. High-resolution color-doppler ultrasound for the study of skin growths. Arch Dermatol Res. 2015;307:559–66.
10. Yamaoka M, Kuramochi A, Takeuchi K, Saitoh T, Ikebuchi K. Sonographic appearance of benign subcutaneous nodules--including color doppler sonography. Rinsho Byori. 2014;62:432–9.

How to cite this article: Kawamoto H, Fujii K, Aoki M, Goto K, Ikoma T, Tozawa T, et al. Ultrasound findings of endocrine mucin-producing sweat gland carcinoma mimicking epidermal cysts: A case series and diagnostic challenges. J Dermatol. 2025;52:939–942. https://doi.org/10.1111/1346-8138.17694

Received: 17 November 2024 | Accepted: 12 March 2025

DOI: 10.1111/1346-8138.17722

THE JOURNAL OF DERMATOLOGY

CONCISE COMMUNICATION

Transurethral resection and oral mucosal grafting for urethral-involved extramammary Paget disease: A function-preserving approach

Katsuhiko Nishihara[1] | Kazuyasu Fujii[1] | Megumi Aoki[1] | Sotaro Yamamoto[1] | Shuichiro Kawahira[2] | Shigeto Matsushita[1]

[1]Department of Dermato-Oncology, NHO Kagoshima Medical Center, Kagoshima, Japan

[2]Department of Urology, NHO Kagoshima Medical Center, Kagoshima, Japan

Correspondence
Kazuyasu Fujii, Department of Dermato-Oncology, NHO Kagoshima Medical Center, Kagoshima, Japan.
Email: k7597938@kadai.jp

Abstract

Extramammary Paget disease with urethral involvement presents considerable challenges, primarily because of the difficulty in achieving clear surgical margins while preserving urinary function. This report describes four women with urethral extramammary Paget disease who were treated using transurethral resection followed by oral mucosal grafting for urethral reconstruction. The primary objective was complete excision of the diseased area while minimizing postoperative complications, with a particular focus on preservation of urinary function. Transurethral resection enabled precise resection of the urethral mucosa without compromise of the urethral sphincter. Pathological analysis confirmed negative margins in three of the four patients; one patient had preoperative evidence of tumor cell invasion at the internal urethral orifice. Urinary function was preserved in all patients, and postoperative complications such as urethral stricture were successfully managed using dilation. No recurrences were observed during follow-up. This approach, which combines transurethral resection and oral mucosal grafting, offers a minimally invasive and function-preserving surgical option for urethral-involved extramammary Paget disease, demonstrating favorable oncological and functional outcomes.

KEYWORDS
extramammary Paget disease, minimally invasive surgical procedures, quality of life, transurethral resection, urethral neoplasms

1 | INTRODUCTION

Extramammary Paget disease (EMPD) is a rare cutaneous intraepithelial malignancy that primarily affects areas rich in apocrine glands, such as the genital, perianal, and axillary regions. A notable feature of EMPD is its ability to invade adjacent structures, including the urethra, vagina, and anus. The mucosal border is involved in approximately one-third of cases,[1] and boundary area tumor involvement is a major risk factor for incomplete excision, local recurrence, and poor survival outcomes.

When EMPD invades the mucous membranes of the anus or genitals, the standard approach has been wide local excision; however, complete excision is difficult using wide local excision alone. More invasive procedures such as excision of the vulva, perineum, rectum, or urethra; total cystectomy; and total pelvic exenteration may be performed with the aim of achieving a wide excision.[2] These surgical methods may lead to substantial tissue loss and require extensive reconstruction, leading to serious functional impairment and deformity and reducing the patient's quality of life. However, incomplete resection of the primary tumor reportedly has no significant association with a poor prognosis.[1,3] Therefore, a less invasive surgical approach that preserves anogenital[4] and urinary[5] function may be acceptable as a first-line treatment for resectable EMPD.

Transurethral resection (TUR) is commonly used to treat certain urinary and prostate conditions, particularly prostate enlargement[6] or bladder tumors.[7] It is also used to treat certain

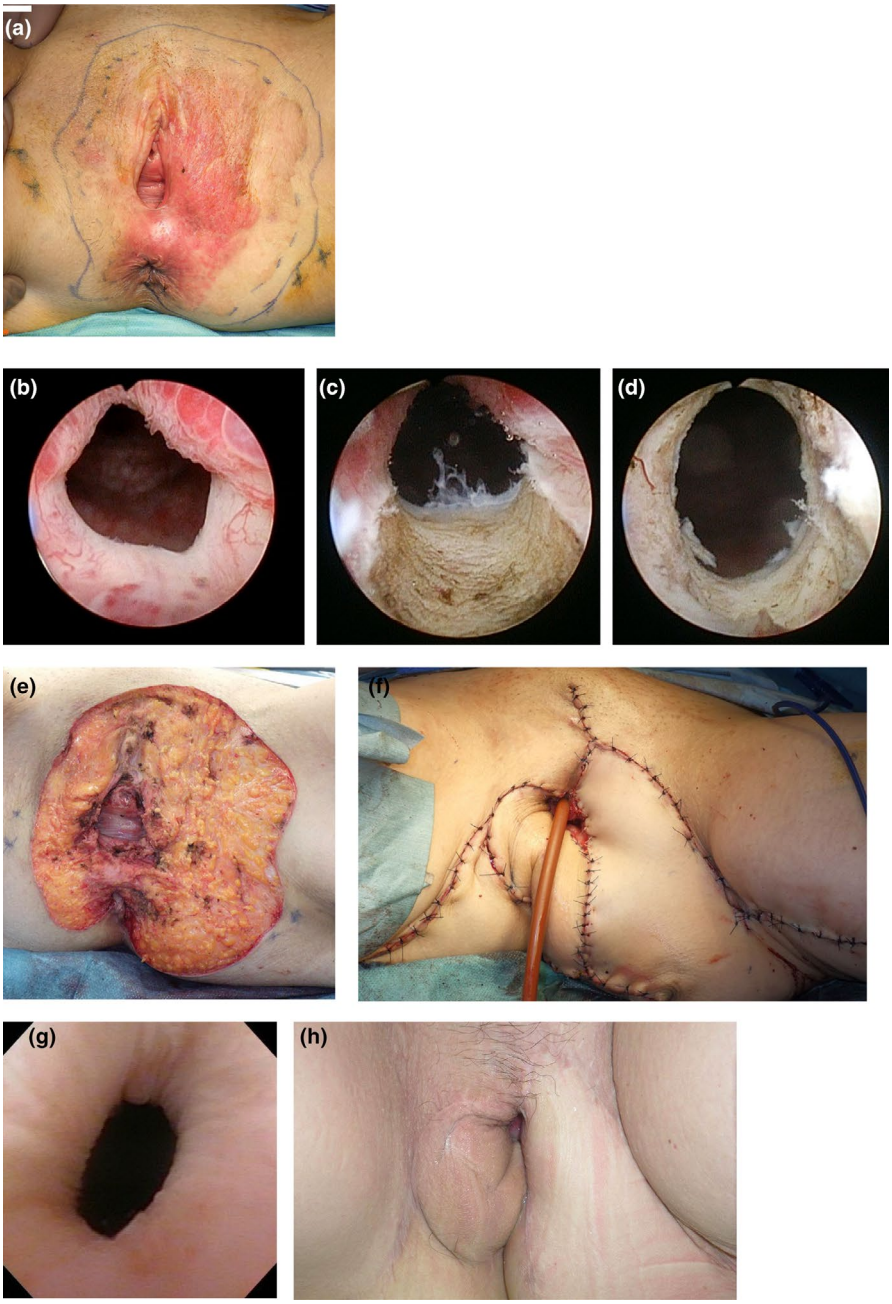

FIGURE 1 (a) Clinical appearance before surgery. The dotted line indicates the preoperatively estimated skin boundary of the tumor, while the solid line represents the skin incision line. Cystoscopy images showing the urethra before transurethral treatment (b), after resection of one-quarter of the urethral mucosa (c), and after complete circumferential resection of the urethral mucosa (d). (e) Clinical appearance after tumor excision. (f) Final clinical appearance after surgery. The skin defects on both sides were repaired using gluteal fold flaps. Endoscopic findings (g) and clinical appearance (h) 1 year after surgery.

types of urethral cancer. In the 2020 European Association of Urology guidelines on primary urethral carcinoma, TUR is indicated primarily for small distal urethral tumors, particularly in patients in whom the tumor is noninvasive or minimally invasive.[8] The procedure involves inserting a resectoscope through the urethra to access bladder or urethral lesions. A wire loop with electric current is used to remove the tumor, and the tissue is sent for pathological evaluation. The technique is precise and allows tumor removal without external incision. TUR offers a less invasive, bladder-preserving treatment with fewer complications than traditional surgical methods.

Herein, we describe four patients with vulvar EMPD with suspected urethral involvement, all of whom were treated surgically using TUR.

2 | CASE REPORT

A 55-year-old woman was referred to our clinic because of vulvar erythema that had persisted for 7 years (Figure 1a). Histologically, she was diagnosed with EMPD, and mapping biopsy revealed tumor invasion of the epithelium of the external urethral meatus. Although bladder cystoscopy did not reveal macroscopic or histological tumor invasion, the presence of tumor cells at the external urethral meatus increased the likelihood of urethral invasion, so it could not be completely ruled out. This consideration led us to proceed with urethral resection. The urethral mucosa was completely resected from the internal urethral orifice using TUR, while the urethral sphincter was preserved (Figure 1b–d). The skin lesions were excised 10 mm from the visible tumor margins. The vaginal mucosa was excised along

the negative mapping biopsy line, and the anal lesion was resected based on the negative mapping biopsy results, with preservation of the anal sphincter (Figure 1e). The skin defects on both sides were reconstructed using gluteal fold flaps (Figure 1f). Urethral reconstruction was performed using a buccal mucosal graft harvested from the left buccal mucosa and oral vestibule. The graft was sutured to the external urethral meatus, incorporating the sphincter and flap. The internal urethra was grafted using a urethral catheter, for compression, to ensure graft adherence. Postoperative tissue examination was performed specifically at the internal urethral opening, at the pathologist's discretion, and no tumor cells were detected at this site. Postoperatively, the patient developed bladder irritation as a complication; however, her symptoms resolved within 2 weeks, after antibiotic therapy. One year after surgery, no recurrence has been observed (Figure 1g,h).

Further details of the patients included in this study are summarized in Table 1. In cases 2 and 3, as in case 1, tumor invasion of the external urethral opening was confirmed by preoperative biopsy. In all cases, resection of the urethral mucosa was performed up to the internal urethral orifice. Histopathological examination confirmed that the side margin facing the bladder was negative, and no tumor cells were detected at the internal urethral opening. In case 4, preoperative biopsy revealed the presence of tumor cells, not only in the external urethral meatus but also in the internal urethral meatus. However, considering the patient's advanced age and overall activities of daily living, we decided to forgo more aggressive surgical interventions, such as total urethrectomy or urinary diversion, and treated her using TUR-based urethrectomy. In case 2, urethral reconstruction was performed using the lip mucosa, whereas in the other patients, the buccal mucosa was used. The difference in mucosal harvesting sites did not affect the surgical difficulty or occurrence of postoperative complications.

All patients successfully underwent TUR without intraoperative complications. Postoperative pathology confirmed negative surgical margins except in case 4. Urinary function was preserved in all cases. Two patients developed postoperative urethral strictures that were effectively managed using urethral dilation using a multiple-use bougie. In case 2, no recurrence was observed for 7 years, whereas in case 3, no recurrence was observed for 3 years and 3 months. In case 4, no disease progression was observed for 2 years and 9 months.

3 | DISCUSSION

In cases of EMPD extending to the urethral mucosa, traditional surgery typically involves excision of the urethral mucosa, followed by skin grafting, which often results in postoperative complications, particularly urethral strictures.[5] Urethral strictures can affect patients' quality of life by causing urinary dysfunction, such as difficulty in voiding and urinary spraying. To address this, Nakamura et al.[5] introduced a novel technique involving implantation of buccal mucosa between the remaining urethral mucosa and the skin graft after excision. This method successfully prevented urethral stricture and maintained normal urinary function for up to 2 years after surgery. However, this technique requires partial urethral resection, which leads to postoperative shortening. Urethral shortening may result in long-term complications including a higher risk of urinary incontinence, reduced voiding function, instability of urethral support structures, and higher susceptibility to infections.[10]

In contrast, our surgical technique involves complete excision of the urethral epithelium from the external meatus to the internal meatus, replacement of the entire urethra with mucosal tissue, and preservation of all sphincter muscles. Even after consideration of the potential contraction of the transplanted mucosa postoperatively, a key feature of this approach is that urethral length is maintained relative to the extent of mucosal excision. EMPD is an intraepithelial neoplasm that tends to spread horizontally within the epithelium; however, vertical invasion is rare. Therefore, TUR, which allows epithelial removal with preservation of the urethral sphincter, is an appropriate treatment technique.

A potential limitation of this surgical method is the risk of residual tumor tissue. Consistent postoperative follow-up and regular monitoring are essential for effective management of this risk.

In conclusion, TUR with oral mucosal grafting is a promising, minimally invasive alternative to traditional excision of EMPD with urethral involvement. This approach, which uses oral mucosa for

TABLE 1 Summary of the four cases.

Case	Age, y	Sex	EMPD stage	Resection margins (urethral side)	Postoperative complications	Management of complications	Time to symptom resolution	Last follow-up
1	55	Female	0	Negative	Bladder irritative symptoms	Antibiotic therapy	2 wk	ANED, 1 y
2	59	Female	1	Negative	Urethral stricture	Urethral dilation (bougie)	3 mo	ANED, 7 y
3	53	Female	0	Negative	Urethral stricture	Urethral dilation (bougie)	2 mo	ANED, 3 y 3 m
4	89	Female	0	Positive	None	Not applicable	Not applicable	AWD, 2 y 9 m

Note: Extramammary Paget disease (EMPD) staging was based on a report by Ohara et al.[9]

Abbreviations: ANED, alive with no evidence of disease; AWD, alive with disease.

urethral reconstruction, effectively preserves urinary function, minimizes postoperative morbidity, and promotes healing. While recurrence was not observed in three of the four patients during follow-up, further studies with larger sample sizes and extended follow-up should be performed to confirm these findings, refine patient selection criteria, and fully assess the long-term outcomes.

CONFLICT OF INTEREST STATEMENT

None declared.

INFORMED CONSENT

Written informed consent was obtained from each patient.

ORCID

Katsuhiko Nishihara https://orcid.org/0000-0002-3801-4278
Kazuyasu Fujii https://orcid.org/0000-0002-6482-8953
Sotaro Yamamoto https://orcid.org/0009-0003-8617-6444
Shigeto Matsushita https://orcid.org/0000-0003-2001-5341

REFERENCES

1. Hashimoto H, Kaku-Ito Y, Furue M, Ito T. Mucosal invasion, but not incomplete excision, has negative impact on long-term survival in patients with extramammary Paget's disease. Front Oncol. 2021;11:642919.
2. Geisler JP, Gates RW, Shirrell W, Parker SM, Maloney CD, Wiemann MC, et al. Extramammary Paget's disease with diffuse involvement of the lower female genito-urinary system. Int J Gynecol Cancer. 1997;7:84–7.
3. Okumura M, Ogata D, Namikawa K, Takahashi A, Akiyama M, Yamazaki N. Functional preservation benefits of minimal surgery for extramammary Paget's disease. Exp Dermatol. 2023;32:1644–50.
4. Yamamura K, Matsushita S, Shimaoka S, Kitazono M, Maeda T, Nuruki K, et al. Anorectal function preserving surgery with endoscopic submucosal dissection in patients with perianal extramammary Paget's disease. J Dermatol. 2021;48:E520–1.
5. Nakamura M, Hakozaki Y, Iwata S, Sato Y, Makino K, Kawai T, et al. Novel operative technique of advancement urethral meatoplasty utilizing buccal mucosa for vulvar Paget's disease with urethral invasion: two case reports. J Med Case Reports. 2021;15:136.
6. Wasson JH, Reda DJ, Bruskewitz RC, Elinson J, Keller AM, Henderson WG. A comparison of transurethral surgery with watchful waiting for moderate symptoms of benign prostatic hyperplasia. The Veterans Affairs Cooperative Study Group on Transurethral Resection of the Prostate. N Engl J Med. 1995;332:75–9.
7. Herr HW, Donat SM. Quality control in transurethral resection of bladder tumours. BJU Int. 2008;102:1242–6.
8. Gakis G, Bruins HM, Cathomas R, Compérat EM, Cowan NC, van der Heijden AG, et al. European Association of Urology guidelines on primary urethral Carcinoma-2020 update. Eur Urol Oncol. 2020;3:424–32.
9. Ohara K, Fujisawa Y, Yoshino K, Kiyohara Y, Kadono T, Murata Y, et al. A proposal for a TNM staging system for extramammary Paget disease: retrospective analysis of 301 patients with invasive primary tumors. J Dermatol Sci. 2016;83:234–9.
10. Lapides J. Surgical therapy for abnormalities of the urinary sphincter in the female. Br J Urol. 1965;37:609–19.

How to cite this article: Nishihara K, Fujii K, Aoki M, Yamamoto S, Kawahira S, Matsushita S. Transurethral resection and oral mucosal grafting for urethral-involved extramammary Paget disease: A function-preserving approach. J Dermatol. 2025;52:1094–1097. https://doi.org/10.1111/1346-8138.17722

Radiological Physics and Technology (2024) 17:938–946
https://doi.org/10.1007/s12194-024-00840-8

TECHNICAL NOTE

Optimum delineation of skin structure for dose calculation with the linear Boltzmann transport equation algorithm in radiotherapy treatment planning

Keisuke Hamada[1,2] · Toshioh Fujibuchi[3] · Hiroyuki Arakawa[3]

Received: 27 October 2023 / Revised: 23 August 2024 / Accepted: 25 August 2024 / Published online: 9 September 2024

Abstract
This study investigated the effectiveness of placing skin-ring structures to enhance the precision of skin dose calculations in patients who had undergone head and neck volumetric modulated arc therapy using the Acuros XB algorithm. The skin-ring structures in question were positioned 2 mm below the skin surface (skin A) and 1 mm above and below the skin surface (skin B) within the treatment-planning system. These structures were then tested on both acrylic cylindrical and anthropomorphic phantoms and compared with the Gafchromic EBT3 film (EBT3). The results revealed that the maximum dose differences between skins A and B for the cylindrical and anthropomorphic phantoms were approximately 12% and 2%, respectively. In patients 1 and 2, the dose differences between skins A and B were 9.2% and 8.2%, respectively. Ultimately, demonstrated that the skin-dose calculation accuracy of skin B was within 2% and did not impact the deep organs.

Keywords Skin-surface dose · Skin-ring structure · Volumetric modulated arc therapy · Acuros XB · Head and neck

1 Introduction

Acute radiation dermatitis (ARD) is a common adverse effect observed in patients undergoing radiation therapy for head and neck cancer [1]. The number of ARD cases has decreased due to advancements in irradiation technology, specifically the shift from three-dimensional conformal radiotherapy to volumetric modulated arc therapy (VMAT) [2–4]. However, ARD still occurs in many patients, and there have been reports of severe cases [1, 5]. Therefore, accurate skin-dose calculations using treatment-planning systems (TPSs) are crucial. Currently, there are no available radiotherapy guidelines for assessing skin doses [6]. As a result, skin doses are not evaluated using a dose–volume histogram.

The skin-dose evaluation lacks a defined ring structure due to the inaccuracies found in calculations based on the percentage depth dose for photon beams from a single direction [7, 8]. However, with the introduction of VMAT irradiation technology, the skin is now exposed to radiation from multiple directions, and it is important to investigate the damage caused to the skin as it is affected by both the incoming and outgoing directions. In this study, we compared the dose measured from the Gafchromic EBT3 film (EBT3) with the dose calculated using the TPS, examined the dose gradient at the skin–air interface, and investigated the average dose in the target volume and organs at risk.

2 Materials and methods

2.1 Contour definition of the skin structure and verification conditions

Skin A was the default setting in Eclipse version 13.6 (Varian Medical Systems, Palo Alto, CA, USA), where the external body contour was automatically constructed after importing computed tomography (CT) images. Skin A had

✉ Keisuke Hamada
hamada.keisuke.we@mail.hosp.go.jp

1 Department of Radiological Technology, National Hospital Organization Kagoshima Medical Center, 8-1 Shiroyama-cho, Kagoshima 892-0853, Japan

2 Department of Health Sciences, Graduate School of Medicine, Kyushu University, Fukuoka, Japan

3 Department of Health Sciences, Faculty of Medical Sciences, Kyushu University, Fukuoka, Japan

a thickness of 2 mm and was obtained from the skin surface as described in previous studies [9, 10] (Fig. 1a, b). Skin dose calculations for the TPS were only performed inside the body contour [11, 12]. In skin B, the skin surface was located at the center of the skin ring structure. Skin B had a 1-mm structure in front of and behind the skin surface. The external body contour included skin B, extending 1 mm outward from the default settings (Fig. 1c, d). The extension of the external body contour included an air layer on the skin surface. Notably, thermoplastic masks and couches can significantly affect the skin dose of a patient [13–15]. Therefore, these were included in the external body contour to measure the effect of scattered radiation [11].

To create skins A and B, the TPS used the "extract wall" function to create a skin-ring structure. A structural functional margin was used to extend the external body contours. The treatment data from two patients were fused to an acrylic cylindrical phantom in Fig. 2 and anthropomorphic phantoms in Fig. 3 (QUART, Zorneding, Germany) using the TPS. The cylindrical phantom had a diameter of 12 cm and length of 15 cm, representing the neck area. The photon energy used was 6 MV, the calculation algorithm was Eclipse version 13.6 Acuros XB (AXB), and the calculation grid size was 1.5 mm. Treatment-planning CT images with a slice thickness of 2 mm were imported into the TPS. CT was performed using SOMATOM Definition AS 64 Open (Siemens Healthineers, Erlangen, Germany). The field of view of the CT images was 500 mm, and the pixel size was 0.9765 mm.

2.2 Target volume, organs at risk, and planned organ-risk volume

Contouring and plan optimization are briefly summarized here, with a more detailed description available in the literature [16, 17]. The target volumes were defined as shown

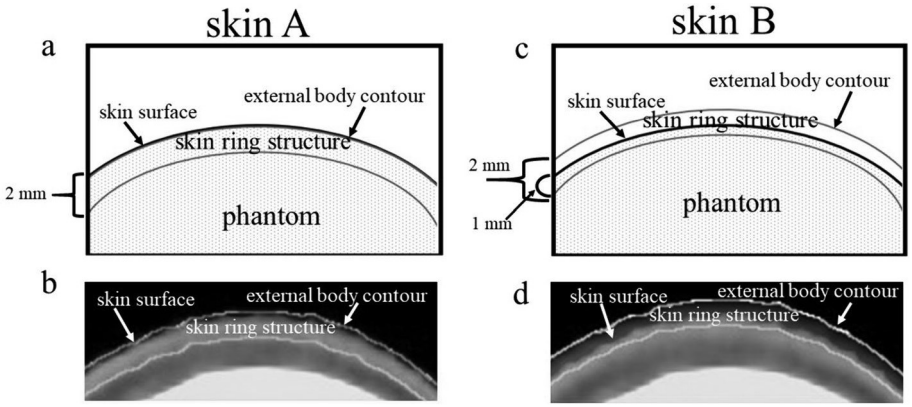

Fig. 1 **a** Skin A is a skin-ring structure located 2 mm below the skin surface. The external body contour is contoured at the same location as the skin surface with default settings. **b** Dose distribution in skin A and the skin surface of the treatment-planning system. The doses are calculated at a depth of 2 mm from the skin surface. **c** Skin B is a 2-mm skin-ring structure with its center on the skin surface. The external body contour is extended outward by 1 mm. **d** Dose distribution in skin B and the skin surface of the treatment-planning system

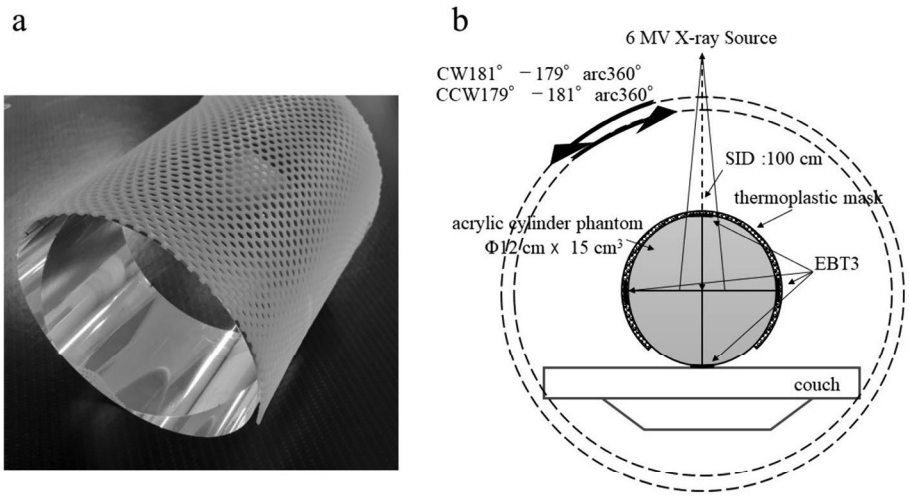

Fig. 2 **a** Acrylic cylindrical phantom simulating the neck. **b** TPS calculation conditions and the measurement position of the EBT3 film are shown. The cylindrical phantom has a diameter of 12 cm and length of 15 cm. The measured doses from the EBT3 film and the calculated doses from the TPS are compared at the same location on the acrylic cylindrical phantom. TPS, treatment-planning system; EBT3, Gafchromic EBT3 film

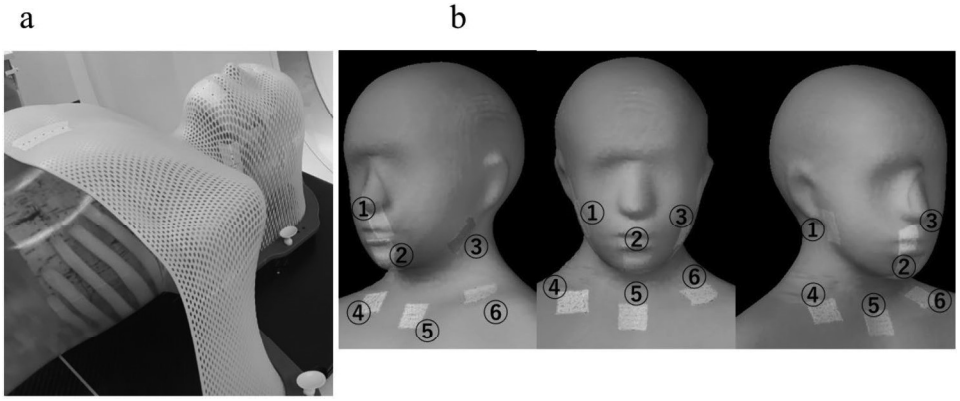

Fig. 3 **a** Anthropomorphic phantom covered with a thermoplastic mask. **b** Skin-ring structure of the TPS and location of the EBT3 film. (1) Right parotid gland, (2) chin, (3) left parotid gland, (4) right clavicle, (5) sternum pattern, and (6) left clavicle. TPS, treatment-planning system; EBT3, Gafchromic EBT3 film

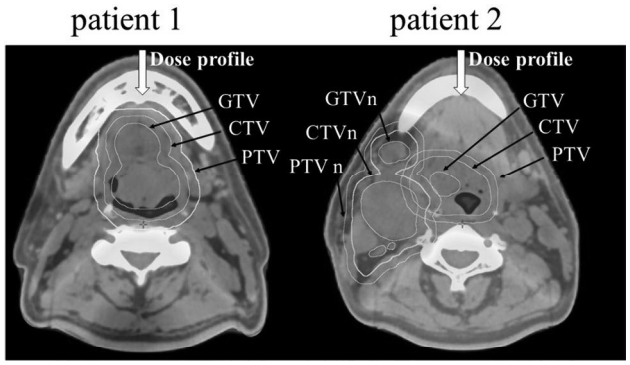

Fig. 4 Patient 1 is a stage II patient with a T2, N0, and M0 TNM classification for oropharyngeal cancer. Patient 2 is a stage I patient with a T1, N1, and M0 TNM classification for oropharyngeal cancer. The target volume and dose distribution are shown. A 2-mm portion of the PTVn in patient 2 is excluded from the skin surface. Dose profiles are calculated at the arrow positions. PTVn, planning target volume of potentially metastatic lymph node enlargement

in Fig. 4. The gross tumor volume (GTV) included the gross extent of the primary disease and lymph-node metastases, taking into account clinical and radiologic findings. The clinical target volume (CTV) was defined as the GTV plus a 5-mm margin, considering anatomic and clinical oncologic features. The planning target volume (PTV) was defined as the CTV plus a 5-mm margin. To prevent a skin overdose, a 2-mm exclusion zone was created around the PTV, assuming no sacrifice in CTV dose.

Gross enlarged lymph nodes (GTVns) with potential for metastasis were defined based on clinical and radiologic findings. The CTV of potentially metastatic lymph nodes (CTVns) included the GTVn plus a 5 mm margin, considering anatomic and clinical oncologic features. The PTV of potentially metastatic lymph-node enlargement (PTVn) was defined as the CTVn plus a 5-mm margin. The organs at risk included the skin, brain, brainstem, lungs, spinal cord, right parotid gland, left parotid gland, trachea, brainstem, planned organ-risk volume (PRV), spinal cord PRV, right parotid PRV, and left parotid PRV.

2.3 Gafchromic film EBT3 dosimetry

EBT3 is a reliable instrument for skin dosimetry [18, 19]. The irradiated EBT3 (Ashland Inc., Bridgewater, NJ, USA) was read 24 h later using an EPSON ES-10000G flat-head scanner (Seiko Epson Corporation, Suwa, Nagano, Japan). The films were individually placed at the center of the scanner. Film data were analyzed using Dose-Difference Analysis version 14 (*R*-TEC Inc., Itabashi, Tokyo, Japan). To ensure measurement reliability, the data were obtained from three separate irradiations under identical conditions, and the average value was used. The EBT3 was carefully placed in close contact with an anthropomorphic phantom, as depicted in Fig. 3. For the anthropomorphic phantoms, a 1.6-mm thick thermoplastic mask (CIVCO Radiotherapy, Orange City, IA, USA) with a 4-mm diameter hole was employed. A 1-mm spherical plastic was positioned at each of the four corners of the EBT3 as a landmark, corresponding to the TPS skin-ring structure. The analysis of EBT3 was performed using *D-D* Analysis version 14. The region of interest and the skin-ring structure for EBT3 were 2.5 cm long and 3 cm wide. EBT3 had a three-phase structure with a thickness of 0.278 mm.

2.4 Comparison of the measured dose of EBT3 and the calculated dose of TSP

This section compares the dosimetry of the EBT3 and TPS calculations for cylindrical and anthropomorphic phantoms in patients 1 and 2. The TPS contour tool was used to create a skin-ring structure with dimensions of 2.5 cm length and 3 cm width on both the cylindrical and anthropomorphic phantoms. The ring structures on the TPS were referred to as skins A and B (Fig. 1). The positions of the TPS calculations and EBT3 measurements were the same. A thermoplastic mask was applied to the phantom. The EBT3 and TPS were

placed at four locations on the cylindrical phantom: upper to 0° beam angle, left to 90° beam angle, bottom to 180° beam angle, and right to 270° beam angle (Fig. 2). In the anthropomorphic phantom, the EBT3 and TPS structures were placed at six arbitrary locations: right parotid gland, chin, left parotid gland, right clavicle, left clavicle, and sternal pattern (Fig. 3).

The TPS and EBT3 doses were compared using Eq. (1).

$$\text{Difference}\,(\%) = \{(D_{\text{TPS}} - D_{\text{EBT3}})/D_{\text{EBT3}}\} \times 100, \cdots, \quad (1)$$

where D_{TPS} represents the TPS dose and D_{EBT3} represents the EBT3 dose.

2.5 Dose gradient at the skin–air interface

The skin–air interface of various skin-ring structure arrangements was examined. The skin–air interface dose profiles for patients 1 and 2 were examined by selecting the location with the largest GTV diameter and the steepest dose gradient that strongly dose constrains the dose (Fig. 4). The clinical irradiation conditions included a dose of 2.0 Gy per session, a total of 35 sessions, and a total dose of 70 Gy administered five times per week.

2.6 Comparison of the target volume mean dose, risk-organ mean doses, and planned organ-risk volume

The target volumes of skins A and B, as well as the doses to normal organs, were investigated in patients 1 and 2. In patient 1, the skin, GTV, CTV, and PTV were investigated, while in patient 2, the investigation included the skin, GTV, CTV, PTV, GTVn, CTVn, and PTVn. The organs at risk included the skin, brain, brainstem, lungs, spinal cord, right and left parotid glands, trachea, brainstem PRV, spinal cord PRV, right parotid PRV, and left parotid PRV. The dose to the skin-ring structure, the average dose to the target volume, and the average dose to the organs at risk for skins A and B were compared using Eq. (2).

$$\text{Difference}\,(\%) = \{(\text{skin}\,A - \text{skin}\,B)/\text{skin}\,A\} \times 100, \cdots. \quad (2)$$

3 Results

3.1 Comparison between the measured dose of EBT3 and the calculated dose of TSP

Figure 5 shows the results of irradiating a cylindrical phantom. The maximum and minimum dose differences between skin A and EBT3 were 12.5% and 2.72%, respectively. The dose difference between skin B and EBT3 was approximately 2.0%. The bottom of the cylindrical phantom showed a small dose difference of 1% (skin A) to 2% (skin B) with EBT3. A comparison between the EBT3 dose and TPS dose calculations for anthropomorphic phantoms showed a maximum difference of 13.4% and a minimum of 6.27% for skin A and within approximately ± 2.0% for skin B (Fig. 6). Skin B matched the EBT3 dose, regardless of the measurement site.

3.2 Dose gradient at the skin–air interface

The dose gradients at the skin–air interfaces for patients 1 and 2 are shown in Fig. 7a and b, respectively. Dose gradients differed between skin A and B in patient 1. For skin A, the dose calculation began 3.0 mm outside the skin surface (Fig. 7a (1)), and the dose increased by approximately 600 cGy for

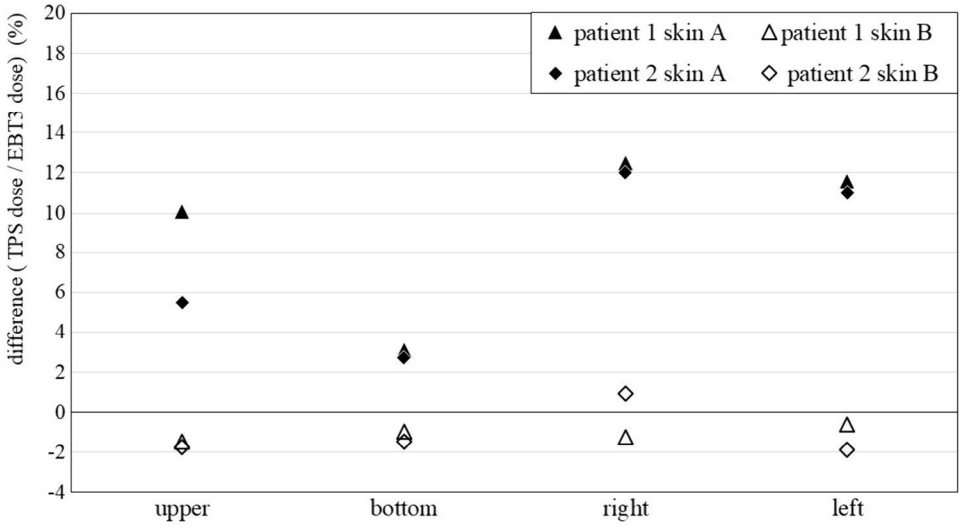

Fig. 5 Comparison between EBT3-measured doses and TPS-calculated doses for skin A and B in a cylindrical phantom. For skin A, the TPS-calculated doses are higher than those measured by EBT3. In contrast, the dose difference for skin B is within 2% of the EBT3 measurements. In addition, for skin A, the dose difference between TPS and EBT3 is smaller at the bottom of the phantom compared to the top, right, and left sides. TPS, treatment planning system; EBT3, Gafchromic EBT3 film

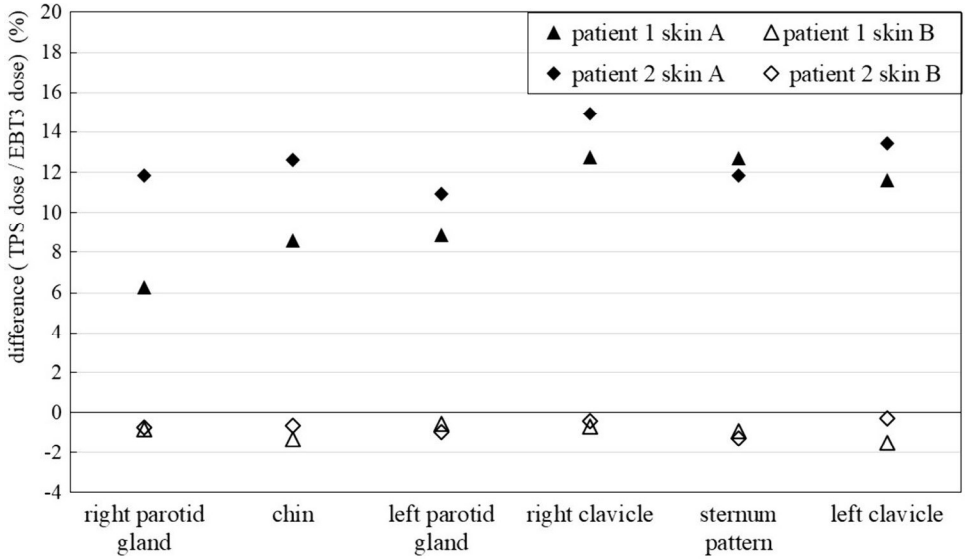

Fig. 6 Comparison between EBT3-measured doses and TPS-calculated doses for skin A and B in anthropomorphic phantoms. Skin A is overestimated by up to 15%, whereas skin B improved the dose difference to within 2%

each 1 mm depth to the skin surface (Fig. 7a (2)). For skin B, the dose calculation began approximately 6.0 mm (Fig. 7a (3)) from the skin surface and 4.5 mm outside the external body contour (Fig. 7a (4)). In addition, the dose profile of skin B increased by approximately 250 cGy at a depth of 1 mm (Fig. 7a (5)). Similarly, patient 2 displayed different dose gradients for skin A and B. For skin A, the dose calculation began 1.5 mm outside the skin surface (Fig. 7b (1)), and the dose increased by approximately 750 cGy/mm (Fig. 7b (2)). Dose calculations for skin B began approximately 3.0 mm from the skin surface (Fig. 7b (3)) and 2.0 mm from the body contour (Fig. 7b (4)). The dose profile of skin B exhibited an increase of approximately 300 cGy for each depth of 1.0 mm (Fig. 7b (5)). Notably, the 1-mm extension of the external body contour was calculated using the calculation starting point more than 1 mm outward due to the effect of voxel resolution [11, 20].

3.3 Comparison between target volume and risk-organ doses

The dose differences for the skin, GTV, CTV, and PTV for skins A and B in patient 1 were 8.8%, 0.00031%, 0.00025%, and 0.00008%, respectively. The dose differences for the skin, GTV, CTV, PTV, GTVn, CTVn, and PTVn for skins A and B in patient 2 were 7.6%, −0.00015%, −0.00014%, 0.00015%, 0.00011%, 0.00018%, and 0.00019%, respectively. The dose differences for all organs at risk in patients 1 and 2 were ≤0.01% (Table 1).

4 Discussion

This study investigated the placement of skin-ring structures to improve the accuracy of skin-dose calculations in patients undergoing full-arc head and neck VMAT. In the dose comparison between EBT3 and TPS, the conventional method for skin A showed a maximum dose difference of approximately 13%, which is consistent with the results reported in previous studies [21–23]. On the other hand, skin B significantly improved the accuracy of the skin-dose calculation by approximately 2%. Notably, some studies have extrapolated EBT3 doses to accurately measure skin doses [24–26]. However, other studies on the accuracy of TPS calculations have reported low accuracy due to the omission of measurement-depth issues [11, 27–29].

There is a limit to the thickness of the skin-ring structures created by the TPS. The thickness of the skin-ring structures depends on the voxel size. In this study, the field of view was 500 mm and the matrix was 512 × 512. Since one pixel corresponds to 0.9765 mm, the minimum thickness of the skin-ring structure is 2 mm. However, it is not possible to further decrease the thickness of the skin-ring structures by simply adjusting their dimensions, as demonstrated in skin A. Therefore, alternative methods need to be considered. Notably, skin B has a structure that extends beyond the body contour and is not originally

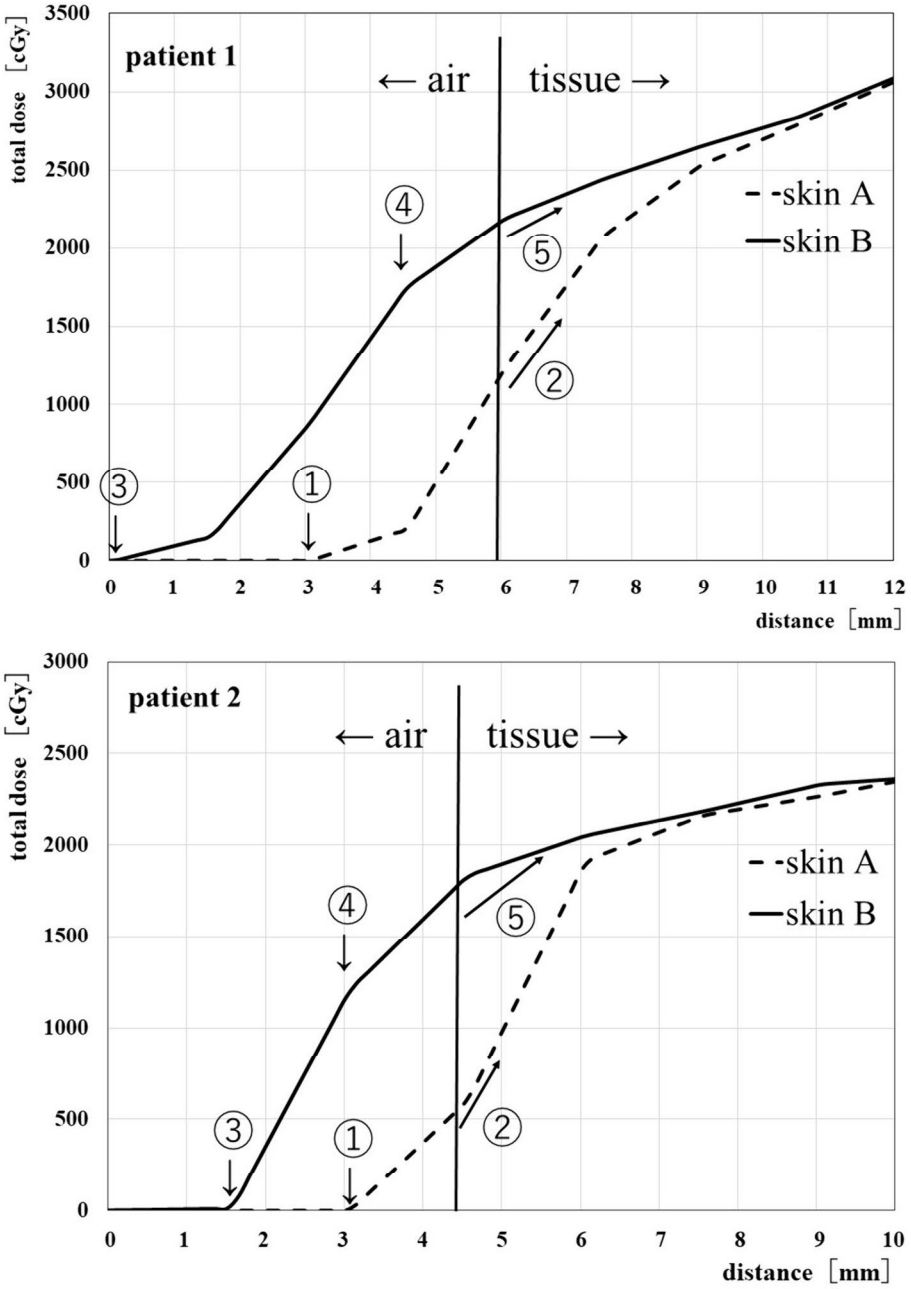

Fig. 7 **a** Dose profile of patient 1 at any position. When the external body contour is extended outward by 1 mm, the calculation starting point for skin B moved away from the skin, and the slope of the dose incident on the skin decreased. **b** Dose profile at any position of patient 2. As in Fig. 7a, the calculation starting point is farther away from the skin, and the slope of the dose incident on the skin is slower. The extension of the external body contour contributes to the dose distribution at the boundary between the air and the patient/phantom

present. However, the accuracy of the model-based calculation algorithm can improve the accuracy of the calculation as it approaches the entrance. In essence, the skin-dose reduction is greater without a thermoplastic mask [30]. Nevertheless, in VMAT, the exit dose contributes significantly to the skin dose [15, 31]. This is another factor that improves the calculation accuracy by avoiding a sharp decline on the exit side [32, 33].

Skin B did not affect the target volume or at-risk organs, with a dose difference of $< 0.01\%$ (Table 1). This result aligns with the findings reported by Tanaka et al. [20]. This is because the build-up effect is smaller when the effective depth is ≥ 4 mm [30]. Another factor is that with a 360-degree rotating VMAT, even better scattering conditions can be achieved using a fixed device, such as a thermoplastic mask, "behind" the patient [31]. In addition, skin B follows the usual depth-dose percentage curve [15, 32, 33] and does not affect the target volume or risk-organ dose. To explore this further, we investigated the volume structures outlined in the TPS, such as the skin-ring structures, target volumes, and organs at risk. As shown in Fig. 7a and b, the dose profiles provide a survey of point doses at various locations. Notably, the VMAT skin doses were speckled [31], indicating that skin B doses were higher than skin A

Table 1 Comparison between the mean doses of the target volumes and organs at risk, as well as the percentage changes, due to extension of the external body contour

(a)				
Patient 1				
Structure	DVH parameter	Skin A	Skin B	{(Skin A-skin B) skin A} 100 (%)
Skin	D_{mean}	685.2	624.8	8.8
GTV	$D_{99\%}$	7120.8	7122.4	0.00031
CTV	$D_{99\%}$	7113.8	7115.6	0.00025
PTV	$D_{99\%}$	7075.4	7076.0	0.00008
GTVn	$D_{99\%}$	–	–	–
CTVn	$D_{99\%}$	–	–	–
PTVn	$D_{99\%}$	–	–	–
Brain	D_{mean}	91.9	92.2	0.00325
Brainstem	D_{mean}	209.8	210.3	0.00238
Lung	D_{mean}	197.7	198.0	0.00152
Spinal cord	D_{mean}	1545.2	1546.0	0.00052
Rt. parotid gland	D_{mean}	1728.0	1729.7	0.00098
Lt. parotid gland	D_{mean}	1736.4	1738.5	0.00121
Trachea	D_{mean}	1293.6	1293.3	−0.00023
Brainstem PRV	D_{mean}	228.1	228.7	0.00262
Spinal cord PRV	D_{mean}	1557.6	1558.4	0.00051
Rt. parotid PRV	D_{mean}	1101.8	1104.7	0.00263
Lt. parotid PRV	D_{mean}	1096.9	1100.4	0.00318
(b)				
Patient 2				
Structure	DVH parameter	Skin A	Skin B	{(Skin A-skin B) skin A} 100 (%)
Skin	D_{mean}	869.1	803.2	7.6
GTV	$D_{99\%}$	7112.4	7111.3	−0.00015
CTV	$D_{99\%}$	6960.3	6959.3	−0.00014
PTV	$D_{99\%}$	6772.2	6771.2	−0.00015
GTVn	$D_{99\%}$	7079.1	7078.3	−0.00011
CTVn	$D_{99\%}$	7088.2	7086.9	−0.00018
PTVn	$D_{99\%}$	7009.6	7008.3	−0.00019
Brain	D_{mean}	250.8	251.2	0.00159
Brainstem	D_{mean}	685.4	685.8	0.00058
Lung	D_{mean}	427.4	427.4	0.00000
Spinal cord	D_{mean}	2049.6	2049.5	−0.00005
Rt. parotid gland	D_{mean}	2604.3	2606.2	0.00073
Lt. parotid gland	D_{mean}	1787.6	1789.8	0.00123
Trachea	D_{mean}	1943.5	1941.3	−0.00113
Brainstem PRV	D_{mean}	743.7	744.1	0.00054
Spinal cord PRV	D_{mean}	2062.4	2062.2	0.00010
Rt. parotid PRV	D_{mean}	1328.5	1330.8	0.00173
Lt. parotid PRV	D_{mean}	1234	1236.5	0.00202

doses, in contrast to the aforementioned results. Since even slight differences in measurement points can alter the profile shape, caution is advised when examining skin doses using arbitrary profiles. In our study, we believe that arbitrary profiles are unreliable for skin-dose evaluation and that it is better to evaluate skin dose by volume.

Therefore, skin B allows for a more realistic evaluation of the surface doses obtained using EBT3.

5 Conclusion

This study aimed to improve the accuracy of skin-dose calculations in patients who underwent full-arc head and neck VMAT using skin-ring structures. Skin B, calculated using AXB, exhibited a dose difference of approximately 2% compared to that of EBT3. In the phantom study, skin A (with a conventional skin-ring structure) showed a dose difference of 13%, whereas skin B (new skin-ring structure) showed an improvement of approximately 10% (within 2%). In clinical cases, improvements of 8.2% and 9.2% were observed in patients 1 and 2, respectively, for skin B. Furthermore, extending the external body contour of skin B by 1 mm did not affect the dose delivered to the target or organ at risk. Overall, skin B can be used as an indicator to evaluate skin dose during the treatment-planning phase.

Acknowledgements Not applicable

Funding This study was funded internally by Kyushu University.

Data availability All authors share our data by network attached storage.

Declarations

Conflict of interest All authors declare that they have no conflict of interest.

Ethical approval This study was approved by the ethics committee of Kyushu Cancer Center (2022–30) and was conducted according to the Declaration of Helsinki.

References

1. Bozec A, Culié D, Poissonnet G, Dassonville O. Current role of total laryngectomy in the era of organ preservation. Cancers. 2020;12:584. https://doi.org/10.3390/cancers12030584.
2. Leventhal J, Young MR. Radiation dermatitis: recognition, prevention, and management. Oncology. 2017;31:885–7, 894–9. https://europepmc.org/article/med/29297172.
3. Gamez ME, Blakaj A, Zoller W, Bonomi M, Blakaj DM. Emerging concepts and novel strategies in radiation therapy for laryngeal cancer management. Cancers. 2020;12:1651. https://doi.org/10.3390/cancers12061651.
4. Kaidar-Person O, Gil Z, Billan S. Precision medicine in head and neck cancer. Drug Resist Updates. 2018;40:13–6. https://doi.org/10.1016/j.drup.2018.09.001.
5. Lalla RV, Brennan MT, GoRDon SM, Sonis ST, Rosenthal DI, Keefe DM. Oral mucositis due to high-dose chemotherapy and/or head and neck radiation therapy. JNCI Monographs. 2019;53:lgz011. https://doi.org/10.1093/jncimonographs/lgz011.
6. Lin D, Lapen K, Sherer MV, et al. A systematic review of contouring guidelines in radiation oncology: analysis of frequency, methodology, and delivery of consensus recommendations. Int J Radiat Oncol Biol Phys. 2020;107:827–35. https://doi.org/10.1016/j.ijrobp.2020.04.011.
7. Chung H, Jin H, Dempsey JF, et al. Evaluation of surface and build-up region dose for intensity-modulated radiation therapy in head and neck cancer. Med Phys. 2005;32:2682–9. https://doi.org/10.1118/1.1992067.
8. Higgins PD, Han EY, Yuan JL, Hui S, Lee CK. Evaluation of surface and superficial dose for head and neck treatments using conventional or intensity-modulated techniques. Phys Med Biol. 2007;52:1135. https://doi.org/10.1088/0031-9155/52/4/018.
9. Baba MH, Singh BK. In-vivo skin dose measurement using gafchromic EBT3 film dosimetry in the radiation therapy of Head and Neck cancers: 2DRT versus IMRT. J Radiat Res Appl Sci. 2022;15:170–4. https://doi.org/10.1016/j.jrras.2022.05.019.
10. Sheykholeslami N, Parwaie W, Farzin M, Vaezzadeh V, Geraily G. An investigation into the surface dose using eclipse treatment planning system and film dosimetry for treatment of breast cancer. Front Biomed Technol. 2023;2023(10):27–31. https://doi.org/10.18502/fbt.v10i1.11509.
11. Wang L, Cmelak AJ, Ding GX. A simple technique to improve calculated skin dose accuracy in a commercial treatment planning system. J Appl Clin Med Phys. 2018;19:191–7. https://doi.org/10.1002/acm2.12275.
12. Eclipse Photon and Electron Algorithms Reference Guide: This document provides reference information about the algorithms supported in Eclipse, version 13.6. California: Varian medical systems; 2015. 286.
13. Chiu-Tsao S, Sim S, Chan MF. The impact of patient immobilization devices on skin dose during IMRT: a radiochromic EBT film dosimetry study in phantom. Int J Radiat Oncol Biol Phys. 2008;72:S659. https://doi.org/10.1016/j.ijrobp.2008.06.346.
14. Olch AJ, Gerig L, Li H, Mihaylov I, Morgan A. Dosimetric effects caused by couch tops and immobilization devices: report of AAPM task group 176. Med Phys. 2014;41:061501. https://doi.org/10.1118/1.4876299.
15. Hadley SW. Effects of immobilization mask material on surface dose. J Appl Clin Med Phys. 2005;6:2005. https://doi.org/10.1120/jacmp.v6i1.1957.
16. Merlotti A, Alterio D, Vigna-Taglianti R, et al. Technical guidelines for head and neck cancer IMRT on behalf of the Italian association of radiation oncology-head and neck working group. Radiat Oncol. 2014;9:1–32. https://doi.org/10.1186/s13014-014-0264-9.
17. Fiorino C, Dell'Oca I, Pierelli A, et al. Simultaneous integrated boost (SIB) for nasopharynx cancer with helical tomotherapy. Strahlenther Onkol. 2007;183:497. https://doi.org/10.1007/s00066-007-1698-x.
18. Baba MH, Singh BK. In-vivo skin dose measurement using gafchromic EBT3 film dosimetry in the radiation therapy of Head and Neck cancers: 2DRT versus IMRT. J Radiat Res Appl Sci. 2020;15:170–4. https://doi.org/10.1016/j.jrras.2022.05.019.
19. Dreindl R, Georg D, Stock M. Radiochromic film dosimetry: considerations on precision and accuracy for EBT2 and EBT3 type films. Z Med Phys. 2014;24:153–63. https://doi.org/10.1016/j.zemedi.2013.08.002.
20. Tanaka Y, Monzen H, Matsumoto K, Inomata S, Fuse T. Dose distribution comparison in volumetric-modulated arc therapy plans for head and neck cancers with and without an external body contour extended technique. Reports Pract Oncol Radiother. 2019;24(6):576–84. https://doi.org/10.1016/j.rpor.2019.09.003.
21. Avanzo M, Drigo A, Kaiser SR, et al. Dose to the skin in helical tomotherapy: results of in vivo measurements with radiochromic films. Physica Med. 2013;29:304–11. https://doi.org/10.1016/j.ejmp.2012.04.004.

22. Mahur M, Singh M, Semwal M K, Gurjar O P. Evaluation of surface dose calculations using monaco treatment planning system in an indigenously developed head and neck phantom. Medical Journal of Dr. DY Patil University. 2023. https://journals.lww.com/mjdy/toc/2023/16050.
23. Giuliano A, Ravaglia V. 149. Skin dose in radiotherapy: results of in vivo measurements with Gafchromic EBT3 films. Phys Med Eur J Med Phys. 2018;56:156–7. https://doi.org/10.1016/j.ejmp.2018.04.160.
24. Devic S, Seuntjens J, Abdel-Rahman W, et al. Accurate skin dose measurements using radiochromic film in clinical applications. Med Phys. 2006;33:1116–24. https://doi.org/10.1118/1.2179169.
25. Chiu-Tsao ST, Chan MF. Photon beam dosimetry in the superficial buildup region using radiochromic EBT film stack. Med Phys 36(6Part1). 2009;36:2074–83. https://doi.org/10.1118/1.3125134.
26. Kern A, Bäumer C, Kröninger K, et al. Determination of surface dose in pencil beam scanning proton therapy. Med Phys. 2020;47:2277–88. https://doi.org/10.1002/mp.14086.
27. Fleckenstein J, Eschler A, Kremp K, Kremp S, Rübe C. Dose distribution and tumor control probability in out-of-field lymph node stations in intensity modulated radiotherapy (IMRT) vs 3D-conformal radiotherapy (3D-CRT) of non-small-cell lung cancer: an in silico analysis. Radiat Oncol. 2015; 10: 1–7. https://rdcu.be/dose6.
28. Joosten A, Matzinger O, Jeanneret-Sozzi W, Bochud F, Moeckli R. Evaluation of organ-specific peripheral doses after 2-dimensional, 3-dimensional and hybrid intensity modulated radiation therapy for breast cancer based on Monte Carlo and convolution/superposition algorithms: implications for secondary cancer risk assessment. Radiother Oncol. 2013;106:33–41. https://doi.org/10.1016/j.radonc.2012.11.012.
29. Lu CC, Wang FN, Lin HH, Hsu CH, Lin JP, Lai LH. Dosimetric measurement of testicular dose for colorectal cancer using optically-stimulated luminescent dosimeters in radiotherapy. Radiat Phys Chem. 2020;172:108792. https://doi.org/10.1016/j.radphyschem.2020.108792.
30. Kry SF, Smith SA, Weathers R, Stovall M. Skin dose during radiotherapy: a summary and general estimation technique. J Appl Clin Med Phys. 2012. https://doi.org/10.1120/jacmp.v13i3.3734.
31. Lowther NJ, Marsh SH, Louwe RJ. Dose accumulation to assess the validity of treatment plans with reduced margins in radiotherapy of head and neck cancer. Phys Imag Radiat Oncol. 2020. https://doi.org/10.1016/j.phro.2020.05.004.
32. Velec M, Waldron JN, O'Sullivan B, et al. Cone-beam CT assessment of interfraction and intrafraction setup error of two head-and-neck cancer thermoplastic masks. Int J Radiat Oncol Biol Phys. 2010;76:949–55. https://doi.org/10.1016/j.ijrobp.2009.07.004.
33. Penoncello GP, Ding GX. Skin dose differences between intensity-modulated radiation therapy and volumetric-modulated arc therapy and between boost and integrated treatment regimens for treating head and neck and other cancer sites in patients. Med Dosim. 2016;41:80–6. https://doi.org/10.1016/j.meddos.2015.09.001.

編集後記

令和 6 年度（2024 年 4 月～2025 年 3 月）における臨床研究部の活動を取りまとめた「研究業績集 第 25 号」が、このたび完成いたしました。本業績集には、臨床研究および治験の成果をはじめ、英文原著論文、和文原著・著書、学会発表、研究会、学術講演会など、多岐にわたる研究実績を収録しております。

2024 年度より、私が臨床研究部長を拝命し、研究基盤の再構築と新たな研究体制の確立に取り組んでまいりました。本年度は、各診療科・部署において臨床データに基づくエビデンス創出が積極的に推進され、基礎研究から臨床応用へと展開する多角的な研究活動が着実に進展いたしました。

英文原著論文においては、循環器領域、脳血管領域、皮膚腫瘍領域を中心に顕著な成果が得られました。英文論文の掲載数は 27 編に達し、過去 3 年を上回った前年度とほぼ同数を維持しております。そのうち、職員が筆頭著者を務めた原著英文論文は 8 編、原著以外の英文論文が 6 編であり、全体の半数以上を占めました。これらの成果は、当施設における研究の質的向上および国際的な認知の高まりを示すものであり、日々の診療業務と研究活動を両立させながら研鑽を重ねている職員各位の不断の努力の賜物と深く敬意を表する次第です。

さらに、2024 年度より鹿児島大学大学院との連携講座「臨床情報医工学」が開講され、臨床現場と基礎研究を有機的に結ぶ教育・研究体制が一層充実いたしました。これにより、次世代の医療研究者を育成するという新たな使命に向けた取り組みが本格的に始動しております。

今後とも、研究支援体制のさらなる整備・強化を図りつつ、倫理的かつ科学的に妥当な臨床研究の推進に努め、地域および社会の健康増進に資する研究成果の創出を目指してまいります。本業績集が、当施設の研究活動を広く周知する一助となり、新たな研究交流および協働の契機となることを期待しております。

最後に、本業績集の作成にご尽力賜りました臨床研究部スタッフならびに関係各位に、謹んで深謝申し上げます。

令和 7 年 3 月吉日

国立病院機構鹿児島医療センター

臨床研究部長 松下 茂人